AFML-TR-75-42

Volume II

ADA029934

PROCEEDINGS OF THE 1974 TRISERVICE CORROSION OF MILITARY EQUIPMENT CONFERENCE, 29-31 OCTOBER 1974
Volume II. Sessions IV through VII

AERONAUTICAL SYSTEMS BRANCH
SYSTEMS SUPPORT DIVISION

SEPTEMBER 1975

TECHNICAL REPORT AFML-TR-75-42, Volume II
FINAL REPORT FOR PERIOD 31 OCTOBER 1974 — 1 FEBRUARY 1975

Approved for public release; distribution unlimited

DDC

SEP 20 1976

A

AIR FORCE MATERIALS LABORATORY
AIR FORCE WRIGHT AERONAUTICAL LABORATORIES
Air Force Systems Command
Wright-Patterson Air Force Base, Ohio 45433

REPORT DOCUMENTATION PAGE	READ INSTRUCTIONS BEFORE COMPLETING FORM

1. REPORT NUMBER	2. GOVT ACCESSION NO.	3. RECIPIENT'S CATALOG NUMBER
AFML-TR-75-42, Volume II	(1974)	(9)

4. TITLE *(and Subtitle)*	5. TYPE OF REPORT & PERIOD COVERED
PROCEEDINGS OF THE 1974 TRISERVICE CORROSION OF MILITARY EQUIPMENT CONFERENCE	Final Technical Report. 31 Oct 74 - 1 Feb 75.
held at Dayton, Ohio on 29-31 Oct 74. Volume II. Sessions IV through VII.	6. PERFORMING ORG. REPORT NUMBER

7. AUTHOR(s)	8. CONTRACT OR GRANT NUMBER(s)
Fred H. Meyer, Jr. (Editor)	

9. PERFORMING ORGANIZATION NAME AND ADDRESS	10. PROGRAM ELEMENT, PROJECT, TASK AREA & WORK UNIT NUMBERS
Aeronautical Systems Branch (MXA) Air Force Materials Laboratory Wright-Patterson AFB, Ohio 45433	73810701

11. CONTROLLING OFFICE NAME AND ADDRESS	12. REPORT DATE
Systems Support Division (MX) Air Force Materials Laboratory Wright-Patterson AFB, Ohio 45433	Sep 1975
	13. NUMBER OF PAGES
	379

14. MONITORING AGENCY NAME & ADDRESS*(if different from Controlling Office)*	15. SECURITY CLASS. *(of this report)*
AFML-TR-75-42-Vol-2	UNCLASSIFIED
	15a. DECLASSIFICATION/DOWNGRADING SCHEDULE

16. DISTRIBUTION STATEMENT *(of this Report)*

Approved for public release; distribution unlimited.

AF-7381   738107

17. DISTRIBUTION STATEMENT *(of the abstract entered in Block 20, if different from Report)*

18. SUPPLEMENTARY NOTES

19. KEY WORDS *(Continue on reverse side if necessary and identify by block number)*

Corrosion

20. ABSTRACT *(Continue on reverse side if necessary and identify by block number)*

This report is a compilation of papers presented at the 1974 Triservice Corrosion of Military Equipment Conference held in Dayton, Ohio, 29-31 October 1974.

DD FORM 1473 EDITION OF 1 NOV 65 IS OBSOLETE

FOREWORD

This report was compiled by the Aeronautical Systems Branch, Systems Support Division, Air Force Materials Laboratory, Wright-Patterson AFB, Ohio. It was initiated under Project 7381, "Materials Applications," Task 738107, "Corrosion Control and Failure Analysis," with Mr. Fred H. Meyer, Jr. as the Project Engineer. The 1974 Triservice Conference is a follow-up to three similar conferences held in 1967, 1968, and 1972.

The report includes all available papers from the 1974 Triservice Corrosion of Military Equipment Conference.

This technical report was submitted by the author in February 1975.

Proceedings of prior conferences are available in AFML Technical Report TR-67-329 (1967) and in Metals and Ceramics Information Center Report MCIC 73-19.

The purpose of the 1974 Conference was to continue interservice coordination in the areas of corrosion research and corrosion prevention and control. Specifically, the objectives were to make Department of Defense personnel, contractors and interested individuals aware of the important corrosion problems in military equipment, to present the status of significant corrosion research projects currently pursued by the military services and to provide a general forum for exchange of corrosion prevention and control information.

TABLE OF CONTENTS

Preceding Page Blank

TABLE OF CONTENTS (continued)

AFML-TR-75-42
Volume II

TABLE OF CONTENTS (continued)

TABLE OF CONTENTS (concluded)

SESSION IV

ENVIRONMENT INDUCED CRACKING PHENOMENA

EVALUATING STRESS CORROSION CRACK PROPAGATION RATES IN HIGH
STRENGTH ALUMINUM ALLOYS WITH BOLT LOADED PRECRACKED DOUBLE
CANTILEVER BEAM SPECIMENS

by

D. O. Sprowls, J. W. Coursen and J. D. Walsh

ABSTRACT

Propagation rates for stress-corrosion cracking (SCC) of high
strength aluminum alloys determined with mechanically precracked
double cantilever beam (DCB) specimens provide a quantitative
means of comparing the resistance to SCC of alloys and tempers.
The determination of precise propagation rates for relatively
resistant materials, however, can be markedly influenced by
test conditions and interpretation of the crack growth data.
This paper describes a relatively simple, accelerated testing
method for determining SCC "plateau velocities" that rank the
SCC behavior of aluminum alloys in the same order as SCC propa-
gation rates in a seacoast or industrial atmosphere. Rankings
of alloys with the "plateau velocities" also are boradly similar
to rankings with "threshold stresses" estimated from tests of
smooth specimens. Practical difficulties associated with this
test method, however, warrant further evaluation to justify
this as a primary method of testing.

INTRODUCTION:

The primary objective in performing a stress corrosion test with fracture mechanics type precracked specimens is to determine the threshold stress-intensity below which stress-corrosion cracking (SCC) will not occur for a specific material and test orientation in a specific environment (1). Another objective is to determine the rate of SCC propagation, da/dt, as a function of the mechanical crack driving force, K_I, under controlled test conditions (2). It is generally agreed that in order to fully characterize the resistance to SCC by this test method, it is preferable to obtain the complete curve of K_I vs da/dt.

A convenient type of specimen for determining SCC propagation rates is a double cantilever beam (DCB) loaded by constant displacement to a stress-intensity at or just below the critical stress-intensity required for mechanical fracture. With such extremely high stress-intensity SCC will start quickly in highly susceptible materials and proceed for a time at a fairly constant rate before it slows down to approach an arrest as the crack lengthens and K_I decreases. When (and if) the crack growth comes to an "arrest", the stress-intensity can be said to be at the threshold for SCC (K_{Iscc}). A typical SCC crack growth curve and the relationship of the SCC propagation rate with the decreasing stress-intensity is shown for a relatively susceptible material in Figure 1. (Note that the graphs are plotted in a rather unorthodox manner in order to relate the performance with the crack growth shown in the specimen.) The purpose of the present paper is to consider the use of SCC "plateau velocities", as illustrated in Figure 1, for comparing the resistance to SCC of aluminum alloys and to describe a simple test procedure for obtaining such data. The significance of the "plateau velocity" is that it is the highest SCC propagation rate that a material will sustain for an appreciable crack extension under the controlled test conditions.

Procedure Used for Determining SCC Plateau Velocities

The specimen configuration shown in Figure 2 was used for most of the experiments described below. The specimen orientation (S-L) was such that stress was applied in the short transverse direction to the grain structure and the SCC growth was in the longitudinal direction. The precrack was produced by loading with either one or two bolts until fracture (pop-in) occurred and the crack was advanced until it was about 0.1-inch long on the sides of the specimen. A few drops of 3.5% NaCl solution (reagent grade NaCl and deionized water) were added to the notch during pop-in. Loaded specimens were placed in a vertical position with the notched end up, and a few drops of 3.5% NaCl solution were added to the notch three times daily (once daily on weekends). Crack lengths were measured every one or two days to the nearest 0.01 inch on both sides of the specimen and the measurements averaged. Upon termination of exposure after thirty or forty days, the specimens were broken open to examine the fracture surfaces; in some cases specimens were sawed in half lengthwise so that one-half could be broken open and the other half sectioned for metallographic examination of the crack tip.

SCC propagation rates, like the threshold stress or stress-intensity, depend upon the conditions of test. The effect of the corrosive environment is illustrated by the test results shown in Figures 3 and 4 for specimens of alloy 7079-T651 exposed to the atmosphere under various conditions. The SCC growth curves in Figure 3 show that the crack growth was relatively rapid at first; but in the laboratory and the outdoor industrial atmosphere, the crack growth increased only very slightly after about 250 days. Although these curves were plotted only to 365 days, the exposures were continued for at least another year and the extended curves were used for the derivations of K_I and da/dt in Figure 4. Wide variations both in the plateau velocities and the apparent K_{Iscc} values were observed, depending upon the atmospheric conditions. Corrosion of the crack faces with the formation of wedges of corrosion product prevented crack arrest and the estimation of K_{Iscc} values for the seacoast atmosphere and the 3.5% NaCl solution tests. It is noteworthy, also, that in the dry air in the desiccator no SCC growth occurred in a period of 39 months; this was confirmed for the interior of the specimen by breaking the specimen open and examining the fracture surface.

It is easy to determine plateau velocities for materials with a relatively low resistance to SCC, such as 7079-T651 alloy plate when stressed in the short transverse direction; however, the procedure is not so easy for resistant materials which develop only small amounts of crack growth. The initial SCC crack growth for the more resistant materials is likely to be erratic because the extremely high local stress concentration at the crack tip may cause a sudden small initial burst of cracking, or conversely localized plastic deformation can have a crack-blunting effect that will delay the initiation of SCC. Consequently, estimates of the initial crack velocity can be misleading.

Examples of the variation encountered in the environmental crack growth curves of materials with relatively high resistance to SCC are shown in Figure 5. Various approaches were tried for determining realistic plateau velocities, and it was concluded that the simplest procedure that is subject to the least error in interpretation is to divide the total crack growth by the total exposure time for some arbitrary period. The period should be long enough to ensure an opportunity for SCC to initiate and to include the initial sustained crack growth, yet not long enough to include excessive crack growth caused by corrosion product wedging. This method will not only identify the materials with relatively low resistance to SCC (such as the 7075-T651) but will also provide a useful measure for the highly resistant materials that may not develop a K_I vs da/dt curve with a definite plateau.

A comparison of plateau velocities calculated by this method (c) with two other procedures (a and b) is shown below (the more realistic estimates of the plateau velocity are marked with an *):

3

Alloy	Plateau Velocities, in./hr. x 10^{-5}			
	(a) First Growth	(b) Growth Peaks	(c) Average Growth	
			15 Days	30 Days
7075-T651	160*	--	110*	80
7050-T76511	90*	--	60*	40
2124-T851	100	40*	30*	30*
7075-T7X51	30	12*	19*	17*
7050-T73651	60	--	20	10*
7075-T7351	10	6	3*	6

(a) Average slope of the initial portion of the crack growth curve beginning at the time when growth starts and extending until the curve starts to bend over.

(b) Slope of a straight line drawn tangent to the crack growth curve at successive growth peaks exemplified by the curve for 7075-T7X51.

(c) Slope of straight line from zero time to the amount of growth at 15 or 30 days.

The propagation rate calculated from the slope of the first growth (Procedure (a)) appears to be meaningful for the alloys having lower resistance to SCC but are exaggerated for the alloys with higher resistance. Procedure (b) is not applicable to all growth curves. The 15-day average rates determined by Procedure (c) are the most generally applicable and the procedure is not subject to interpretation.

Effect of Variations in Test Procedure

A series of experiments was performed to determine whether the SCC growth would be affected by several variations that would simplify or increase the flexibility of the test procedure. For example, it would be advantageous to be able to compare the results from tests of DCB specimens of different heights because of the necessity of testing S-L orientation specimens from materials of various thicknesses. Therefore, tests were performed on specimens with beam heights of 0.5, 1.0 and 2.0 inches. A comparison also was made of a straight notch vs the chevron notch in the 1.0-inch high specimen because considerable data in the literature have been obtained with the straight notch (3,4). The chevron notch and higher (stiffer) beams have the advantage of causing less plastic deformation during the precracking of specimens of tougher alloys and tempers. In an effort to minimize plasticity effects during tension precracking, a deeper notch (1.5 inch vs 0.625 inch) was tested also with the 1.0 inch high specimen. One other experiment was carried out in which drops of the 3.5% NaCl solution were added to the test specimens only once a day instead of three times. For all of the above experiments, tests were made on single specimens of each of three tempers of 7075 alloy plate artificially aged to provide different SCC performances (Table I).

The plateau velocities based on 15-day exposures are summarized in Table II, and certain comparisons are illustrated graphically in Figures 6-8. Varying the beam height did not appreciably affect the average SCC plateau velocities for any of the three tempers. However, the other variations in specimen configuration (straight notch or increased notch depth) and the reduced frequency of wetting with 3.5% NaCl solution did reduce the SCC propagation rates for 7075-T7X51 and T7351--although not for the T651 temper. The relative extent of SCC crack growth in the three different tempers is shown in the photograph of fracture surfaces in Figure 9.

SCC plateau Velocities in Natural Environments

Plateau velocities in the 3.5% NaCl test for a variety of alloys and tempers are compared in Table III with similarly obtained maximum sustained velocities observed in the seacoast atmosphere at Point Judith, Rhode Island, and in an inland industrial atmosphere at New Kensington, Pennsylvania (4). It is significant that a ranking of these materials by the 3.5% NaCl test places them in the same general categories as SCC propagation rates in outdoor atmospheric exposures. The velocities in the accelerated test were about five to ten times greater than the velocities in the atmosphere depending on the alloy and temper, and velocities tended to be equal or about twice as great in the seacoast atmosphere as in industrial atmosphere. The more corrosive conditions at the seacoast also caused more rapid mechanical fracturing of the highly resistant 2XXX alloys as a result of corrosion product wedging.

SCC Ranking with Precracked vs Smooth Specimens

It appears from tests conducted on a variety of aluminum alloy products (3,4,5,6) that general trends derived from DCB specimen data agree with established trends derived from smooth specimen threshold data. Data from both types of tests provide a clear-cut distinction between alloys and tempers with high or low resistance to SCC. HOWEVER, NEWLY DEVELOPED MATERIALS WITH CONTROLLED RANGES OF INTERMEDIATE RESISTANCE TO SCC PROVIDE A CHALLENGE TO BOTH TYPES OF TESTING.

Data for groups of 2XXX-T8 and 7XXX-T7 materials are arranged in Table IV in the order of increasing SCC plateau velocities so that rankings can be compared for the two test methods (materials with higher plateau velocities would be expected to have lower threshold stress values). For materials with plateau velocities of 30×10^{-5} in./hr. and above the rankings are similar for the two methods, but for plateau velocities ranging from 3 to 30×10^{-5} in./hr. they are not, and comparisons can be confusing. For example, in the case of the 2XXX-T8 alloys, four plates had plateau velocities ranging from 8 to 22×10^{-5} in./hr. that are meaningless because no SCC could be detected in any instance; yet SCC resulted in failure of smooth specimens from two of the items at applied stresses of 46-48 ksi (75% Y.S.). Thus, the smooth specimen tests could rank the four materials into two categories but the DCB tests could rank

them only as being not susceptible to SCC or the test must be considered as indeterminate under the test conditions. In the case of the 7XXX-T7 alloys, the situation was different. There are listed four items with plateau velocities of 3 or 20 x 10^{-5} in./hr., and there is no similarity with the rankings indicated by the test results from the smooth specimens. Probably the confusion in the rankings of these 7XXX-T7 materials can be attributed to the mixtures of alloys and products involved.

Thus, plateau velocities in the 3.5% NaCl test ranging from 3 to about 25 x 10^{-5} in./hr. do not, in themselves, provide information about the resistance to SCC unless it is verified that crack growth is really SCC and not mechanical fracture. Also, it appears that plateau velocities can be used to best advantage for ranking a series of materials of the same alloy and product, as for example, the three tempers of 2.5-inch 7075 alloy plate listed in Table IV.

Complete K_I - da/dt Curves

For DCB specimens of this type, the stress intensity can be expressed in terms of V, the crack opening displacement at the load line, crack length a, beam height (2h), and the modulus of elasticity E according to the following relationship (3):

$$K_I = \frac{VEh(3h(a + 0.6\ h)^2 + h^3)^{1/2}}{4((a + 0.6\ h)^3 + h^2\ a)}$$

For the tougher alloys a significant amount of plastic deformation at the crack tip or in the arms of the specimen occurs during the tension precracking, and the total value of V is so large that the calculated K_I is greater than the K_{Ic} value. Thus, all subsequent K_I values calculated after various increments of SCC growth also will be too large. However, if only the elastic part of V and the crack length measured on the fracture are used in the calculations, adjusted K_{Ii} values can be obtained that are consistently close to K_{Ic} values, as shown in the following examples selected from Table V.

Alloy and Temper	K values in ksi $\sqrt{in}$.		
	K_{Ic}	Nominal K_{Ii}	Adjusted K_{Ii}
7075-T651	15.7	20.4	14.5
7075-T7X51	19.9	28.6	18.7
7075-T7351	19.2	30.9	18.7

Adjusted K_{Ii} values close to K_{Ic} also were obtained with the variations in beam height (0.5 inch, 1.0 inch and 2.0 inch) for which data are given in Table V and for the various other types of aluminum alloys tested (4). Thus, it appears that the use of the elastic portion of V and the crack length measured on the fracture will provide meaningful K levels to drive the environmental crack propagation. Although the plastic behavior obtained during tension precracking technically may invalidate the calculations of stress-intensity, it appears for aluminum alloys that the SCC propagation rate is not appreciably affected (4).

6

In conducting the SCC test, it is not advisable to unload and reload the test specimen. Therefore, if it is desired to calculate stress-intensities, it is proposed that a pop-in test as described in the footnotes in Table V be performed on a duplicate specimen to estimate the elastic component of V to be used in the calculations of K_I for the SCC test specimen. Also, the SCC test specimen should be broken open at the end of the test to obtain a more realistic measurement of the total crack length. This procedure was used for the K_I - da/dt curves in Figure 4.

SUMMARY

The method described above for estimating "plateau" or maximum sustained SCC velocities at stress-intensities at or just below the critical stress-intensity has several advantages for screening tests of alloys and tempers. The test is fairly rapid; it is sensitive to various degrees of susceptibility to SCC; it does not require determination of stress-intensities, and it simplifies the interpretation of the crack growth curves. It is essential, however, for materials that show only small amounts of environmental crack growth, especially in the case of 2XXX alloys, to establish that the crack growth is really SCC and not simply mechanical fracture caused by corrosion product wedging. The mode of cracking can be readily determined either by fractographic examination or metallographic examination of the crack tip (Figure 10).

Although SCC plateau velocities obtained by this method are not directly applicable in the design of structures, knowledge of relative SCC propagation rates can be useful in special situations for appraising the hazard of SCC and determining suitable inspection intervals.

Practical difficulties involved in measuring small amounts of SCC growth, however, warrant further evaluation to justify this as a primary method of testing.

ACKNOWLEDGMENTS

References:

(1) Brown, B. F., <u>Stress Corrosion Cracking in High Strength Steels and in Titanium and Aluminum Alloys</u>, Naval Research Laboratory, Washington, D.C., 1972. (Sponsored by the Advanced-Research Projects Agency ARPA Order No. 878), pp. 1-16 (Fundamentals).

(2) Wei, R. P., Novak, S. R., and William, D. P., "Some Important Considerations in the Development of Stress-Corrosion Cracking Test Methods", <u>AGARD Conference Proceedings No. 98</u>, Specialists Meeting on Stress Corrosion Testing Methods, Brussels, Belgium, 5 and 6 October, 1971, pp. 5-1 thru 8.

(3) Speidel, Markus O. and Hyatt, Michael V., "Stress Corrosion Cracking of High Strength Aluminum Alloys", <u>Advance in Corrosion Science and Technology</u>, Vol. 2, Edited by Mars G. Fontana and and Roger W. Staehle (Plenum Press, 1972), p. 158.

(4) Sprowls, D. O., Shumaker, M. B., Walsh, J. D. and Coursen, J. W., "Evaluation of Stress Corrosion Cracking Susceptibility Using Fracture-Mechanics Techniques", Final Report-Part I of Contract No. NAS 8-21487, prepared for George C. Marshall Flight Center, May 31, 1973.

(5) Babilon, C. F., Wygonik, R. H., Nordmark, G. E. and Lifka, B. W., "Mechanical Properties, Fracture Toughness, Fatigue, Environmental Fatigue Crack Growth Rates and Corrosion Characteristics of High-Toughness Aluminum Alloy Forgings, Sheet and Plate", Technical Report AFML-TR-73-83, April 1973, USAF Contract No. F33615-71-C-1571.

(6) Davies, R. E., Nordmark, G. E., and Walsh, J. D., "Design Mechanical Properties, Fracture Toughness, Fatigue Properties, Exfoliation and Stress Corrosion Resistance of 7050 Sheet, Plate, Extrusions, Hand Forgings and Die Forgings", Final Report for NASC Contract No. N00019-72-C-0512. To be published.

(7) "Standard Method for Stress Corrosion Testing and an Improved System for Rating the Relative Resistance to Stress-Corrosion Cracking of High Strength 7XXX Aluminum Alloy Products", Report of AA/ASTM Task Group G01.06.91 by D. O. Sprowls, Chairman. Also presented at this conference.

Table I

CHARACTERISTICS OF 2.5-IN. THICK 7075 ALLOY
PLATE USED TO EVALUATE VARIATIONS IN TEST PROCEDURE

Temper	Electrical Conductivity % IACS	Long-Transverse			Short-Transverse			K_{Ic} ksi $\sqrt{in.}$
		T.S. ksi	Y.S. ksi	El. % in 4D	T.S. ksi	Y.S. ksi	El. % in 4D	
T651	33.5	80.2	71.7	8.0	74.8	66.6	2.0	15.7*
T7X51	38.7	73.9	63.3	10.0	70.4	60.8	4.0	19.9
T7351	41.0	68.0	56.6	9.5	65.0	54.4	4.0	19.2

	Chemical Composition - Per cent (Remelt Analysis)									
Temper	Si	Fe	Cu	Mn	Mg	Zn	Cr	Ni	Ti	Be
T651, T7351	0.08	0.31	1.80	0.02	2.38	6.02	0.19	0.00	0.03	0.002
T7X51	0.10	0.24	1.80	0.03	2.44	5.87	0.18	0.00	0.04	0.002

*Value meaningful, although not technically valid according to ASTM
criteria.

Table II

EFFECT OF VARIATIONS IN TEST PROCEDURE ON SCC PROPAGATION RATES IN DCB SPECIMENS OF 7075 ALLOY IN VARIOUS TEMPERS

Beam Height (2h) (in.)	Notch Type	Notch Depth (in.)	Frequency of 3.5% NaCl Application	Average Plateau Velocity in./hr. x 10-5 (1) T651	T7X51	T7351
0.5	Chevron	0.625	3 times/day	110	14	6
1.0	Chevron	0.625	3 times/day	110	20	3
2.0	Chevron	0.625	3 times/day	170	14	4
1.0	Straight	0.625	3 times/day	125	8	$<3^{(2)}$
1.0	Chevron	1.500	3 times/day	100	8	$<3^{(2)}$
1.0	Chevron	0.625	1 time/day	110	6	$<3^{(2)}$

Notes: (1) Based on an exposure period of 15 days.

(2) No SCC growth until 16 to 32 days.

Table III

COMPARISON OF MAXIMUM SCC PROPAGATION RATES IN THE 3.5% NaCl ACCELERATED TEST AND IN OUTDOOR ATMOSPHERES (1)

Alloy and Temper	Average Plateau Velocity in./hr. x 10^{-5}		
	3.5% NaCl (15 days)	Seacoast (6 mo.)	Industrial (6 mo.)
7079-T651	320	35	25
7039-T6351	220	30	25
5456-Sens.	210	40	2
2219-T37	210	35	20
2014-T651	120	15	10
2024-T351	100	20	10
7075-T651	100	20	10
2021-T81	30(2)	6(2)	2(2)
2219-T87	20(2)	4(2)	1(2)
2024-T851	20(2)	2(2)	0.5(2)
5456-H117	6(2)	<0.2	<0.2
6061-T651	6(2)	<0.2	<0.2
7075-T7351	3	<0.2	0.4

Notes: (1) Tests on 1-in. high, straight notch DCB specimens (Ref. 4).

(2) Mechanical fracture rather than SCC.

Table IV

COMPARATIVE SCC RANKING BY DCB AND SMOOTH SPECIMENS IN ACCELERATED TESTS

Alloy and Temper	Product	Plateau Velocity(1) in./hr. x 10⁻⁵	Estimated Threshold Stress, ksi(3)	Reference to Source of Data
2XXX Alloy Products				
2124-T851	4.5" plate	8(2)	>45	5
2124-T851	2.5" plate	12(2)	<48 >37	5
2024-T851	2.5" plate	17(2)	<46 <27	4
2219-T87	2.0" plate	22(2)	>43	4
2124-T851	1.75" plate	30	<30	5
2024-T351	2.5" plate	100	<10	4
7XXX Alloy Products				
7075-T7351	2.5" plate	3	>43	-
7049-T73	<1" die forging	3	<35	5
7050-T73651	4.0" plate	20	>45	6
7075-T7X51	2.5" plate	20	<35 >25	-
7050-T736	1-2" die forging	30	<35 >25	6
7050-T76511	3.5" x 7.5" extrusion	80	<25	6
7075-T651	2.5" plate	110	<10	-

Notes:
(1) Average plateau velocity during 15-day exposure to 3.5% NaCl added dropwise. The 7XXX alloy specimens had a chevron notch and the 2XXX alloy specimens a straight notch.

{2} Mechanical fracture, not SCC.

{3} 0.125" dia. tension specimens exposed 84 days to 3.5% NaCl by alternate immersion (Federal Method 823).

Table V

COMPARISON OF STRESS INTENSITIES DETERMINED BY POP-IN OF DCB SPECIMENS OF VARIOUS CONFIGURATIONS

Alloy and Temper	Beam Height (2h) (in.)	Crack Opening (V), in. (1)		Crack Length, in. (2)		K_{I1}, ksi $\sqrt{in.}$			
						V-Total		V-Elastic	
		Total	Plastic	Surface	Fracture	Surface	Fracture	Surface	Fracture
7075-T651 (K_{Ic}=15.7 ksi $\sqrt{in}$)	0.498	0.037	0.008	0.755	0.858	23.9	19.4	18.7	15.2
"	1.001	0.017	0.003	0.785	0.875	20.4	17.6	16.8	14.5
"	1.001	0.049	0.004	1.605(3)	1.740	20.4	17.9	18.7	16.4
"	1.997	0.015	0.001	0.935	1.158	24.1	18.8	22.5	17.5
7075-T7X51 (K_{Ic}=19.9 ksi $\sqrt{in}$)	0.496	0.042	0.011	0.715	0.835	29.4	22.9	21.7	16.9
"	1.001	0.021	0.004	0.715	0.840	28.6	23.0	23.1	18.7
"	1.001	0.064	0.009	1.545(3)	1.725	28.3	23.7	24.3	20.3
"	1.998	0.016	0.002	0.925	1.113	26.0	21.0	22.8	18.4
7075-T7351 (K_{Ic}=19.2 ksi $\sqrt{in}$)	0.498	0.043	0.014	0.715	0.805	30.3	25.0	20.4	16.9
"	1.001	0.024	0.005	0.745	0.908	30.9	23.9	24.5	18.7
"	1.002	0.063	0.008	1.525(3)	1.717	28.5	23.5	24.9	20.5
"	1.998	0.016	0.001	1.005	1.173	23.7	19.7	22.8	18.5

Notes: (1) Values for V were obtained from measurements of 2h at the bolt line before loading (d_0), after loading (d_1) and after unloading (d_2). V-total=d_1 - d_0 and V-plastic=d_2 - d_0.

(2) Black ink was added to the cracks after loading to mark the crack fronts, and the specimens broken open so that the crack length could be measured on the fracture surface.

(3) A deeper crack starter notch was machined for this configuration.

13
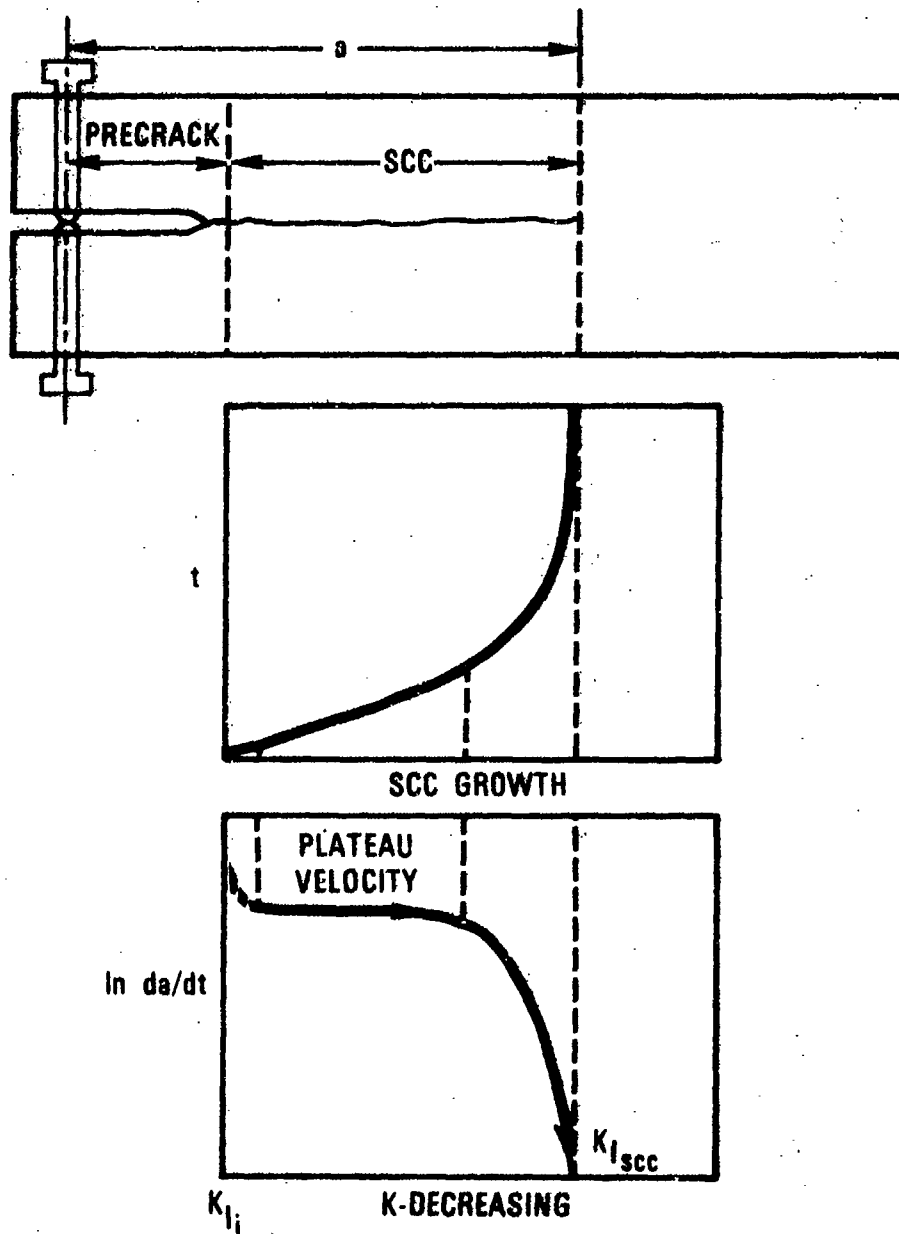
SCHEMATIC ILLUSTRATION OF SCC GROWTH AND THE
RELATIONSHIP BETWEEN THE SCC PROPAGATION
RATE AND THE DECREASING STRESS INTENSITY
IN A BOLT LOADED DCB SPECIMEN

Fig. 1

1/4 DIA-28NF TAP

B=1.000

.500

.375

.625

W=5.0

2h=1.000

.500

.063

32 ✓ ALL OVER

MILL WITH
60° CUTTER

.063

NOTCH ROOT
RADIUS 0.01 MAX

SECTION ON ℄

45°

45°
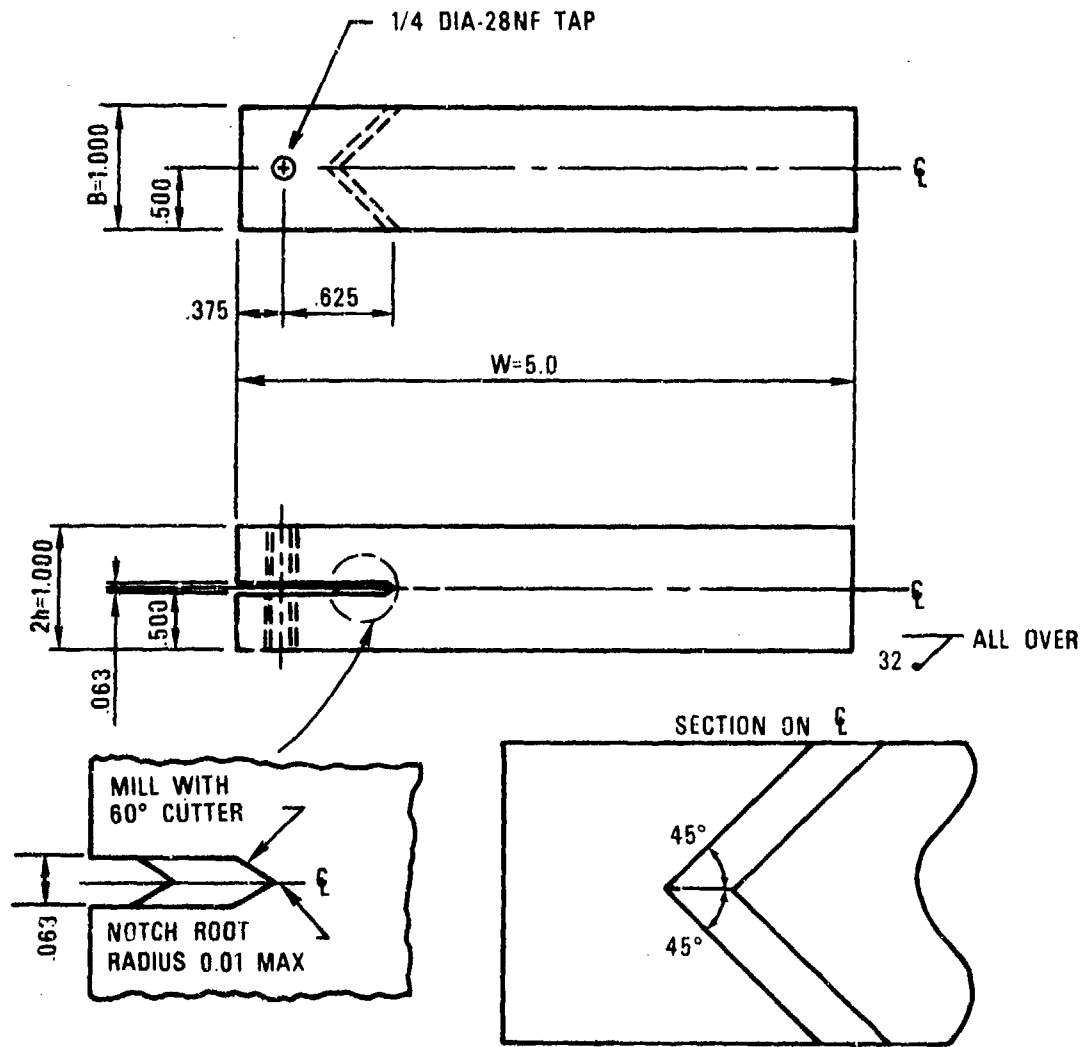
**CONFIGURATION OF DOUBLE CANTILEVER BEAM
(DCB) SPECIMEN USED FOR SCC TESTS**

Fig.2

15
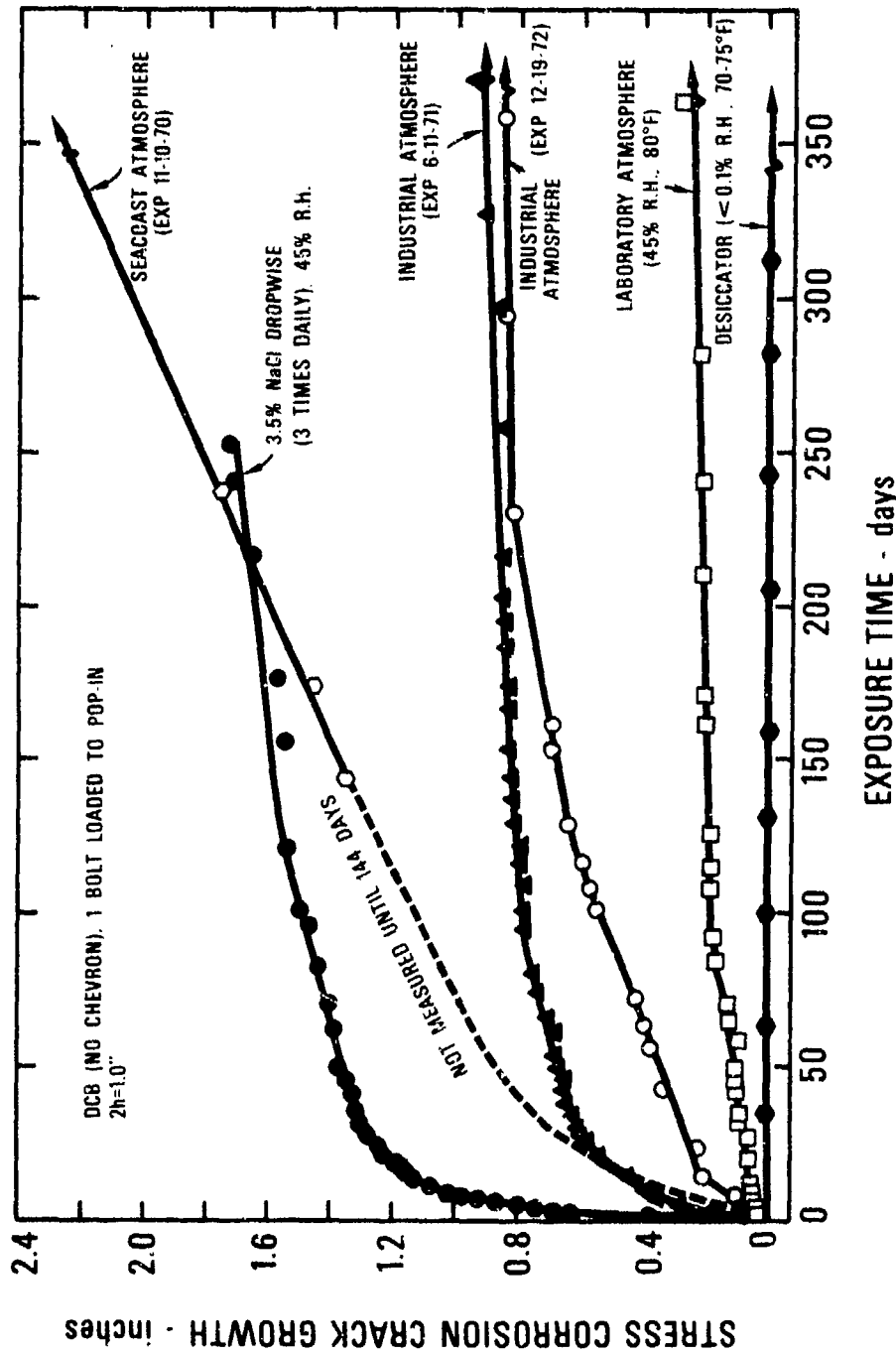
EFFECT OF CORROSIVE ENVIRONMENT ON S.C.C. PROPAGATION
IN 7079-T651 ALUMINUM ALLOY PLATE (2.5 in. THICK)

Fig. 3

16

OCB (NO CHEVRON), 1 BOLT LOADED TO POP-IN
2a=1.0

3.5% NaCl DROPWISE
(3 TIMES DAILY), 45% R.H.

INDUSTRIAL ATMOSPHERE
(EXP 6-11-71)

SEACOAST ATMOSPHERE
(EXP 11-10-70)

INDUSTRIAL ATMOSPHERE
(EXP 12-19-72)

LABORATORY ATMOSPHERE
(45% R.H., 80°F)

DESICCATOR
(<0.1% R.H., 80°F)
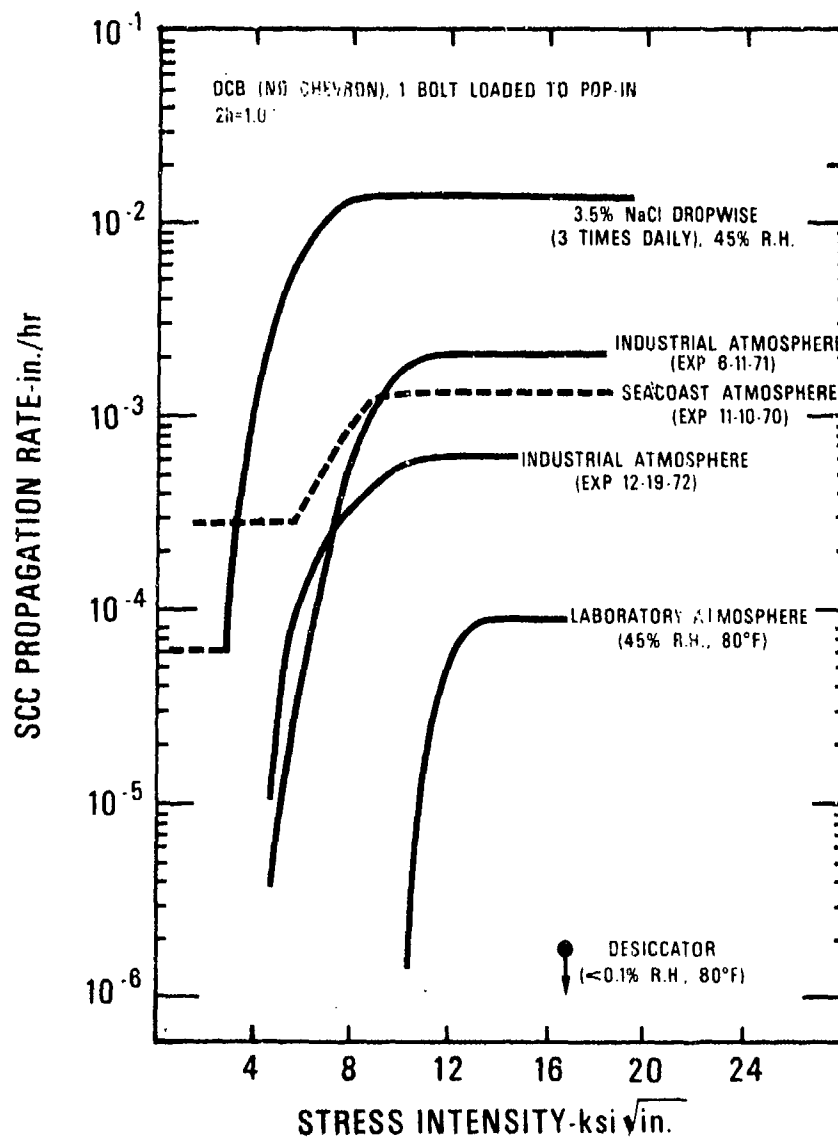
**EFFECT OF CORROSIVE ENVIRONMENT ON SCC PROPAGATION
RATE IN 7079-T651 ALLOY PLATE (2.5-in. THICK)**

Fig. 4
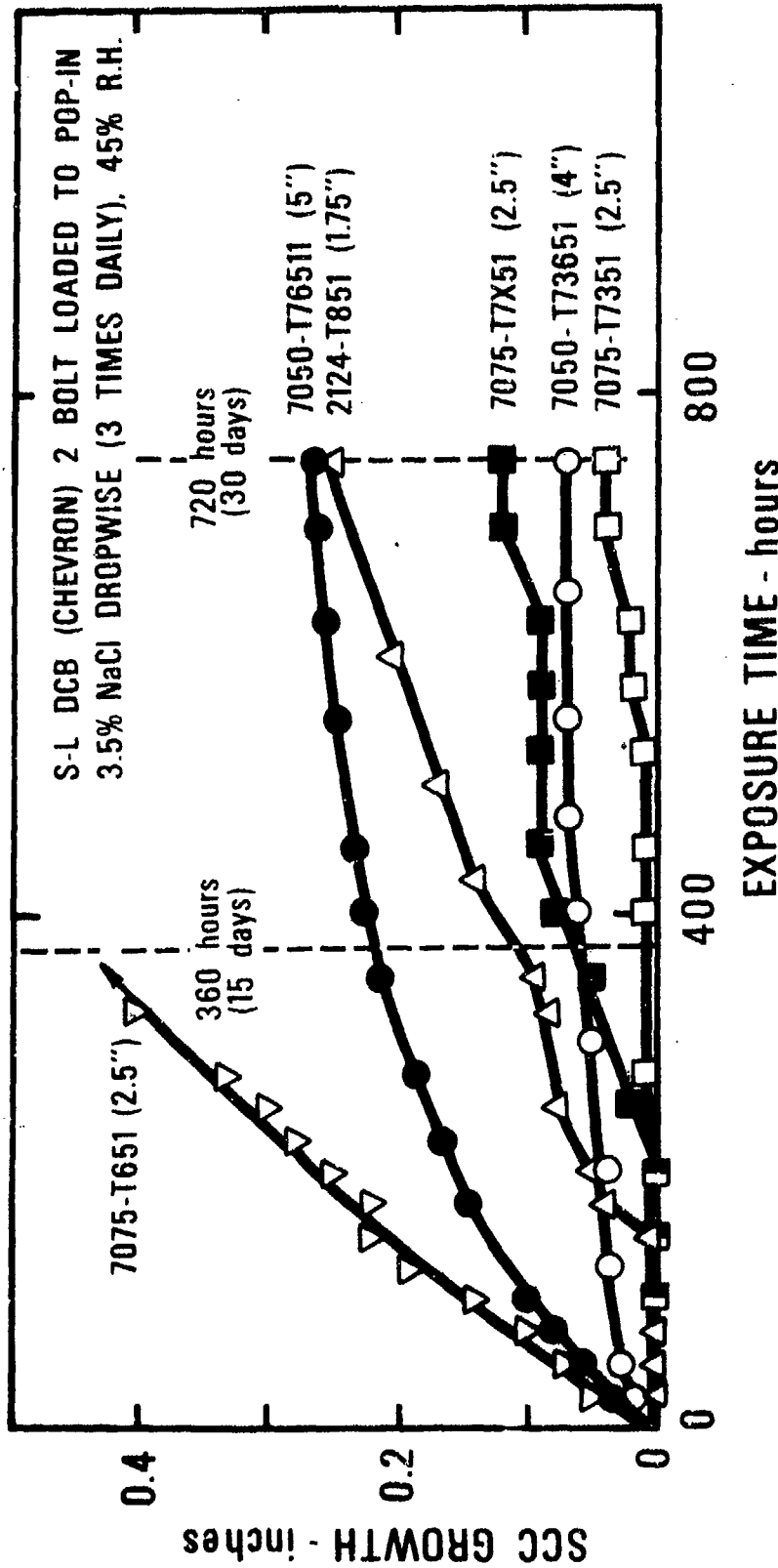
EXAMPLES OF SCC CRACK GROWTH IN VARIOUS MATERIALS WITH RELATIVELY HIGH RESISTANCE TO SCC

Fig. 5
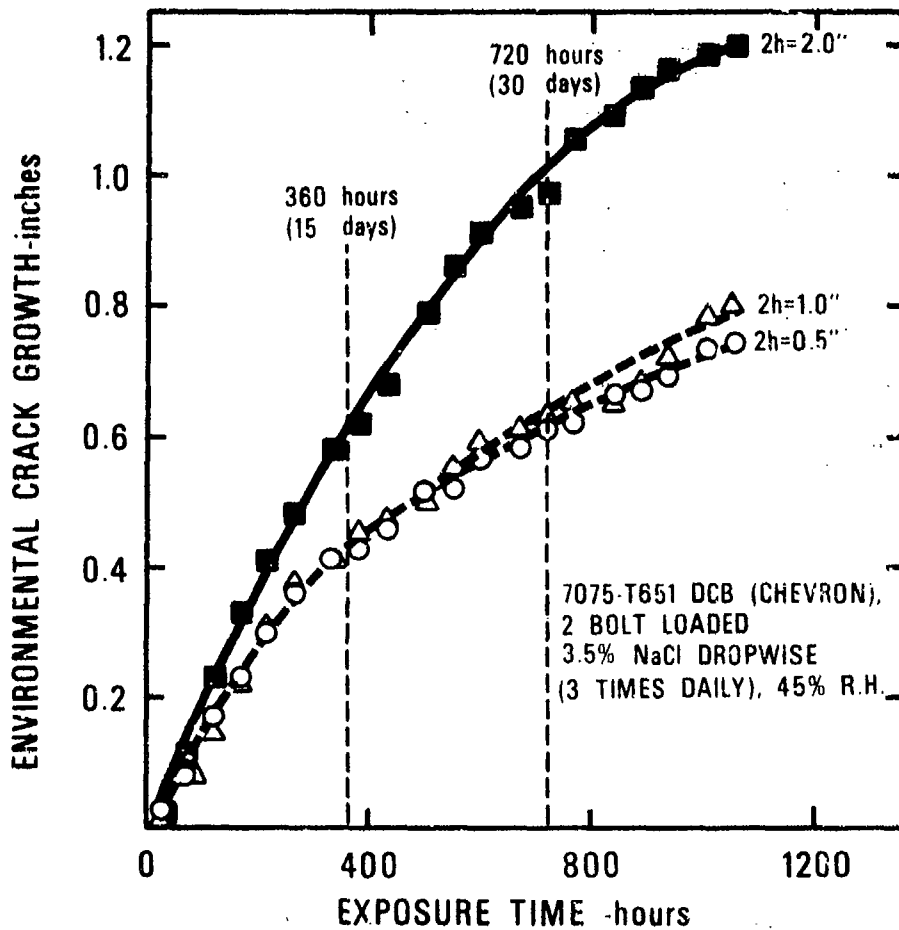
EFFECT OF BEAM HEIGHT (2h) ON ENVIRONMENTAL CRACK GROWTH IN S-L SPECIMENS FROM 7075-T651 ALLOY PLATE

Fig. 6

DCB (CHEVRON), 2 BOLT LOADED
O 2h=0.5"
△ 2h=1.0"
■ 2h=2.0"
3.5% NaCl DROPWISE
(3 TIMES DAILY), 45% R.H.
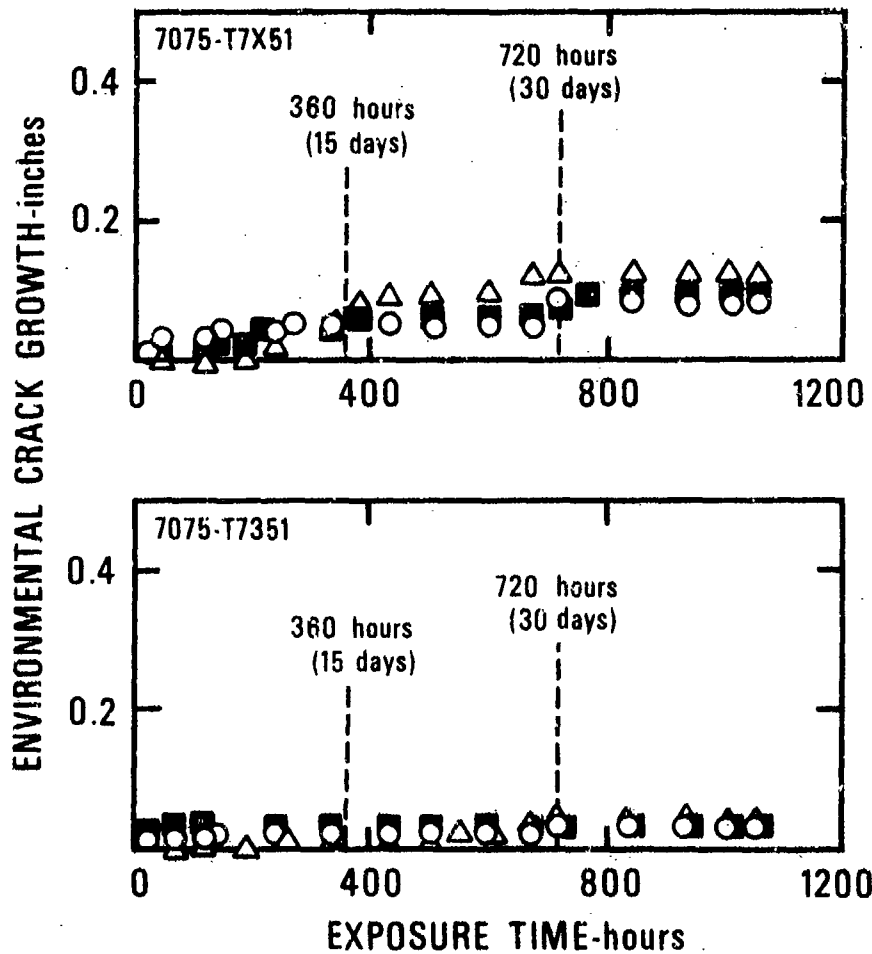
EFFECT OF BEAM HEIGHT (2h) ON ENVIRONMENTAL CRACK GROWTH IN S-L SPECIMENS FROM 7075-T7X5 1 AND 7075-T735 1 ALLOY PLATE

Fig. 7

DCB (CHEVRON), 2 BOLT LOADED
2h=1.0"
3.5% NaCl DROPWISE
45% R.H.

ENVIRONMENTAL CRACK GROWTH-inches

7075-T7X51

0.4

720 hours
(30 days)

360 hours
(15 days)

0.2

3 TIMES DAILY

1 TIME DAILY

7075-T7351

720 hours
(30 days)

0.4

360 hours
(15 days)

0.2

3 TIMES DAILY

1 TIME DAILY

0   400   800   1200

EXPOSURE TIME-hours
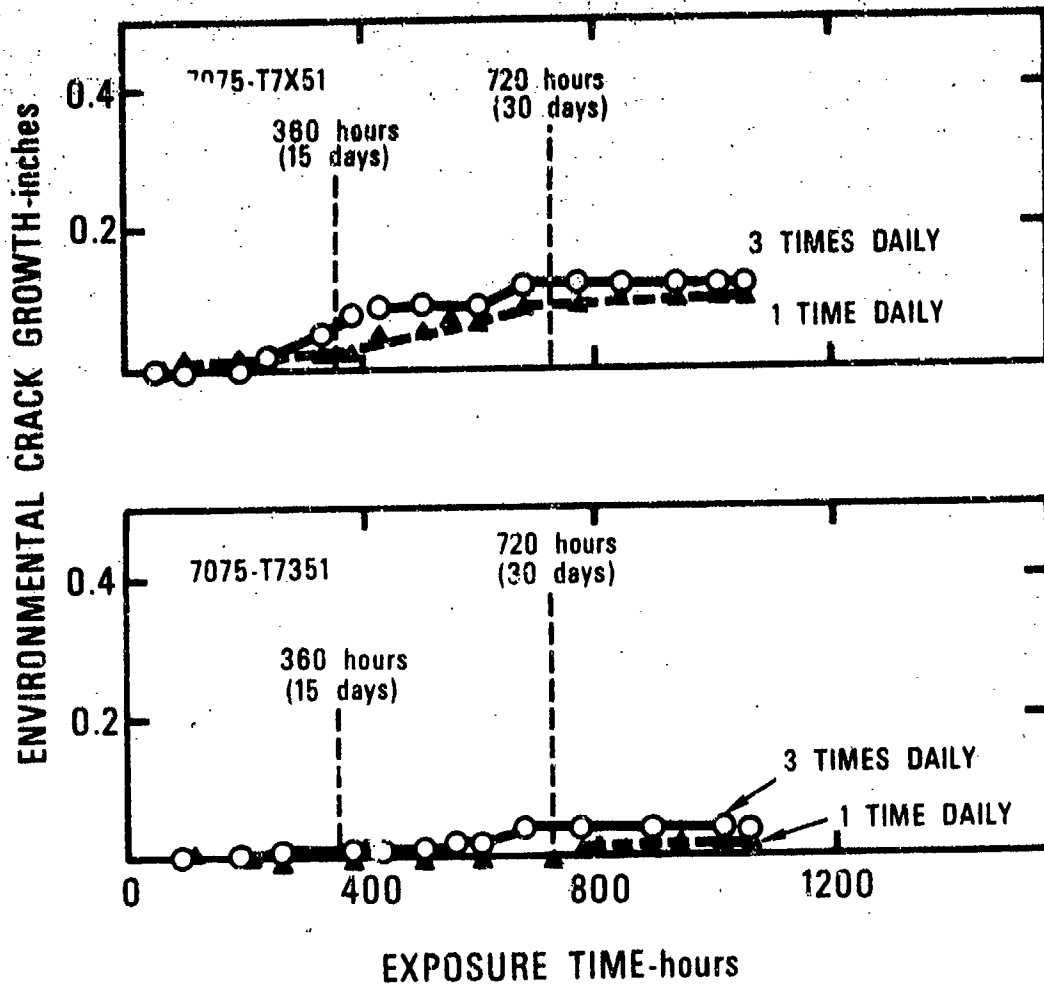
EFFECT OF DAILY WETTING FREQUENCY ON THE
ENVIRONMENTAL CRACK GROWTH IN S-L SPECIMENS
FROM 7075-T7X51 AND 7075-T7351 ALLOY PLATE

Fig. 8

21
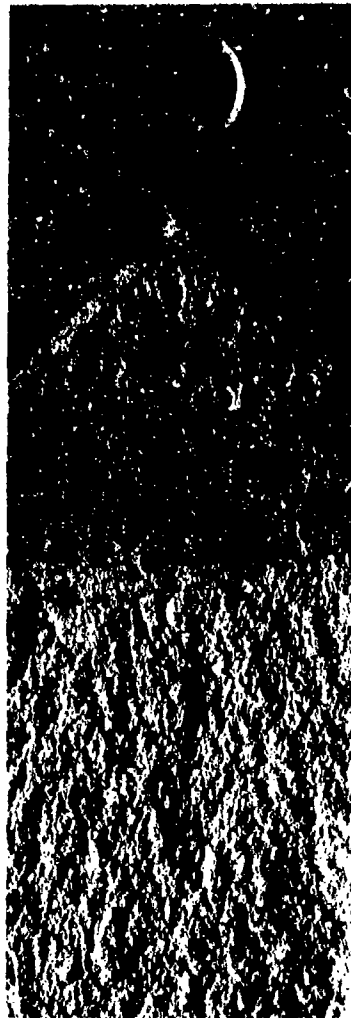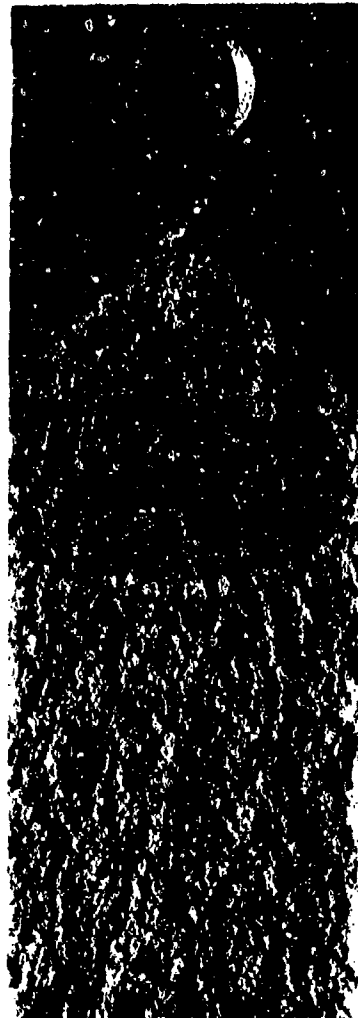
T651   T7X51   T7351

FRACTURE SURFACES OF DCB SPECIMENS SHOWING RELATIVE SCC
GROWTH FOR SEVERAL TEMPERS OF 7075 ALLOY PLATE

FIG. 9
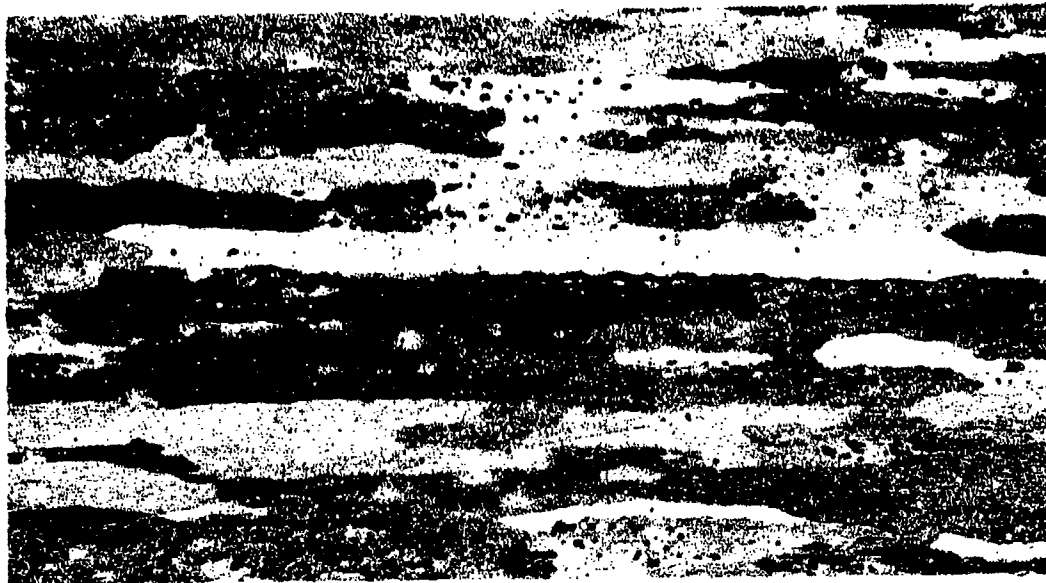
SCC

MECHANICAL

MICROGRAPHS (100X) OF TIP OF ENVIRONMENTAL CRACK

GROWTH IN DCB SPECIMENS OF 2124-T851 ALLOY PLATE

FIG. 10

HYDROGEN CONCENTRATIONS IN 7075 ALUMINUM ALLOY SURFACES
AFTER STRESS CORROSION EXPOSURE

P. N. Adler,[†] G. M. Padawer,[‡] and E. A. Kamykowski[‡]

Research Department
Grumman Aerospace Corporation
Bethpage, New York 11714

ABSTRACT

We have used a recently developed method of nuclear microanaly-
sis, the lithium nuclear microprobe (LNM), to measure hydrogen con-
centrations within the first few microns of the surfaces of selected
metals. The technique utilizes the resonant nuclear reaction
$^1H(^7Li,\gamma)^8Be$, which is initiated by fast ^7Li ions delivered to
the target sample by a Van de Graaff accelerator. The yield of
gamma rays is proportional to the hydrogen concentration at a depth
at which the bombarding ^7Li ions have been slowed to 3.075 MeV,
the resonance energy. By raising the bombarding energy above this
threshold level, deeper lying regions in the host material can be
successively assayed. The depth resolution of the LNM technique
for aluminum is typically 0.2 μm. The sensitivity, established on
the basis of interfering background levels and concentration cali-
bration standards, is better than 5 ppm (weight).

We will describe this technique and report on measurements ob-
tained in 7075 aluminum alloy. Both higher strength, T651, and
overaged, T7351, tempers of 7075 aluminum alloy were exposed to a
3.5 percent aqueous chloride solution at pH = 2 and at stress
levels of 0, 25, and 50 ksi. We find that very high hydrogen
concentrations are introduced as a result of environmental ex-
posure. In overaged material, which is not susceptible to stress
corrosion attack, the observed hydrogen concentrations are found
to depend on the applied stress levels during exposure; a lesser
dependence is observed for the higher strength temper. As demon-
strated by this work, the LNM offers a sensitive technique for in-
vestigating hydrogen-related corrosion phenomena. This work was
partially supported by Navy Contract N00019-72-C-0404.

[†] Materials and Structural Mechanics

[‡] Nuclear and Astrophysics

Introduction

The importance of hydrogen to stress corrosion attack in 7000 series high strength aluminum alloys has long been a point of controversy. A good deal of recent evidence suggests that stress corrosion of these alloys is a form of hydrogen embrittlement. Montgrain and Swann (Ref. 1) have reported evolution of molecular hydrogen during deformation and intergranular fracture of an Al - 7% Zn - 3% Mg alloy exposed to a saturated water vapor environment. In addition, they observed the embrittling effect of unstressed pre-exposure in this environment. Speidel (Ref. 2) has reviewed the possibility of hydrogen embrittlement of aluminum alloys and suggested that stress corrosion cracking of aluminum alloys in gases containing water vapor can be attributed to hydrogen embrittlement and that stress corrosion of these alloys in aqueous solutions could be due to hydrogen embrittlement.

Localized hydrogen measurements of the concentrations in the critical region preceding a stress corrosion crack or in the grain boundary region where attack takes place would be of great value in resolving the influence of hydrogen. An attempt to determine whether hydrogen concentrates at grain boundaries in a cathodically charged pure Al - 4% Zn - 3% Mg alloy was made using an autoradiographic technique with a tritium tracer (Ref. 3). Although some indication of tritium segregation at grain boundaries was observed in stressed as opposed to unstressed samples, the results were not conclusive.

The present work reports on an exploratory investigation that was conducted as part of a broader program concerning the development of the lithium nuclear microprobe (LNM) for localized, in situ, hydrogen measurements in surfaces (Ref. 4). The work represents the first stage of an effort to evaluate the role of hydrogen in the stress corrosion attack of high strength aluminum alloys. Specifically, the hydrogen concentration in surfaces of both susceptible and nonsusceptible tempers of 7075 aluminum alloy exposed to stress corrosion environments is evaluated.

Experimental

"Dog-bone" type flat specimens of both highly susceptible T651 and nonsusceptible overaged T7351 tempers of 7075 aluminum alloy were prepared from a commercial rolled bar, 3 in. x 6 in. x 12 ft.

26

Slices of 0.150 in. thickness were cut from the bar, and five tensile specimens were machined from each slice maintaining the short transverse direction of the bar in the eventual uniaxial loading direction. The specimens had a reduced center section of 1.500 in. length x 0.500 in. width x 0.050 in. thickness. The T7351 temper was obtained from the "as-received" T651 material by heat treatment at 175°C for 9 hours.

Samples of both tempers were exposed to a 3.5 percent aqueous chloride environment at pH 2.0 for approximately 2700 min at stresses of 0, 25, or 50 ksi. These stresses are approximately 0, 35, and 70 percent of the average yield strength of these tempers. For the stressed specimens, the exposure was sufficient to initiate and propagate stress corrosion cracking on specimens that were originally smooth surfaced. For all cases, only one of the two flat surfaces was exposed to the chloride solution; the other surface acted as a control for stress exposure. Details of surface preparation and stress corrosion testing have been reported (Ref. 5).

The basic features of the LNM for localized hydrogen analysis have been described previously (Refs. 4, 6, 7, and 8) and are illustrated in Fig. 1. Essentially, ^{7}Li ions at a kinetic energy of 3.075 MeV react with hydrogen nuclei in the surface to form the fifth excited state of ^{8}Be, which decays promptly by emitting either a 17.64 or 14.74 MeV gamma ray. The number of gamma rays emitted is directly proportional to the number of hydrogen nuclei at the particular depth probed. By control of the energy of the incident ^{7}Li beam, the probed depth can be varied. This depth can be determined accurately by knowing the incident beam energy and the stopping power property of the target material. Measurements can be made to several microns depth with an approximate 0.2 μm resolution. Since only a small percentage of the existing hydrogen nuclei react and the structure of the host is not significantly affected by the incident ^{7}Li ions, the technique can be considered nondestructive. Hydrogen concentration calibration was attained over a composition range from 32 ppm (0.0032 wt % H) to 2.64 wt % H with a ±8% estimated uncertainty. Three NBS hydrogen-in-titanium standards (NBS 352, 353, and 354) and Kapton, a polyimide film, were used for the calibration. Details of calibration have been fully described (Ref. 4).

Hydrogen concentrations were measured approximately six months after stress corrosion exposure. A ¼-in. diameter ^{7}Li beam impinged normal to the 0.420 in. x 0.560 in. surface area of dog-bone

specimens that were exposed to the aqueous chloride environment. Measurements at specific depths of 1.2 μm and 2.6 μm were made using beam energies of 3.7 and 4.4 MeV, respectively. For concentration-depth profile measurement, beam energies from 3.05 to 4.80 MeV were utilized. Beam currents were generally 1 μA for the measurements at constant depth and 0.050 μA for the depth profile; these currents resulted in power densities of approximately 0.8 and 0.04 watts/in.^{2}, respectively.

Results

The nature of surface attack for the two tempers examined in the 3.5 percent aqueous chloride environment is illustrated in Fig. 2. A localized type of grain boundary attack, characteristic of stress corrosion cracking, is evident for the highest strength stress corrosion susceptible T651 temper in Fig. 2a, whereas a general type of pitting erosion, characteristic of corrosion, is evident for the overaged, nonsusceptible T7351 temper in Fig. 2b. Within each temper, the mode of attack was found to be independent of the applied stress.

Hydrogen concentrations in the unexposed surfaces of T651 and T7351 that had been stressed at 25 and 0 ksi, respectively, were found to be less than 5 ppm. On the other hand, very high concentrations were found in exposed surfaces, as evidenced by the concentration-depth profile illustrated in Fig. 3 for the T651 temper after exposure at 50 ksi. Surface concentrations of 8000 ppm were observed, decreasing to 2000 ppm at a depth of 3 μm.

The effect of stress on hydrogen concentration in the exposed T651 at a specific depth of 1.2 μm is shown in Fig. 4. Hydrogen concentration at this depth as a function of deposited beam energy is illustrated. This representation shows the change in concentration that accompanies sample heating by the lithium beam. A time-dependent concentration decrease, related to hydrogen diffusion during sample heating, was generally observed at the 0.8 watt/in.^{2} power density used for the constant depth measurements. The concentrations after exposure of the T651 temper at 0 and 50 ksi are quite similar. In contrast, results for the T7351 temper, shown in Fig. 5, indicate that applied stress levels of 25 and 50 ksi lead to much higher hydrogen concentrations than that of 0 ksi loading. In fact, the intermediate stress exposure at 25 ksi led to the highest surface hydrogen concentration.

The effect of beam heating on subsequent probes is illustrated in Fig. 6 for T7351 samples exposed at 25 ksi. After an initial probe at 1.2 μm, a second probe was made at a 2.6 μm depth. Beam-induced heating did not affect the concentration during the 2.6 μm probe. However, the concentration of an initial probe at the 2.6 μm depth on a duplicate sample was affected by beam-induced heating. After beam heating effects were stabilized, both samples had identical concentrations at the 2.6 μm depth. Because higher concentrations were measured at the 1.2 μm depth, a concentration gradient, similar to that shown in Fig. 3, is indicated for this exposure.

Concentrations measured during probes at a 2.6 μm depth, subsequent to initial 1.2 μm probes, are shown in the table. These measurements were generally independent of beam-induced heating effects, as illustrated by the second probe shown in Fig. 6. For one case, T651 exposed at a 25 ksi stress, the 2.6 μm depth was probed initially, but no beam-induced heating effect was observed. The results shown in the table indicate that higher surface hydrogen concentrations exist in T7351 than in T651 after exposure, and that the concentration of hydrogen for both tempers does not increase monotonically with applied stress.

HYDROGEN CONCENTRATIONS[†] IN 7075 ALUMINUM ALLOY
AFTER STRESS CORROSION EXPOSURE

Condition	Applied Stress (ksi)		
	0	25	50
Maximum Strength T651	223 ± 18 ppm	1789 ± 135 ppm[‡]	611 ± 48 ppm
Overaged T7351	446 ± 37 ppm[‡]	2018 ± 153 ppm	1377 ± 105 ppm

[†] At 2.6 μm depth subsequent to measurements at 1.2 μm

[‡] Initial probe at 2.6 μm (independent of beam-induced heating)

[‡] Beam-induced heating effect

Discussion

The preceding LNM results indicate three significant factors:

1. Very high hydrogen concentrations are present to a depth of at least 3.5 μm in the surface of 7075 aluminum alloy exposed to an aqueous chloride solution environment.

2. Higher hydrogen concentrations are present in the stress corrosion exposed surfaces of the nonsusceptible T7351 temper than in the susceptible T651 temper.

3. The hydrogen concentration is at a maximum for samples exposed at the intermediate applied stress of 25 ksi.

The hydrogen concentrations measured are of the order of 4000 ppm by weight or approximately 10 atomic percent. Since the solid solubility of hydrogen in aluminum is approximately 3 ppb by weight at 400°C (Ref. 9), these exceedingly high values must be indicative of something other than hydrogen in solution. We suggest that these high hydrogen concentrations are related to the corrosion product on the exposed sample surface. A white residue was observed in the sample surface exposed to the solution. We attempted to identify this corrosion product using X-ray diffraction, but the results were not conclusive. This product could be a hydrated form of $AlCl_3$ or $Al(OH)_3$, but because of the acidic environment, the former is more likely (Ref. 10). The measured hydrogen concentration would then relate to the hydrogen constituency of the corrosion product and the amount of corrosion product present.

The amount and/or hydrogen constituency of this corrosion product appears to be enhanced by stress to a greater degree in the T7351 temper than in the T651 temper as shown in Figs. 4 and 5 and in the table. Considering the basic difference in attack mode between these tempers (see Fig. 2) it appears likely that the general erosion mode of attack in the T7351 temper results in a greater coverage of the surface by the corrosion product than in the more localized attack mode of the T651 temper. This, in turn, could lead to the greater sensitivity to stress exhibited by the corrosion product of the T7351 temper. Additional study would be required to clarify the significance of these measurements; nonetheless

the applicability of the LNM technique to evaluating corrosion characteristics is evident.

Finally, the maximum in hydrogen concentration observed for the intermediate 25 ksi exposure, as shown in Fig. 4 for the T7351 temper and in the table for both tempers, suggests an interesting stress dependent corrosion phenomenon. Stress appears to enhance corrosion product formation if loading on the specimen is essentially elastic. Whereas 50 ksi is below the 0.2 percent offset yield strength of both tempers, a good deal of microstrain would be anticipated. Plastic deformation may be acting as a deterrent to corrosion product formation. Additional studies should be performed to evaluate this speculation since it relates directly to the stress assisted corrosion of high strength aluminum alloys.

Conclusions

1. Very high hydrogen concentrations are introduced into the surface of 7075 aluminum alloy as a result of exposure to an acidic aqueous chloride environment; these high concentrations appear to be related to formation of a corrosion product.

2. Application of stress during exposure increases the hydrogen concentration in the corrosion product of the T7351 temper to a greater extent than in the corrosion product of the T651 temper.

3. A hydrogen concentration maximum is observed in both tempers for samples exposed at an intermediate stress level.

4. Direct measurement of hydrogen in exposed surfaces may be of significance in understanding corrosion product formation as well as in evaluating relative corrosion susceptibility.

Acknowledgments

at Oak Ridge National Laboratory. We are grateful to the staff of this facility, and in particular, we cite the help of Dr. J. A. Biggerstaff and Dr. C. D. Moak. We are also pleased to acknowledge the assistance of our colleagues Dr. E. J. Schneid and F. J. Kuehne in performing this study and constructive discussions with Dr. G. I. Geschwind, Dr. M. C. Stauber, and M. D. D'Agostino.

References

1. Montgrain, L. and Swann, P. R., in Hydrogen in Metals, ed. by I. M. Bernstein and A. W. Thompson, ASM, p. 575, Metals Park, Ohio, 1974.

2. Speidel, M. A., in Hydrogen in Metals, ed. by I. M. Bernstein and A. W. Thompson, ASM, p. 249, Metals Park, Ohio, 1974.

3. Haynie, F. H. and Boyd, W. K., Proc. of Conference of Fundamental Aspects of Stress Corrosion Cracking, ed. by R. W. Staehle, A. J. Forty, and D. van Rooyen, NACE, p. 580, Houston, Texas, 1969.

4. Padawer, G. M., Adler, P. N., Kamykowski, E. A., Schneid, E. J., Kuehne, F. J. Jr., Stauber, M. C., and D'Agostino, M. D., Final Report for Contract N00019-72-C-0404, October 1973.

5. Geschwind, G., Soltz, G. C., and Adler, P. N., Corrosion, Vol. 26, p. 165, 1970.

6. Padawer, G. M. and Schneid, E. J., Trans. ANS, Vol. 12, p. 493, 1969.

7. Padawer, G. M., Larson, D. J. Jr., and Adler, P. N., Met. Trans., Vol. 2, p. 2287, 1971.

8. Adler, P. N., Kamykowski, E. A., and Padawer, G. M., Hydrogen in Metals, ed. by I. M. Bernstein and A. W. Thompson, ASM, p. 623, Metals Park, Ohio, 1974.

9. Brandt, J. L., Aluminum, Vol. 1 - Properties, Physical Metallurgy and Phase Diagrams, ed. by K. R. Van Horn, ASM, p. 26, Metals Park, Ohio, 1967.

10. Ibid, p. 24.
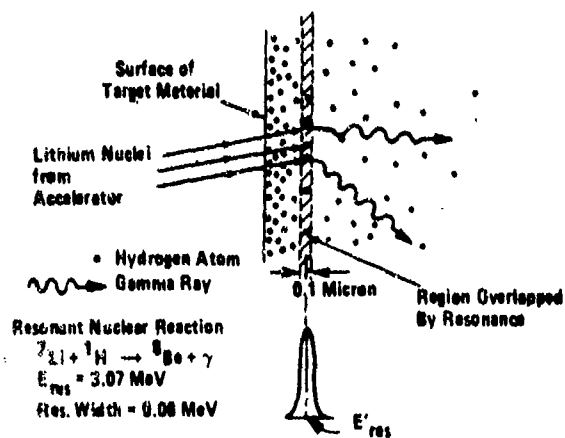
Fig. 1   Lithium Nuclear Microprobe (LNM) Fundamentals
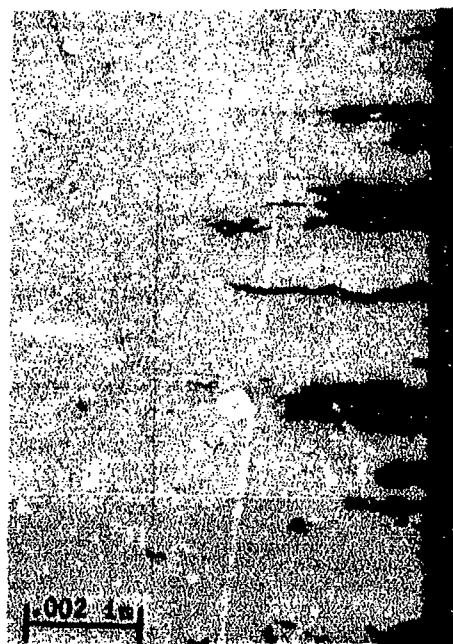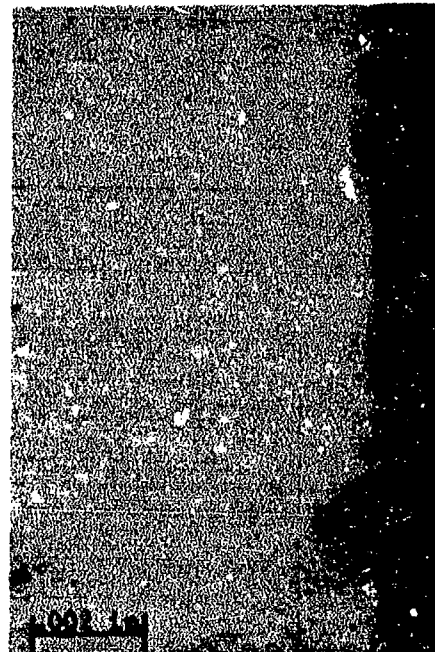
a) T651   b) T7351

Fig. 2   Surface Attack in 7075 Aluminum Alloy Exposed
         in a 3½% Aqueous Chloride Solution at
         pH = 2.0 for 2700 min at 25 ksi
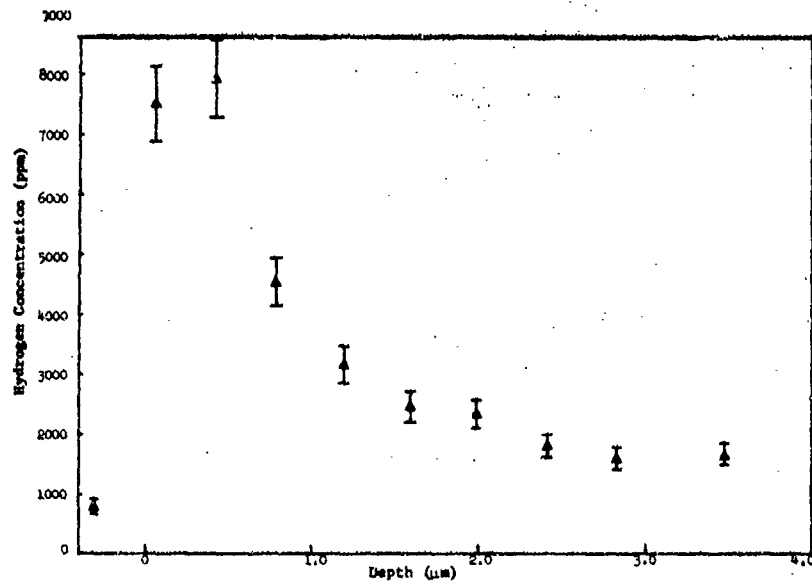
Fig. 3   Hydrogen Concentration-Depth Profile in
         7075-T651 Aluminum Alloy After
         Environmental Exposure at 50 ksi
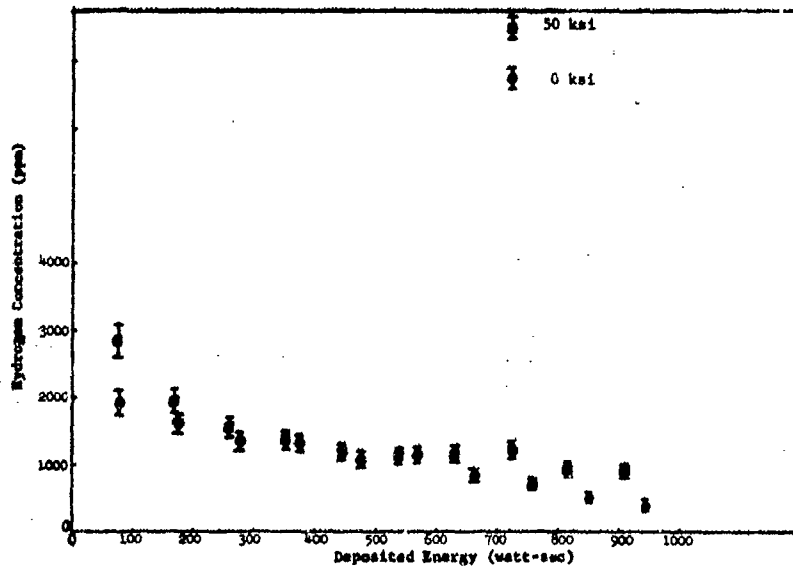
Fig. 4   Hydrogen Concentration in 7075-T651
         Aluminum Alloy at 1.2 μm Depth
         After Environmental Exposure
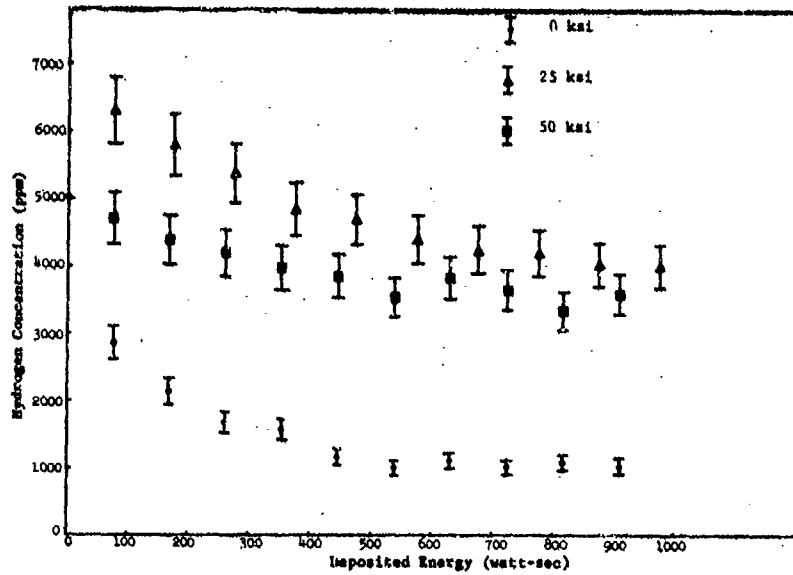
Fig. 5 Hydrogen Concentration in 7075-T7351
        Aluminum Alloy at 1.2 μm Depth
        After Environmental Exposure
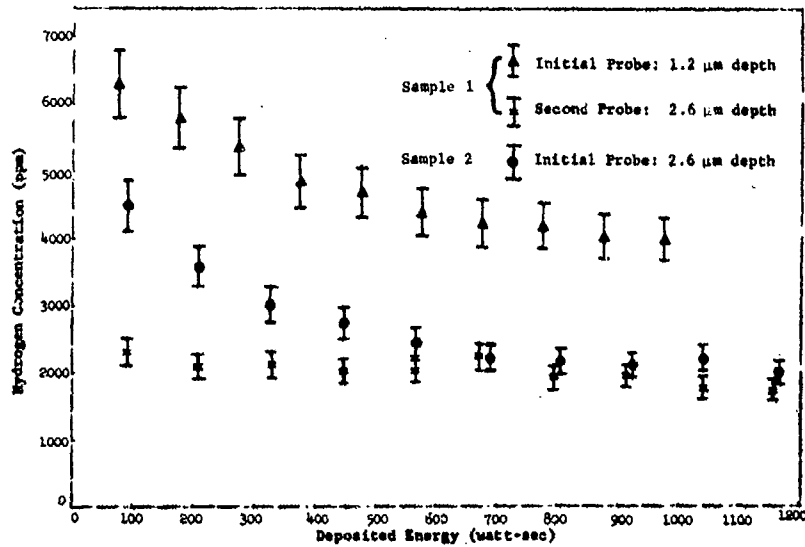
Fig. 6 Hydrogen Concentration in 7075-T7351
        Aluminum Alloy After Environmental
        Exposure at 25 ksi

SESSION V

CORROSION OF HYDROSPACE EQUIPMENT

PROTECTIVE SYSTEM FOR FASTENER AREAS
OF CARRIER-BASED NAVAL AIRCRAFT

by

Robert N. Miller
Gwen G. Seeliger
Wilbum A. Boggs

Lockheed-Georgia Company
Marietta, Georgia

Abstract

Results are presented for a three-year program to develop a full temperature range (-65 to 325°F) protective system for the fastener areas of carrier-based Navy aircraft. In the laboratory phase of the program a selected group of primers and topcoats were subjected to screening tests which included thermal stability at 350°F, scribe tests, moisture permeability, tensile and elongation properties at -65°F, and bend and impact tests of coated panels at -65°F. Aluminum panels, coated with the candidate systems, were exposed to sun and salt spray for six months at a Florida sea coast site.

The primers and topcoats which passed the screening tests were applied to aluminum and titanium fatigue specimens which had a typical aircraft joint with eight fasteners. After five cycles of a simulated flight spectrum, the specimens were checked for coating defects, corrosion, gloss retention, and coating adhesion. Representative specimens were stripped, disassembled and examined for evidence of exfoliation and general corrosion.

The results of the laboratory evaluation indicate the best coating combinations to be three-layer systems. These were composed of an inhibited polysulfide or MIL-P-23377 epoxy-polyamide primer, an aliphatic linear polyurethane topcoat, and intermediate coats of elastomeric polyurethane, inhibited polysulfide, or fluoroelastomer. These were applied in August 1973 to test areas on the upper center wing Navy C-130 Aircraft No. 149787 stationed at Barber's Point, Oahu. They were also applied to five A-5 carrier-based Navy aircraft in the fall of 1974.

Introduction

Carrier-based Naval aircraft, because they must withstand ocean spray, stack gases from the aircraft carrier, and temperatures ranging from -65 to 325°F, pose an unusually severe maintenance problem. When the wings are flexed at the subzero temperatures of high altitude flight, the coating systems in current use crack in the fastener areas. Upon its return to the flight deck, the aircraft is exposed to sea water mist which penetrates the cracks adjacent to the fasteners and initiates corrosion reactions.

For the past two years the Lockheed-Georgia Company, under a Naval Air Systems Command contract, has been developing a protective system for the fastener areas of carrier-based Naval aircraft. Mr. T. A. Johnston of NASC is the Project Monitor. It is the objective of this program to develop and test a protective system for aircraft fastener areas which will:

(a) prevent the entry of corrosive media associated with a marine environment,

(b) not degrade significantly around stressed fasteners under cyclic flight loads anticipated during three years of aircraft operation with repeated exposures to the extremes of the temperature range -65 to 325°F,

(c) be compatible with a chemical pretreatment (over aluminum and titanium) and a subsequently applied white aliphatic polyurethane topcoat, MIL-C-81773A,

(d) not be readily damaged in service but, if damaged, will be readily repairable at the organizational maintenance level, and

(e) be 5 mils or less in thickness with minimum weight consistent with desired performance.

Selection of Materials

Some of the coatings which were used in this program were selected on the basis of their performance in previous laboratory tests. Others were modified by the manufacturer to obtain balance of flexibility and toughness in the primers, and flexibility and gloss retention in the topcoats.

The primers and intermediate coats included epoxy-polyamides, modified epoxy-polyurethanes, elastomeric polyurethanes, polysulfides, and a fluoroelastomer. Tedlar and aluminum foil tapes were also evaluated as potential intermediate coats for fastener patterns. The topcoats were aliphatic linear polyurethanes produced by a variety of manufacturers. The metal substrates used in this study were 7075-T6 aluminum, 2024-0 aluminum, and 6Al-4V titanium.

Screening Tests

The candidate coatings were first subjected to a battery of screening tests which included thermal stability at 350°F, and -65°F tensile elongation, bend, and impact tests.

Thermal Stability Test

The thermal stability tests were conducted on a Mettler Thermogravimetric Analyzer shown in Figure 1. A sample of each material was heated to 350°F and held there for two hours. During the test, simultaneous plots were made of temperature and sample weight. Table I lists the percent weight losses of some of the candidate coatings at the conclusion of the 4-hour test period.

TABLE I

SUMMARY OF THERMAL STABILITY

Material	% Weight Loss	Observations
Tedlar Film *	2.7	Shrank in size
Aliphatic PU, Bostik-Finch	5.7	Some loss of flexibility, discolored
Elastomeric PU, 3M	1.9	Soft and tacky
Elastomeric PU, Hughson	13.3	Soft and pliable
Elastomeric PU, LTV	35.2	Soft and pliable
Elastomeric PU, PRC	1.9	Darker on one side
Aliphatic PU, Andrew Brown	29.7	Loss of flexibility, discolored

*Polyurethane

All coatings which embrittled during the heating cycle or which sustained weight losses of more than 15%, were considered unacceptable.

Tensile and Elongation Tests

Free films for the tensile and elongation tests were made by applying the coatings to a non-adhering surface to give a 20 mil thickness. The coatings were fully cured and dumbbell-shaped tensile specimens were stamped from the film. The specimens were 1/4" wide in the test section. Three specimens of each coating were tested at -65°F. Table II summarizes the average tensile and elongation data.

The Hughson elastomeric polyurethane and the PRC polysulfide have the best low temperature elasticity of the primers and intermediate coats. The DeSoto topcoat, which is a MIL-C-83286 aliphatic linear polyurethane, had an elongation of 18.9% at -65°F. This is more than double the elongation of any of the other topcoats which were evaluated. All the polyurethanes have high tensile strengths - 5,450 to 14,000 psi.
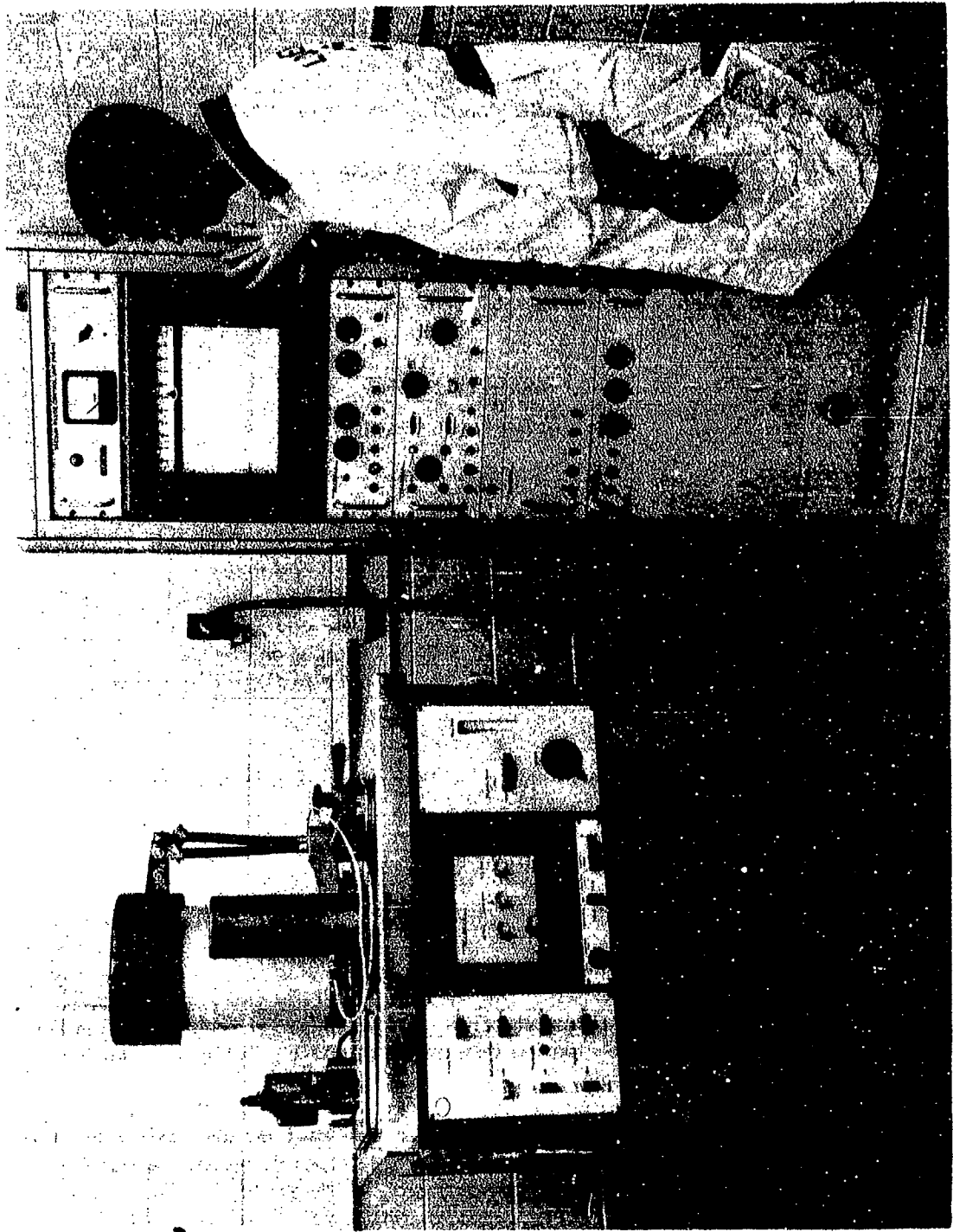
FIGURE 1

METTLER THERMOGRAVIMETRIC UNIT WHICH WAS USED TO DETERMINE THERMAL STABILITY

TABLE II

TENSILE STRENGTH AND ELONGATION RESULTS AT -65°F

Coating	Tensile Strength (Lbs/In^2)	Percent (%) Elongation
Aliphatic PU*, Bostik-Finch	9,470	10.7
Elastomeric PU, 3M	5,450	62.8
Polysulfide, PRC	296	100.0
Elastomeric PU, Hughson	5,433	100.0
Elastomeric PU, LTV	5,630	75.1
Elastomeric PU, PRC	6,180	36.7
Aliphatic PU Topcoat, DeSoto	14,100	18.9
Aliphatic PU Topcoat, Andrew Brown	9,866	9.9

*Polyurethane

Impact Flexibility

The impact flexibility test specimens, 3" wide by 6" long by .030" thick, were made of 2024-0 aluminum with a chromate conversion coating. Each panel was coated with a combination of primer, intermediate, and topcoat to give a total coating thickness of 4 + 1 mils. Specimens were cooled to -65°F. Individual specimens were removed from the low temperature environment and the impact flexibility was determined by allowing a 2 pound weight, 1 inch in diameter, to fall upon the panel from a height of 20 inches. The test was conducted in accordance with the procedure outlined in Federal Test Method 141, Method 6226.

Figure 2a is an example of a coating system which had enough flexibility to withstand the -65°F impact test without cracking. Figure 2b illustrates a brittle coating system.

Bend Tests

The specimens used for the impact flexibility test were again cooled to -65°F. Individual specimens were removed from the low temperature environment and within 3 seconds the specimens were bent 180° over a mandrel 1/4" in diameter. The test was conducted by the procedure outlined in Federal Test Method 141, Method 6221. In general, the coatings which performed best on the impact flexibility test also performed well on the bend test. Examples of the better systems are:

(1) DeSoto polyurethane topcoat over PRC polysulfide intermediate coat and Andrew Brown epoxy-polyamide primer (Figure 3a).

(2) DeSoto topcoat over Hughson elastomeric polyurethane intermediate coat and Andrew Brown epoxy-polyamide primer.

Figure 3B is an example of a brittle system.
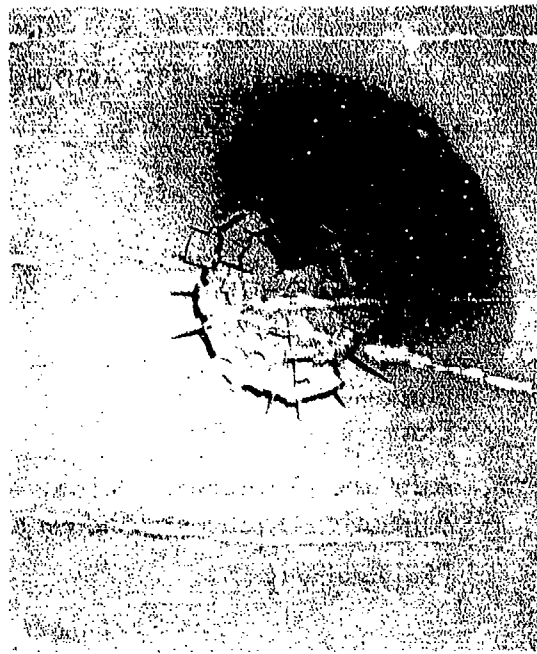
FIGURE 2. -65°F IMPACT SPECIMENS FOR (a) FLEXIBLE AND (b) BRITTLE COATINGS
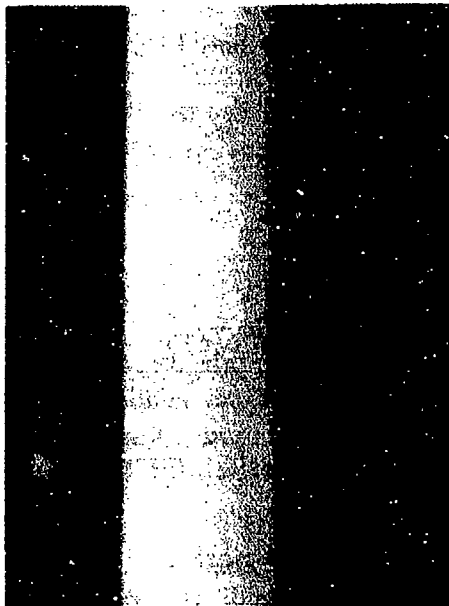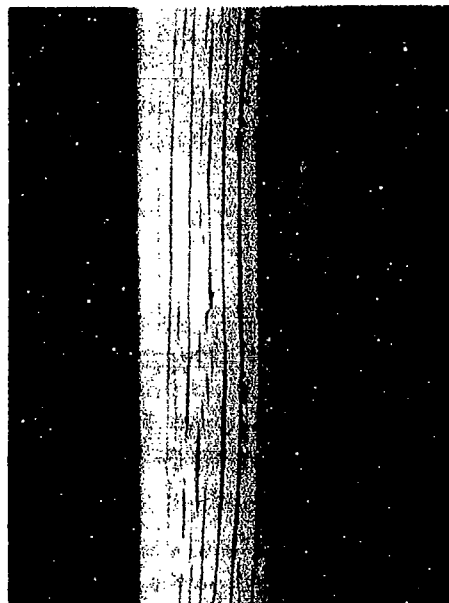
FIGURE 3. -65°F BEND TEST SPECIMENS WITH (a) FLEXIBLE AND (b) BRITTLE
COATING SYSTEMS

Florida Exposure Specimens

Seacoast exposure tests were conducted on three sets of 2024-0 aluminum panels, 6" x 12" x .032" which were anodized, dichromate sealed, and coated with the candidate protective system. The back of each panel was coated with a clear polyurethane to assure that corrosion would not initiate on the back side. Gloss measurements were made for each specimen. They were then sent to Miami Marine Research Laboratories at Miami Beach, Florida for marine atmospheric exposure tests and mounted on a raft in Biscayne Bay facing the south for maximum exposure to sunlight. This exposure to intense ultraviolet radiation and salt spray serves as a test of gloss retention. One set of specimens was returned after 6 months and checked for gloss retention. All specimens were in excellent condition and the gloss readings were only a few points below the original readings.

Coated Fatigue Specimens for Simulated Flight Spectrum

Specimen Preparation

Fatigue specimens made of aluminum and titanium, illustrated in Figure 4, were prepared for the environmental cycling tests. Half of the specimens were made from 7075-T6 aluminum and the other half made from 6Al-4V titanium. Each specimen had a pattern of eight fasteners. Prior to assembly a MIL-C-5541 conversion coating was applied to the aluminum specimens and a phosphate conversion coating was applied to the titanium specimens.

During the first year of the program the fasteners were not wet installed in the fastener holes and a large number of exfoliation defects were noted when the specimens were stripped after the environmental cycling tests. All fasteners were wet installed with inhibitive sealant in specimens prepared during the remainder of the program. The specimens were coated to a thickness of 4-5 mils with combinations of the primers, intermediate coatings and topcoats which performed best in the screening tests.

Environmental Cycling

The specimens were subjected to the simulated flight spectrum diagrammed in Figure 5. At the conclusion of the environmental cycling the specimens were carefully examined for cracks, blisters, and evidence of substrate corrosion. Intercoat adhesion and adhesion of primer to substrate were checked by the wet tape test. The fasteners were removed from representative specimens and the fastener holes were checked for corrosion.

Results of Environmental Cycling Tests - During the first heating cycle, most of the specimens with the aluminum and Tedlar tapes blistered in the taped areas due to the vaporization of residual solvents in the polysulfide bonding layer (Figure 6). In addition, one of the elastomeric polyurethane coating systems wrinkled severely. Both groups of specimens were removed from the test program. At the conclusion of the five environmental cycles, the most prevalent defects were fine cracks in the coating around fasteners on some of the titanium specimens, as illustrated in Figure 7. In comparison with the results of tests

43
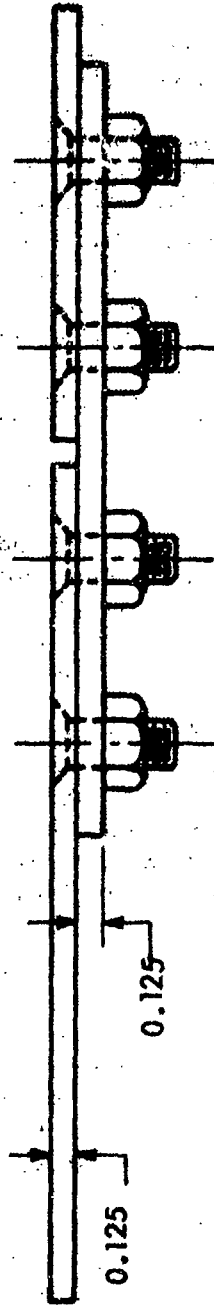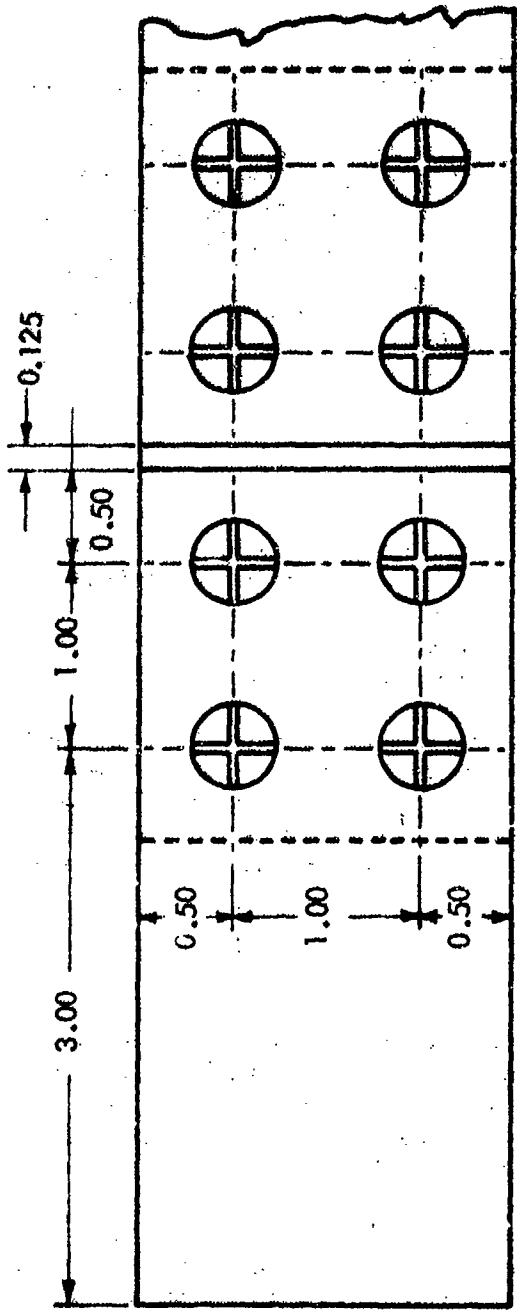
SPECIMEN MATERIAL

7075-T6 Al Non-clad
6Al-4V Titanium

FASTENER MATERIAL

Cd Plated Steel
Titanium

FIGURE 4.

FATIGUE SPECIMEN CONFIGURATION FOR -65°F CYCLIC LOADING AND EXPOSURE
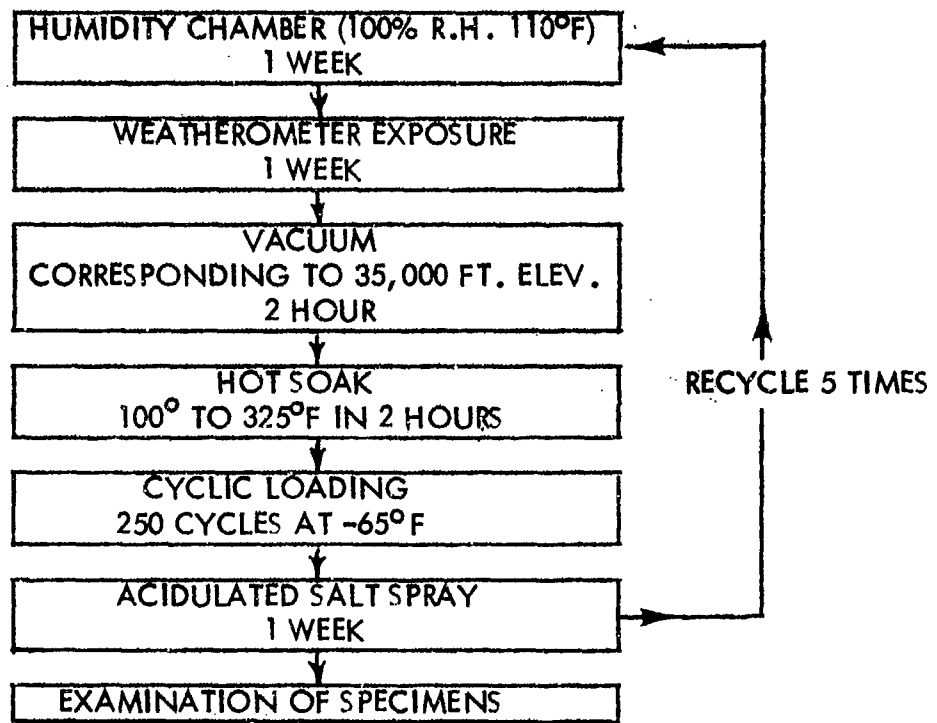
FIGURE 5. SIMULATED FLIGHT SPECTRUM DIAGRAM

FIGURE 7. FINE CRACKS AROUND FASTENERS

FIGURE 6. BLISTERS UNDER TEDLAR (LEFT)
AND ALUMINUM TAPE (RIGHT)

conducted in 1972, there was a very low incidence of exfoliation corrosion around fasteners. This is attributed to the fact that the fasteners were wet installed with inhibited polysulfide sealant.

None of the two-component systems, composed of a primer and topcoat, met all the target requirements. Except as noted, almost all of the fatigue specimens with the three-component coating systems were in excellent condition at the end of the five environmental cycles. Figure 8 shows two of the specimens after the environmental exposure tests.

The concept of a three-component coating system for fastener areas is quite compatible with the current procedures for painting carrier-based Naval aircraft. The entire aircraft is given a MIL-P-23377 primer coat, a flexible coating is applied over the fastener patterns only, and a topcoat is applied over the total surface.

The wet tape tests which were made at the conclusion of the environmental cycling revealed that the elastomeric polyurethanes had poor adhesion when they were applied directly to aluminum or titanium substrates but had good adhesion over a MIL-P-23377 primer. Therefore, the presence of a primer base coat is essential.

Application of Test Coatings to C-130 Aircraft

The coating systems which gave the best performance in all the laboratory tests conducted on this program during 1972 and 1973 were applied to test areas on the upper center wing of Navy C-130, No. 149787, on 24 August 1973. The center wing is one of the more highly stressed structural components of the aircraft and is made of anodized 7075-T73 aluminum extrusions. Figure 9 is a photograph of the aircraft in the paint hanger.

The MIL-P-23377, epoxy-polyamide primer performed well in most of the laboratory tests and is also already in use as a primer on military aircraft. For these reasons, it was selected as the primer for use on the C-130 field service test. The MIL-P-23377C epoxy-polyamide primer and the MIL-C-83286 aliphatic linear polyurethane topcoat were used on all test areas, with intermediate coats of elastomeric polyurethane, inhibited polysulfide, and fluoroelastomer. On two additional test areas, 5% strontium chromate inhibitor was blended with the elastomeric polyurethane intermediate coats.

Figures 10 and 11 are views of one of the test areas before and after painting. The test C-130 was flown back to Barber's Point on the island of Oahu in September 1973. There it is being exposed to solar radiation, rain, and salt spray in a semi-tropical environment.

The aircraft is being inspected at intervals of approximately six months for evidence of coating deterioration on the test areas. The test aircraft was inspected in February and September of 1974. All test areas were in excellent condition. At the conclusion of the three-year test period, the test areas will be stripped, inspected, and recoated with the standard coating system.
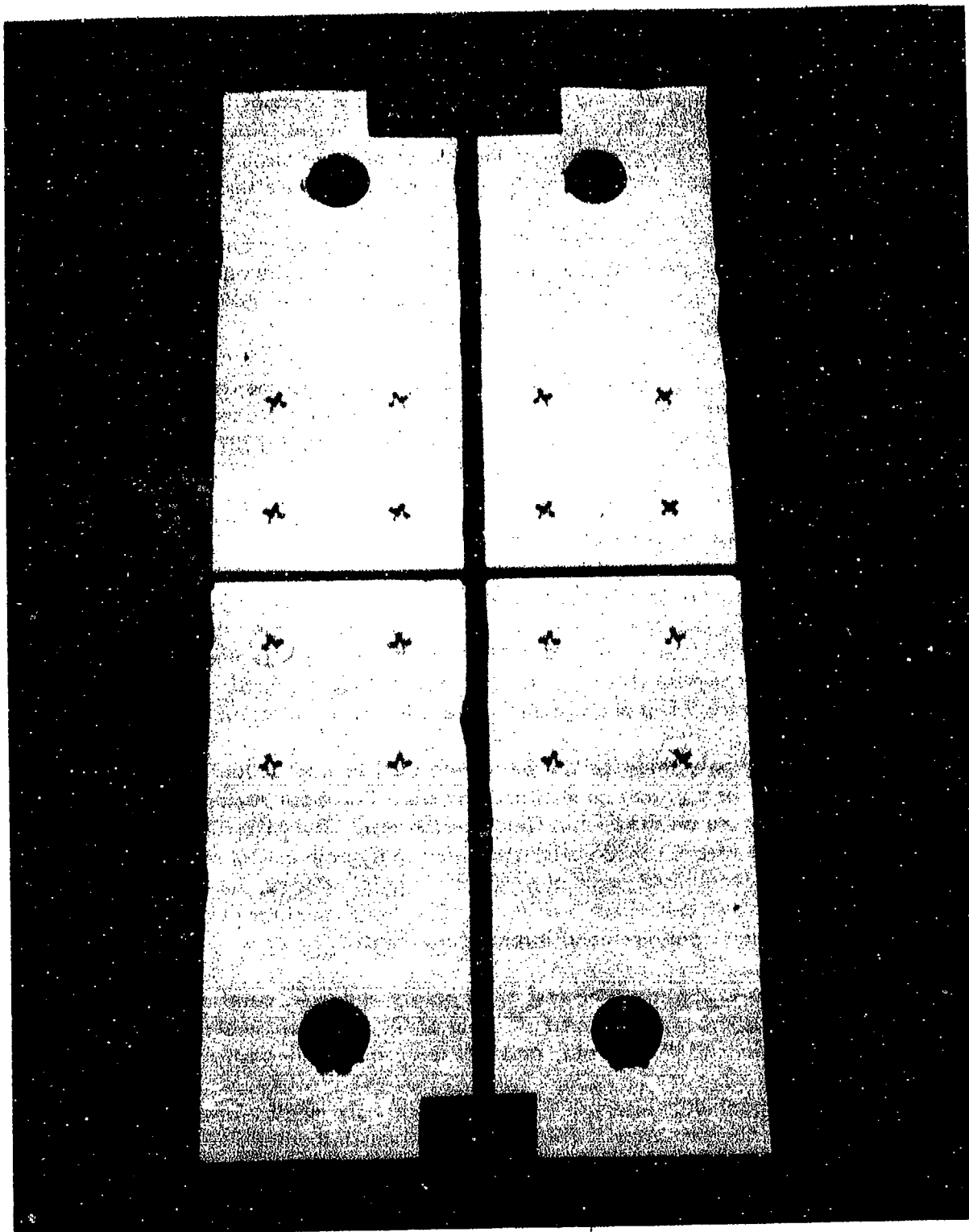
FIGURE 8. FATIGUE SPECIMENS WITH THREE-COMPONENT COATINGS AFTER
ENVIRONMENTAL EXPOSURE TESTS
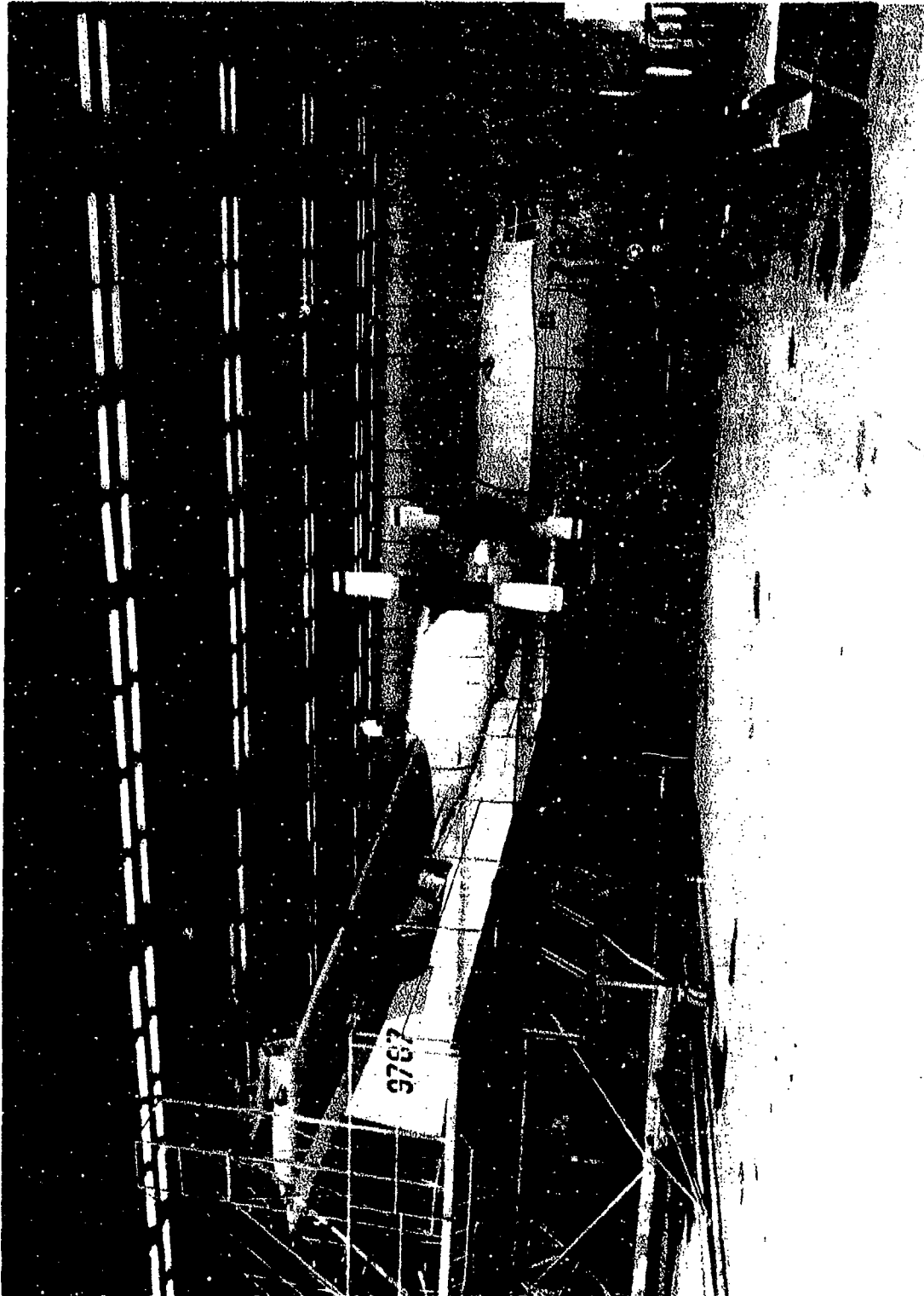
FIGURE 9. NAVY C-130F AIRCRAFT NO. 149787.

FIGURE 11. TEST AREAS AFTER PAINTING

TEST AREA NO. 2
TEST AREA NO. 4
TEST AREA NO. 5
ST AREA NO. 6
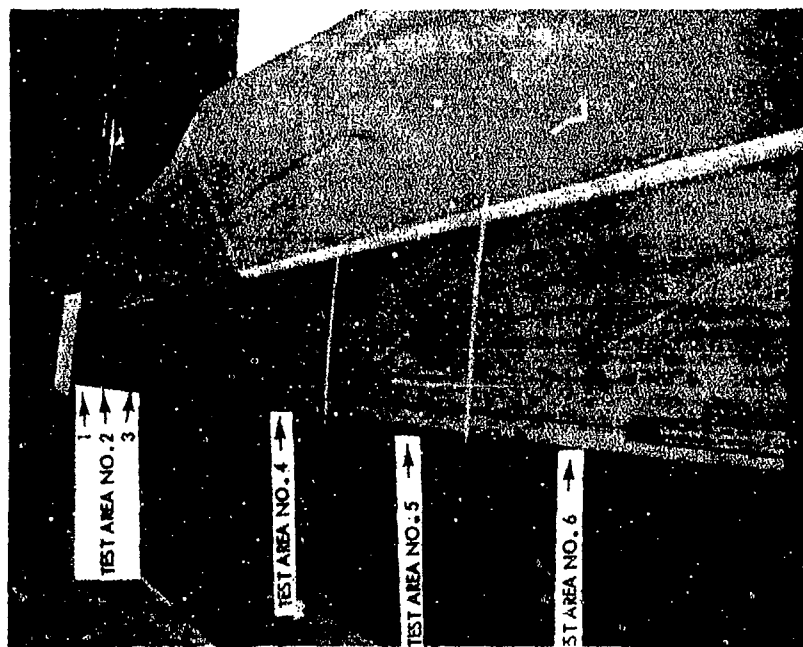
FIGURE 12. TEST AREAS BEFORE PAINTING

Application of Test Coatings to A-5 Aircraft

For a final long-term field service evaluation, the most promising coating systems, plus two additional systems, were applied to five carrier-based A-5 supersonic aircraft in the fall of 1974. Factors which were considered in a final selection were: performance in laboratory tests, application properties cost, and availability. One of the additional systems utilizes an epoxy-polyurethane primer and intermediate coating material developed by the Naval Air Development Center at Warminster, Pennsylvania. In another system, a corrosion-inhibitive polysulfide material is used as the primer and intermediate coating. This system was developed by Lockheed-Georgia and has been applied to several Air Force C-130's, C-141's, F-104's, and B-52's. Table III describes the five coating systems used in the field service evaluation. The starboard and port side of five aircraft will be painted with a different system. Each system will be applied to the port side of one aircraft and the starboard side of another.

All five of the A-5 aircraft will utilize the Lockheed-Georgia walkway coating system on the upper fuselage. This system is composed of 3 mils of inhibitive polysulfide primer, 3 mils of aluminized inhibitive polysulfide, and a polysulfide topcoat which contains asbestos fibers. This coating system protects the upper wing of Air Force C-130's.

After their return to the aircraft carriers, the A-5's will be inspected at six-month intervals for a three-year period. The results of the rigorous laboratory evaluations, plus the perfect condition of the C-130 test coatings at the end of six months, indicate that most of the coating systems will meet the target requirements.

Conclusions

1. The only topcoat which meets the low temperature flexibility requirements of this program is DeSoto MIL-C-83286, aliphatic linear polyurethane.

2. Wet sealing of fasteners during installation is essential to the prevention of countersink corrosion and reduction of cracking or blistering of the coatings in the fastener areas.

3. Protective coating systems composed of a linear polyurethane topcoat, an elastomeric polyurethane or inhibited polysulfide intermediate coat, and an epoxy-polyamide or inhibited polysulfide primer, provided excellent protection for both the aluminum and titanium specimens during the environmental cycling tests.

4. Tedlar or aluminum foil tapes are unsuitable for use as an intermediate coating on fastener patterns because, due to solvents or air pockets beneath the tape, they would tend to blister at elevated temperatures.

5. Three-layer coating systems which were applied to Navy C-130 aircraft No. 149787, composed of a MIL-C-83286 polyurethane topcoat, an elastomeric intermediate coat, and a MIL-P-23377C epoxy-polyamide primer, are in excellent condition after one year of service and should provide good protection for the fastener areas of carrier-based aircraft for three years.

TABLE III

COATING SYSTEMS APPLIED TO FIVE AIRCRAFT

AIRCRAFT NO.	PORT SIDE		STARBOARD SIDE	
1	Primer:	(Andrew Brown) MIL-P-23377, Epoxy-Polyamide	Primer:	(NADC) 90-50M, Epoxy-Polyurethane
	Sealant:	(PRC) PR-1436G, Polysulfide	Sealant:	(NADC) 90-50M, Epoxy-Polyurethane
2	Primer:	(NADC) 90-50M, Epoxy-Polyurethane	Primer:	(Andrew Brown) MIL-P-23377, Epoxy-Polyamide
	Sealant:	(NADC) 90-50M, Epoxy-Polyurethane	Sealant:	(Hughson) M413/M200, Elastomeric Poly-urethane
3	Primer:	(Andrew Brown) MIL-P-23377, Epoxy-Polyamide	Primer:	(Andrew Brown) MIL-P-23377, Epoxy-Polyamide
	Sealant:	(PRC) RW-1025-83, Elastomeric Polyurethane	Sealant:	(PRC) PR-1436G, Polysulfide
4	Primer:	(Andrew Brown) MIL-P-23377, Epoxy-Polyamide	*Primer:	(PRC) PR-1432GP, Polysulfide
	Sealant:	(Hughson) M413/M200, Elastomeric Polyurethane	Sealant:	(PRC) PR-1432GP, Polysulfide
5	*Primer:	(PRC) PR-1432GP, Polysulfide	Primer:	(Andrew Brown) MIL-P-23377, Epoxy-Polyamide
	Sealant:	(PRC) PR-1432GP, Polysulfide	Sealant:	(PRC) RW-1025-83, Elastomeric Poly-urethane

NOTE: TOPCOAT: All aircraft shall be topcoated with the DeSoto MIL-C-83286 (grey) and the Andrew Brown MIL-C-81773 (Insignia white)

* The (PRC) polysulfide, PR-1436G, shall be used in high temperature areas as primer and sealant.

CORROSION AND CATHODIC PROTECTION OF WIRE ROPES IN SEAWATER

T. J. Lennox, Jr., M. H. Peterson
and R. E. Groover (Retired)
Naval Research Laboratory, Washington, D.C.

ABSTRACT

Eleven different alloys were exposed as unstressed wire ropes in seawater. Ropes were exposed totally immersed with and without cathodic protection and partially immersed with the ropes extending through the tidal zone. Rope construction was of three types; independent wire rope core (IWRC), wire strand core (WSC), and fiber strand core (FSC).

The corrosion characteristics and response to cathodic protection are reported. Recommendations are made for selection of wire rope for up to 2 years service in seawater with or without cathodic protection.

INTRODUCTION

There are many Naval applications which require the use of wire rope or armored electrical cable in a submerged or partially submerged condition. Wire ropes are an essential component of most deep ocean mooring systems. Deep ocean moors range from large complex systems to relatively simple single point moors used for oceanographic instrument packages, meterological data buoys, or underwater weapons.

There has been a definite need for engineering data on the corrosion characteristics of wire ropes and on the response of wire rope to cathodic protection. To obtain data of this type wire ropes of 11 different materials were studied in 790-day experiments at the NRL Marine Corrosion Research Laboratory, Key West, Florida.

EXPERIMENTAL PROCEDURES

Some of the wire ropes were fabricated from a single metal or alloy; in others the wires were coated with a second metal or alloy such as aluminum, zinc, or copper-nickel. It was not possible to obtain all of the wire ropes with an independent

wire rope core (IWRC) construction; some of the ropes had a
wire strand core (WSC) and others a fiber strand core (FSC).
The ropes were generally selected so that the minimum diameters
of the individual wires were similar but this was impossible
for the smaller diameter wire ropes.

The construction, rope diameter, wire diameter, and
coating thickness, where applicable, are shown in Table 1.
Three specimens of each material, except for one of the cobalt
alloys with limited availability, were studied in an unstressed
condition. Two specimens were 4 feet long and were used for
the total immersion phase of the study; one with cathodic
protection from a zinc anode and the second unprotected. The
third specimen was 10 feet long and was exposed partially
immersed.

All of the specimens were suspended beneath a pier in
clean, quiescent seawater with a resistivity of 19 ± 2 ohm-cm,
a pH of 8.3 ± 0.2, and a temperature range of 62° to 90°F.
More detailed information on the preparation of the specimens
and on the seawater characteristics is available in Reference 1.

At the conclusion of the exposure period, the specimens
were cleaned according to ASTM procedures (2). Each strand of
the chemically cleaned rope was examined at 20X magnification
under a stereo microscope. In some instances the strands were
intentionally unraveled and individual wires were also examined
under the microscope.

At the completion of the microscopic examination it was
evident that a comparison of the initial and final diameters
of the individual wires would not produce meaningful data
because of the highly localized nature of the corrosion on some
of the materials and that a qualitative evaluation of the
specimens would be adequate to characterize the corrosion and
the effectiveness of cathodic protection.

Complete details of the specimen preparation and mounting
procedures, specimen cleaning procedures, photomacrographs of
corroded areas and potential-time data for some of the ropes
may be found in Reference 1.

ANALYSIS OF CORROSION

The degree and type of corrosion and other observations on
each wire rope material under the various exposure conditions
are shown in Table 2. To assist in the selection of wire rope
for marine service a qualitative estimate of the degree of

corrosion on each material has been plotted as a function of exposure zone with respect to mean low water (MLW) and mean high water (MHW) on Figures 1-9. The estimations of the severity of corrosion were based on the most severe corrosion observed under each exposure condition.

Phosphor Bronze

Phosphor bronze, Figure 1, was one of the least corrosion resistant rope materials studied. The most severe corrosion occurred at the tidal zone of the partially immersed specimen but severe corrosion was observed on the unprotected ropes under all exposure conditions. The cathodically protected specimen was only slightly corroded, but the alkali generated in the cathodic protection process resulted in unacceptable deterioration of the FSC.

Visual examination of the rope at 183 days indicated that appreciable corrosion had occurred prior to the inspection. Noticeable localized reduction in the diameters of the individual wires was observed in the totally immersed specimen at this time. There was an accumulation of green corrosion products on the partially immersed specimen both in the immersed zone and in the zones above MHW. At a 325-day inspection multiple broken wires were found in the tidal zone of the partially immersed specimen and a heavy accumulation of green corrosion products was observed on the totally immersed unprotected specimen.

Galvanized Steel

The IWRC (Source 2) galvanized rope was less severely corroded than the hemp FSC rope (Source 1) except in the splash zone and above where severe corrosion occurred on both materials, Figure 2. This difference in behavior was first noted at the 183-day inspection when corrosion in the form of rust was observed on both the partially immersed and totally immersed unprotected specimen of the rope with the FSC. Rust on the IWRC rope was limited to the splash zone of the partially immersed specimen at the 183-day inspection.

This difference in corrosion behavior cannot be fully explained but the more severe corrosion on the Source 1 material is believed to be associated with the FSC construction. From Table 1 it is evident that the thickness of the zinc coating on the two ropes were essentially equal. It is therefore doubtful that this factor contributed to the difference in behavior.

The possibility that the slightly larger individual wire diameters on the IWRC rope contributed to its superior corrosion resistance cannot be completely discounted.

Galvanizing (up to 0.6 mil Zn) protected the IWRC rope for slightly more than one year except for the splash zone where the coating failed in less than 6 months. The galvanizing (up to 0.9 mil Zn) on the FSC rope failed in less than 6 months on both the totally immersed and partially immersed specimens.

Cathodic protection from a zinc anode extended the life of the galvanized wire ropes to over 2 years but caused severe deterioration of the hemp FSC of the Source 1 rope.

Aluminized Steel

In the totally immersed condition, aluminized-steel wire rope was one of the most corrosion resistant materials studied, Figure 3. As for the galvanized ropes, however, the hemp FSC aluminum rope showed less inherent corrosion resistance than the IWRC rope. This difference was particularly evident in the tidal and splash zones where severe to very severe corrosion was noted on the FSC rope as compared to the slight to moderate corrosion found on the IWRC rope. Both ropes showed excellent corrosion resistance in the totally immersed condition with only slight to moderate corrosion after 790 days.

The hemp FSC is believed to be the major factor in the reduced corrosion resistance although differences in the initial individual wire diameters may also have been a contributing factor. In this regard, it should be noted that the FSC of the partially immersed rope was severely deteriorated, but only in the tidal zone.

The aluminized-steel wire ropes responded well to cathodic protection. Zinc anodes extended the rope life to well over 2 years. After 790 days the ropes were essentially free of corrosion with much of the aluminum coating still intact. The hemp FSC, however, was severely deteriorated in the cathodically protected rope.

Copper-Nickel Clad Stainless Steel (Types 304L and 205)

Type 304L Stainless Steel

Type 216 Stainless Steel

Discussion of these ropes have been grouped because of their similar behavior. The 90-10 copper-nickel clad stainless steels (Figures 4 and 5), the Type 304L stainless steel (Figure 6), and the Type 216 stainless steel (Figure 7) were among the least corrosion resistant of the materials studied. The primary type of corrosion on the stainless steel ropes, both clad and unclad, was localized crevice corrosion and tunneling with resultant individual wire breakage. Both unprotected specimens of the Type 216 stainless steel rope were completely severed by crevice corrosion in the immersed zone.

External visual examination of stainless steel wire ropes can lead to serious misjudgement on the extent of the corrosion. In some instances individual wires which appeared to be in excellent condition were found to be completely hollow and were readily perforated by moderate pressure with a needle probe. Such hollow wires obviously retain only a small fraction of their original breaking strength.

The copper-nickel clad wire ropes were no more corrosion resistant in quiescent seawater than unclad 304L stainless steel rope which showed inherently poor corrosion resistance.

The performance of these ropes as a group was much improved by cathodic protection from a zinc anode, but localized corrosion was completely eliminated only on the Type 216 stainless, and the copper-nickel clad Type 304L stainless steel ropes. All of the other ropes in the group showed some evidence of crevice corrosion.

Nickel and Cobalt Based Alloys

Wire ropes constructed from some of the materials previously discussed have been in use for many years and their mechanical and engineering properties have been well established. Ropes constructed from "super-alloys" have been available for only a few years and then only as special order items. Thus the total engineering experience with ropes constructed from these materials is extremely limited.

All of these alloys show outstanding resistance to corrosion in seawater and the following evaluation of corrosion resistance is intended to apply between alloys of this class with the understanding that the group as a whole has corrosion resistance at least an order of magnitude better than the alloys previously discussed.

62Ni-22Cr-9Mo-2Fe-3.75Cb+Ta

This nickel based alloy exhibited excellent corrosion resistance under all marine exposure conditions (Figure 8, Table 2). Crevice corrosion was limited from slight to moderate localized corrosion under an area at the lower end of the specimen wrapped with polyvinyl chloride tape. Even this slight corrosion was virtually eliminated by cathodic protection from a zinc anode.

It should be noted that wires drawn from this alloy may become extremely brittle if the alloy is heated. Zinc socketing should not be used for ropes constructed from this alloy as the embrittlement phenomenon can occur below red heat.

40Co-20Cr-15Ni-7Mo-2Mn-Rem.Fe

This alloy was also resistant to corrosion in seawater; the corrosion observed was confined to a general surface etch on the wires with slight crevice corrosion under the polyvinyl tape on the completely immersed specimen (Figure 9, Table 2). Wire embrittlement was found on individual wires even though they had not been heated after receipt of the rope. The embrittled areas were under the polyvinyl chloride tape and were found on wires both with and without cathodic protection. For this alloy the embrittlement phenomenon does not appear to be associated with a heat affected zone as efforts to embrittle wires by heating to red heat and cooling were unsuccessful.

The data for this alloy is consistent with a mechanism of embrittlement by hydrogen generated either by the corrosion process in the crevice or by the cathodic polarization process. Ropes constructed from this alloy should be used with caution until the conditions leading to embrittlement are more fully investigated.

35Co-35Ni-20Cr-10Mo

Because of the limited amount of rope available, this alloy was exposed in only two conditions, i.e., totally immersed in seawater with and without cathodic protection. Corrosion was

confined to slight crevice corrosion (etching) which occurred
both between individual wires and under the polyvinyl chloride
tape. Crevice corrosion was reduced somewhat but not eliminated
by cathodic protection from a zinc anode.

Individual wires were embrittled in the heat affected
zone when heated and allowed to cool in air to room temperature
but no embrittled wires were found in the rope sections which
had been exposed to seawater with or without cathodic protection
and not given a post exposure heat treatment. Zinc socketing
should not be used for ropes constructed from this alloy.

73Ti-13V-11Cr-3Al

The titanium alloy wire rope had very good inherent corrosion
resistance (Table 2). Corrosion on the unprotected specimens
was limited to occasional microscopic pitting and etching.
Because of the excellent corrosion resistance of the alloy, a
plot of the degree of corrosion as a function of exposure
condition has not been shown. Such a plot would show a vertical
straight line located at the "none" position on the abscissa.

Despite the excellent corrosion resistance, the utility
of titanium wire rope in seawater would be limited to non-working
ropes because of reported excessive wear of titanium ropes run
over sheaves.

SUMMARY

A summary of the corrosion characteristics and response to
cathodic protection of non-working wire ropes in seawater is
shown in Table 3. There is no wire rope alloy now available
which can be unreservedly recommended for long term use in the
marine environment. If only corrosion characteristics are
considered aluminized steel, the "super-alloys", and titanium
alloy ropes are suitable for 2-year service. Longer life would
be expected in the case of titanium, the "super-alloy" ropes or
larger diameter aluminized steel ropes with an IWRC or WSC.
However, the utility of the "super-alloy" ropes is limited both
by high initial cost and the incompletely resolved problems with
embrittlement. The utility of the titanium alloy rope is
severely limited by cost and by the very poor wear properties
of the rope.

Most of the alloys studied are suitable for service for
2 or more years in IWRC or WSC construction if adequate cathodic
protection can be applied to the rope. However, the application

of cathodic protection to long lengths (over 200 feet) of wire rope often leads to unacceptable restrictions on the design and emplacement of wire rope structures.

ACKNOWLEDGMENT

REFERENCES

1. T. J. Lennox, Jr., R. E. Groover, and M. H. Peterson, "Corrosion Characteristics and Response to Cathodic Protection of Eight Wire Rope Materials in Sea Water," NRL Report 7584, Sep 1973.

2. ASTM: G1-72, Recommended Practice for Preparing, Cleaning, and Evaluation Corrosion Test Specimens, 1974 Annual Book of ASTM Standards - Part 10, p. 489.

Table 1

Wire-Rope Construction Details.

Material	Construction Details			Metallic-Coating Thickness (Mils)
	Rope Diameter (in.)	Individual Wire Diameter (Mils)	Number of Wires per Strand	
Phosphor Bronze	5/16 6 x 19FSC Warrington	18 - 24	19	None
Galvanized Steel Source 1	1/2 6 x 37FSC Warrington-Seale	16 - 25 core:40	41	0.1 - 0.9 zinc
Galvanized Steel Source 2	1/2 6 x 19(IWRC)	19 - 40 core:48	19	0.1 - 0.6 zinc
Aluminized Steel Source 1	1/2 6 x 37FSC	19 - 26	37	0 - 0.7 aluminum
Aluminized Steel Source 2	1/2 6 x 19(IWRC)	20 - 40 core:48	19	0.1 - 0.9 aluminum
90/10 Cu-Ni Clad Type 304L-SS	1/2 6 x 19(IWRC)	20 - 40 core:47	19	1.0 - 2.8 90/10 Cu-Ni
90/10 Cu-Ni Clad Type 205-SS	1/2 6 x 19(IWRC)	20 - 40 core:47	19	1.0 - 2.6 90/10 Cu-Ni
Type 304L-SS	1/2 6 x 19(IWRC)	19 - 40 core:47	19	None
216 Stainless Steel	1/4 7 x 19	17 core:19	19	None
62Ni-22Cr-9Mo-2Fe-3.75Cb+Ta	1/4 7 x 19	16 - 18 core:19+	19	None
40Co-20Cr-15Ni-7Mo-2Mn-Rem.Fe	1/8 7 x 19	8 core:9	19	None
35Co-35Ni-20Cr-10Mo	1/8 7 x 19	8 core:9	19	None
73Ti-13V-11Cr-3A1	1/8 7 x 19	8 - 11	19	None

Table 2

Degree and Type of Corrosion on Wire Rope Specimens
after 200 Days in Seawater at Key West, Florida

Material	Total Immersion		Partial Immersion – No Cathodic Protection				
	No Cathodic Protection	Cathodic Protection Zinc Anode	Immersed Zone	Immersed – Near Surface Zone	Tidal Zone	Splash Zone	Above Splash Zone
Phosphor Bronze	Very severe corrosion; wires broken	Slight intermittent evidence crevice corrosion	Severe general and pitting corrosion; necked down	Wires badly thinned; severe pitting	All wires severely corroded and broken	Quite severe to 6" above mean high water	Laminar, generalized corrosion
Fiber core	Could not be broken by hand	Could be broken by hand	Could not be broken by hand	Could not be broken by hand	–	Could not be broken by hand	Could not be broken by hand
Galvanized Steel Source 1	Very severe corrosion; wires broken	Slight rust and roughened surface	Very severe corrosion; broken wires	Very severe corrosion; broken wires	Wires broken	Badly whiskered and reduced wire diameter	Very severe corrosion
Hemp fiber core	Could not be broken by hand	Could be broken by hand	Could not be broken by hand	Could not be broken by hand	Could not be broken by hand	–	Could not be broken by hand
Galvanized Steel Source 2	Slight-to-moderate corrosion and pitting	No corrosion	Moderate-to-severe corrosion	Considerable general corrosion	Moderate-to-severe corrosion	Very severely corroded	Severe general corrosion; broken wires
IWRC	Essentially no corrosion	No corrosion	Relatively small amount corrosion	Wires thinned	Moderate-to-severe corrosion; some broken wires	Very severely corroded	Severe general and local corrosion
Aluminized Steel Source 1†	Rust stained; essentially no bright aluminum remained	Small amount of superficial rusting	Some scattered rust areas	Some superficial rust	Top 3" – quite severe rusting	Very severe corrosion to 5" above mean high water	No rust; 30-80% bright aluminum present
Hemp fiber core	Could not be broken by hand	Could be broken by hand	Could not be broken by hand	Could not be broken by hand	Could be broken by hand	Could not be broken by hand	Could not be broken by hand
Aluminized Steel Source 2	Scattered rust areas	95% bright aluminum remaining, except under tape	Scattered flaking and corrosion	Scattered rust-stained areas	Scattered superficial rusting; <40% bright aluminum	Rust stains scattered areas; 30% bright aluminum	Localized flaking and corrosion
IWRC	Scattered rust areas	95% bright aluminum remaining, except under tape	Scattered flaking and corrosion	Scattered rust-stained areas	Scattered superficial rusting; essentially no bright aluminum present	Rust stains scattered areas; 30% bright aluminum	Localized flaking and corrosion
90/10 Cu-Ni Clad Type 304L Stainless Steel	Irregular corrosion	No corrosion and some mechanical deformation	Tunneling	Crevice corrosion	Severe tunneling	Mechanical deformation	Corrosion corrosion and blistering
IWRC	Crevice corrosion and tunneling; Cu-Ni present	No corrosion and some mechanical deformation	Tunneling	Severe tunneling	Severe tunneling	Very severe tunneling	Very severe tunneling
90/10 Cu-Ni Clad Type 205 Stainless Steel	Crevice corrosion and pitting	Discolored and some mechanical deformation	Crevice corrosion	Crevice corrosion	Some crevice corrosion and pitting	Severe tunneling	Very severe corrosion tunneling to 3" above high water
IWRC	Very severe tunneling	Some crevice corrosion	Severe tunneling	Very severe tunneling	Very severe tunneling	Very severe tunneling	Very severe corrosion tunneling to 3" above mean high water
Type 304L Stainless Steel	Severe crevice corrosion under tape	Slightly etched and some shallow pitting	Severe crevice corrosion and tunneling	Rusting, etched and pitting	Considerable crevice corrosion and pitting	Severe crevice corrosion and pitting	Crevice corrosion and pitting
IWRC	Very severe tunneling	Etched and slight crevice corrosion	Badly thinned by crevice corrosion	Tunneling	Some local corrosion	Crevice corrosion, pitting and tunneling	Crevice corrosion and pitting
Type 216 Stainless Steel	Completely severed by crevice corrosion at tape	No evidence crevice corrosion	Completely severed by crevice corrosion	Rust staining and some crevice corrosion	Rust staining and some crevice corrosion	Rust staining and some crevice corrosion	Some rust staining
67Ni-22Cr-9Mo-2Fe-3.75Cb-Ta	Slight crevice corrosion with mechanical delamination	Slight crevice corrosion and microscopic pitting	Crevice corrosion and pitting; necked down under tape	Intermittent and slight crevice corrosion	Intermittent and slight crevice corrosion and microscopic pitting	Intermittent and slight crevice corrosion	Intermittent and slight crevice corrosion
WSC	Slight-to-moderate crevice corrosion under tape with mechanical delamination	No corrosion	Crevice corrosion pitting; necked down under tape	Etched	Evidence slight general corrosion and microscopic pitting	No corrosion	No corrosion
40Co-20Cr-15Ni-7Mo-2Mn-REM-Fe	Slight etch all surfaces, some crevice corrosion‡	Very slight etch all surfaces‡	Slight etch all surfaces of wires	Slight etch all surfaces of wires	Slight etch all surfaces of wires	Slight etch all surfaces of wires	Slight etch all surfaces of wires
35Co-35Ni-20Cr-10Mo	Crevice etched; some reddish areas‡	Only slightly better than unprotected specimen‡	← Initial length of wire rope did not permit including this type of specimen →				
73Ti-13V-11Cr-3Al	Etched; occasional microscopic pitting	Bright and corrosion free‡	Etched	Etched; occasional microscopic pitting	Etched; occasional microscopic pitting	Etched; occasional microscopic pitting	Etched
WSC	Etched; occasional microscopic pitting	Bright and corrosion free	Etched	Etched; occasional microscopic pitting	Etched; occasional microscopic pitting	Etched; occasional microscopic pitting	Etched

*Examined at 20X magnification

†Cross section

‡Embrittled (heat and/or cold) sometimes associated with tape crevice

63

Table 3

Summary of Corrosion Characteristics and Response to Cathodic
Protection of Nonworking Wire Ropes Suitable
for Long-Term Use in Seawater

Service Condition	Materials Judged Suitable for Long-Term (e.g., 2-yr) Service	Remarks
Partial immersion; rope extends from well below the tidal zone to above the splash zone	Aluminized Steel	Avoid hemp FSC; worst corrosion in splash zone
	62Ni-22Cr-9Mo-2Fe-3.75Cb+Ta	Slight-to-moderate corrosion under the tape in the immersed zone; avoid Zn socketing (embrittles)
	40Co-20Cr-15Ni-7Mo-2Mn-Rem.Fe	Etched surfaces
	73Ti-13V-11Cr-3Al	Working over sheaves may cause rapid deterioration
Totally immersed; no cathodic protection	Aluminized Steel	FSC or IWRC; both suitable
	62Ni-22Cr-9Mo-2Fe-3.75Cb+Ta	Slight-to-moderate corrosion seen under the tape; avoid Zn socketing (embrittles)
	40Co-20Cr-15Ni-7Mo-2Mn-Rem.Fe	Slight etch crevice corrosion; embrittled under tape without heat
	35Co-35Ni-20Cr-10Mo	Etched in crevice; some reddish areas; embrittled with heat. (Avoid Zn socketing)
	73Ti-13V-11Cr-3Al	Working over sheaves may cause rapid deterioration
Totally immersed; cathodic protection from Zn anode	Phosphor Bronze, Galvanized Steel, and Aluminized Steel	Avoid hemp FSC
	90/10 Cu-Ni Clad Type 304L Stainless Steel	--
	Type 304L Stainless Steel	Pitting not eliminated
	Type 216 Stainless Steel	--
	62Ni-22Cr-9Mo-2Fe-3.75Cb+Ta	Avoid Zn socketing (embrittles)
	40Co-20Cr-15Ni-7Mo-2Mn-Rem.Fe	Additional studies required to determine suscept. to embrittlement
	35Co-35Ni-20Cr-10Mo	Additional studies required to determine suscept. to embrittlement
	73Ti-13V-11Cr-3Al	Working over sheaves may cause rapid deterioration

Fig. 1 – Degree of corrosion and cathodic-protection response for phosphor bronze wire rope

Fig. 2 — Degree of corrosion and cathodic-protection response for galvanized-steel wire rope

66

Fig. 3 — Degree of corrosion and cathodic-protection response for aluminized steel wire rope

67
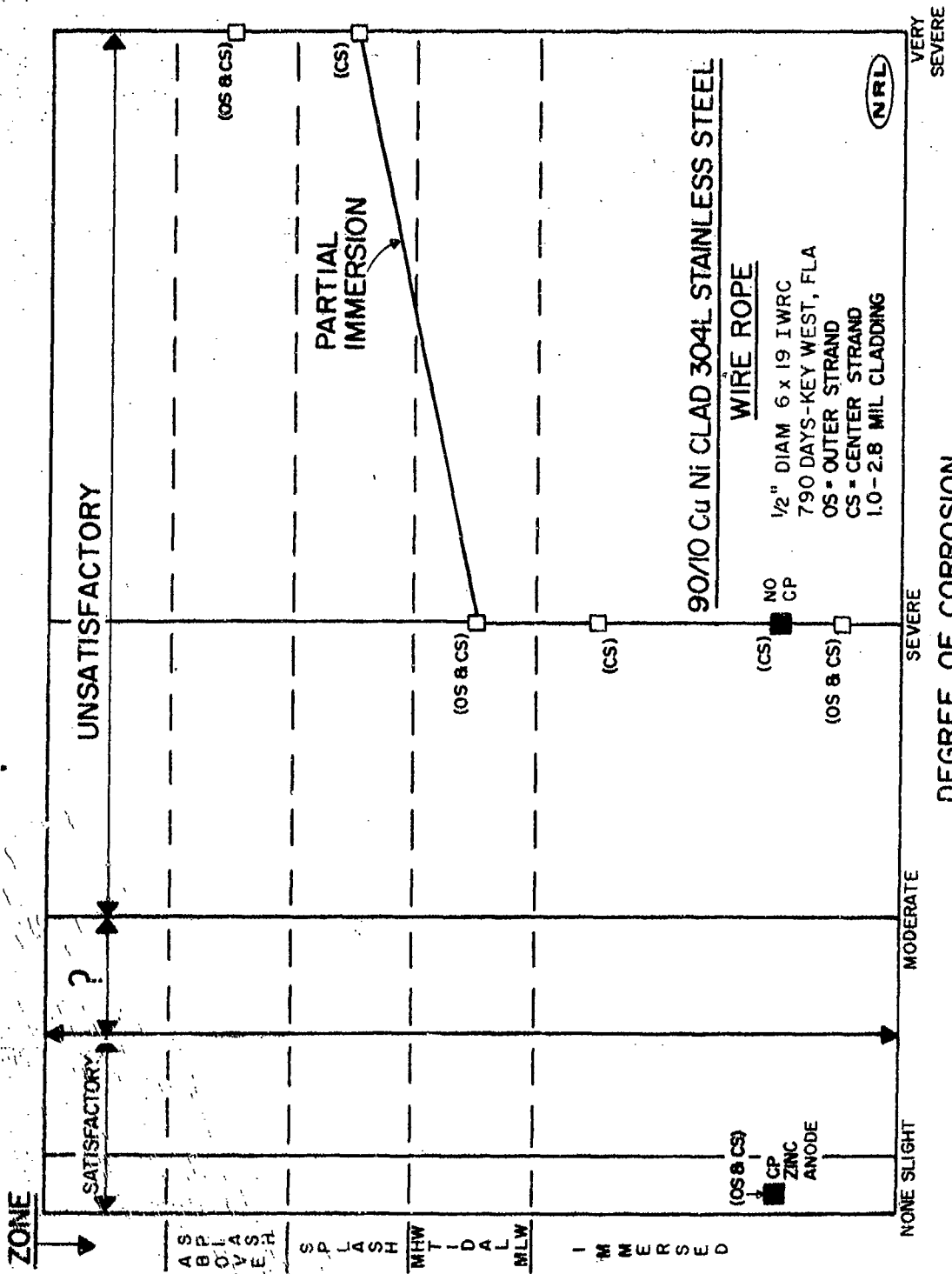
Fig. 4 – Degree of corrosion and cathodic-protection response for 90/10 copper–nickel clad Type 304L stainless steel wire rope
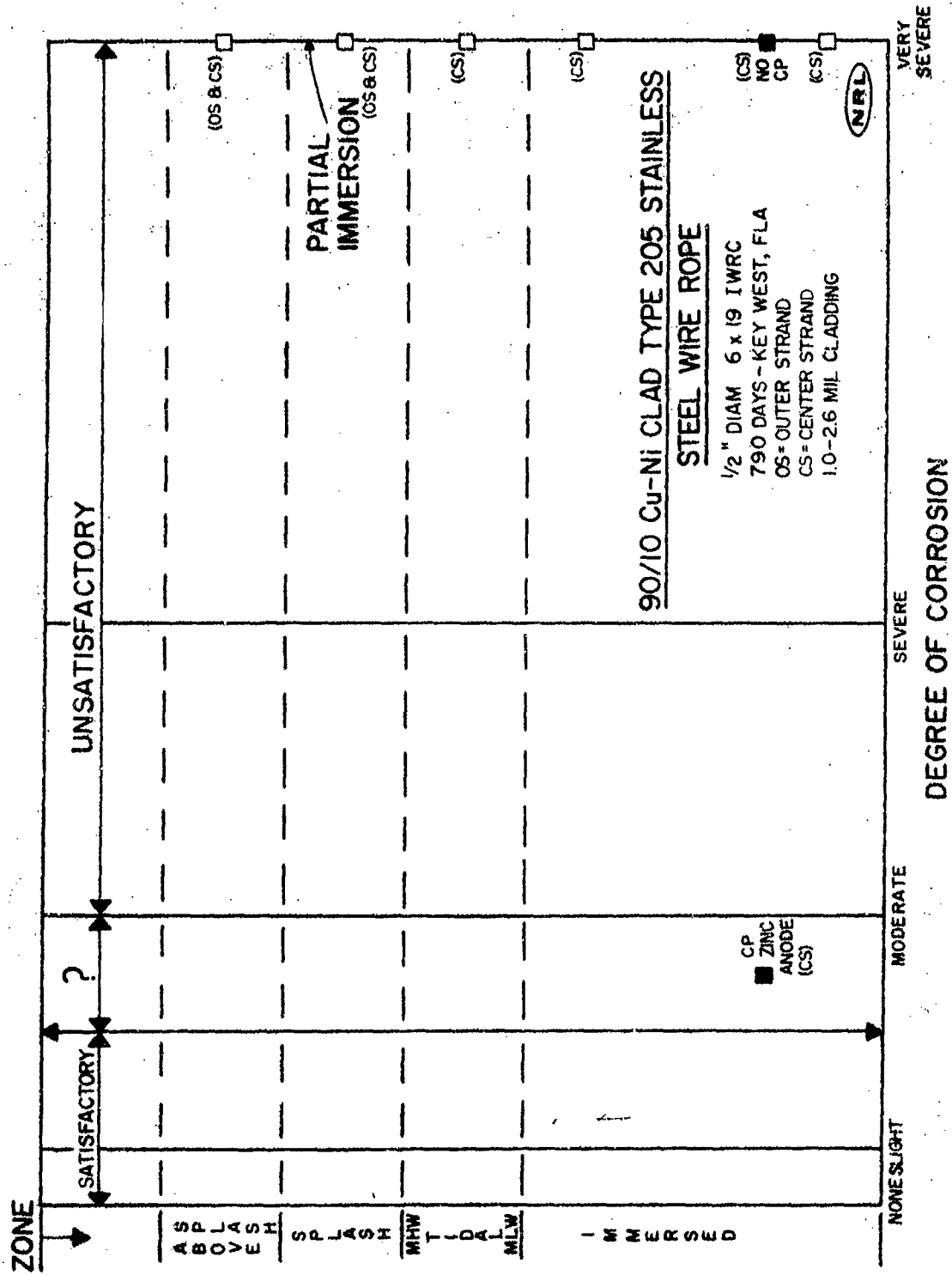
Fig. 5 — Degree of corrosion and cathodic-protection response for 90/10 copper-nickel clad Type 205 stainless steel wire rope

ZONE

SATISFACTORY | ? | UNSATISFACTORY

UNSATISFACTORY

PARTIAL IMMERSION

(OS & CS)

(OS)

(CS)

(OS & CS)

(CS)
NO
CP

(OS & CS)

(NRL)

304L STAINLESS STEEL WIRE ROPE

½" DIAM 6 x 19 IWRC
790 DAYS – KEY WEST, FLA

OS = OUTER STRAND
CS = CENTER STRAND

CP
ZINC
ANODE
(SOME PITTING)
(OS & CS)

ABOVE SPLASH
SPLASH
MHW TIDAL MLW
IMMERSED

NONE SLIGHT | MODERATE | SEVERE | VERY SEVERE

DEGREE OF CORROSION
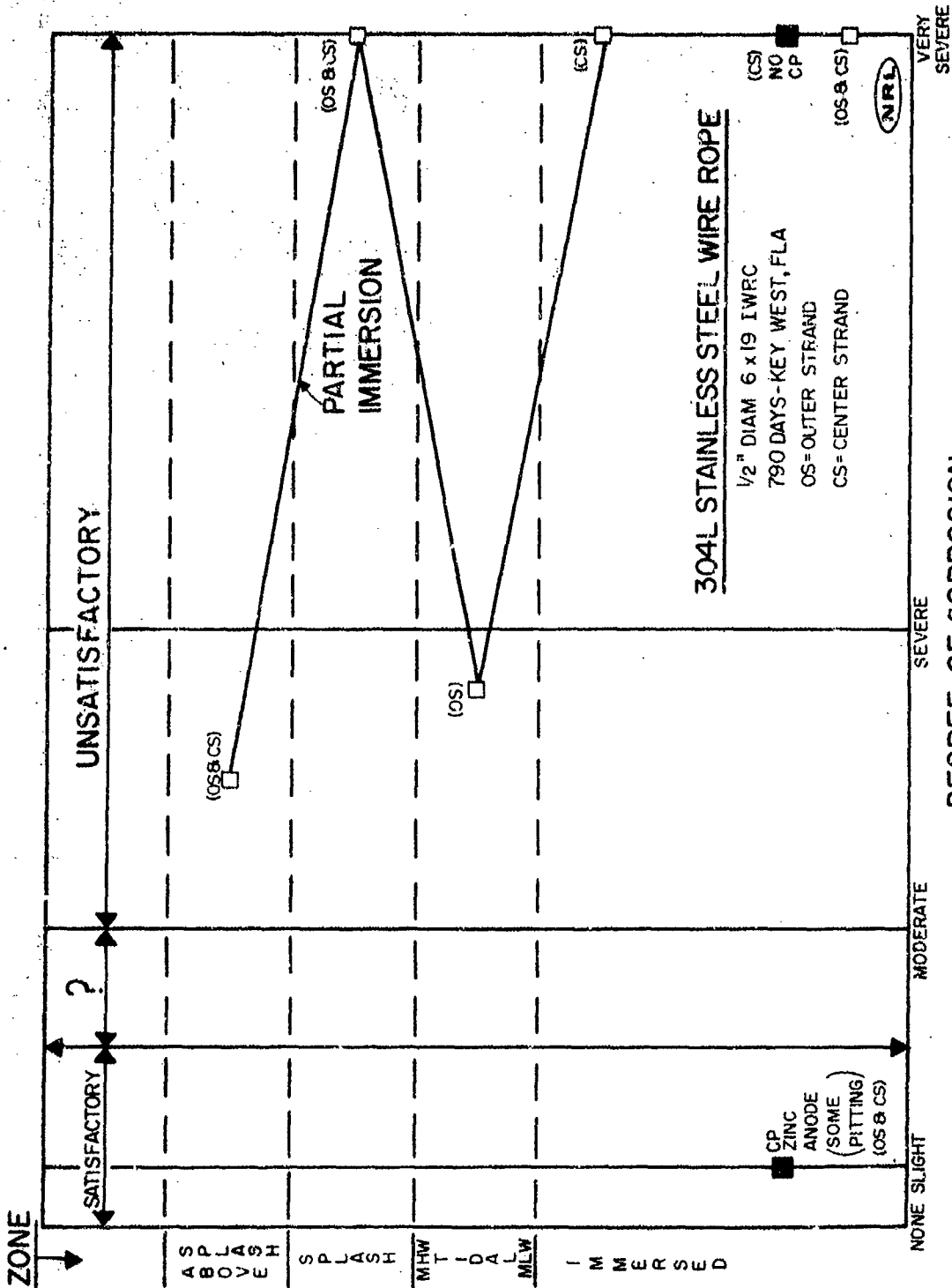
Fig. 6 — Degree of corrosion and cathodic-protection response for Type 304L unclad stainless steel wire rope

70
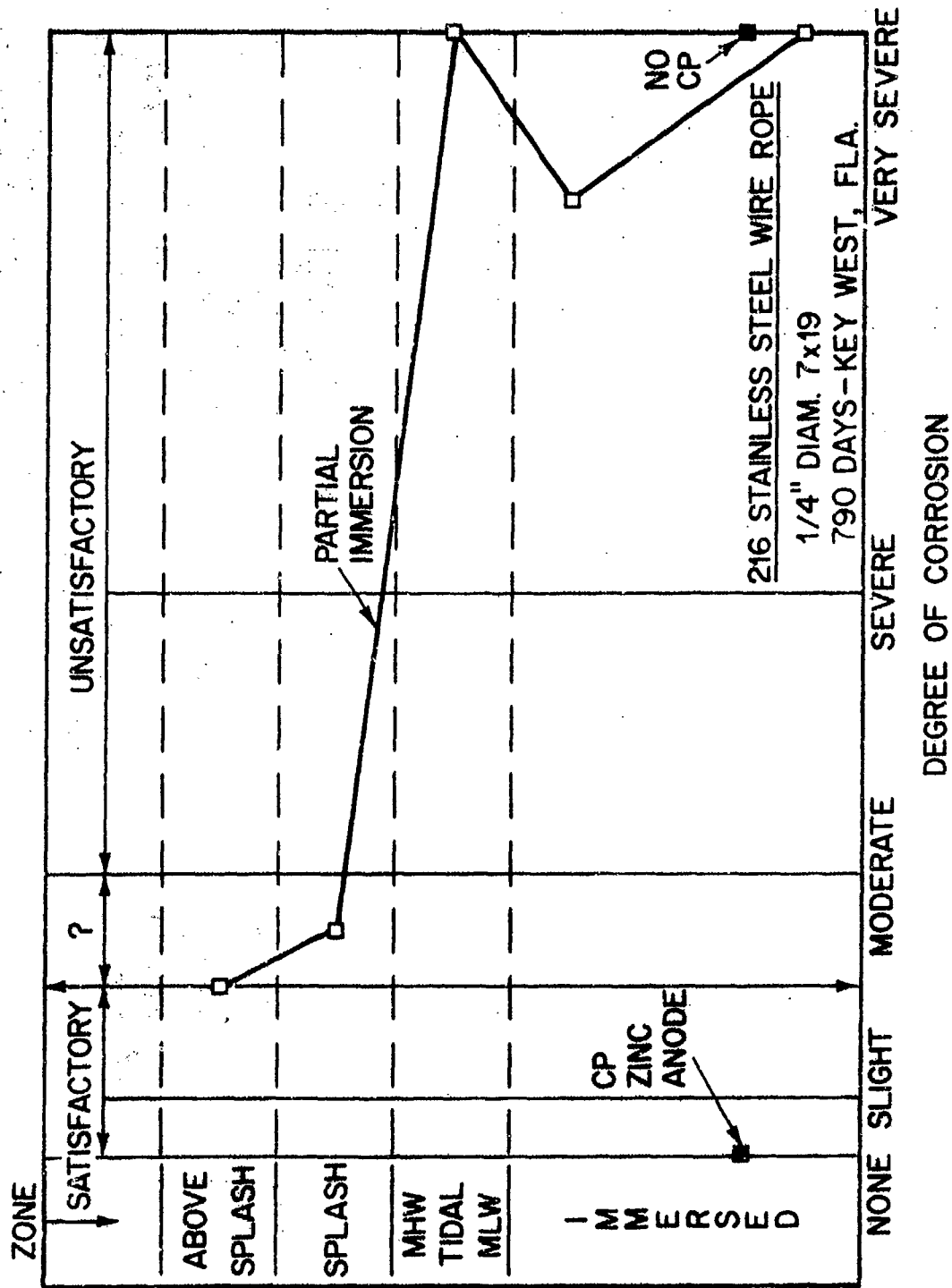
Fig. 7 — Degree of corrosion and cathodic-protection response for 216 stainless steel wire rope
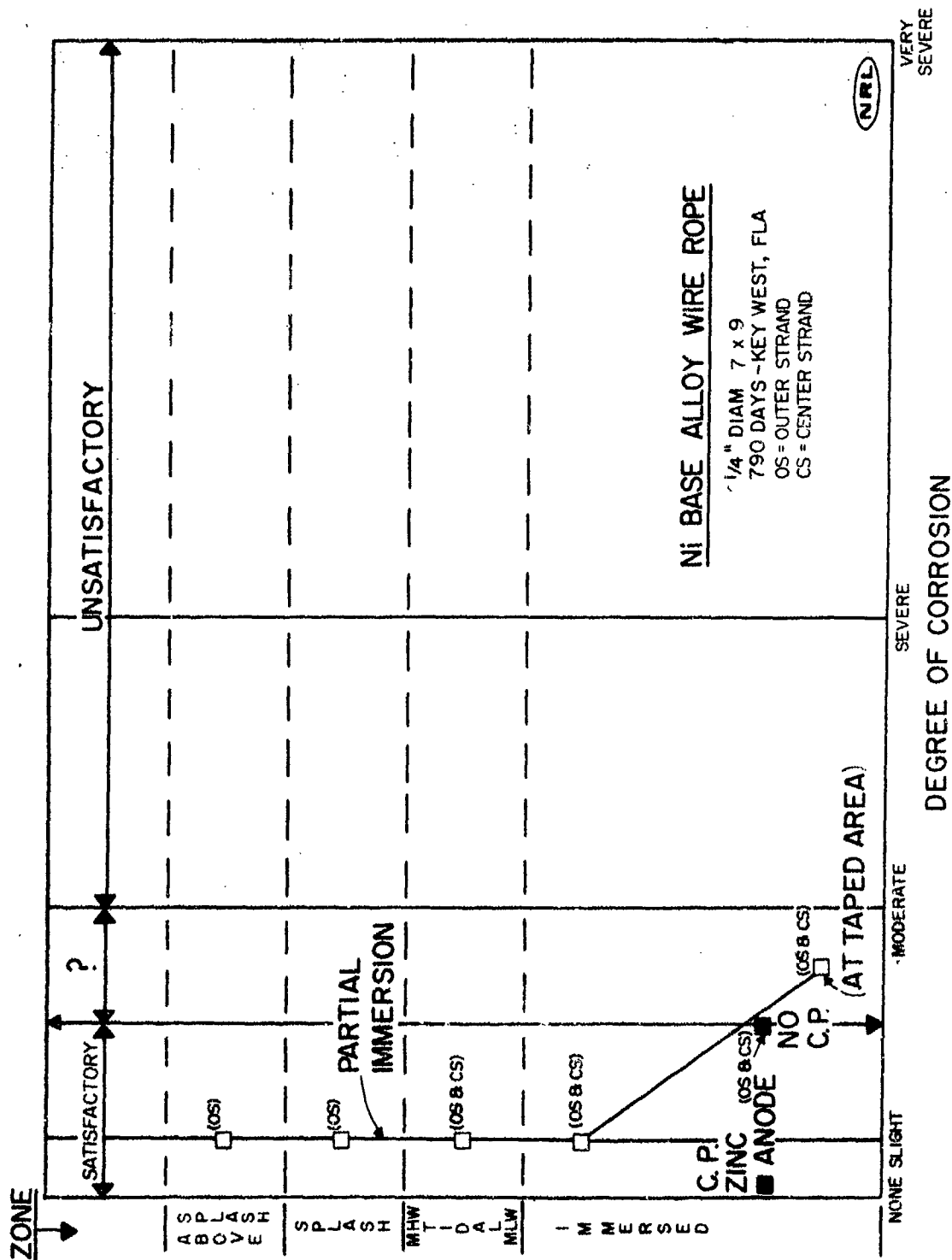
Fig. 8 – Degree of corrosion and cathodic-protection response for nickel-base-alloy wire rope

Fig. 9 – Degree of corrosion and cathodic-protection response for cobalt alloy wire ropes

EVALUATION OF OBJECTS
EXPOSED TO DEEP OCEAN ENVIRONMENTS

By
James F. Jenkins

ABSTRACT

   The Navy's Civil Engineering Laboratory, Port Hueneme, California has partici-
pated in the inspection and evaluation of many objects recovered from the ocean
depths. The purpose of these evaluations was to gather information on the deterior-
ation of materials in deep ocean environments for the design of future equipment as
well as for an assessment of the probable lifetimes of similar in-service equipment.
An attempt has been made to develop standard methods for the inspection, documenta-
tion and evaluation of such objects to permit better correlation between inspections
performed by different personnel.
   The condition of several objects after retrieval as well as the various methods
of inspection, documentation and evalution of the objects are discussed.

, Civil Engineering Laboratory
Naval Construction Battalion Center
Port Hueneme, California 93043

Preceding Page Blank

INTRODUCTION

As man ventures into the sea, the aggressiveness of the marine environment becomes a costly fact of life. In order to combat this hostile adversary man must use his most powerful tool -- knowledge. One of the most successful and therefore widely used methods of acquiring knowledge about the performance of materials and structures in marine environments is to draw on past experience. Almost all of the designs of ships, docks and other structures exposed to near-surface environments are based primarily upon past experience with similar structures in similar environments.

As man, or more often his mechanical eyes and hands, ventures into the ocean depths he is confronted with an almost total lack of experience on which to base his designs. The difference in environment between the surface of the ocean and its depths makes the use of experience in surface waters of questionable value.

While man has been exposing materials to the ocean depths, often inadvertently, for as long as he has ventured to sea, only in the past decades has he been able to recover these objects, analyze their condition, and add the knowledge gained from their analysis to the body of experience which he can use to better fit ocean equipment to the rigors of this hostile environment. This paper is a discussion of the analysis of several objects recovered from the ocean, the objectives of the analyses, the methods used, and the results which were obtained.

OBJECTIVES

The primary aim of the evaluation of objects recovered from the deep ocean is to document the behavior of materials and systems when exposed to marine environments at depth. The information thus obtained can be utilized for several purposes. Firstly, generally applicable information on the behavior of the materials can be used in the design of other ocean equipment. The application of this information must be made with care. The exposure of the material in the new design must be similar to that encountered in the object which was analyzed. Factors such as oceanographic parameters, galvanic coupling, protective coatings, and stress (both static and dynamic) must be considered along with the specific performance requirements in the new design. A good example of the performance requirements of a design is found in the use of aluminum alloys in free-flooding framework structures versus their use in pressure resistant housings. In free-flooding structures the pitting which normally occurs on these alloys is relatively innocuous; however, in a pressure resistant housing, a single pit can result in a leak which renders the entire housing useless.

Secondly, the information obtained from the analyses can be used to identify common design weaknesses which can be rectified in future designs. These design weaknesses are often encountered in widely used "standard" equipment, often of the type sold for marine use. A common example of such a design weakness is the use of stainless steel wire rope. Such rope is commonly used as above-water rigging with satisfactory performance: however, when used as a submerged member, especially in deep ocean, such ropes are susceptible to rapid failure, usually due to crevice corrosion.

A third objective of these analyses is the identification of deficiencies in the ability of deep ocean corrosion technology to predict the behavior of ocean structures. Corrosion technology can normally explain any phenomenon; however, its ability to reliably predict failure is often limited. If a specific phenomenon is found to be a common mode of failure and is, using present knowledge, unpredictable, then the phenomenon is a potential topic for future research.

The information obtained from the inspection of objects recovered from the deep ocean also often has certain specific immediate applications which make the information extremely useful. If the object is one of several identical or very similar objects which are exposed to the same or similar environments, then the condition of one object can be used to infer the condition of the others. Thus the remaining lifetime of both the inspected and uninspected can be determined. This knowledge can be used for many purposes. For example, the object retrieved may be in sufficiently good condition to be replaced after minor repairs; or potential failures of other similar objects can be predicted in advance, thus identifying the need for repair before failure. When the necessity for repair of the object retrieved or of similar objects is discovered during inspection, the cause of the damage can often be determined and repair methods can be identified which often improve upon the original design and extend the object's useful life.

INSPECTION METHODS

The evaluation of an object after exposure to the deep ocean can be divided into three phases: In-situ inspection, visual observations upon retrieval, and laboratory analyses. The evaluation often consists of only one or two of these phases.

In-situ inspection can be performed by manned submersible or remotely operated underwater systems such as the CURV (Cable-controlled Underwater Research Vehicle). The inspection is usually limited to visual observations and photography, although samples can sometimes be retrieved. Underwater observation and photography are limited, using present techniques, in their ability to determine the actual condition of an object. Gross deterioration such as missing or broken components can of course be identified. However, the condition of components which are covered with corrosion products or fouling is often misinterpreted. The ability to remove these deposits could vastly improve the usefulness of these in-situ inspections. If the vehicles are equipped with manipulator arms, the removal of samples of the structure is possible but is usually impractical. One problem encountered in these inspections is the quality of the underwater photographs. They are normally lacking in depth perception and in color reproduction. These deficiences can be overcome by the use of stereo cameras or oblique lighting, and the inclusion of a known color scale in the photograph at the same distance as the subject. In general, the results of inspections made from manned submersibles or from remotely operated vehicles are subject to a wide range of interpretations. Improvements in underwater inspection techniques are needed to improve the quality of the information obtained.

Inspection of underwater objects by divers is now limited to rather shallow depths. The limitations on photography are similar to that encountered with submersible vehicles. The diver has several important advantages, however. He can normally approach the object to a much closer range than the submersible and can easily touch the object, thus determining surface texture, adherence of deposits, etc. This intimate contact with the object vastly improves the quality of information obtained by a well-trained diver over that obtained using an underwater vehicle. The maximum depth for working divers is constantly increasing as new gas mixtures and decompression techniques are developed. Inspection of objects in the deep ocean by divers may become practical in the near future.

The most widely used type of inspection is made after retrieval of the object into the air. This environment allows a vast improvement in the inspector's ability to properly observe and document the condition of the object and to remove samples for further analysis. The most important tool for inspection of any object is the human eye. The most important technique for recording the condition of objects

recovered from the deep ocean is photography. By carefully noting and recording the location, distribution, amount, texture and tenacity of corrosion products on the object a great deal of information is obtained. It is important to inspect the object immediately upon retrieval as the characteristics of the corrosion products will often change rapidly upon contact with the air. The initial stage of inspection is therefore, by necessity, a rapid and fairly cursory one. Further inspection of the underlying material will usually reveal the type and extent of deterioration which has occurred. Disassembly of the object is often necessary to reveal hidden deterioration such as crevice corrosion.

Samples are routinely removed from objects retrieved from the ocean. However, without proper documentation as to their original location and condition and without proper preservation, they are often of limited value. Preservation of samples from objects retrieved from the deep ocean refers only to the preservation of the information available from the sample. It is not necessary, and is usually impossible, to maintain the sample in an "as recovered" condition. Biological samples are normally preserved in formalin. Corrosion samples are usually placed in plastic bags or vials. Metallic material samples should be rinsed in fresh water, then either dried in air or preserved in normal butyl alcohol. The condition of non-metallic materials is often dependent on their content of water which was absorbed under high pressure and is difficult to preserve. These materials are normally wrapped in moistened packing material and stored in plastic bags. Preservation techniques other than those noted above are often successfully applied. The only prerequisite for the selection of a preservation technique is that it retains as much of the information originally contained in the sample as is possible and that any changes in the condition of the sample are such that the original condition can be inferred from later analyses.

CASE HISTORIES OF EVALUATION OF OBJECTS EXPOSED TO DEEP OCEAN ENVIRONMENTS

1. SNAP 7- Acoustic Beacon

    Date of Emplacement - July 1964
    Date of Recovery - November 1969
    Length of Exposure - 64 months
    Location - South of Bermuda
    Water Depth - 2,650 ftms. (15,900 ft.)
    Seawater Characteristics -
        Salinity - 34.6 ppt
        Oxygen Content - 6.3 ml/L
        Temperature - 2.4°C
        pH - 7.4 (50' off bottom)
    Seafloor Soil Characteristics -
        Type - sandy-silty clay
        Analysis - 53% $CaCO_3$, 31% Silicates
        pH of interstitial water - 9.8
    Description of Structure -
        As shown in Figure 1, this installation consisted of 9 miles of bottom-laid grapnel rope and ground tackle with the SNAP 7-E Radioisotope Power Generator (RPG) located in its support structure in approximately the center of the array. From the generator support structure an electromechanical cable extended upwards to an acoustic beacon supported in midwater by a liquid filled float. The beacon and midwater float were lost prior to retrieval.
        Objectives of Evaluation -
            Document condition of RPG and its support structure.

Determine cause of system failure and recommend alternate designs.
Determine condition of other array components.

Results of Evaluation -

Condition of RPG and Support Structure -

Visual observations immediately after recovery showed that the generator capsule was virtually unattacked, as shown in Figure 2. The only deterioration noted was the lifting of a "Underwater Sound Laboratory" decal. No other visible deterioration of the capsule or its paint coating was noted. The dark area at the center of the generator capsule was the result of a penetrating spray lubricant applied in an attempt to limit atmospheric deterioration of the O-ring seal flanges of the generator halves until subsequent disassembly.

The generator and generator support structure were partially disassembled approximately 4 days after recovery. At this time the generator capsule was separated at the central flange for removal of the power converter and inspection of the generator inner housing. The O-ring seal flange between the two capsule halves had corroded slightly, as shown in Figure 3. The maximum penetration near the O-ring seal was less than 0.001-inch. It is not known whether this attack occurred before or after recovery, although the application of a rust-inhibiting penetrating spray lubricant to the seal area immediately after recovery was intended to minimize attack after recovery. No leakage of the primary O-ring was noted and the area between the primary and secondary O-ring grooves was unattacked. There was no evidence of any effect of the zinc anodes adjacent to the flanges in either reducing or accelerating corrosion within the flange.

The electrical penetrator on the top section of the generator capsule was removed for inspection. The O-ring flange on the capsule was covered with a very light film of red rust, as shown in Figure 4. The underlying surface was unattacked. The penetrator flange was more severely rusted, as shown in Figure 5, but showed no attack greater than 0.001-inch.

The support structure was fabricated from mild steel and had been painted. Zinc anodes had been installed at several points on the structure before emplacement. The paint coating was missing from approximately 30% of the structure. In some areas, particularly on the vertical supports surrounding the generator capsule, the paint coating had been lifted from the underlying metal, as shown in Figure 6. This can be attributed to the generation of hydrogen on the steel under the paint coating due to overprotection from zinc anodes which were attached to the structure by the bolts visible at the top of supports in Figure 6. Zinc anodes normally do not cause the lifting of paint coatings on steel; however, the environment near the bottom sediment in this location caused lifting to occur. The single environmental parameter which can best explain such lifting is the pH of the seawater. The pH of the seawater near a marl bottom is higher than that for bulk surface seawater. Zinc is known to be more active and iron less active in solutions of high pH than in more neutral solutions. Thus the criteria used for the design of cathodic protection systems for steel using zinc anodes in or near highly basic marl bottoms should be different than the usual criteria based on experience in less basic surface waters.

The portion of the generator embedded in the bottom sediments was nearly indistinguishable from the portion exposed to the seawater except for the greater deterioration of the paint coating on the portion of the generator support structure immediately below the mudline. Due to the combination of protection by zinc anodes and paint coatings combined with the high pH, low temperature environment to which it was exposed, the steel portions of the generator support structure were uncorroded upon retrieval. However, after less than one hour of exposure on deck, despite fresh water washdowns, the generator support structure showed significant rust staining on the bare steel surfaces.

Cause of System Failure -

The cause of the system failure was loss of the acoustic beacon and float. The electromechanical cable used to attach the acoustic beacon to the power generator had parted at or near the acoustic beacon. The condition of the cable at the break is shown in Figure 7. Inspection of the cable near the break showed that five of the six stainless steel mechanical strength members had corroded nearly through in a conical pattern. The fifth wire was only partially attacked and showed a similar annular pattern of attack. The fifth wire had parted due to overload. The copper conductor wires had broken with a cup and cone fracture and the surfaces at the fracture showed a significant amount of uniform corrosion, although the surfaces were not covered with corrosion products. It was surmised that the stainless steel wires had corroded due to either crevice corrosion, galvanic corrosion, or both, and that failure had occurred at a time well before recovery as indicated by the corrosion of the conductor wires at the fractured surfaces.

The electromechanical cable termination at the generator was similar to that which had failed at or near the acoustic beacon. This termination was disassembled four days after retrieval. The cap over the termination of the mechanical portion of the electromechanical cable showed considerable red rust. Underneath the cap the terminations of the strength members of the cable were found to be intact, as shown in Figure 8. However, the stainless steel wires at the termination had nearly corroded through where they passed through the slotted steel termination plate adjacent to the copper alloy pressed fittings. This corrosion of the wires was due to a combination of galvanic and crevice corrosion. The parting of these stainless steel wires at the upper termination of the acoustic beacon can be attributed to a similar combination of deleterious effects.

Condition of Other Array Components -

The bottom-laid 9x5 manila jacketed galvanized steel core grapnel rope was virtually unaffected by exposure. Tensile tests indicated that there was no appreciable loss in tensile strength.

All steel components which were in contact with the bottom sediments showed no significant corrosion.

2. F6F-3 Aircraft

Date of Exposure - January 1944
Date of Recovery - March 1970
Length of Exposure - 26 years 2 months
Location - Southwest of San Diego, California
Water Depth - 560 ftms. (3,350 ft.)
Seawater Characteristics -
    Salinity - 34.5 ppt
    Oxygen Content - 0.5 ml/L
    Temperature - $3.2^{o}C$
    pH - 7.8
Seafloor Soil Characteristics -
    Type - sandy green cohesive mud
    pH of interstitial water - 7.2
Description of Aircraft -
    This aircraft was forced to ditch shortly after takeoff from the Naval Air Station, North Island, San Diego, California. After loss of power the aircraft was landed on a calm sea. The pilot was rescued by a nearby ship before the aircraft sank. The aircraft was essentially intact upon sinking. The structure of this aircraft is typical of combat aircraft of World War II.

Objectives of Evaluation -
Initial newspaper accounts of the recovery of the aircraft indicated that there was practically no deterioration evident after the 26 year exposure. The objective of this inspection was to verify and explain the lack of deterioration of the aircraft.

Results of Evaluation -
Detailed comprehensive visual observations of the aircraft showed that the information published in newspaper accounts of the condition of the aircraft were in serious error. While the aircraft was virtually intact and had sufficient remaining strength to allow recovery, there was considerable deterioration of the aircraft.

The extent of attack on many materials is given in Table 1. The Magnesium alloy components of the aircraft such as the engine crankcase, (Figure 9), wheels (Figure 10) and electrical junction boxes (Figure 11) were more or less completely destroyed by corrosion. The corrosion products of these components were highly basic when mixed with sea water. A saturated solution of the products in sea water had a pH of 10.3. This led to the attack of adjacent aluminum components such as the engine cowling and the wings just above the main landing gear as shown in Figures 12 & 13. Corrosion of these areas was determined to be from the inside out and points out an important fact: the character of sea water in confined areas may be significantly different from its bulk character.

The corrosion of the magnesium parts of the aircraft gave considerable cathodic protection to the rest of the aircraft. This coupled with the protection afforded the aluminum (mainly 24S or 2024) skin of the aircraft by anodizing, chromate priming and top coting, led to the excellent general appearance of the aircraft. However, these protective measures did not eliminate crevice corrosion of the aluminum components of the aircraft. This crevice attack was especially evident along the main wing spar as shown in Figure 14. Such attack was found at all unsealed crevices and had led to some very severe attack. The most insidious feature of such crevice attack is that it generally remains hidden until exposed by failure - a rather unpleasant way to discover a problem.

Crevice corrosion had, in fact lead to the loss of the propeller blades, wing tips (52S or 5052 alloy) and supercharger access hatches (24S or 2024 alloy). Inside the fuselage, several aluminum junction box covers were located which had corroded at much different rates from one another. All were found to be alloy 3S in the 1/2 H condition (or 3003-H14). One cover was almost completely deteriorated, another was moderately attacked and a third was nearly unattacked. This difference cannot be fully explained at this time but was probably due to differences in the condition of the paint coating on the covers prior to exposure.

Both the magnesium and aluminum components were anodic to the low alloy and carbon steel components of the aircraft. The light film of rust on these steel components as exemplified by the canopy frame shown in Figure 15 was formed upon exposure to the atmosphere after recovery. This can be shown by comparison with the view of the canopy shown in Figure 16 taken immediately before the recovery of the aircraft. This effect shows the importance of inspecting objects recovered from the deep ocean as soon as possible after recovery in order to obtain precise information on corrosion attack.

The stainless steel components of the aircraft such as the pitot tube tip and machine gun ammunition ramps were protected by the magnesium, aluminum and steel components. There was however, considerable crevice attack visible on most of the stainless steel compone ts. In fact, a pit over 3/16" deep was found on an 18-8 stainless steel (AISI Type 304) transmitter hold down clamp. This shows again the inadequacy of cathodic protection in preventing crevice corrosion.

Table 1. Corrosion of various materials of construction on F6F-3.

Material	Component	Description of Attack
Magnesium alloy	Engine casting	Nearly complete destruction
Magnesium alloy	Landing wheels	Nearly complete destruction
Magnesium alloy	Electrical junction boxes in wing tips	Nearly complete destruction
Magnesium alloy	Electrical junction boxes in fuselage	Slight crevice attack on one box, others nearly completely destroyed
Aluminum alloy sheet (52S)	Enginge cowling	Many pits to perforation
Aluminum alloy sheet (24S)	Supercharger compartment access cowling	Lost due to crevice corrosion at attachment
Aluminum alloy sheet (24S)	Fuselage skin	Uncorroded except for crevice corrosion at faying surfaces
Aluminum alloy sheet (24S) (severely deformed in manufacture)	Wing tips	Lost due to crevice corrosion at faying surfaces
Mild steel	Canopy frame	Light rusting
Alloy steel (4130)	Engine mount	Light rusting
Galvanized steel	Control wire ropes	Light rust, some broken wires
Stainless steel (304)	Pitot tube tip	No surface attack, crevice attack at faying surfaces
Stainless steel (304)	Ammunition ramps	No surface attack, light crevice corrosion at faying surfaces

Many other miscellaneous alloys were found on the aircraft. 70-30 brass turnbuckle nuts were only lightly dezincified outside but were heavily dezincified inside. Galvanized steel control cables were only lightly attacked outside but crevice corrosion of the inside wires had reduced their strength by half. A type 431 stainless steel spring from the magneto conductors was only lightly attacked except where crevice attack was severe under a deposit of potting compound.

These and other components generally follow the same pattern of cathodic protection and protective coatings reducing general attack but not preventing crevice corrosion.

3. Barking Sands Test Range Hydrophone

Date of Emplacement - June 1967
Date of Retrieval - October 1971
Length of Exposure - 52½ months
Location - South of Kauai, Hawaii
Water Depth - 880 ftms. (5,280 ft.)
Seawater Characteristics -
    Salinity - 34.6 ppt
    Oxygen Content - 2 ml/L
    Temperature - 3°C
    pH - 7.9
Seafloor Soil Characteristics -
    Type - sandy silt
    Analysis - 36% $CaCO_3$, 58% Silicates
Description of Structure -

The hydrophone support structure is approximately 15 feet high and 12 feet in diameter at its base. A sketch of the structure is shown in Figure 17. The structure was constructed from aluminum alloy bar, plate, channel and extruded tubing, and from PVC, steel, and Ni-Cu alloy 400. Spectrochemical analyses of the aluminum components showed that they were Aluminum-Magnesium alloy 5086 which contains nominally 4% Magnesium. Microstructural analysis of polished component sections showed the plate and tube to be in the strain hardened and stabilized condition (H-32) while the channel and bar were in the as extruded condition (H-111). Welds on the aluminum structure were also analyzed and found to conform to the chemical specifications for alloy 5086. Weld deposits of this composition can be obtained by using the filler wire alloy 5356 as specified. Chemical spot tests confirmed that all fasteners were made from Nickel-Copper alloy 400 (67% Ni-33% Cu).

Objectives of Evaluation -

Document condition of the hydrophone support structure.

Determine probable remaining lifetime of other identical support structures in the test range.

Recommend design changes for future similar structures in the test range.

Results of Evaluation -

Condition of the Hydrophone Support Structure -

Virtually no fouling was found on the structure immediately upon recovery. The only fouling noted was a scattered covering of hydroids. These common deep ocean animals have not been shown to affect the corrosion of underlying materials. Traces of these organisms remained on the structure after drying.

Three basic types of corrosion were found on the structure; galvanic corrosion, pitting corrosion and crevice corrosion. Of these, galvanic corrosion caused the most severe damage, pitting attack caused somewhat less severe damage and crevice corrosion, while even less severe from a structural standpoint, caused the most widespread attack.

The most prominent area where galvanic corrosion had occurred was on the counterweight support pan located at the base of the mast. PVC insulators had been used to electrically isolate the painted steel counterweights from the pan. However, this isolation was not complete and there was, as evidenced by the severe galvanic corrosion shown in Figure 18, an electrical connection between the counterweight support, the Ni-Cu fasteners and the painted steel counterweights. This electrical connection was indicated not only by the condition of the support pan but by the lack of significant attack on the counterweights, even at the areas of paint damage. This attack had resulted in complete penetration of the .250" thick pan in over 25 separate places. Some areas of penetration were up to 1/2 square inch in area. This penetration was usually at areas where either crevice or galvanic attack had caused corrosion of the weight pan. Metallographic inspection of sections cut from the counterweight pan showed intergranular attack typical of that found in strain-hardened and stabilized (H-32) 5086 aluminum alloy. The uncorroded material showed a continuous precipitate of Mg_2Al_3 adjacent to the grain boundaries. This precipate is anodic to the surrounding material and its micro-galvanic corrosion leads to intergranular attack of 5000 series aluminum alloys. Such intergranular attack is undesirable from two aspects. First, components subject to intergranular attack usually corrode faster than those subject only to transgranular attack. Second, due to the difficulty in measuring the depth and extent of attack, such measurements are likely to result in conservative evaluation of corrosion damage. The severity of the attack noted on the bottom of the counterweight support pan can also be partially attributed to the exposure of the pan to the bottom sediments which are normally more aggressive to 5086 aluminum alloy than the seawater above.

The other areas of galvanic corrosion on the structure were of a more subtle nature. They were a result of welding. Although the galvanic potential of the weld bead deposited using 5356 welding wire is closely matched with the potential of the 5086 parent material the match is not exact. Also, welding of 5000 series aluminum alloys can result in an area on the parent material adjacent to the weld bead which is anodic to both the weld bead and the unaffected parent material. On this structure, attack of the weld beads and of the adjacent heat-affected zones was noted at all welded joints. The severity of this attack varied from nearly complete deterioration of the welds to etching of the welds with slight deterioration of the adjacent heat affected zones. Figure 19 shows the severe weld attack noted at the yoke pivot. The weld used to attach the boss to the pivot plate is nearly corroded away. Typical weld attack with accelerated attack in the heat affected zone adjacent to the weld bead is shown in Figure 20. Metallographic examinations of joint sections showed that the corrosion of the weld beads was intergranular.

There was a continuous precipitate of Mg_2Al_3 at the grain boundaries of the weld bead. In the heat affected zone adjacent to the weld bead there was a thin layer where Mg_2Al_3 had precipitated adjacent to the grain boundaries to form a continuous network. Intergranular corrosion was noted in this zone. Attack in the heat affected zone of some joints was up to .086" deep.

Pitting attack on boldly exposed areas of some components of the structure resulted in structurally severe damage. The most severely pitted components were the base ring braces and the yoke. Pitting of the base ring braces, as shown in Figure 21, initiated at the edges of the members and had progressed up to 1" into them at several areas. Metallographic inspection of the base ring brace channel and bar did not show any continuous precipitate at the grain boundaries. The corrosion was transgranular. The clips at the ends of the braces where the base ring was attached were also severely corroded as shown in Figure 20. This attack also initiated at the edges of the clips. Metallographic inspection of sections of these clips revealed a continuous network of Mg_2Al_3 precipitated at the grain

boundaries and the usual attendant intergranual attack. The severity of the attack on the base ring braces can be partially attributed to the exposure of the braces to the bottom sediments.

In several areas on the yoke, pitting attack had caused penetration of the .125" thick tube wall. The pits initiated primarily on the outside of the tube but several internal pits were noted. Metallographic inspection of sections from the pitted areas showed intergranular precipitation of Mg_2Al_3 and the usual attendant intergranular corrosion.

At all points on the structure where there were crevices, crevice corrosion was found. In most areas the attack was not severe. However, in other areas the attack was significant. The area most adversely affected by crevice corrosion was the point where the base ring braces were attached to the mast. Even though the crevices at this joint were sealed with room temperature vulcanizing silicone rubber compound some seawater entered the crevices. This resulted in attack such as shown in Figure 22. In this area the attack was up to .095" deep. Metallographic inspection of sections from this area showed that the channel sections at the base-ring-brace to mast joints had corroded transgranularly. The microstructure of the uncorroded material was typical of as extruded (H-111) 5086 aluminum alloy.

Another area where crevice corrosion had resulted in significant damage was under the compound used to cover the welds on the structure. This compound was applied in an attempt to minimize attack at these areas. However, as shown in Figure 20, attack under the compound was more severe than at adjacent areas.

The Nickel-Copper alloy 400 fasteners used to assemble the structure were not significantly attacked. The only attack noted other than a slight tarnish was slight crevice attack under the heads and on the threads of a few fasteners. This attack was structurally insignificant. The PVC base ring and couplings as well as the various non-metallic insulating sleeves and washers used on the structure were not significantly affected by their exposure at depth. Damage to the base ring was mechanical, as was evidenced by the lack of fouling on the damage-exposed surfaces, and probably occurred during recovery.

Probable Remaining Lifetime of Other Identical Support Structures in the Test Range -

The most significantly attacked components were the counterweight support pan and the base-ring braces. The counterweight support pan was penetrated in many places by intergranular galvanic corrosion due to an electrical connection between the steel counterweights and the support pan. The severity of this attack can be expected to at least double in an additional 4 years exposure. Failure of the pan in from 2 to 4 years was predicted. The base-ring braces were also significantly corroded. The 1" penetration of the braces was due to transgranular pitting and was predicted to sever the members in an additional 5 to 7 years exposure. The intergranular pitting on the base ring attachment clips was predicted to sever these connections in from 5 to 7 years. Thus the additional lifetime to be expected from the remaining structures in the array depends primarily upon the overturning moment applied to the structure. If this moment is small, an additional lifetime in excess of 5 years was predicted. However, if this moment is large, the structures were predicted to be subject to overturning in as little as 2 years additional exposure.

These predictions were based primarily on the results of deep ocean corrosion tests performed by CEL. These tests showed that 5086 alloy corrodes differently in the low oxygen environments found at intermediate depths in the Pacific Ocean than it does when exposed to highly oxygenated surface waters. Not only are the corrosion rates higher at depth but they increase with time. The bottom sediments were found to be more aggressive than the seawater just above them. Specimens showing intergranular precipitation and corrosion corroded at a faster rate than those which corroded transgranularly.

85

Recommended Design Changes for Future Similar Structures in the Test Range -
            The lifetimes of similar structures could be increased by several modifications to the existing design.

            1. Complete isolation of dissimilar metals must be achieved. Inspection of assembled structures to assure isolation was recommended.
            2. Elimination of contact between the bottom sediments and any aluminum structural members was recommended.
            3. Elimination, by design, of any unnecessary crevices was recommended.
            4. The continued use of 5086 aluminum alloy as one of the most corrosive resistant aluminum alloys was recommended. However, 5086 alloy in the as extruded (H-111) condition is preferred to other conditions where intergranular precipitation and its associated accelerated attack is possible.
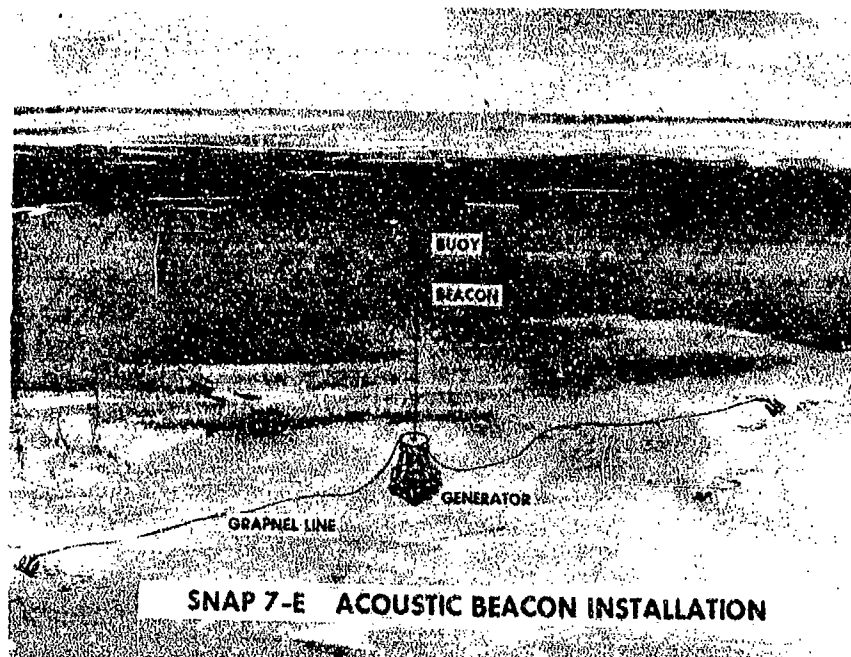
Figure 1.   SNAP 7-E acoustic beacon installation.
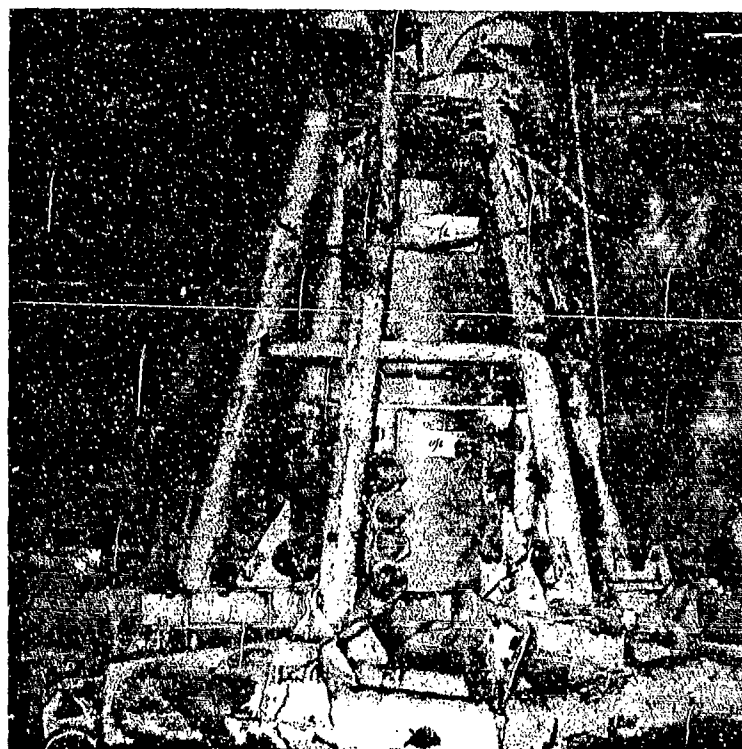
Figure 2.   SNAP 7-E generator capsule in its support
            structure upon retrieval.

Figure 3. Capsule O-ring seal and flange upon disassembly.

Figure 4. Electrical penetrator O-ring seal seat on capsule.
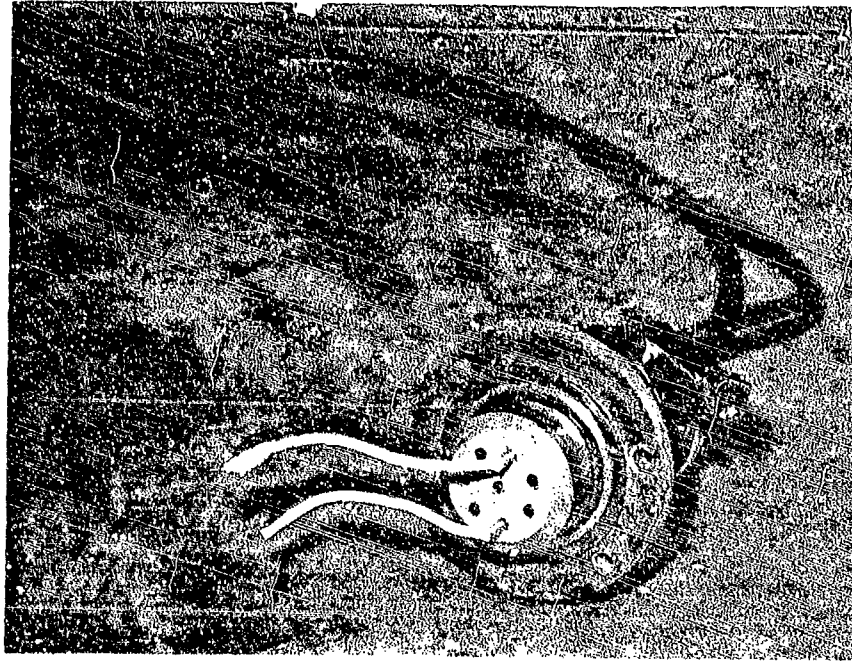
Figure 5. Electrical penetrator O-ring seal flange.
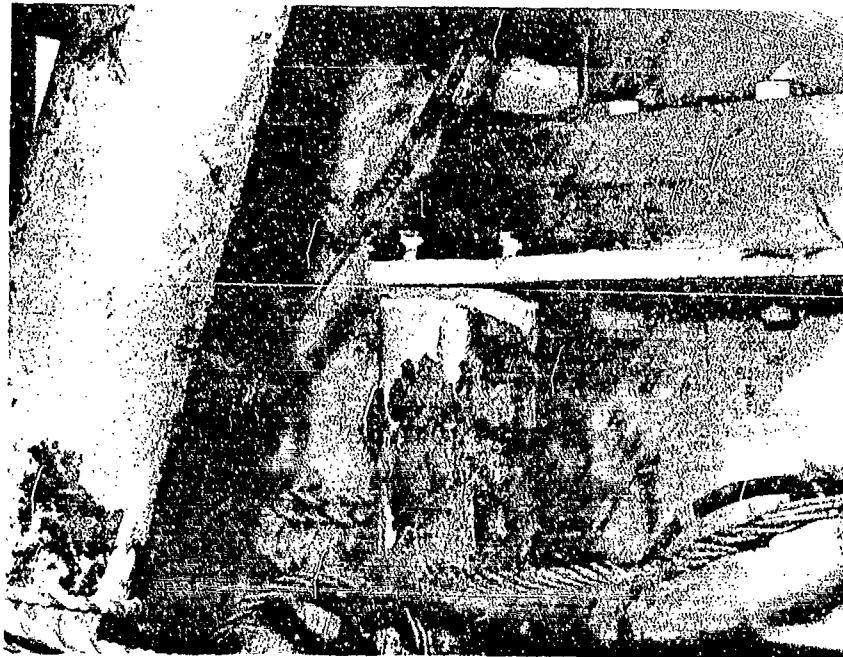

Figure 6. Detail of lifted paint on generator support structure.
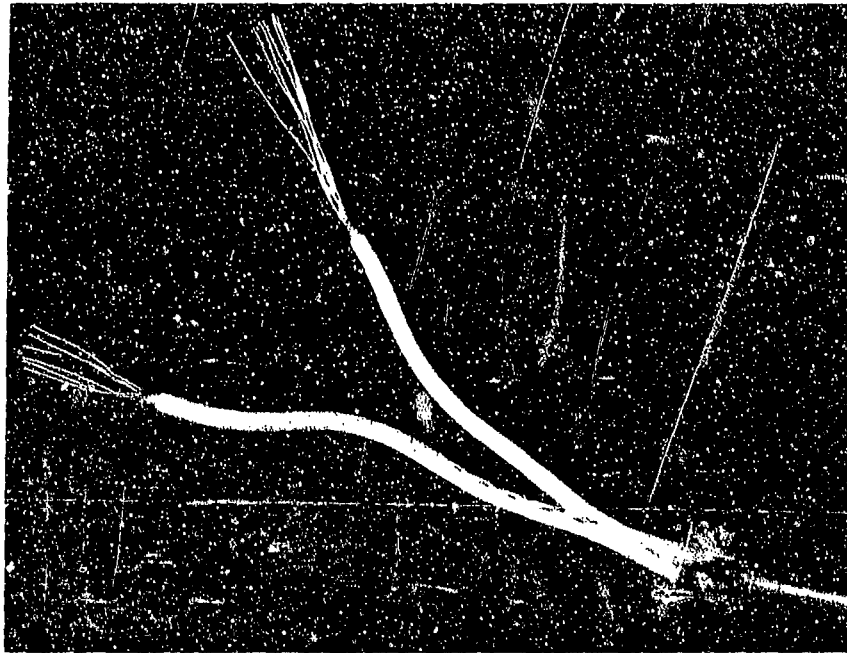
Figure 7. Electromechanical cable at break.

Figure 8. Electromechanical cable termination
at generator structure.

90
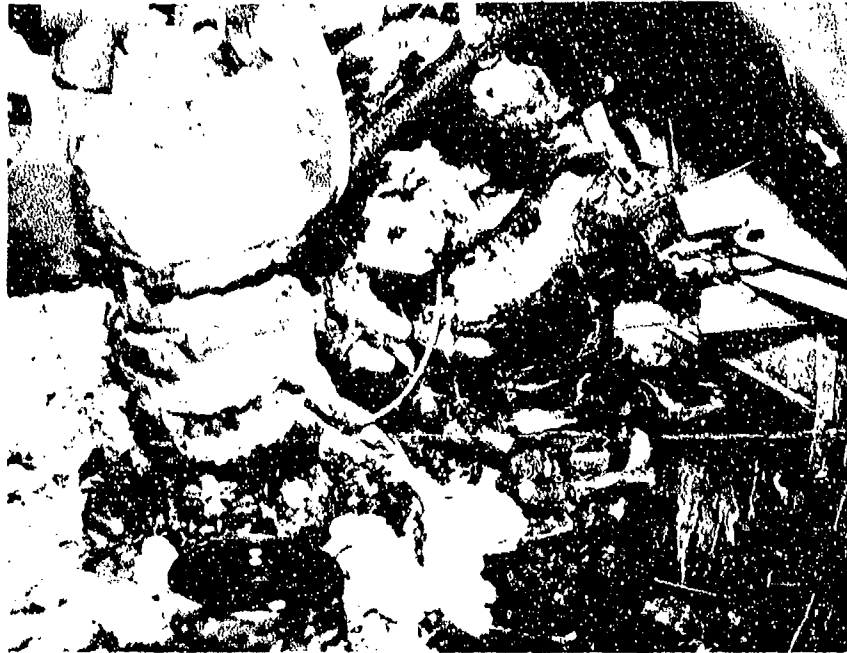
Figure 9.   F6F-3 engine.

Figure 10.   Main landing wheel

Figure 11. Electrical junction box at wing tip.
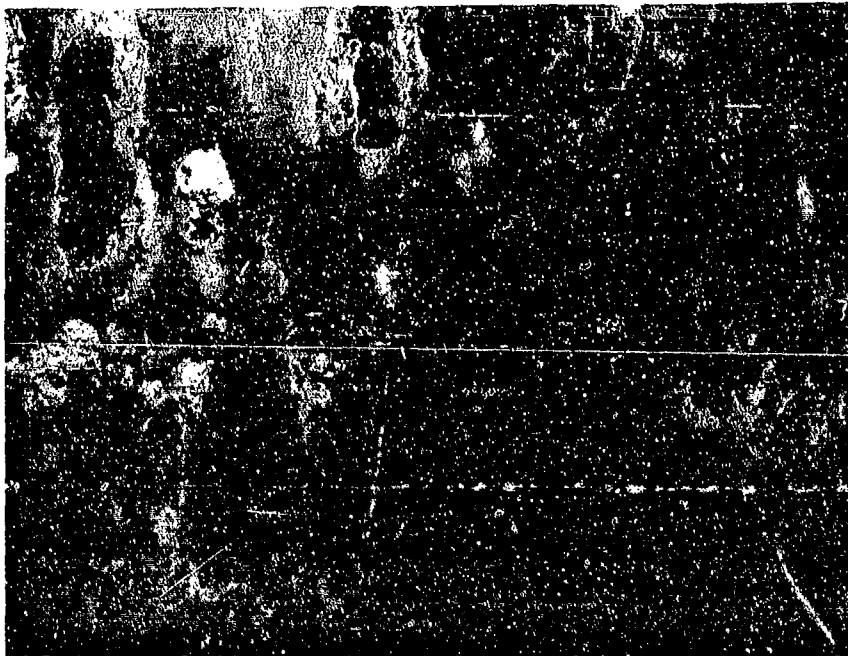
Figure 12. Engine cowling.
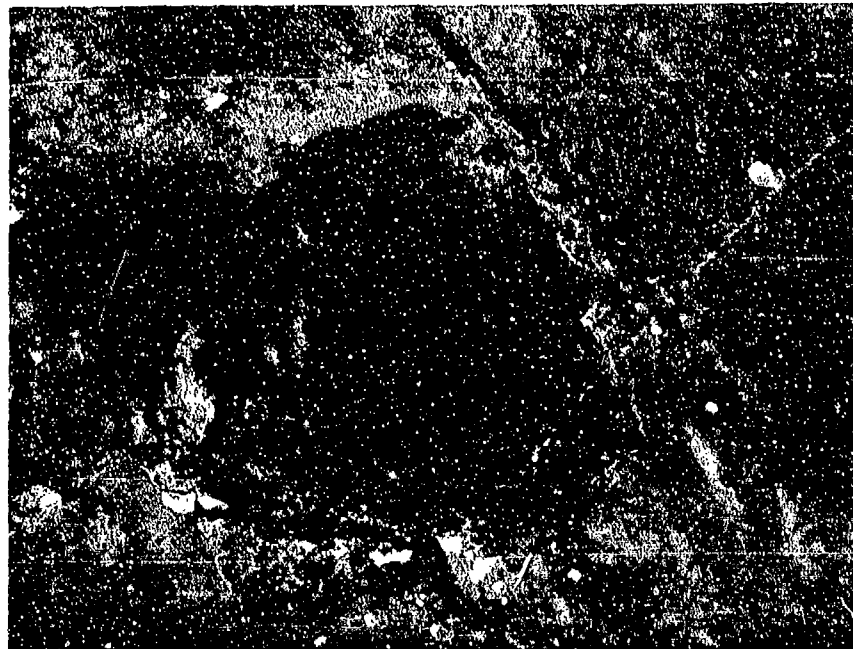
Figure 13.   Wing over main landing gear.

Figure 14.   Crevice corrosion at main wing spar.
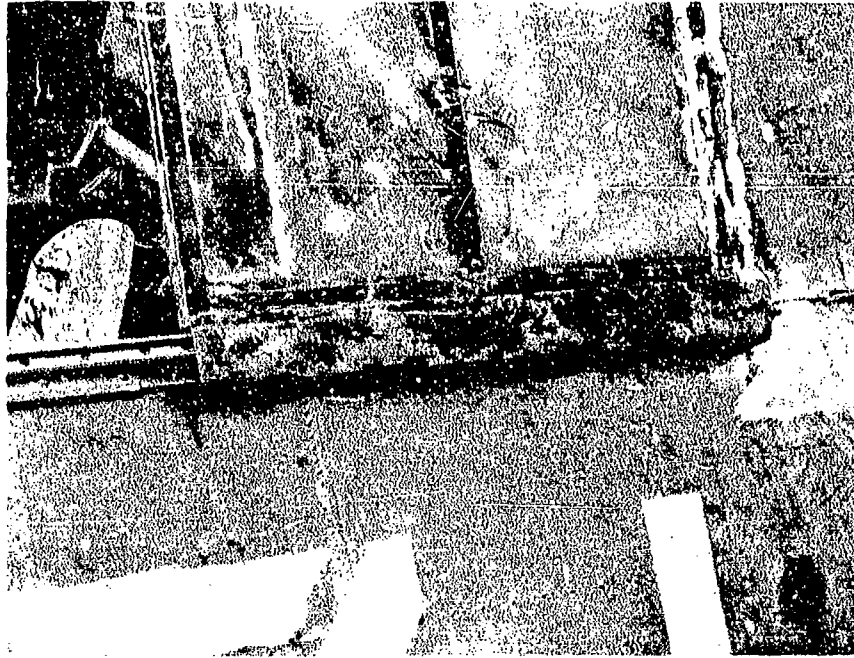
Figure 15. Canopy after retrieval.

Figure 16. Canopy before retrieval.
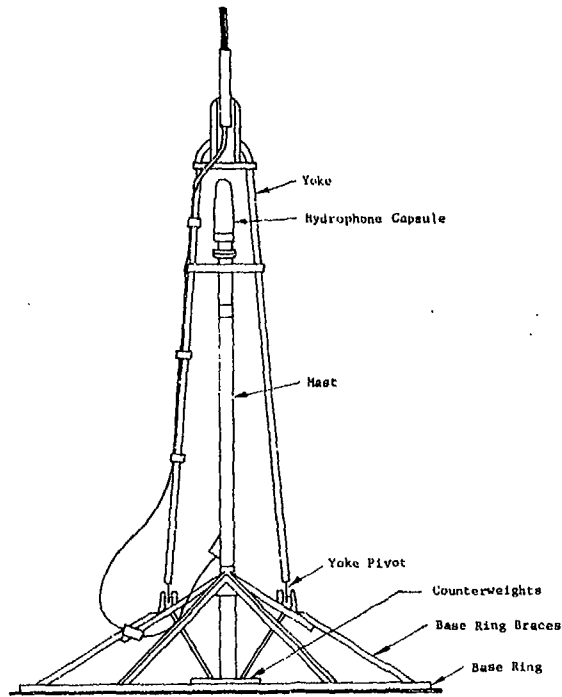
Figure 17.   Sketch of hydrophone support structure.
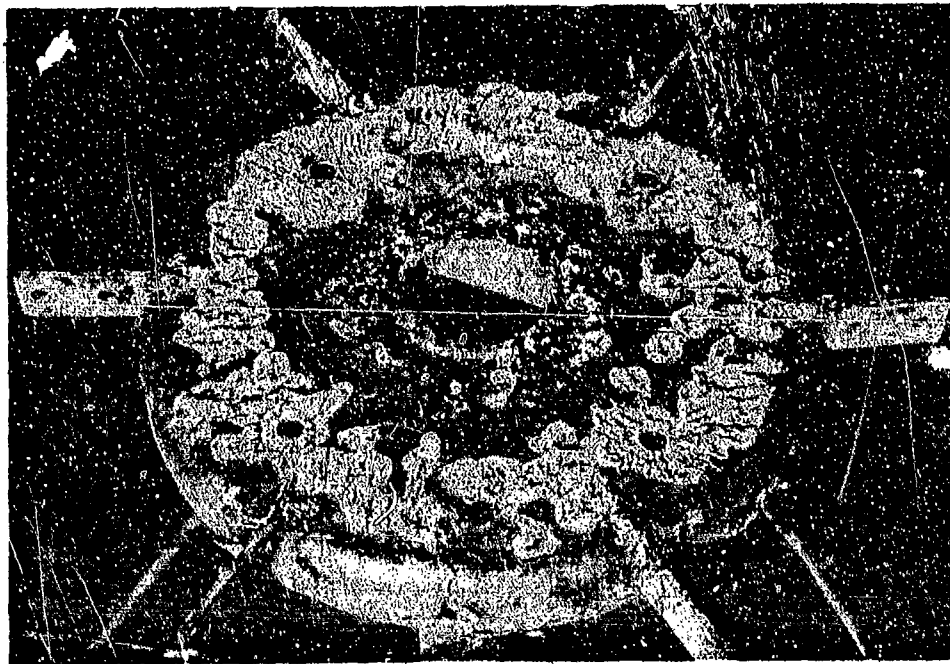
Figure 18.   Galvanic corrosion of counterweight support pan.
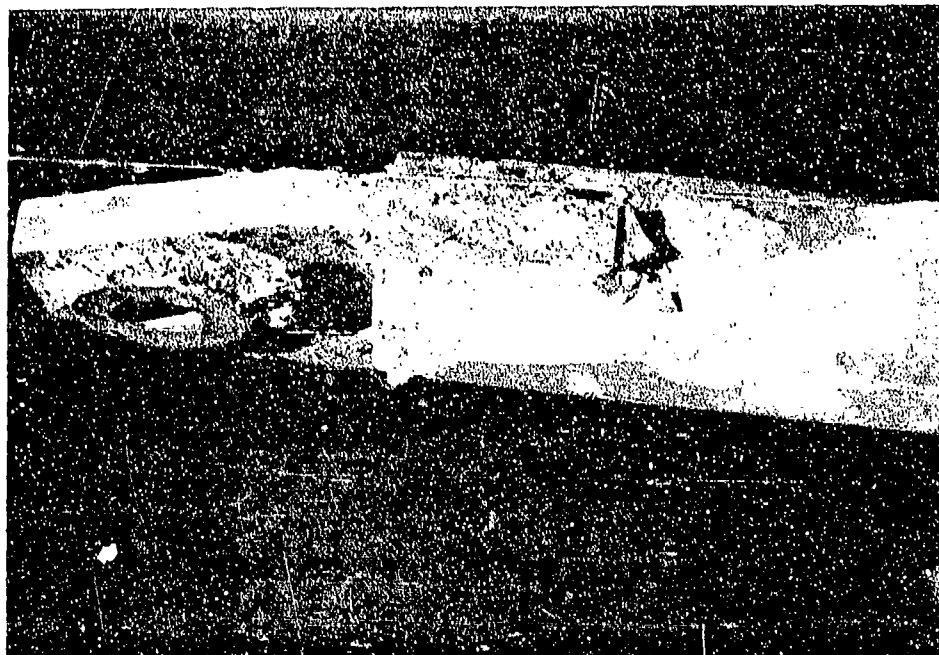
Figure 19.   Weld attack at yoke pivot.

Figure 20.   Weld attack at base ring clip.

Figure 21. Pitting on base ring braces.

Figure 22. Crevice attack on base brace.

ELECTROCOATING OF ALUMINUM COMPONENTS
FOR THE NAVY HARPOON TURBOJET SUSTAINER ENGINE

by

JOHN PRATI
TELEDYNE CAE
TOLEDO, OHIO

ABSTRACT

To provide increased corrosion protection to the aluminum components of the HARPOON turbojet missile engine, an evaluation was made of three electrocoat systems and two anodize systems using a sulfur dioxide (SO_2) salt spray technique to accelerate testing.

Data is presented which shows the superior corrosion resistance of a polyester electrocoat based on the SO_2 salt spray tests. Also presented are results of the polyester electrocoated aluminum components after the engine was exposed to seven months aboard a destroyer and twelve months under an aircraft wing.

INTRODUCTION

The sustainer engine, Teledyne CAE Model J402-CA-400, for the HARPOON missile systems was designed to be a low cost, short life, expendable turbojet, Figure 1. [1] [2]* In addition, one of the major design objectives was that the engine have a five-year storage life in humid and marine environments. To meet this design objective, Teledyne CAE selected materials with inherent corrosion resistance, rather than less resistant materials with protective coatings. One exception was the use of investment cast C355 aluminum on the air inlet duct and stator housing, because of the resulting weight advantage and the component complexity, Figure 2. Although the aluminum castings have some corrosion resistance, these components are given the added protection of electrocoat polyester coating to enhance the five years' storage life which is the subject of this paper.

PROGRAM BACKGROUND

Initially, a sulfuric acid anodize, dichromate sealed, protective coating was selected for the aluminum castings. But early in the engine development program, it was discovered that the residue from the two cartridges used to start the engine was extremely corrosive. Multiple firings of the cartridge during engine starting cycle development severely pitted and corroded all anodize surfaces exposed to the cartridge residue, Figure 3. The residue's corrosive nature was accelerated by high humidities. The corrosive agent in the residue was suspected to be sodium oxide which, when combined with the humidity in the air, formed sodium hydroxide. Since engine acceptance test, which is performed prior

---

* Numbers in parentheses designate references at the end of the paper.

Preceding Page Blank

to storing the missile, contractually required the use of starter cartridges, the corrosive nature of the cartridge residue imposed an additional environmental requirement on the five-year storage goal.

As an alternate approach, spray painting of the castings was evaluated as to its ability to provide protection from both the marine environment and the starter cartridge residue. Achieving a uniform coating by conventional and/or electrostatic spray painting of the stator housing and vanes, Figure 4, was found to be extremely difficult because of the back-to-back position of the two rows of stator vanes which are only separated by approximately 0.060 inch.

When the electrostatic spray process was tested, the deep recessed corners did not coat because of the "Faraday" effect.* A uniform and controlled coating thickness on the vanes is necessary to prevent changes in airfoil shape. A thickness in excess of 0.001 inch tends to choke the engine; for example, a 0.002 inch coating on both sides of 44 vanes represents a 0.176 inch (0.002 inch x two sides x 44 vanes) restriction to the annular flowpath and is equivalent to adding an additional vane. These requirements of a uniform coating and a 0.001 inch maximum thickness build-up on an intricately shaped part led to the evaluation of electrocoatings. Electrocoating has been used in high volume applications in the automobile and appliance industries for many years. Currently, the process is also being used on unique applications requiring a uniform thickness on complicated shapes.

DESCRIPTION OF COATING SYSTEMS

Five protective treatment systems were evaluated for use on the aluminum components and are described in the following sections.

ELECTROCOATING SYSTEM

Electrocoating is similar to plating. The part to be coated is immersed in an electrically charged, water soluable paint bath. The bath, or solution, consists of 5 to 20 percent paint solids in the form of paint resin and paint pigment and 80 to 95 percent de-ionized water with small amounts of solvent and solubilizer. The electric current causes the organic paint resin to deposit on the part. As the resin builds up to a critical thickness, that area becomes insulated, preventing further build-up. Thus, as the exposed surface becomes insulated, resin is deposited on the corners and deep recesses of the part, producing the required uniform coating. Deposition of the resin coating on the part is the result of four distinct reactions which occur simultaneously. They are electrophoresis, electrolysis, electro-osmosis, and polarization. (3)

Briefly, electrophoresis is the movement of colloidal materials dispersed in a liquid medium under the influence of voltage. Electrolysis is the disassociation and movement of ions, in this case the movement of paint solids suspended in the bath. Electro-osmosis, which is the reverse of electrophoresis,

_____

* A charged particle will take the shortest path to an oppositely charged surface.

is the movement of the liquid phase under the influence of voltage. Electroosmosis is the process that forces water from the deposited film coating. The paint film exiting from the bath is between 85 and 95 percent solids.

Polarization is the ability of the deposited film to exhibit electrical resistance. The polarization reaction is the force which makes the film self-insulating, and thus limits the coating action at a certain level to give an exact uniform covering and precise thickness control.

A typical flow chart for the electrocoating of an aluminum part is shown in Figure 5. The first step is a cleaning procedure that removes general dirt and machining oils. The second step is a deoxidize and desmut procedure that chemically cleans the surface of the aluminum part. The third step is a deionized water rinse that reduces carry over of contaminates to the electrocoat bath. The fourth step is the electrocoating, which generally requires one to two minutes to completely coat all wetted surfaces. The part is then rinsed to remove the excess paint clinging to the surface after coating. This may or may not be followed by air drying, depending on the specific paint formula. The final step is a 300 to 400°F cure bake that polerizes the organic resin.

The normal thickness range for electrocoating is 0.0005 inch to 0.002 inch with most coatings about 0.001 inch thick. Under high magnification, the uncured electrodeposited paint has a spongy appearance. During the cure cycle, the coating flows and coalesces to produce the surface gloss. [4] This flow causes the coating to draw away from the edges causing local reduction in film thickness to 0.003 inch at sharp edges.

In addition to providing a reasonably uniform coating, the anodic electrocoating of aluminum results in the simultaneous anodizing and painting of the work because of the applied electric field. This anodize conversion coating is one of the factors that provide good corrosion protection. [4] Additional advantages are that the process reduces labor costs, and when compared to conventional spray processes, reduces required operator skill. Being a low solvent, water base system, electrocoating eliminates most environmental pollution problems. Some of the limitations of electrocoating, as well as a summary of its major advantages and disadvantages, are given in Table I.

The electrocoat paint manufacturers were contacted for assistance in selecting a coating which would meet the following requirements:

    a. Resistant to sea water and humidity (5-year corrosion resistance life).
    b. Capable of surface build-up to approximately 0.001 inch.
    c. Hardness for erosion and chip resistance.
    d. Operational in -60°F to 165°F environment.
    e. Corrosion resistant to highly basic starter cartridge residue.

Three electrocoat coatings were evaluated: a polyester produced by E. I. duPont; an epoxy produced by PPG Industries; and an enamel produced by Standard T.

ANODIZE SYSTEMS

Two anodize systems were evaluated: a standard dichromate sealed sulfuric acid anodize per AMS 2471; and a new duplex seal anodize developed by Lockheed. Testing on AA7075 and 2024 aluminum panels by Lockheed has shown that the duplex seal anodize is capable of providing 2,100 to 14,000 hours' life in a 5 percent salt spray. This salt spray life represents a significant increase in corrosion protection when compared to the standard dichromate sealed sulfuric acid anodize.

TEST PROCEDURE

A new sulfur dioxide (SO_2) salt spray technique was used to evaluate and select the final aluminum protective finishing system. This new technique was developed by the Naval Air Development Center. Naval experience on land and shipboard has revealed that sulfur in the form of oxides, created by ship propulsion systems and by industrial air pollution, causes an increased corrosion of aluminum in marine environments. To simulate this environment. SO_2 gas is included in a normal 5 percent salt spray test. The schedule for the introduction of SO_2 is one hour for each six hours of testing, at a rate of 25 cc/min. Some of the SO_2 combines with water to form sulfurous and/or sulfuric acid, thereby accelerating the testing. Although severe, the procedure accelerated testing while simulating the environmental exposure.[7] At the present time, a correlation between the SO_2 salt spray technique and a standard 5 percent salt spray test has not been established.

To be representative of actual engine hardware, test panels were made from C355-T-61 cast aluminum air inlet ducts from the HARPOON engine. The outer diameter of the duct was cut into quarters. Fifteen panels were cleaned and then three of each were treated with one of the five protective finishes. Each panel was then scribed with an "X" through the coating to bare metal. All fifteen panels were then submitted to the Naval Air Development Center, Warminster, Pennsylvania, for SO_2 salt spray testing for 30 to 45 days.

TEST RESULTS

The following is a description of the results obtained after 30 days testing. Since four of five coatings evaluated failed after 30 days testing, further SO_2 salt spray testing was not conducted.

POLYESTER COATING

The E. I. duPont "370-010 Line" polyester coating provided the best protection of the five finishes evaluated. Figure 6 shows the condition of a coated panel after 7, 14, 21 and 30 days testing. For clarity, a montage photograph of only one of the three panels is shown for all five systems. Considering the severity of the tests, the polyester coating provided excellent corrosion protection. In general, the only areas showing coating deterioration were at the scribed lines and at the sharp edges of the panels. The deterioration in the form of small and scattered blisters was present after 7 days. The blisters increased in size and number as the testing progressed to the 30th day as shown in the last view.

102

Based on its superior corrosion resistance, the electrocoat polyester coating was selected for use on the HARPOON YJ402 and J402 engines.

EPOXY COATING

The PPG Industries "Cationic Power Prime AN6EP322" is an epoxy system in which the coating occurs on the cathode side of an electric cell. In a normal electrocoat set-up, the part is the anode. The condition of one coated panel after 7, 14, 21 and 30 days is shown in Figure 7. After the first 7 days of testing, one of the three panels, not shown in Figure 7, developed localized areas of heavy blistering. As the testing progressed, all of the panels developed heavy blisters. It is possible that modifications to the pre-cleaning procedure would eliminate the blistering; however, due to the excellent results obtained with the polyester coating, no further development was planned for this system.

ENAMEL COATING

Figure 8 shows the condition of the Standard T Chemical Company "217-984 Electrolox Black Enamel" after 7, 14 and 21 days testing. The coating provided protection for 7 days' testing, although some undercutting along the scribe line and vibropeened identification marks were evident. After 14 days' testing, the panels had developed a wrinkled condition, similar to the condition produced by a brush paint stripper. Because of the poor condition of the enamel, testing was terminated after 21 days.

DICHROMATE SEALED SULFURIC ACID ANODIZE AND DUPLEX SEALED ANODIZE

Figures 9 and 10 show the condition of the sulfuric acid anodize (per AMS 2471) and the Lockheed developed duplex sealed anodize panels after 7, 14, 21 and 30 days testing. Both anodize systems developed a few shallow pits after three days of testing. As the testing progressed, the panels showed more and larger pits. Although pitting did occur, both anodize systems provided protection until they failed between the 21st and 30th day of testing. The duplex seal anodize system appeared to provide slightly more protection than sulfuric acid anodize after 30 days' exposure. However, the duplex seal anodize did not provide the corrosion protection obtained with the electrocoat polyester coating, Figure 6.

EVALUATION OF SEA AND AIR TRIAL STORAGE ENGINES

As a preliminary evaluation of the corrosion resistance in a real world environment, development engines were tested by storing for six to twelve months in a simulated missile case. The case, Figure 11, was essentially a closed metal tube with a hole in the bottom to simulate the openings that would be present on an actual missile case. Aerodynamic fairings were added to the aircraft container. Storage tests were conducted on aircraft and shipboard installations. These tests were not to be considered as proof or as qualification tests, but rather as diagnostic type tests to provide engineering data on the corrosion susceptibility. To gain some data on the long term effects of the starter cartridge residue, the engine scheduled for twelve month testing was started using a full set of cartridges during initial acceptance test.

The stator housing and air inlet duct on storage engines were protected with the polyester electrocoat. The following observations were made on the storage engines after exposure to the environments described.

SEVEN MONTH SHIPBOARD EXPOSURE

Although the initial test plan was scheduled for a six-month test, this engine was subjected to seven months' exposure onboard the destroyer U.S.S. Reasoner based at Subic Bay in the Philippines. Initially, the engine was stored in a simulated missile container which was contained in a storage box mounted on the destroyer deck. A few days into the voyage, while enroute from San Diego to Hawaii, the storage box was damaged by high seas. In Hawaii, the storage box was discarded and the simulated missile container was mounted directly to the destroyer rear deck, where it remained for the duration of the exposure test period. During the exposure period, the destroyer was based primarily at Subic Bay with visits to ports in Taiwan, Singapore, Hong King, Ceylon, Austrailia, New Zealand and Tahiti.

After seven months, the polyester electrocoated stator and air inlet duct were in good condition with no deterioration occurring on airflow surfaces, Figure 12. Some minor deterioration had occurred in four exterior locations, Figure 13.

First, some creepage (undercutting) and pitting had occurred around the five mounting pin holes. Corrosion had also occurred on the mounting pins and in the mounting pin holes, which were not coated because of strict tolerance control. Since the holes cannot be painted, it has been recommended that a sealant be used during the installation of the mounting pins to prevent this type of deterioration.

Second, a 3/4 inch diameter spot of coating under the flexible fuel line had failed. The damage was initiated by a mechanical abrading of the coating by the braid wire on the fuel line. It was discovered that the flexible section of all fuel lines had been manufactured one-half inch shorter than designed. Correction of this error has eliminated the wear spot.

The third area of deterioration occurred under the starter cartridge gasket. Analysis revealed that the gasket was not making a complete seal because of insufficient clamping force and incomplete machining of the case boss. To provide proper sealing, RTV silicon rubber is now applied to the joint prior to installation of the cartridge.

The final area of deterioration was a small spot on the fuel line mounting boss. To prevent this type deterioration, all fasteners are now being sprayed with a corrosion preventative compound, MIL-C-81309, after acceptance testing.

TWELVE MONTH AIRCRAFT EXPOSURE

The second engine was stored under the wing of a P-3B aircraft for 12 months. The aircraft accumulated 390 hours, including 175 landings and 16 touch-and-goes. The aircraft, initially based at Key West, Florida, was re-assigned to

Naval Air Station at Patuxent River, Maryland.

The stator housing was in excellent condition from a corrosion standpoint, but had been damaged by the lockwashers and by the short flexible fuel line cutting into the aluminum, Figure 14. The lockwashers have now been replaced by flat washers. A light rub on the axial compressor shroud, which occurred during the initial test, had been touched up with an epoxy paint and was in excellent condition.

The inlet duct was also in like-new condition, except some deterioration had occurred under the alternator strut gasket, Figure 15. This alternator strut has been eliminated from the production engine.

This engine was cartridge started during engine acceptance testing. Although no deterioration was observed on the electrocoated stator housing which was exposed to the cartridge residue, the cast 17-4 Precipitation Hardening Stainless Steel (PHSS) radial compressor rotor was severely corroded. This corrosion was attributed solely to the cartridge residue, since the cast 17-4 PHSS axial compressor, which was not exposed to the residue, was not corroded. Efforts are being made to eliminate the contractual requirement on the use of cartridges for acceptance test.

SUMMARY

The use of E. I. duPont polyester electrocoating is an effective process for providing uniform corrosion protection treatment to complex shaped parts.

The SO_2 Salt Spray testing technique was an effective accelerated method of evaluating corrosion protective treatments. This testing established that the polyester electrocoating provided better corrosion protection than both the duplex sealed and dichromate sealed, sulfuric acid anodize systems.

The evaluation of the storage engine after seven and twelve month exposure has shown that the polyester coating selected for use on the aluminum HARPOON components provided corrosion protection in marine and tropical environments. Some minor material deterioration was observed on exterior surfaces but modifications have been implemented to correct these problems. The storage evaluation has also shown that the residue from the starter cartridge used during engine acceptance testing is corrosive to the 17-4 PH radial compressor but not to the electrocoated aluminum components.

REFERENCES

1. Kidd, W. E., "Turbine Powerplants for Missiles", SAE No. 730364, April 1973.

2. Rogo, Casimir, and Trauth, Richard L., "Design of High Heat Release Slinger Combustor with Rapid Acceleration Requirement", SAE No. 740167, February 1974.

3. Warren, S. C., "Electrocoating High Production Painting Method", Automation, April 1970.

4. Petropoulos, J. C., and Blank, W. J., "A True-False Quiz on Electrocoating", Products Finishing, November 1973.

5. Hutchinson, C. O., "Painting with Electricity Speeds Production, Lowers Costs, Improves the Finish", Metal Progress, June 1968.

6. Saad, K. I., "How to Prepare Metal Surfaces for Electropainting", Products Finishing, May 1969.

7. Brown, S., Goldberg, S., and Shaffer, I., "Optimum Corrosion Protective Finishing Systems for Aluminum Alloys Used in Naval Aircraft", paper presented at 1972 Tri-Service Conference on Corrosion, Houston, Texas, December 1972.

TABLE I

SUMMARY OF THE ADVANTAGES AND DISADVANTAGES OF ELECTROCOATING ALUMINUM*

ADVANTAGES

Good Corrosion Resistance

Uniform Thickness on Complex Parts

Complete Coverage of all Paint Wetted Surfaces

Process Simultaneously Anodizes and Paints (Anodic Process)

Eliminates Runs, Sags and Tears

Reduces Labor Costs

Reduces Required Operator Skill Compared to Spray Process

Eliminates Most Environmental Pollution Problems

Applicable to High Volume Production

Good Paint Utilization

DISADVANTAGES

Work must be Electrically Conductive

Requires Capital Equipment

Requires 300 to 400°F Cure Cycle

Normally Requires the Use of Large Paint Volume

Color Change Difficult

Application of a Second Coat by Electrocoat Process Very Difficult

"Deplates" Surface Dirt to Paint Surface Causing Staining of Light Colors

* References (3), (4), (5) and (6)

T-20108

29.25
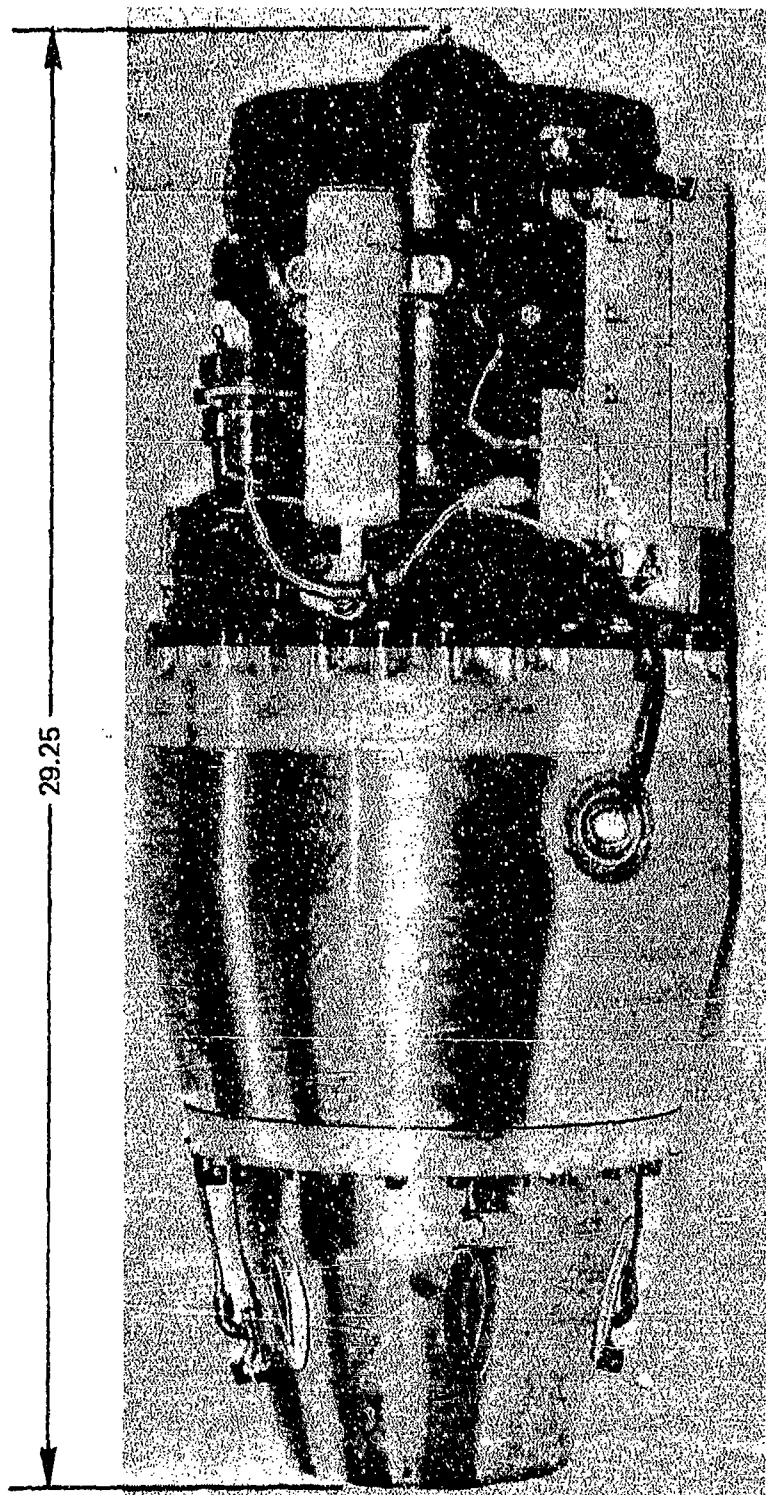
Figure 1. Teledyne CAE J402-CA-400 Turbojet Used to Propel the Navy Harpoon Missile.
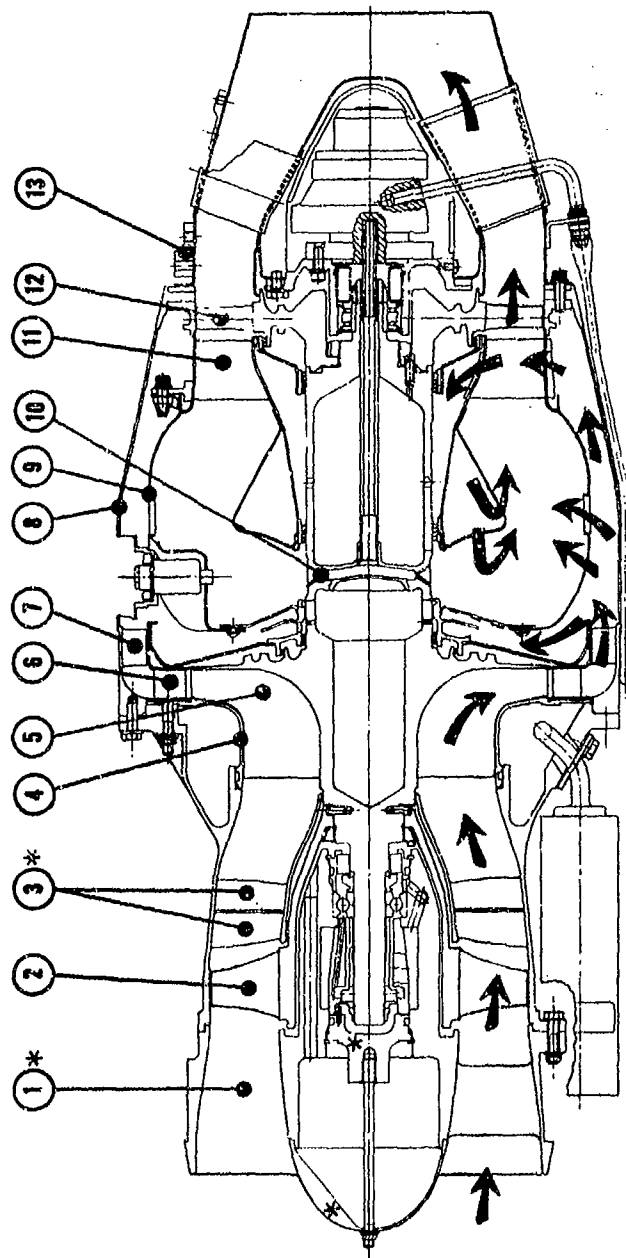
COMPONENT	MATERIAL
1. AIR INLET HOUSING*	C355
2. AXIAL COMPRESSOR ROTOR	CAST 17-4 PH
3. STATOR HOUSING*	L355
4. RADIAL COMPRESSOR SHROUD	CAST 17-4PH
5. RADIAL COMPRESSOR - ROTOR	CAST 17-4 PH
6. RADIAL DIFFUSER	N-155
7. AXIAL DIFFUSER	CAST INCO 718

COMPONENT	MATERIAL
8. COMBUSTOR HOUSING	INCO 718
9. COMBUSTOR SHELL	N-155
10. FUEL SLINGER	17-4 PH
11. TURBINE INLET NOZZLE	N-155
12. AXIAL TURBINE	INCO 100
13. EXHAUST DUCT WITH INTEGRAL NOZZLE	N-155

14121

Figure 2. Cross Section of Harpoon Engine Major Components and Flowpath. Those Components Marked With an Asterisk are Polyester Coated.
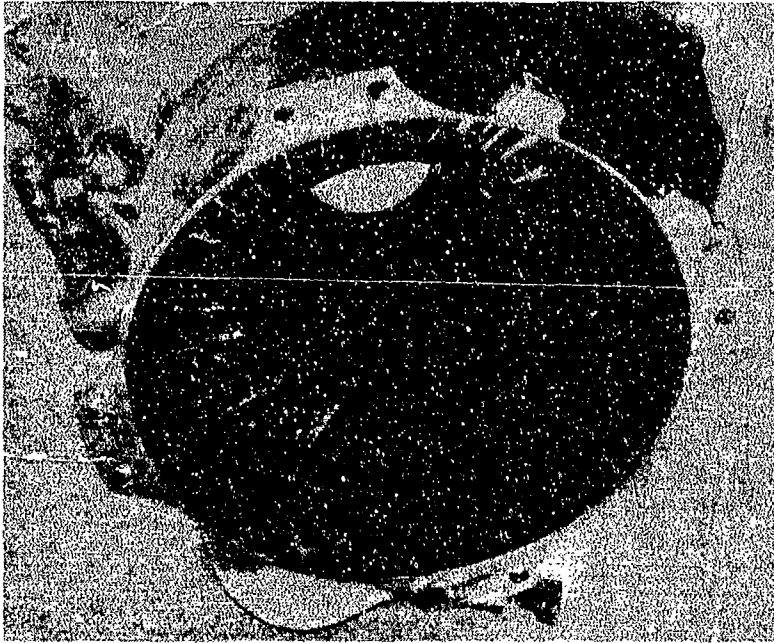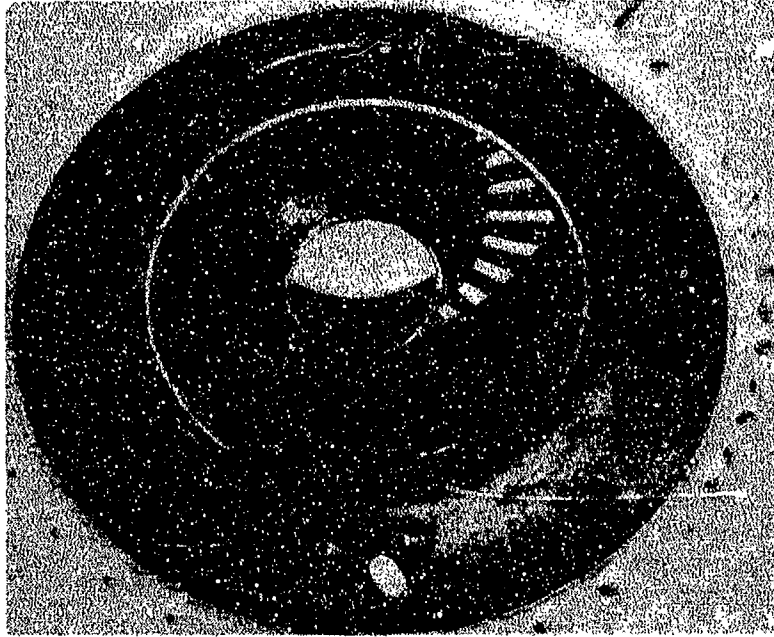
T-8800

Exhaust Side

T-8801

Inlet Side

Figure 3. Corrosion of a Stator Housing Caused by Starter Cartridge Residue. Aluminum Housing was Sulfuric Acid Anodize, Dichromate Sealed.

110

Stator Vanes

12.20"

0.060"

8.26"
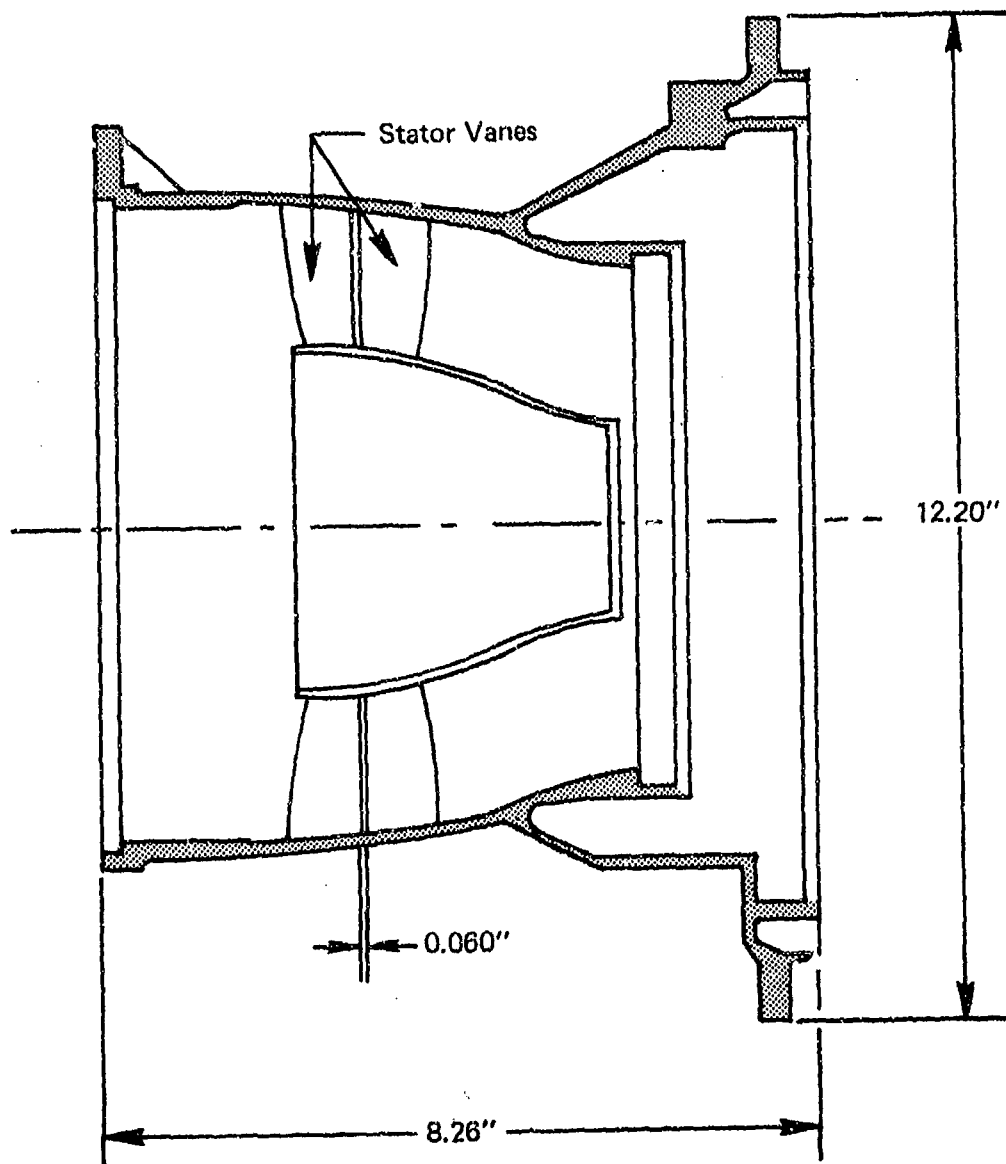
14119

Figure 4.   Cross Section of Stator Housing Showing the Position of the Two Rows of
Stator Vanes.

111
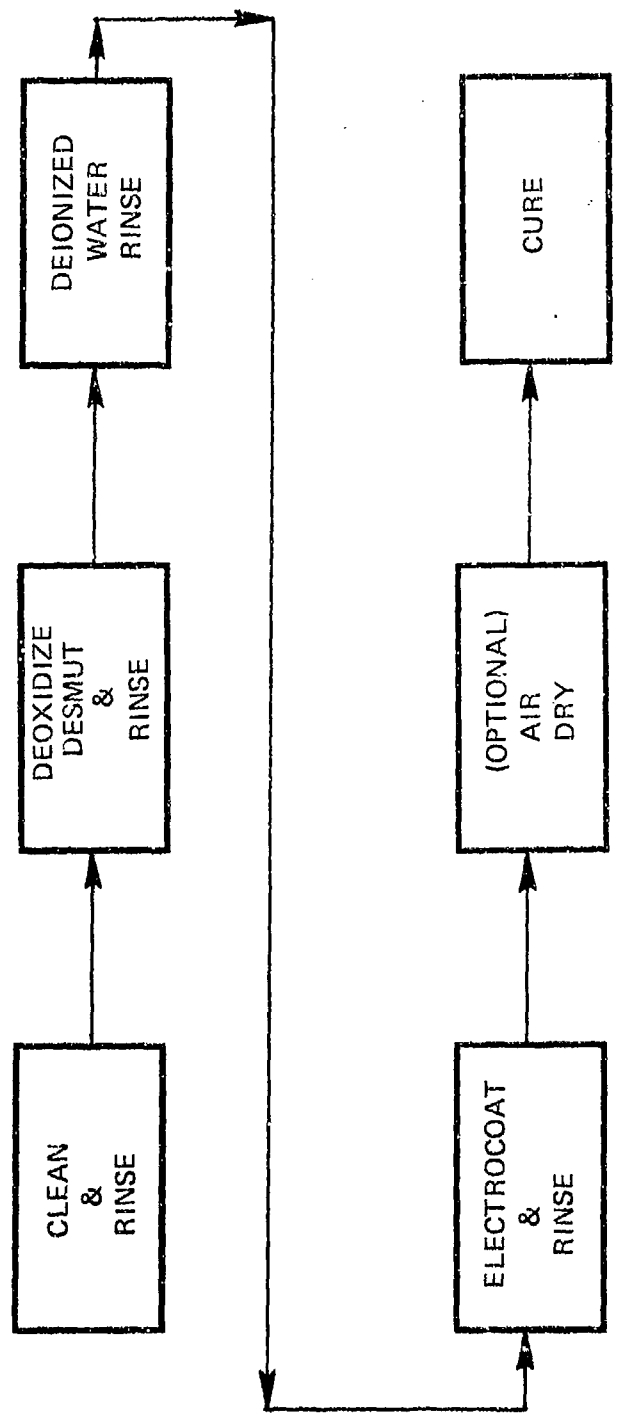
Figure 5. Typical Flow Chart for Electrocoat Processing an Aluminum Component.

14120
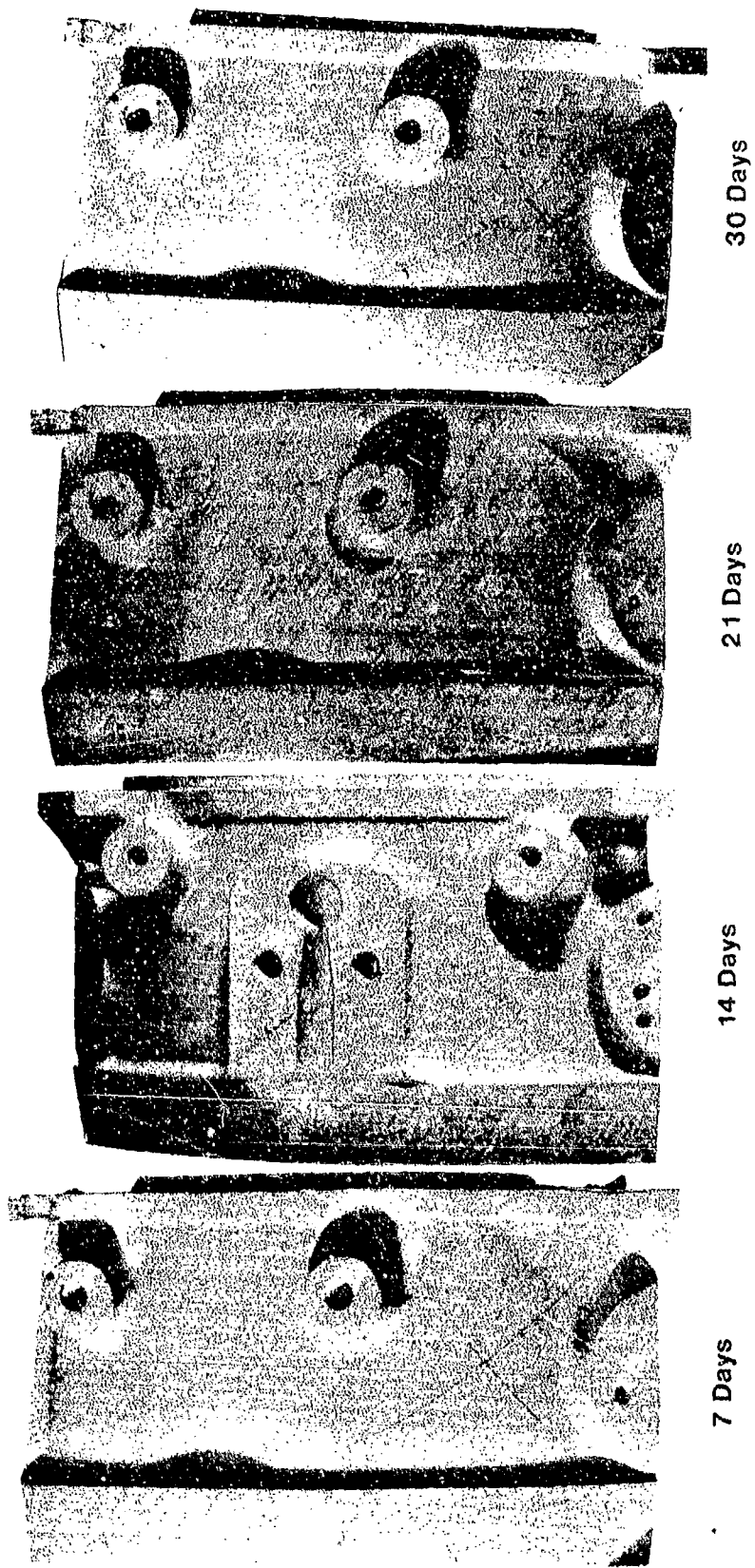
Figure 6. Cast C-355-T61 Aluminum Test Panel After Indicated Exposure to SO$_2$ Salt Spray. Electrocoating: E.I. duPont #370-010 Polyester. Thickness 0.0008 Inch.

7 Days   14 Days   21 Days   30 Days

113

7 Days   **14 Days**   **21 Days**   **30 Days**

Figure 7. Cast C-355-T61 Aluminum Test Panel After Indicated Exposure to SO2 Salt Spray. Electrocoating: PPG Industries #ZN6EP323 Cationic Power Prime Epoxy. Thickness 0.001 to 0.0012 Inch.

Not Tested
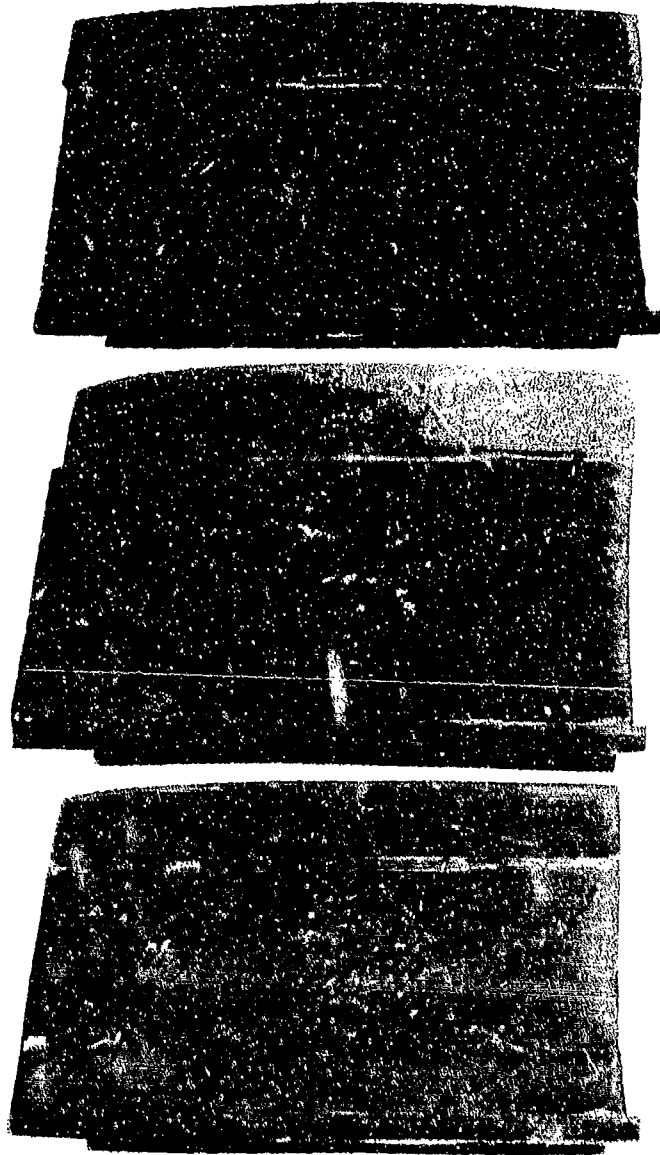
7 Days   14 Days   21 Days   30 Days

Figure 8. Cast C-355-T61 Aluminum Test Panel After Indicated Exposure to SO_2 Salt Spray. Electro-coating: Standard T Chemical #217-984 Electrolox Black Enamel. Thickness: 0.0005 to 0.0006 Inch.
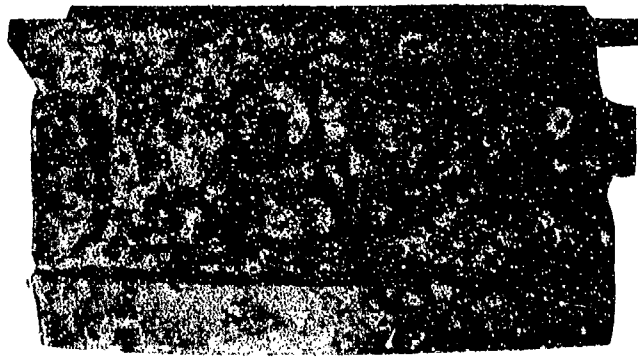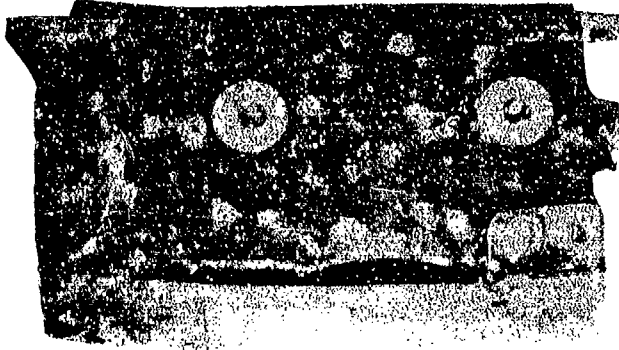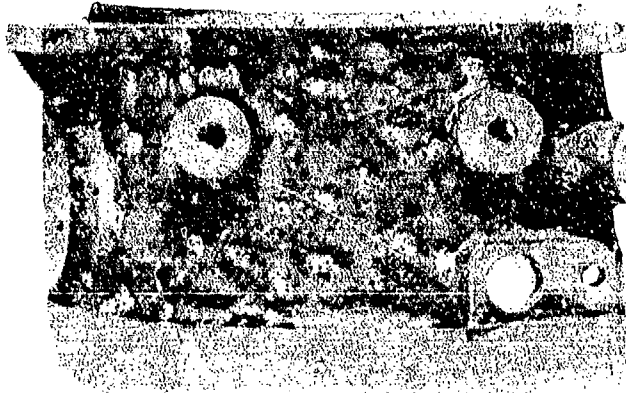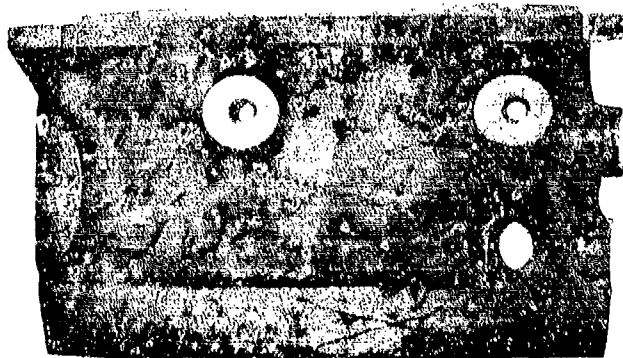
7 Days   14 Days   21 Days   30 Days

Figure 9. Cast C-355-T61 Aluminum Test Panel After Indicated Exposure to SO₂ Salt Spray. Anodize: Dichromate Sealed Sulfuric Acid per AMS 2471.
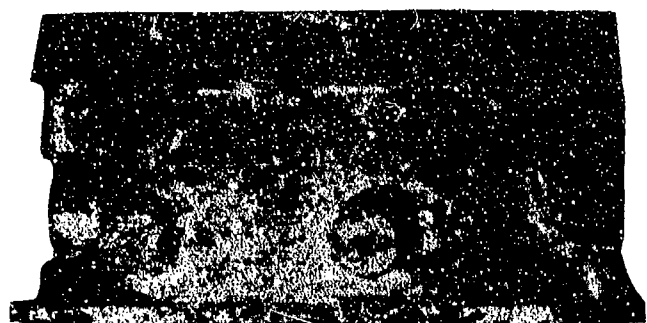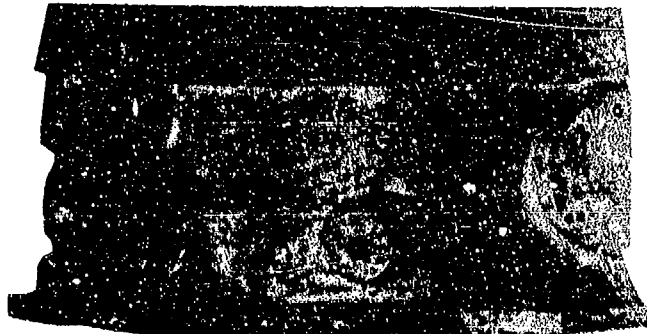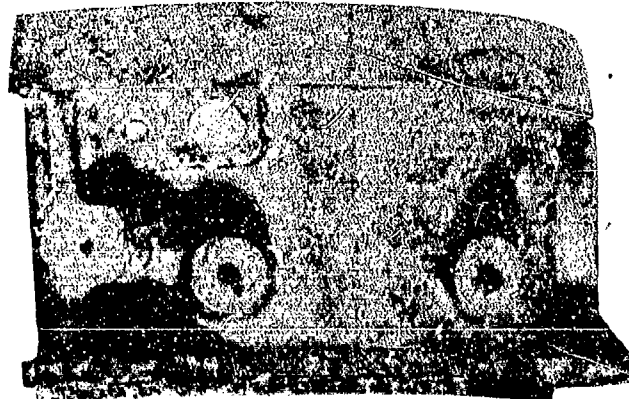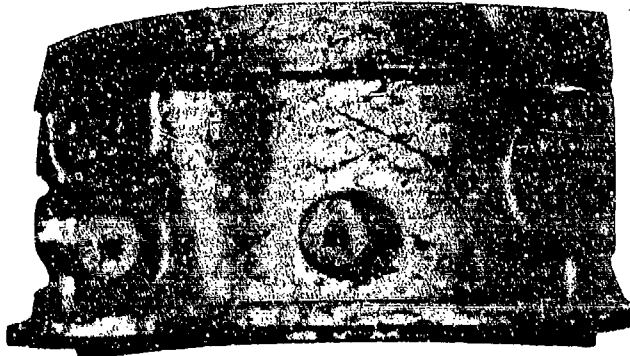
7 Days   14 Days   21 Days   30 Days

Figure 10. Cast C-355-T61 Aluminum Test Panel After Indicated Exposure to SO2 Salt Spray. Anodize: Duplex Seal by Lockheed Corporation Proprietary Process.

AERODYNAMIC
FAIRING

MOUNTING RING

BREATHER HOLE

14122
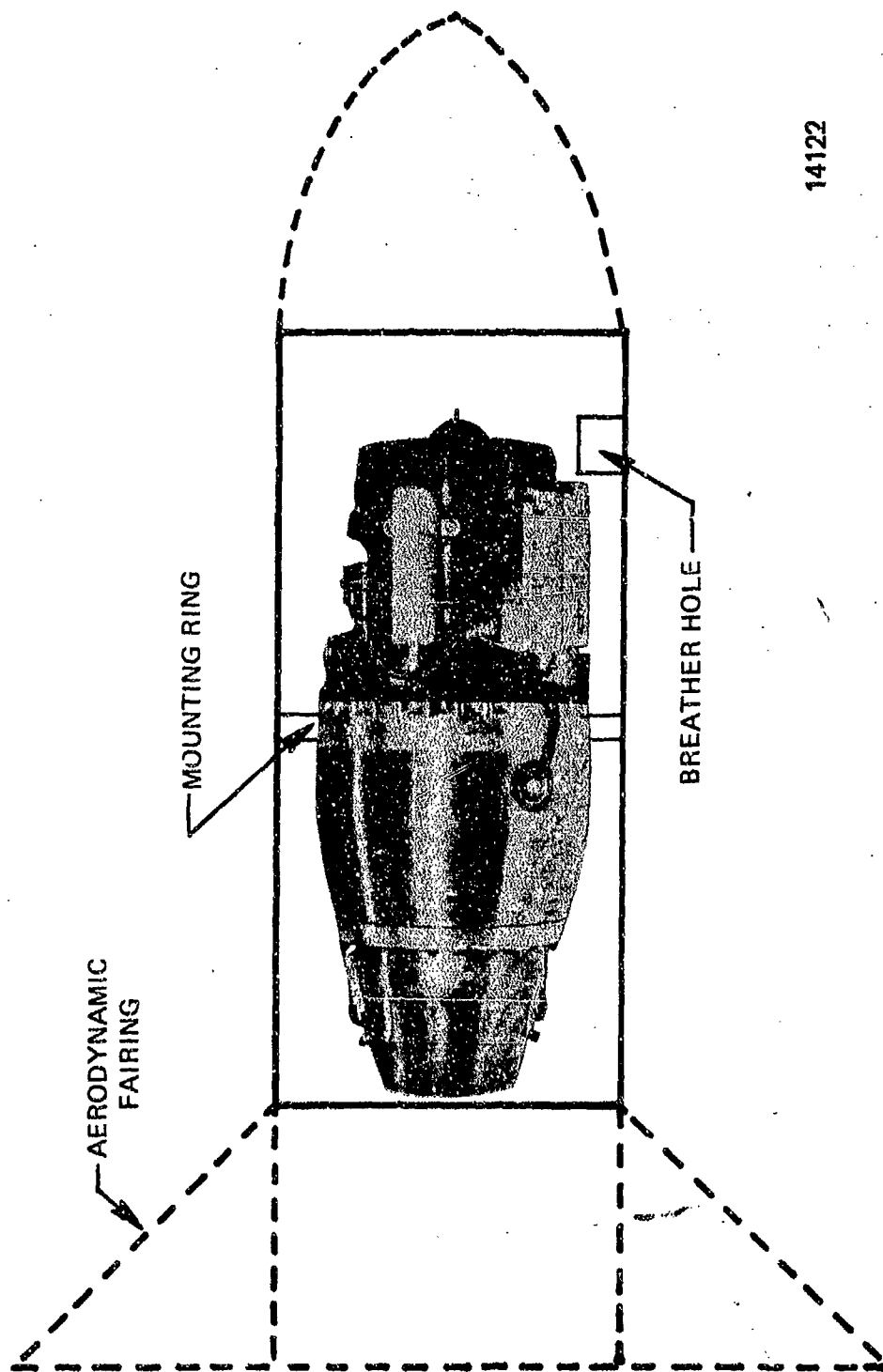
Figure 11. Simulated Missile Case Showing Location of Engine and Hole. The Hole was Sized to Represent the Opening Present on an Actual Missile.
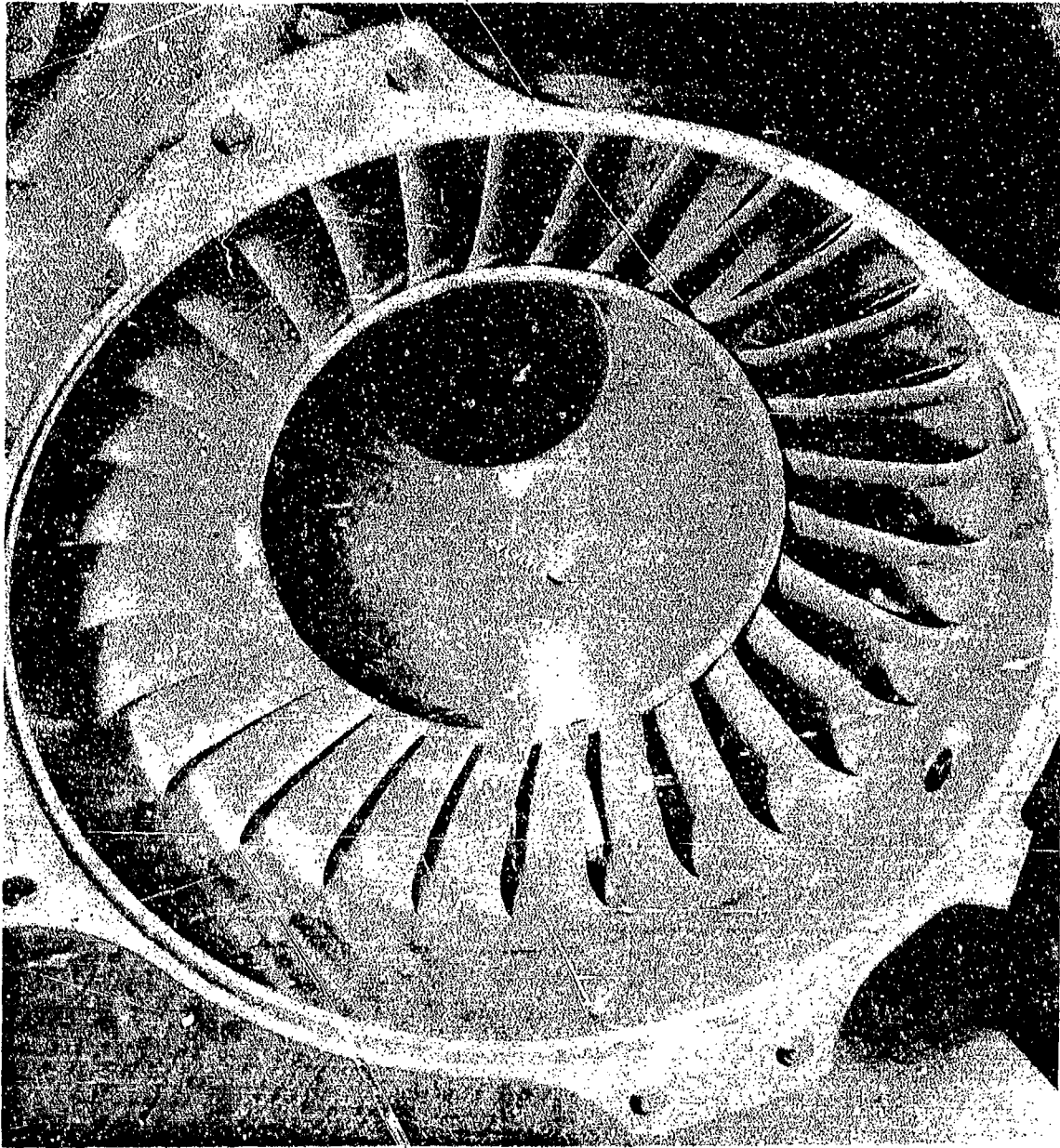
T-20874

Figure 12. Polyester Electrocoated Stator Housing Showing Excellent Condition of the Stator Vanes and Airflow Path After Exposure Aboard a Destroyer Deck for Seven Months.

119
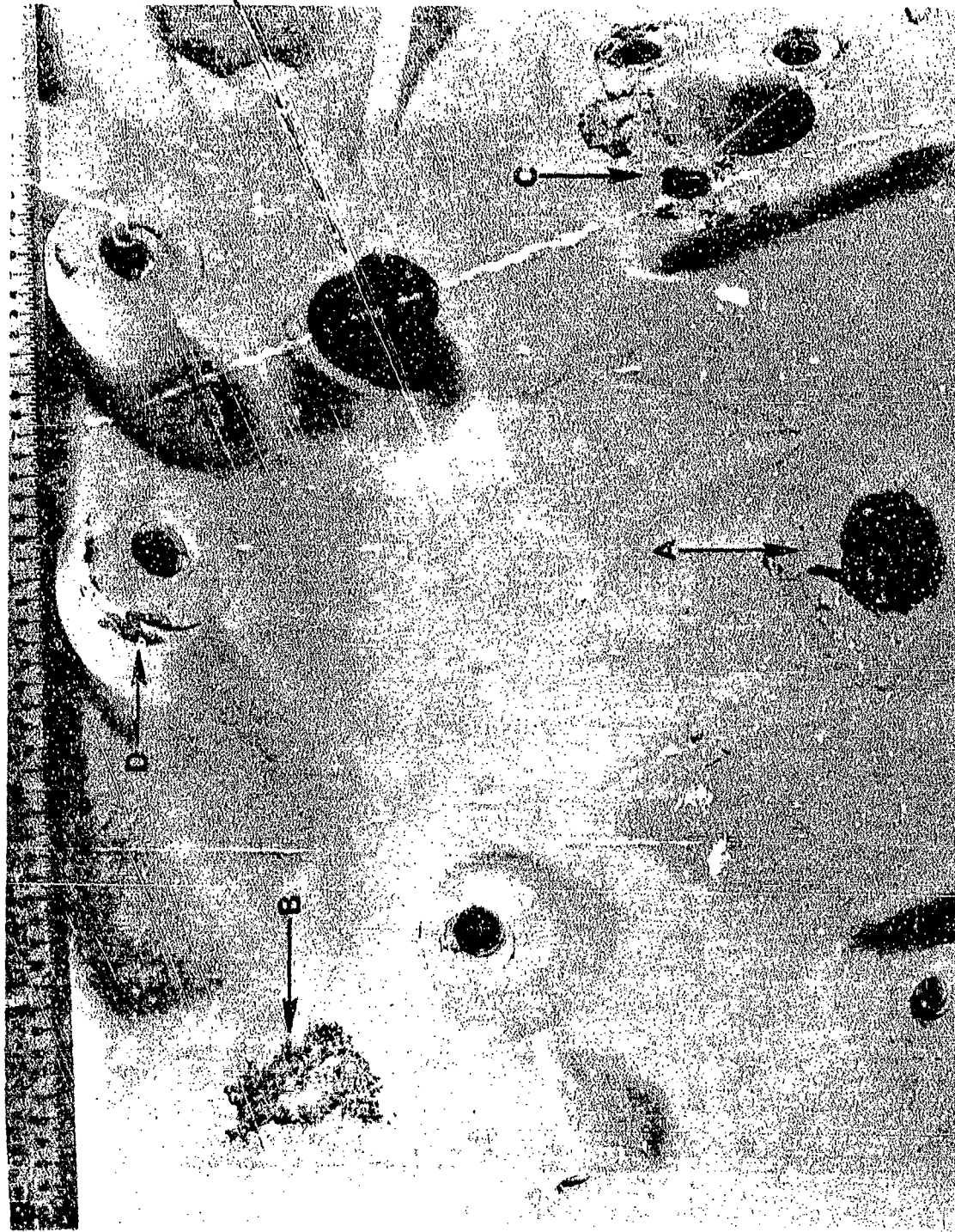
Figure 13. Polyester Electrocoated Stator Housing Showing Some Minor Exterior Deterioration After Seven Months Exposure Aboard a Destroyer. "A" is Mounting Boss Holes; "B" is the Location Under the Fuel Line; "C", Starter Cartridge Gasket Location; and "D" is the Fuel Line Attachment Boss.
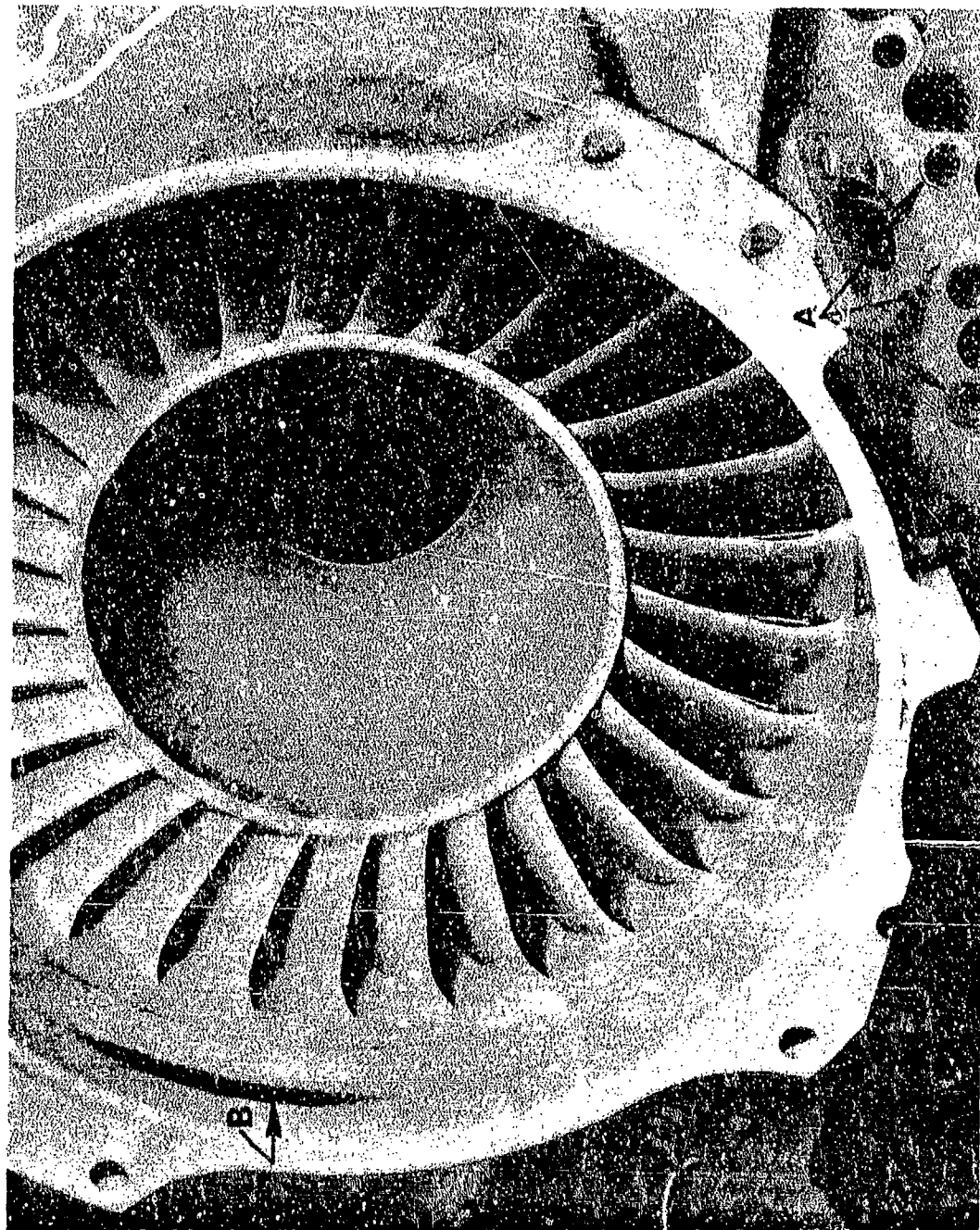
T-20873

Figure 24. Polyester Electrocoated Stator Housing Showing Excellent Condition of Stator Vanes and Airflow Path After 12 Months Exposure Under an Aircraft Wing. "A" is Damage Caused by Lockwashers Cutting into the Aluminum. "B" is a Light Rub on Axial Compressor Shroud Which Occurred During the Initial Acceptance Test. This Area was Touched up with an Epoxy Paint and was in Excellent Condition.
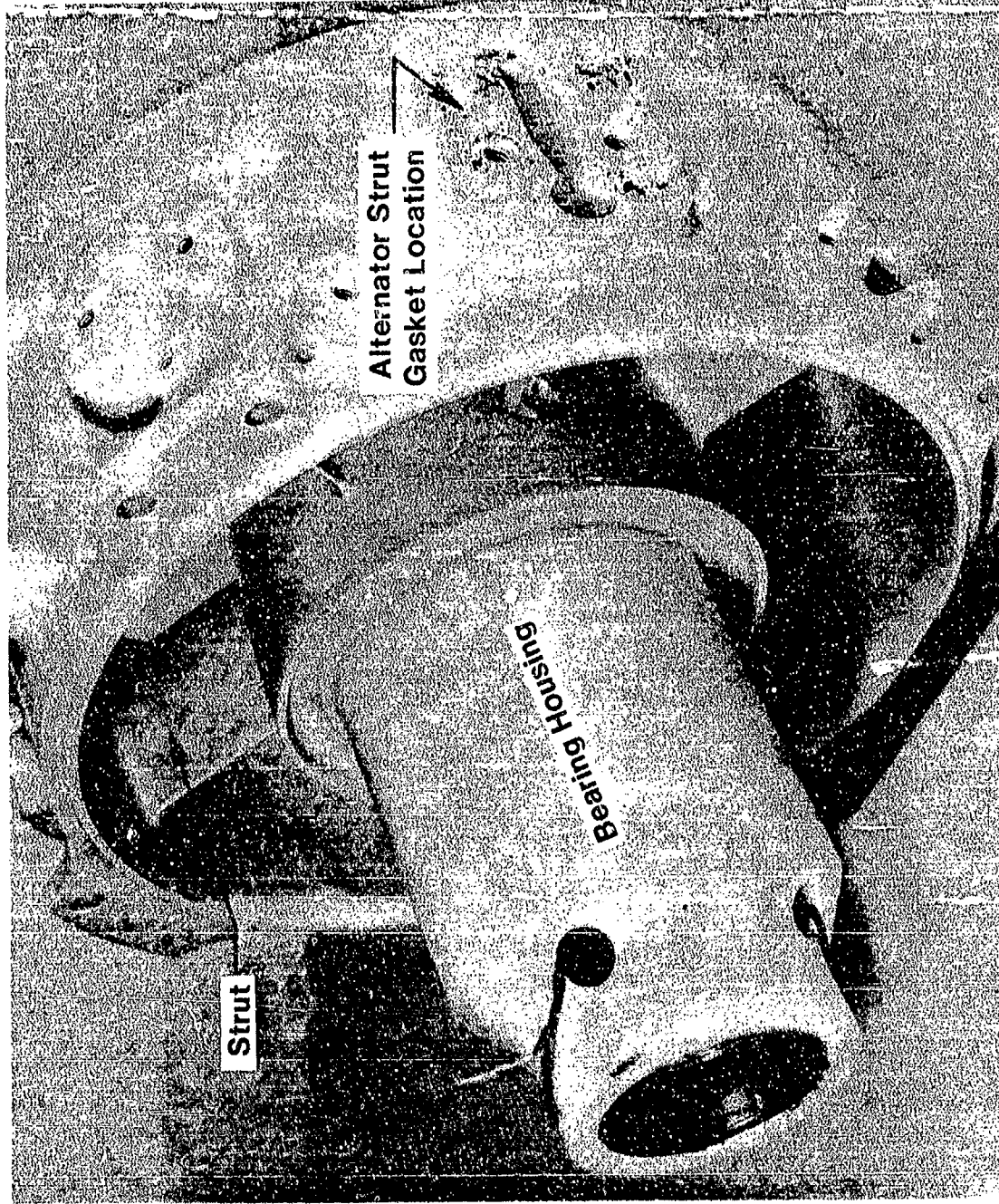
T-20875

Figure 15. Polyester Coated Air Inlet Duct Showing Excellent Condition of Air Passage Struts and Bearing Housing After 12 Months Under an Aircraft Wing. Some Minor Creepage had Occurred Under Alternator Strut Gasket.

CORROSION OF ALUMINUM ALLOYS IN
EXFOLIATION-RESISTANT TEMPERS EXPOSED TO MARINE
ENVIRONMENTS FOR 2 YEARS

by
E. J. Czyryca and H. P. Hack

Naval Ship Research and Development Center
Bethesda, Maryland 20084

ADMINISTRATIVE INFORMATION

ACKNOWLEDGEMENT

INTRODUCTION

The aluminum-magnesium alloys, 5086, 5083, and 5456, are attractive materials for naval construction because of their marine corrosion resistance, high strength-to-weight ratio, and weldability. The alloys have been used by the Navy for light-weight superstructures and as the primary structural metal for high-speed, high-performance ships and craft. The most desirable combination of properties in sheet and plate was achieved in a mildly cold-worked temper (quarter-hard) designated as 5086-H32, 5083-H321, and 5456-H321. However, under certain conditions, exfoliation corrosion problems were experienced with the standard temper. Exfoliation or lamellar corrosion is a type of inter-granular corrosion causing delamination in thin plate material.

To solve the exfoliation problem, the aluminum industry developed rolling procedures for tempers meeting the mechanical property requirements specified for the H32 and H321 tempers and having a metallurgical structure resistant to exfoliation-type corrosion.[1,2] These tempers for sheet and plate high-Mg, 5000-series alloys are designated H116, developed by Reynolds Metals Company, and H117, developed by Alcoa. These exfoliation-resistant tempers are included in Interim Federal Specifications QQ-A-00250/19 and QQ-A-00250/20 for 5086 and 5456 alloys, respectively.

The purpose of this investigation was to study the corrosion behavior of the three high-strength, Al-Mg alloys, 5086, 5083, and 5456, in the exfoliation-resistant tempers when exposed to three marine environments. This report summarizes the results for exposure durations of 6 months, 1 year, and 2 years.

METHOD OF INVESTIGATION

Panels were cut from plates of 5086-H116, 5086-H117, 5083-H116, 5456-H116, and 5456-H117 alloys. The test panel size, thickness, and source are listed in table 1. Specimen panels were exposed with the as-rolled surface finish and with saw-cut or sheared edges.

Panels were tested in two conditions, viz, as-rolled and sensitized. The sensitizing treatment, 1 week at 100° C* in a laboratory oven, is an accelerated aging process to simulate the worst possible condition of the alloy microstructure after long-term service. Such a condition might occur in deck and super-structure applications where exposure to the sun and tropical temperatures are experienced.

---

[1] Superscripts refer to similarly numbered entries in the Technical References at the end of the text.
*Abbreviations used in this text are from the GPO Style Manual, 1973, unless otherwise noted.

TABLE 1
MATERIALS UNDER INVESTIGATION

Alloy and Temper	Plate Thickness inch	NSRDC* Code Letters	Test Panel Size inch	Source
5086-H116	1/4	EST	12 x 3	Reynolds Metals Company
5086-H116	3/4	ESX	12 x 3	Reynolds Metals Company
5086-H117	1/4	ETJ	8 x 3	Alcoa
5083-H116	1/4	ETC	12 x 3	Reynolds Metals Company
5083-H116	1/2	ETD	12 x 3	Reynolds Metals Company
5456-H116	1/4	ESY	12 x 3	Reynolds Metals Company
5456-H116	1/2	ESZ	12 x 3	Reynolds Metals Company
5456-H117	1/4	ETK	8 x 3	Alcoa
5456-H117	1/2	ETF	12 x 3	Alcoa

*NSRDC - Naval Ship Research and Development Center

Panels in both conditions were exposed to three different marine environments at the Francis L. LaQue Corrosion Laboratory, Wrightsville Beach, North Carolina. The three environments were:

- Completely submerged in a trough of slowing flowing sea water (2 to 3 ft/s).

- Exposure in a "splash and spray" zone which is the level of wave breaking.

- Exposure to a marine atmosphere 80 feet from the shore.

Where sufficient material was available, duplicate specimens were tested for every exposure condition. A total of 282 specimens was included in the program. Specimens were removed after exposures of 6 months, 1 year, and 2 years. Note that specimens were not cleaned, inspected, and reexposed; rather, each exposure was for the total duration, and specimens were left undisturbed during the entire period of the specific test.

RESULTS AND DISCUSSION

MICROSTRUCTURES

Exfoliation or lamellar corrosion is a specific type of intergranular corrosion attack which can occur along grain boundaries parallel to the metal surface of aluminum products having an elongated grain structure, such as light gage plate or extruded shapes. The generation of corrosion products forces the

uncorroded layers apart and causes the metal to swell and delaminate or flake apart. For those Al-Mg alloys containing greater than 3% Mg, susceptibility to exfoliation is dependent on the amount of cold work introduced.[3] Plate and sheet having been severely rolled show a striated grain structure with precipitate in the grain boundaries as a continuous line (figure 1). The precipitate (Mg_2Al_3) is anodic to the solid solution in the grain bodies and corrodes preferentially.[3] It is the continuity of the precipitate which makes the structure liable to exfoliation attack.

The H32 and H321 tempers apply to products which are strain hardened and then stabilized by a low-temperature heat treatment to slightly lower the strength and to increase ductility and stress-corrosion resistance. This process can result in a microstructure in which the precipitate is present in a continuous line. Microstructures of as-received 5456-H321 plate and the same material sensitized (1 week at 100° C) are shown in figure 1. With heavy lamellar precipitate already present in the as-received microstructure, sensitizing had little effect in furthering the precipitation.

The new tempers, H116 and H117, apply to products which are strain hardened less than quarter-hard and do not undergo a stabilizing heat treatment. The objective of these tempers is to provide material having a metallurgical structure with a discontinuous network of precipitate. Such a structure should not be susceptible to exfoliation. Figures 2 through 10 show the microstructures of the new tempers for the alloys and plate thicknesses under the present investigation in both as-received and sensitized conditions. Note the discontinuous network of the precipitate in the as-received plates.

Interim Federal Specifications QQ-A-00250/19 (Navy-Ships) for 5086 plate and sheet and QQ-A-00250/20 (Navy-Ships) for 5456 plate and sheet in the H116 and H117 tempers require, as part of the material qualification procedure, that samples of production lots be examined metallographically. The examination must show a microstructure predominantly free of a continuous grain boundary network of Al-Mg precipitate. The as-received microstructures of plates of all alloys and thicknesses for the H116 and H117 tempers in this study meet the requirement (figures 2 through 10).

The H116 and H117 tempers represent two different approaches for providing a discontinuous precipitate network. In the H116 temper, the precipitate is dispersed throughout the metal in disconnected paths, while the H117 process prevents the formation of paths of precipitate along the grain boundaries. It was observed that in the as-received condition, the alloys in H117 temper (figures 4, 9, and 10) had a sparse population of precipitates in comparison to those in H116 temper. However, after the sensitizing treatment, the H117 tempers show heavy, continuous "stringers" of precipitate, whereas the alloys in the H116 temper show only a slight increase in precipitate density and continuity. It seems,

therefore, that inherent in the H116 tempering procedure is a stabilizing process which inhibits further growth of precipitate. The H117 tempers appear to hold much Mg in solution. Consequently, this less stable condition is more responsive to the sensitizing treatment.

The sensitization treatment may be more severe than natural aging. Sensitization treatments may be considered a means of obtaining a conservative evaluation of long-term corrosion performance when long-term data are not available, and the long delay involved in complete evaluation under conditions of natural aging and exposure is unreasonable.

CORROSION

The results of exposure to the three environments are summarized in table 2 for panels exposed to marine atmosphere, in table 3 for panels exposed to splash and spray, and in table 4 for the fully submerged panels. The results are given in terms of corrosion rates in mils per year, based on weight loss and exposed surface area. In general, the calculated rates for any exposure and condition were less than 1 mil/yr and decreased with time, i.e., the initial attack is highest.

The panels exposed to marine atmosphere and to splash and spray showed a scattered light pitting on surfaces, with a slightly greater intensity in the latter exposure. The pitting can best be described as "pinpoint" and of insignificant depth. The one exception to this general behavior was that of the sensitized, 1/4-inch-thick 5456-H117 panels. In both environments, the attack on these panels appeared as a minor scattered surface blistering. The attack was first noted after 1 year of exposure, being the only instance of increased corrosion rate at that time; however, the rates after 2 years of exposure show the attack to have virtually ceased.

Surface attack on the as-received and the sensitized 5456-H117 1/4-inch panels after 2 years of exposure to splash and spray and marine atmosphere is compared in figure 11. White corrosion product was present under the blisters, and an area about 1/2 x 1/8 inch near the edge of the sensitized panel exposed to splash and spray showed evidence of delamination (figure 12). Corrosion rates based on weight losses of the 1/4-inch panels ranged from nil to 0.10 mil/yr in both the splash and spray exposure and marine atmosphere.

TABLE 2
CORROSION TEST RESULTS FOR ALUMINUM ALLOYS IN
MARINE ATMOSPHERE 80 FEET FROM OCEAN

Alloy and Temper	Plate Thickness inch	Corrosion Rate mil/yr			Corrosion Description After 2 Years
		6 Months	1 Year	2 Years	
As-Rolled Condition					
5086-H116	1/4	0.10	0.09	Nil	
5086-H117	1/4	0.10	0.13	Nil	
5083-H116	1/4	Nil	0.11	Nil	
5456-H116	1/4	0.10	0.11	Nil	Scattered light pitting
5456-H117	1/4	0.10	0.13	0.10	
5083-H116	1/2	0.30	0.13	0.10	
5456-H116	1/2	0.35	0.13	0.05	
5086-H116	3/4	0.50	0.12	0.10	
Sensitized Condition					
5086-H116	1/4	Nil	0.17	Nil	Scattered light pitting
5086-H117	1/4	0.20	0.17	Nil	Scattered light pitting
5083-H116	1/4	Nil	0.33	Nil	Scattered light pitting
5456-H117	1/4	0.30	0.65	Nil	Moderate light blistering
5083-H116	1/2	0.40	0.31	0.05	Scattered light pitting
5456-H116	1/2	0.40	0.23	0.10	Scattered light pitting
5086-H116	3/4	0.50	0.26	0.10	Scattered light pitting

TABLE 3
CORROSION TEST RESULTS FOR ALUMINUM ALLOYS IN
SPLASH AND SPRAY ZONE

Alloy and Temper	Plate Thickness inch	Corrosion Rate mil/yr			Corrosion Description After 2 Years
		6 Months	1 Year	2 Years	
As-Rolled Condition					
5086-H116	1/4	0.10	0.11	Nil	
5086-H117	1/4	0.10	0.09	Nil	
5083-H116	1/4	Nil	0.07	Nil	
5456-H116	1/4	0.10	0.09	0.10	
5456-H117	1/4	0.20	0.13	0.10	Scattered light pitting
5083-H116	1/2	0.35	0.08	0.05	
5456-H116	1/2	0.35	0.13	0.10	
5086-H116	3/4	0.30	0.12	0.10	
Sensitized Condition					
5086-H116	1/4	0.15	0.14	Nil	Scattered light pitting
5086-H117	1/4	0.10	0.13	Nil	Scattered light pitting
5083-H116	1/4	0.25	0.17	Nil	Scattered light pitting
5456-H117	1/4	0.10	0.26	Nil	Moderate light blistering
5083-H116	1/2	0.30	0.13	0.10	Scattered light pitting
5456-H116	1/2	0.35	0.21	0.05	Scattered light pitting
5086-H116	3/4	0.40	0.14	0.10	Scattered light pitting

TABLE 4
CORROSION TEST RESULTS FOR ALUMINUM ALLOYS
FULLY SUBMERGED IN FLOWING SEA WATER

Alloy and Temper	Plate Thickness inch	Corrosion Rate mil/yr			Corrosion Description After 2 Years	Edge Attack After 2 Years
		6 Months	1 Year	2 Years		
As-Rolled Condition						
5086-H116	1/4	0.80	0.53	0.45	Light uniform attack, moderate slight pitting	Moderate
5086-H117	1/4	0.90	0.52	0.40	Light uniform attack, no pitting	None
5083-H116	1/4	0.75	0.47	0.40	Light uniform attack, minor incipient pitting	Very slight and local
5456-H116	1/4	0.80	0.48	0.40	Light uniform attack, no pitting	None
5456-H117	1/4	0.70	0.48	0.30	Light uniform attack, no pitting	None
5083-H116	1/2	0.85	0.47	0.50	Light uniform attack, minor incipient pitting	Moderate and local
5456-H115	1/2	0.70	0.50	0.45	Light uniform attack, minor incipient pitting	Moderate and local
5456-H117	1/2	0.60	0.50	-	Light uniform attack, no pitting*	None*
5086-H116	3/4	1.00	0.43	0.30	Light uniform attack, no pitting	Slight and local
Sensitized Condition						
5086-H116	1/4	0.70	0.57	0.40	Light uniform attack, no pitting	Slight
5086-H117	1/4	0.80	0.52	0.40	Light uniform attack, no pitting	None
5083-H116	1/4	0.70	0.51	0.80	Light uniform attack, severe shallow pitting	Severe
5456-H117	1/4	0.70	0.56	0.50	Light uniform attack, no pitting	None
5083-H116	1/2	1.15	0.56	0.40	Light uniform attack, minor shallow pitting	Moderate
5456-H116	1/2	1.85	1.02	1.15	Light uniform attack, minor incipient pitting	Severe
5456-H117	1/2	0.80	0.85	-	Light uniform attack, no pitting*	Severe*
5086-H116	3/4	1.10	0.55	0.40	Light uniform attack, no pitting	Moderate

*After 1 year in test.

The highest corrosion rates resulted from the fully sub-merged exposure where the surface generally showed a light, uniform corrosion with minor pitting in some cases. Severe edge attack occurred in most alloys and thicknesses in both the as-received and sensitized conditions. Based on weight loss, the average corrosion rate for the 1/4-inch-thick panels which experienced no edge attack (5086-H117, 5456-H116, and 5456-H117) was 0.80 mil/yr in the first 6 months (i.e., 0.40 mil of metal loss in 6 months). The average corrosion rate after the first year was 0.52 mil/yr (0.52 mil of metal loss) and 0.39 mil/yr after the second year (0.78 mil of total metal loss). Thus, the actual corrosion rate in the second 6 months was 0.24 mil/yr (or 0.12 mil of metal loss in the second 6 months) and 0.26 mil/yr in the second year (or 0.26 mil of metal loss in the second year). This analysis indicates that the general corrosion rate reduces to a low, uniform rate after the initial attack of the first 6 months.

The pitting attack on the fully immersed panel surfaces was minor and shallow in the alloys of H116 temper; alloys of the H117 temper experienced no significant local surface attack. Severe shallow pitting was experienced, however, in the sensitized 5083-H116, 1/4-inch plate, as shown in figure 13.

Edge attack generally occurred in the same panels that exhibited some form of pitting attack. Attack was most severe in the sensitized 5083-H116, 1/4-inch plate and sensitized 5456-H116, 1/2-inch plate. Figures 14 and 15 show the attack in these speci-mens compared to the as-received condition and different thick-nesses. Although the attack occurred in some of the as-received plates, sensitized specimens showed the more severe attack. The alloys in the H117 temper did not exhibit edge corrosion except for the sensitized 1/2-inch-thick 5456-H117. Both the massive pitting and the severe edge attack were found to be conventional intergranular corrosion. By this process, corrosion of the grain boundaries tends to spread out in all directions, removing whole grains, and causing an area of intense local attack.

The slight pitting and edge attack in the as-received plates were insignificant and would probably be prevented in service by paint; however, buttering of exposed edges with weld metal below the waterline is suggested for complete immunity to edge attack. Although alloys in a sensitized condition showed an increased severity of pitting and edge attack, none of the observations indicates a corrosion problem beyond routine maintenance in the long-term usage of these alloys in marine applications.

In a previous investigation,[4] the same alloys in several sheet gages in standard tempers (0, -H14, -H34, and -H321) were partially immersed in sea water for exposure times up to 7 years. General corrosion damage was mild, characterized by shallow pitting. The present study confirms the excellent marine corro-sion resistance of the commercial 5000-series alloys in the new H116 and H117 tempers.

CONCLUSIONS

The results of the investigation reported herein may be summarized as follows:

● Metallographic analysis of as-received plates of Al-Mg alloys 5086, 5083, and 5456 in H116 and H117 tempers in thicknesses from 1/4 to 3/4 inch showed structures with discontinuous or randomly dispersed precipitate network necessary for exfoliation resistance.

● The alloys in H117 temper showed continuous precipitate network after a sensitizing treatment. The same alloys in H116 temper realized only a slight increase in precipitate density and continuity, suggesting that the H116 temper produces material less susceptible to natural aging.

● The results of 2 years of exposure to marine environments (marine atmosphere, splash and spray, and fully submerged in sea water) indicate that alloys 5086, 5083, and 5456 in the H116 and H117 tempers have good corrosion resistance. No exfoliation attack was evident on any test panel.

TECHNICAL REFERENCES

1 - Brooks, C. L., "Aluminum-Magnesium Alloys 5086 and 5456-H116," Naval Engineers Journal, Vol. 82, No. 4, pp. 29-32 (Aug 1970)
2 - Wood, C., Jr., "Selecting Wrought Aluminum Alloys for Marine Use," Aluminum Company of America (June 1969)
3 - Binger, W. W., et al, "Resistance to Corrosion and Stress Corrosion," Aluminum, Vol. 1, Chapter 7, Amer. Soc. for Metals (1967)
4 - Niederberger, R. B., et al, "Corrosion and Stress Corrosion of 5000-Series Al Alloys in Marine Environments," Corrosion, Vol. 22, No. 3, pp. 68-73 (Mar 1966)

As Received   Sensitized 1 Week at 100° C

Figure 1
Microstructure of 5456-H321
1/4-Inch Plate (500X)

As Received   Sensitized 1 Week at 100° C

Figure 2
Microstructure of 5086-H116
1/4-Inch Plate (500X)
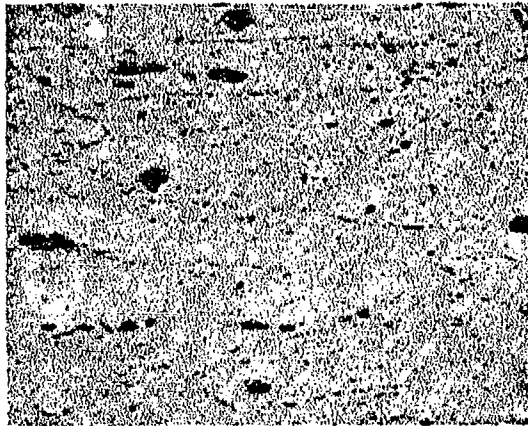
As Received   Sensitized 1 Week at 100° C
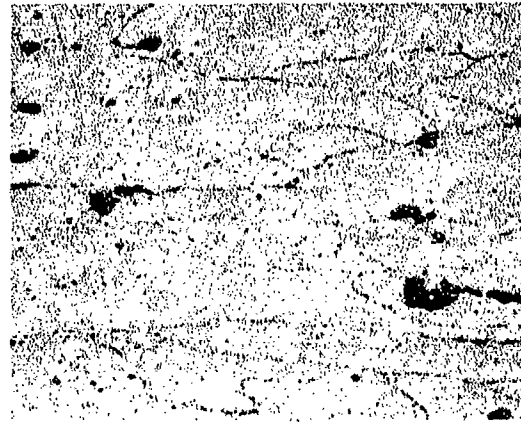
Figure 3
Microstructure of 5086-H116
3/4-Inch Plate (500X)

As Received   Sensitized 1 Week at 100° C
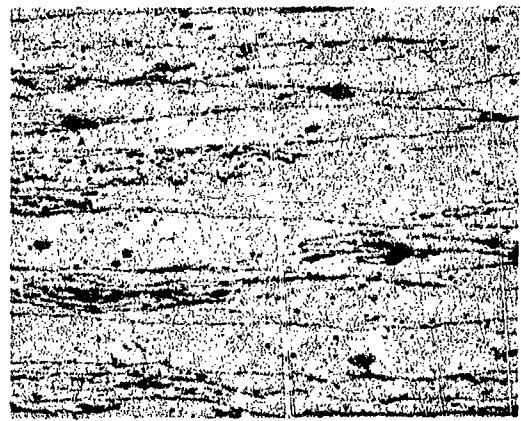
Figure 4
Microstructure of 5086-H117
1/4-Inch Plate (500X)

133
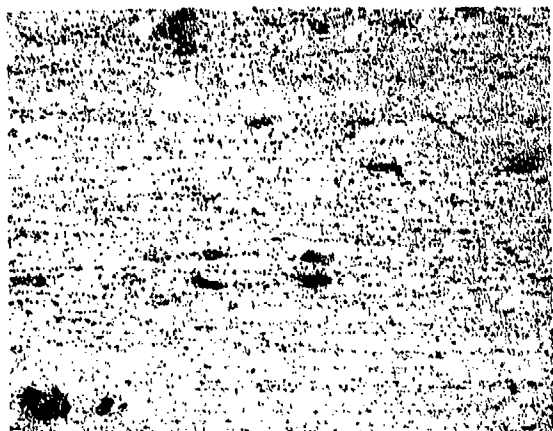
As Received   Sensitized 1 Week at 100° C
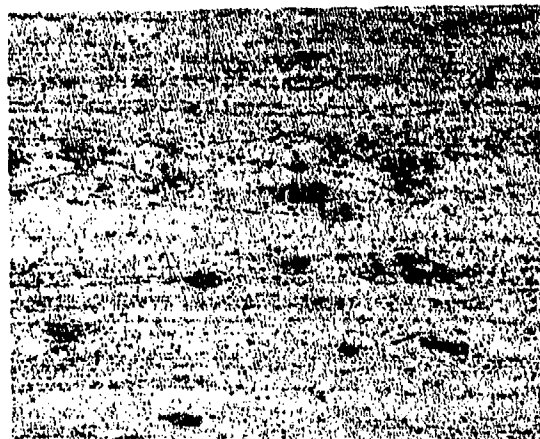
Figure 5
Microstructure of 5083-H116
1/4-Inch Plate (500X)
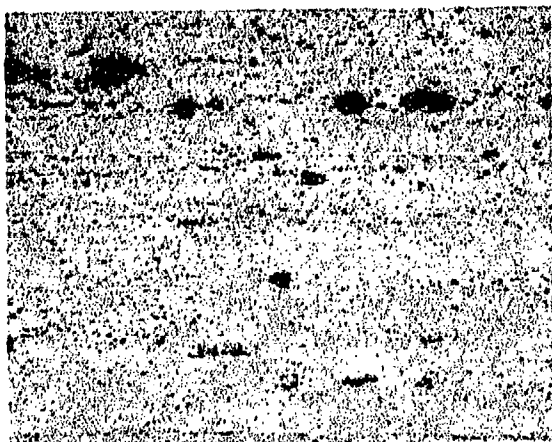
As Received   Sensitized 1 Week at 100° C
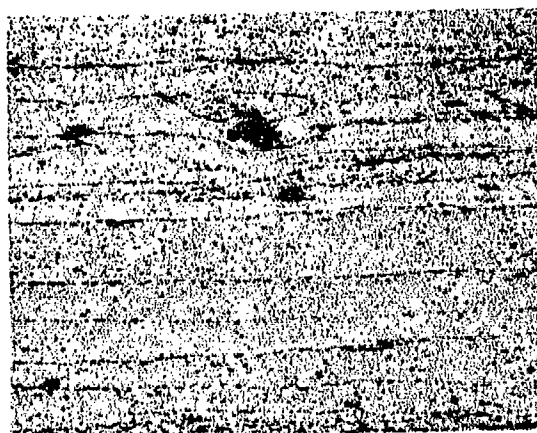
Figure 6
Microstructure of 5083-H116
1/2-Inch Plate (500X)
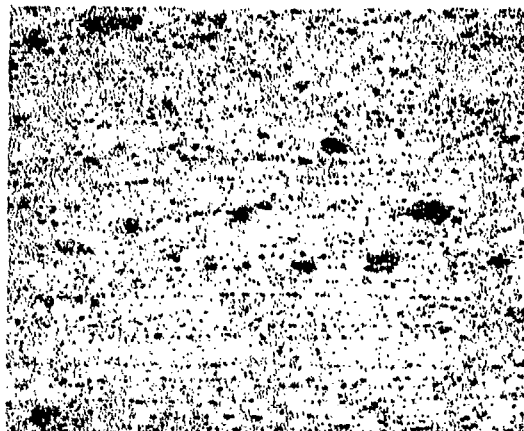
As Received

Figure 7
Microstructure of 5456-H116
1/4-Inch Plate (500X)
(Sensitized Condition Not Tested)

As Received

Sensitized 1 Week at 100° C

Figure 8
Microstructure of 5456-H116
1/2-Inch Plate (500X)

135

As Received   Sensitized 1 Week at 100° C

Figure 9
Microstructure of 5456-H117
1/4-Inch Plate (500X)

As Received   Sensitized 1 Week at 100° C
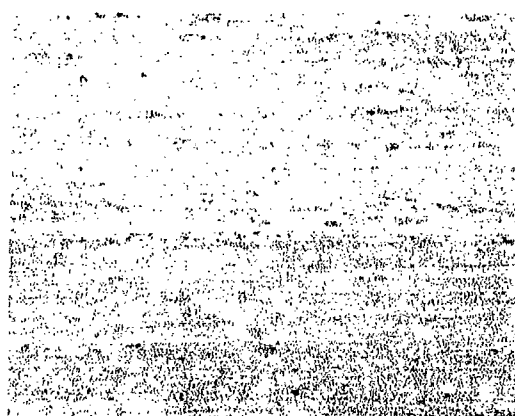
Figure 10
Microstructure of 5456-H117
1/2-Inch Plate (500X)

As Received   Sensitized

Marine Atmosphere
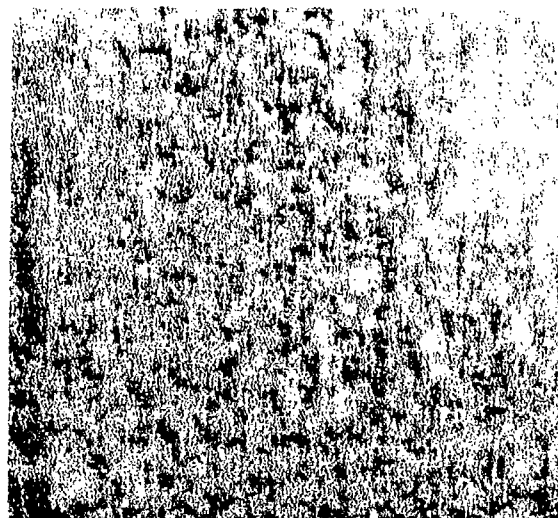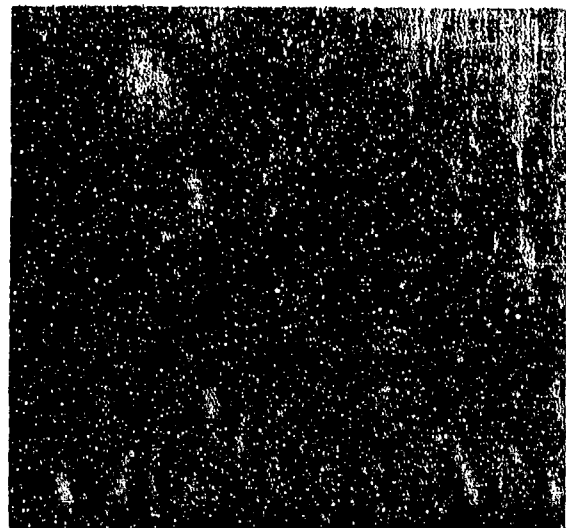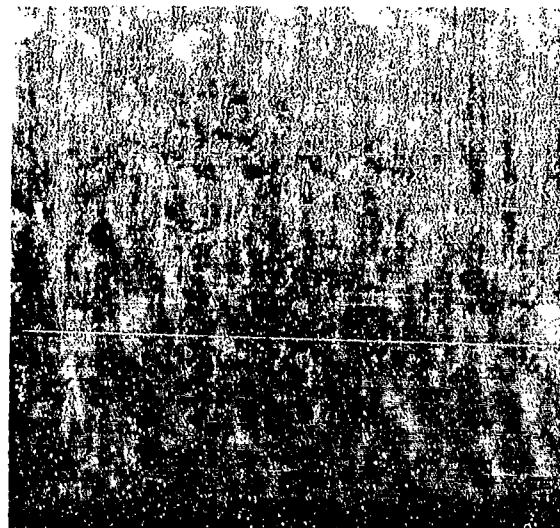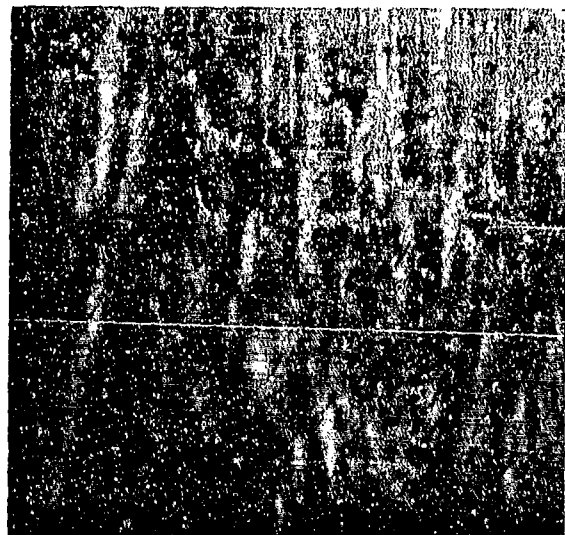
Splash and Spray

Figure 11
Comparison of Surface Attack on As-Received
and Sensitized 5456-H117 1/4-Inch Plate Exposed
to Splash and Spray and Marine Atmosphere

137
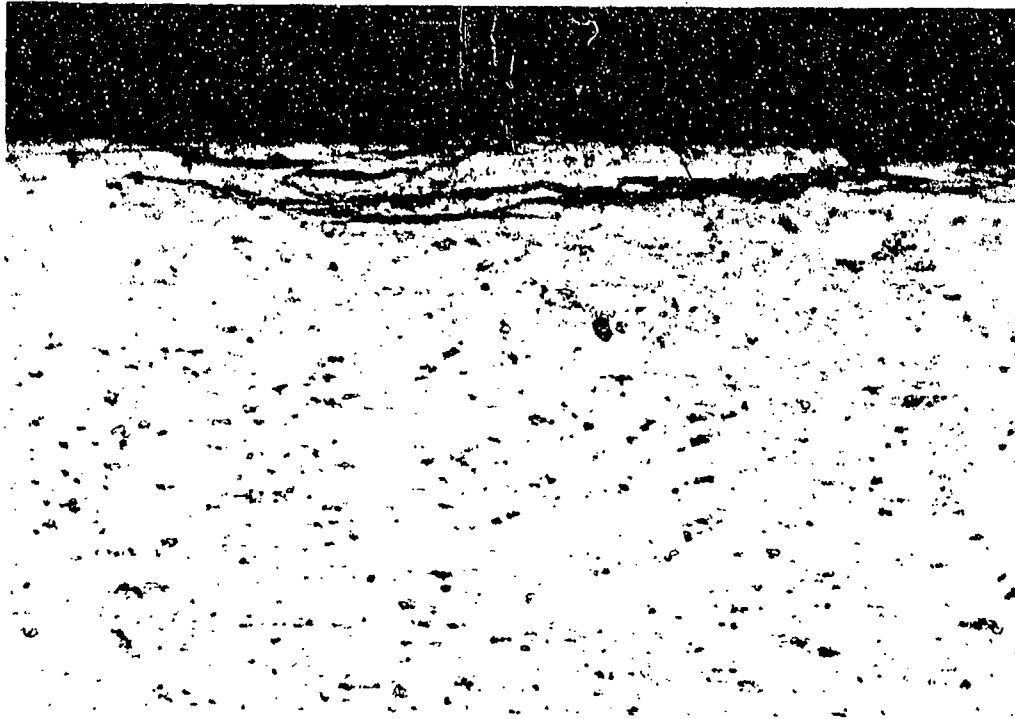
Figure 12
Delamination Under Blistering on
Sensitized 5456-H117 1/4-Inch Plate
After Splash and Spray Exposure
(250X)

As Received   Sensitized
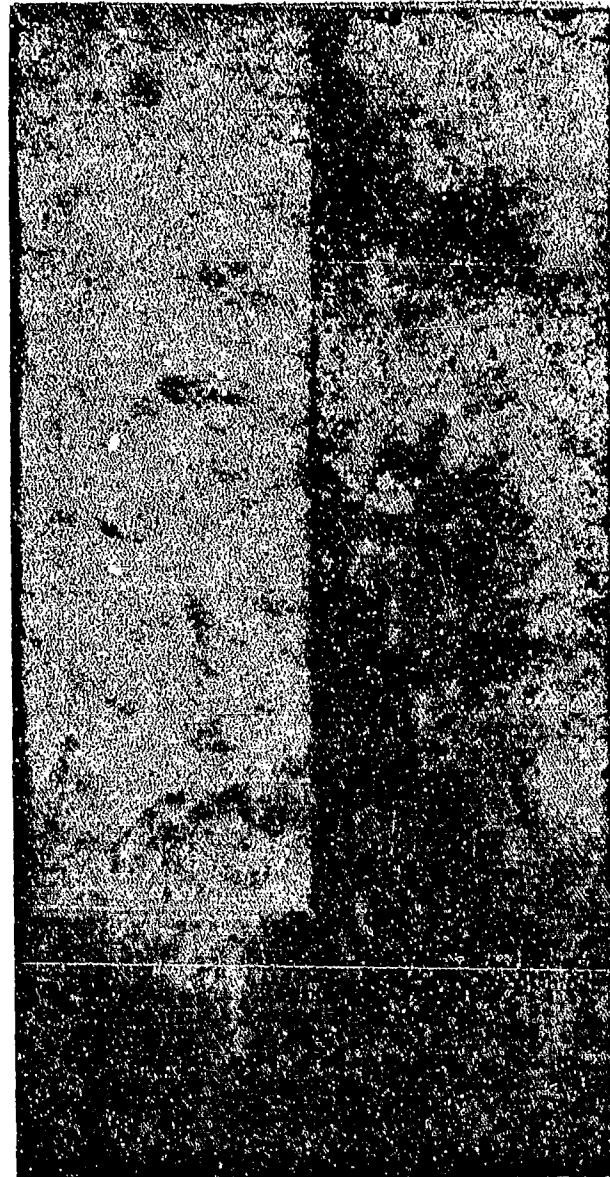
Figure 13
Wide, Shallow Pitting in
Sensitized 5083-H116
1/4-Inch Plate After Fully
Immersed Exposure

Side Edge

End Edge

A – 1/4-Inch Plate, As Received
B – 1/4-Inch Plate, Sensitized
C – 1/2-Inch Plate, As Received
D – 1/2-Inch Plate, Sensitized

Figure 14
Edge Corrosion on 5083–H116 Panels
Exposed to Flowing Sea Water

140

Side Edge
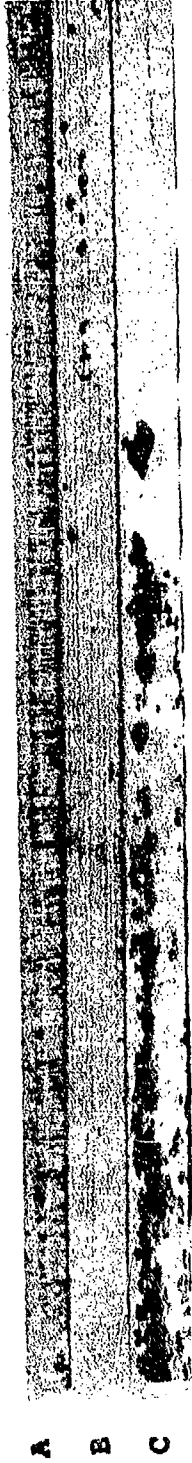
End Edge

A – 1/4-Inch Plate, As Received
B – 1/2-Inch Plate, As Received
C – 1/2-Inch Plate, Sensitized

Figure 15
Edge Corrosion on 5456-H116 Panels
Exposed to Flowing Sea Water

A

B

C

A

B

C

CAVITATION CHARACTERISTICS OF SEA WATER PIPE SYSTEM COMPONENTS

Authors: Y Boccadoro[*] and B Angell[✗]

* Southampton University, Department of Mechanical Engineering

✗ Admiralty Materials Laboratory, Holton Heath, Poole, UK

SYNOPSIS

Through-life costs of sea water systems in HM Ships could be greatly improved
if rapid erosion of valves and other pressure reducing devices could be avoided.
This can only be achieved if designers and operators are provided with adequate
design criteria. To establish such criteria is the aim of a current research
programme undertaken jointly by AML and Southampton University.

The orifice plate, being the simplest pressure reducer was first studied in some
detail. Flow visualisation techniques, using fresh water, were supplemented by
long term experiments in which full-scale systems carrying sea water were built to
resemble construction and operating conditions. Diaphragm valves were also
investigated thoroughly, since little data seemed to be available in the literature.
The results were used, together with a theoretical estimate of the pressure losses,
to produce simple and practical data, which may be used with valves and other
pressure reducers. It is concluded that the proposed design criterion is adequate
to minimise risk of cavitation erosion in piping systems.

Preceding Page Blank

INTRODUCTION

The piping systems which circulate sea water around a ship to satisfy fire
fighting and cooling requirements are expensive to build and maintain. This is
particularly true in warships where sophisticated materials may be used to ensure
reliability. It follows that every effort should be made to preserve their
integrity during the life of the vessel. The object of research at AML
(Admiralty Materials Laboratory) in this field is to minimise through-life costs
while taking advantage of developments in new materials. It is well known that
sea water is a particularly corrosive fluid which, even when static, may cause
deterioration of metallic materials in which it is contained by a number of
corrosion processes. When the sea water is flowing the situation is altered by
the decreasing severity of some mechanisms but others are introduced which are
influenced by the hydrodynamic characteristics of the piping system. These are
impingement corrosion and cavitation erosion and are often descriptively coupled
together in the term "corrosion/erosion".

While this paper is concerned principally with cavitation and its prevention it
is important that the relationship between these two effects should be emphasised.
Cavitation erosion is mechanical in nature and does not require a corrosive
medium. Impingement corrosion requires mechanical energy resulting from hydro-
dynamic forces to establish and maintain areas of differing potential so that the
predominantly electrochemical wastage process may take place. It is easy to
appreciate, therefore, that in a piping system carrying sea water at, typically,
3 metres/second the presence of a source of cavitation may result in the
deterioration of component materials by these effects wither singly or in com-
bination. Impingement corrosion severely limited design velocities in copper
sea water systems and resulted in the development of a series of alloys, described
later, which possessed increasing resistance to this phenomenon and where these
materials are properly used failures are rare. However this situation may be
radically changed if a component is forced into cavitation. Considerable
experimental and service experience has shown that cavitation must be prevented
if high maintenance costs are to be avoided.

As a result of studying the hydrodynamic characteristics of some commonly used
pipework components it was concluded that, in an otherwise well designed and
constructed system, pressure and velocity conditions suitable for the inception
of cavitation were only found in devices which dissipate energy in order to
control flow. Pressure reducing orifice plates and control valves fall within
this category. It was confirmed that, in service, this was an area where little
guidance was available to designers and operators on the permissible operating
limits of these devices whilst avoiding serious corrosion/erosion of valve com-
ponents and downstream pipework. The lack of data frequently led designers into
assuming that when sizing valves in flow control terms, materials problems could
be avoided by ensuring that local velocities did not exceed values at which
significant corrosion occurred. It was of some concern to AML to find from a
literature survey that what data did exist was not directly relevant to the
diaphragm valves which had been generally adopted for use in controlling sea
water flow in surface ships. It should perhaps be emphasised that in most systems
where pump performance matches the loss characteristics there will be no
requirement to reduce pressure to the extent where any component is forced into
cavitation. Invariably the problem is confined to subsidiary cooling systems
which are coupled to the fire main either for convenience or by necessity. As

a result pressure must be reduced from values in excess of 7 bar (100 psig) to perhaps 1-2 bar to achieve the desired flow rate. In this paper it is proposed that several devices are used in cascade under controlled non-cavitating conditions rather than a single valve or orifice plate. For this purpose a suitable parameter has been evolved for use with orifice plates and diaphragm valves which should minimise the risk of cavitation.

<div align="center">

NOTATION:
</div>

$p_1\ v_1$	Pressure and velocity measured 5 diameters upstream
$A_1 = A_3$	Upstream and downstream pipe section area
$p_T,\ v_T,\ A_T$	Pressure and velocity and area measured at Vena contracta, (and valve 'throat')
$p_3\ v_3$	Pressure and velocity measured 10-12 diameters downstream
p_v	Saturated vapour pressure of fluid
m	Area ratio at Vena contracta
M_o	Area ratio of orifice plate
β	Diameter ratio of orifice plate
C_c	Contraction coefficient $(= \frac{m}{M_o})$
ξ	loss coefficient $(= \frac{p_1-p_3}{\frac{1}{2} v_1^2})$
σ K_d	Cavitation parameters
ρ	Density of fluid

MATERIALS

Copper alloys are now used almost exclusively in the construction of sea water systems for HM Ships and, since their use offers greater reliability in spite of higher initial cost compared to ferrous systems, they are increasingly found in commercial vessels. As mentioned earlier the piping materials in use today were developed to provide good resistance to impingement corrosion. These are the cupro-nickel alloys covered by BS 2871 Section 2 CN 102 and CN 107 and aluminium brass (CZ 110). For naval applications CN 102 (90/10 cupro-nickel) has been used in surface ships since the mid sixties with composition limits modified slightly to conform with Ministry of Defence specifications.

Cast components, such as valve bodies, are usually made from lead containing gunmetals although aluminium bronze, Monel and phosphor bronze may also be used. These materials generally have good corrosion resistance in sea water but with the exception of aluminium bronze and Monel their cavitation erosion resistance is relatively low. With the rising price of copper alloys diaphragm valves with cast iron bodies completely protected internally by a lining material are becoming popular. Linings may be chosen to suit many fluids and several polymeric and thermoplastic materials offered have better cavitation resistance than gunmetal. However considerable confidence in a lining material is required since in a copper alloy sea water system perforation would lead to rapid corrosion of the ferrous component.

THE RESEARCH PROGRAMME

The content of this paper describes a part of a collaborative project between Southampton University and AML to study the hydrodynamic factors which affect cavitation erosion and impingement corrosion. Having emphasised earlier the relationship between these phenomena cavitation alone will be considered here since the hydrodynamic conditions which promote impingement corrosion and the extent of interaction are still under investigation.

The need for hydrodynamic measurements using flow visualisation and acoustic techniques supported by practical experiments in simulated shipboard systems conveniently divided the work between the facilities available at the University and research establishment. A simple recirculatory system of 50 mm nominal bore was constructed at Southampton in which Towns water could be pumped through the components of interest under a variety of velocity and pressure conditions. Lengths of transparent acrylic pipe permitted flow visualisation and facilities were available for photography and detection of sound emitted from collapsing cavities. At AML the sea water test facilities provided practical data from full-scale, long duration (5000 hour) experiments with recirculated and 'once-through' sea water. Six identical 50 mm bore pipe systems similar in configuration to that at Southampton contained orifice plates and partially closed diaphragm valves to study cavitation effects at velocities in the range 2.5 - 6 metre/second. In addition other test systems were used to obtain supporting evidence for the proposed design parameter by including diaphragm valves set at known cavitation levels.

Initial literature surveys of cavitation in piping systems by Southampton University revealed that some data were available on the cavitation characteristics of orifice plates and several valves but not the diaphragm type. To use a systematic approach a study was made of the orifice plate using several orifice ratios. The parameters obtained from the consideration of this relatively simple hydrodynamic case were applied to the diaphragm valve using a number of basic assumptions. The loss coefficient characteristics of a 50 mm valve were determined for various degrees of closure leading to the inception of cavitation and finally the choking condition. In a similar independent exercise a 38 mm valve was characterised in a sea water system at AML. The methods of cavitation detection varied between the two sets of experiments. At Southampton visual and aural observations were combined with sound level measurements with a Bruell and Kjaer sound meter fitted with microphone and operating in the 16 kHz octave band. Aural detection aided by a piezoelectric crystal probe device under development, were used at AML.

DERIVATION OF A CRITERION TO AVOID CAVITATION

The initial assumption made in deriving the design criterion was that the geometry of a valve is the same as an orifice plate. Since the non-cavitating loss coefficient provided an ideal basis on which to formulate the criterion this was derived in terms of the physical properties of the orifice plate (Appendix A). Equations (1) and (1)' were compared with the experimental results of Numachi, Ball and Lienhard (Refs 1,2,3) as shown in Figure 1. It was found that the curve derived from equation (1) also corresponded to data published in British Standard 1042 (Ref 4). The three cavitation numbers most widely used in the literature are:-

$$\sigma_T = \frac{p_T - p_V}{\frac{1}{2}\rho v_T^2} \tag{2}$$

$$\sigma_3 = \frac{p_3 - p_V}{p_1 - p_3} \tag{3}$$

$$\sigma_3' = \frac{p_3 - p_V}{p_1 + \frac{1}{2}\rho v_1^2 - p_3} \tag{4}$$

σ_T is in nature slightly different from the others because it gives the difference between the average minimum pressure in the system and the vapour pressure when cavitation starts.

The reason for considering the other cavitation parameters is that σ_T is not easily obtainable when valves are studied instead of orifice plates, since the location of the minimum pressure is not known and might even vary with the degree of opening. Numachi investigated the variations of a slightly different coefficient $K_d = \sigma_T/C_o^2$ and found that it was independent of both area ratio and flow conditions. Since for values of β as high as 0.7 C_o can be considered constant this means that $\sigma_{Tcritical}$ is also independent of area ratio and flow conditions. This was confirmed at Southampton University by S B Au (Ref 5) and Y Boccadoro (Ref 6). Using this result together with an estimate of the losses by Borda's equation an approximation for the critical value of σ_3 or σ_3' was obtained.

$$\sigma_3 = \frac{p_3 - p_T}{p_1 - p_3} + \frac{p_T - p_V}{p_1 - p_3}$$

$$\sigma_3 = \frac{2m}{1 - m} + \frac{\sigma_T}{(1 - m)^2} \tag{5}$$

The same process may be repeated with σ_3'; however σ_3' is very simply related to σ_3 by:

$$\sigma_3 = \sigma_3' \left(1 + \frac{1}{\xi}\right) \tag{6}$$

so that only σ_3 is considered here.

The introduction of σ_T essentially avoids the assumption that the pressure in the section of minimum area is equal to vapour pressure at cavitation inception. This would correspond to $\sigma_T = 0$. However equation (5) is still difficult to use because with valves neither Mo nor M are generally known. The pressure loss between locations 1 and 3 is usually easy to measure. By eliminating m between equations (1) and (5):

$$\sigma_3 = \sigma_T + \frac{2(1 + \sigma_T)}{\sqrt{\xi}} + \frac{\sigma_T}{\xi} \qquad (7)$$

Equation (7) is therefore proposed as a design criterion to avoid cavitation damage. Y Boccadoro (Ref 6) showed that the optimum value of σ_T for orifice plates was 0.8 based on more than 100 data points for $0.3 \leqslant \beta \leqslant 0.7$.

To use this criterion with valves it was first assumed that σ_T is effectively independent of opening and flow conditions; although this would be difficult to check the assumption seemed reasonable Viscous losses, particularly from changes in the direction of flow, were considered; and it was concluded that they only affect the estimate of σ_3 at very low loss coefficients, so that in practice they can be ignored (Ref 6).

LOCATION AND INTENSITY OF DAMAGE BEHIND A CAVITATING ORIFICE PLATE

S B Au of Southampton University (Ref 4) studied visually the location of impingement of the small bubbles released by a cavitating orifice plate. The results were qualitatively quite interesting and helped to confirm that the erosion experienced in piping systems could indeed be caused by cavitation. However no information on damage could be obtained from a visual study because it did not take into account the variation in the energy of the impinging bubbles. Far more enlightening was the study made by Lobo Guerrero (Ref 7). The potential damage resulting from a cavitating step in a two dimensional channel (analagous to the orifice plate situation) was assessed by counting the number of pits per second of running, on a thin metallic foil located downstream of the step. Of course the actual damage would depend on the material but this method can be used to compare accurately the potential damage under different conditions. For a given velocity the influence of the cavitation number may be described as follows:

(a) near incipience, bubbles begin to appear in the shear layer but no damage can be observed.

(b) For lower σ_T a cloud of small bubbles develops and initial damage is experienced, starting from behind the dead water region (Fig 2b).

(c) Lowering the cavitation number results in increased cavity length; this displaces the location of maximum attack downstream and increases its intensity. The cavity also begins to pulsate backwards and forwards and this causes minor erosion right up to the bottom of the step, as shown in Fig 2(c).

(d) The pulsations reach their maximum strength and amplitude resulting in maximum erosion. Substantial attack can be experienced just behind the step (Fig 2d).

(e) Lowering σ_T then tends to reduce the intensity of the pulsations. The cavity length is even more unstable and the erosion is far less localised with diminishing intensity. Zone (a) is filled with very large bubbles. (Fig 2e).

(f) Finally when choking is reached the erosion is distributed as in Fig 2(f). The zone of attack is centred around the end of the cavity which grows longer as σ_T is lowered even further. Zone (a) then becomes filled with vapour so that no attack is experienced just behind the step.

The distances downstream were expressed in terms of the step height. Obviously a true similarity should take into account both the step height H and the section diameter D. However for $\frac{2H}{D}$ of the order of 0.5 it is considered that H is the most relevant parameter. When the cavitation number was held constant and the velocity varied it was found that the erosion intensity increased as V^α where $(2 \leqslant \alpha \leqslant 5)$. The intensity, but not the distribution of erosion, was found to be affected by velocity so that a comparison with the velocity increasing/cavitation number decreasing situation, as in the AML experiments, was still valid accepting the differences in magnitude.

The distribution of erosion established by Lobo Guerrero was generally confirmed in the experiments at AML but the results were not sufficient to support any theory satisfactorily since the operating cavitation numbers did not cover adequately the values of interest. Damage to 90/10 cupro-nickel pipes downstream of identical orifice plates with $\beta = 0.6$ was observed after a 5000 hour test. With the range of velocities stated earlier cavitation numbers of $\sigma_m = 5.0, 1.4, 0.38, 0.36$ were obtained. The presence of cavitation was not detected at $\sigma_T = 5.0$ and 1.4 and only scattered impingement corrosion pitting was found. However at $\sigma_m = 0.38$ and below general erosion wastage to an average depth of 0.2 mm occurred between 1 and 3 diameters downstream.

By correlating the available experimental data it is considered that the potential damage resulting from cavitating orifice plates may be summarized as follows:-

$\sigma_T > 0.8$ possible bubbles in the shear layer - no or negligible attack.

$0.8 > \sigma_T > 0.4$ light to moderate cavitation - some possible damage concentrated within 1 and 3 D downstream.

$0.4 > \sigma_T > 0.2$ moderate to heavy cavitation - increased potential damage in the same zone with some attack possibly immediately behind the plate.

$0.2 > \sigma_T > 0$ potential damage very high spread out over a larger area with maximum attack further downstream (4-5 diameters).

$\sigma_T = 0$ choking is reached- high potential damage over 5 or more diameters located where the cavity collapsed. In this condition the

remainder of the system downstream may be
exposed to corrosion/erosion effects.

It is considered that the summary above should be a useful guide to the
designers of sea water piping systems. Having chosen σ_T corresponding to the
degree of attack that can be tolerated σ_3 can be computed using equation (7).
When possible a value of $\sigma_T \geq 1$ should be chosen to ensure that the risk of
erosion damage is minimised.

LOCATION AND INTENSITY OF ATTACK ASSOCIATED WITH
DIAPHRAGM VALVES

In attempting to characterise the diaphragm valve (shown in section in Fig 3)
in cavitation terms the following steps must be taken:-

(a) Recognise when the valve is cavitating and determine the conditions under
which maximum damage to the valve interior will occur.

(b) Identify the conditions which will produce damage to downstream piping.

In order to use the cavitation criterion derived from work on orifice plates the
non-cavitating loss coefficient of the 50 mm diaphragm valve was measured for
various degrees of closure (Fig 4). The behaviour of the loss coefficient was
quite complex and after a thorough investigation it was concluded that it could
not be used with any degree of accuracy to determine cavitation incipience. It
could however, be used to indicate the choking condition which is the state when
maximum flow for a given upstream pressure is reached. Cavitation inception and
desinence were then recorded for six different positions of the 50 mm valve
(17%, 23%, 31%, 39%, 54% and 100% open), and a wide range of pressure and
velocity. Noise measurements were used as described earlier but the signal
obtained was not always reliable particularly at low upstream pressures and large
valve openings, which could explain the scatter in the data. In a similar manner
the choking condition was identified in each case. The experimental values of
σ_3 for cavitation desinence and choking were compared with loss coefficient and
curves derived from values of $\sigma_T = 1.0$ and 0.2 were superimposed (Fig 5). It
was found that $\sigma_T = 1.0$ is a fair estimate of cavitation inception while choking
is represented by $\sigma_T = 0.2$ and not zero which would indicate "breakdown" by the
formation of a clear cavity at vapour pressure.

This result was in agreement with the data obtained by Lobo Guerrero and
indicated that the maximum damage to the valve interior would be expected just
prior to the choking condition. Lowering σ_3 still further would tend to bring
the cavity outside the valve into the downstream pipe therefore displacing the
location of maximum attack (related to the end of the cavity). High speed
photography confirmed that only a few scattered bubbles were seen downstream of
the valve when choking was reached. When the cavitation number was lowered
further the cavity was clearly seen several diameters downstream. However Tullis
observed that the length of the cavity was highly dependent on the general
environment downstream (Ref 8). Due to the variety of conditions found in ship-
board systems a detailed survey of the cavity location was not considered

necessary. Based on the study of the 50 mm valve, equation (7) with $\sigma_T = 0.2$ is probably a fair estimate of when the pipe downstream would be damaged by cavitation erosion, the rate of attack depending on the material used.

Having determined the cavitation parameters for a 50 mm valve it was felt that their reliability might be demonstrated if agreement could be obtained when applied to another of different nominal bore. As an example the 38 mm valve used for independent cavitation studies at AML has a loss coefficient of 70 at 20% open. Therefore at cavitation inception represented by $\sigma_T = 1.0$, $\sigma_{3c} = 1.5$ from equation (7).

Now
$$\frac{p_1 - p_v}{\frac{1}{2}\rho v_1^2} = \frac{p_1 - p_v}{p_1 - p_3} \cdot \frac{p_1 - p_3}{\frac{1}{2}\rho v_1^2} = (\sigma_3 + 1)\xi \qquad \approx 175.$$

Curves of critical upstream pressure versus velocity for cavitation inception for four valve positions, were compared with the AML experimental data (Fig 6). The correlation was good over the effective operating range (20–40% open) and although the valves did not differ greatly in size some confidence was drawn from the result.

A total of ten gunmetal diaphragm valves were examined after 5000 hour tests in sea water piping systems. Seven were throttled to give loss coefficients in the range 50–100. Of the latter, two operated at $\sigma_3 \approx 1.6$, and the valve interiors of these suffered moderate cavitation erosion downstream of the seats. The seats were only slightly attacked. Five valves were operated at $\sigma_3 = 0.5$ and at the lower cavitation number both seats and downstream areas of the bodies were severely eroded. The remaining three valves operated at values of σ_3 between 2.0 and 4.0 with loss coefficients in the range 20–8 and no erosion of the interior was noted. Significant erosion wastage of 90/10 cupro-nickel piping downstream of valves occurred at $\sigma_3 = 0.5$ which supported results expressed earlier. At greater values of σ_3 corrosion/erosion effects were more dependent on velocity than cavitation number.

RECOMMENDATIONS FOR DESIGN

The results of studies on diaphragm valves have confirmed that equation (7) with $\sigma_T = 1.0$ can be used conveniently to avoid any major cavitation damage in pressure reducing devices. This yields

$$\left[\frac{p_3 - p_v}{p_1 - p_3}\right]_{critical} = \sigma_{3c} = 1 + \sqrt{\frac{4}{\xi}} + \frac{1}{\xi} \qquad (8)$$

or for $\xi > 10$ a simplified form is derived

$$\sigma_{3_0} \approx 1 + \frac{4}{\sqrt{\xi}} \qquad\qquad (9)$$

It is considered that if σ_3 is kept larger than σ_3 critical defined by equation (8) or (9) little or no cavitation erosion of either the fitting or the downstream pipe should be experienced. However if it is important that cavitation should be avoided completely a more conservative value of σ_T must be used and a value of 1.2 to 1.5 is suggested.

The present criterion has the great advantage of simplicity since it only involves knowing the upstream or downstream pressure, the pressure drop and the velocity. However the cavitation number σ_3 does not depend directly on velocity. It was emphasized earlier that at constant cavitation number the damage was an exponential function of velocity. The situation is further complicated by the risk of impingement corrosion at favourable local turbulence conditions which are also dependent on velocity. Therefore when applied to copper alloy sea water systems it is suggested that equation (8) be used only for velocities less than 5 m/s. This satisfies the requirements of sea water systems as defined by BS MA18 'Salt Water Piping Systems in Ships'. Since the cavitation parameters were derived mainly using Town's water the recommendations obviously apply to piping systems carrying this fluid and may be used with more confidence since the risk of impingement corrosion will be absent.

An example in the use of the design criterion may clarify its use. Assume that a permanent drop in pressure is required from 760 kN/m^2 absolute to 200 kN/m^2 with a flow rate corresponding to an average velocity of 3 m/s. The use of only one orifice plate would result in a cavitation number of approximately 0.36 and severe erosion of the downstream pipe would occur. Applying the proposed criterion three orifice plates would be required which would drop the pressure successively whilst maintaining values of σ_3 greater than σ_{3crit}. Such an arrangement should be free of corrosion/erosion effects. If a measure of control is required the last orifice plate may be replaced by a diaphragm valve provided that its operation falls within the limits specified earlier.

CONCLUSIONS

A design criterion to avoid major damage resulting from cavitation in pressure reducing devices has been developed. A single curve expresses the critical cavitation number σ_3 versus loss coefficient. This was supported by a thorough investigation of the cavitation characteristics of orifice plates and diaphragm valves including long term experiments using sea water. Recommendations for its use in sea water systems have acknowledged the influence of velocity and impingement corrosion on damage to the component and its associated pipework.

The dependence of the criterion upon knowledge of the non-cavitation loss coefficient of the pressure reducing device emphasised the need for accurate data on valves which should be provided by the manufacturer. Such data on orifice plates is already available in British Standard 1042. Although the data

now reported is intended primarily for the system designer its effectiveness should be checked by the operator. In short, it is considered that greater emphasis should be placed on the provision of means for monitoring pressure and velocity in installed systems if the long term economic advantages offered by the use of the design criterion are to be realised.

ACKNOWLEDGEMENTS

REFERENCES

(1)   NUMACHI F. "Cavitation effect on discharge coefficient of the sharp edge orifice plate.. Trans. ASME (D) vol 82 pp 1 1960.

(2)   BALL J W. "Sudden enlargement in pipelines" ASCE Journal Power Div. vol 88 paper 3340 December 1962.

(3)   LINENHARD J H. "Influence of Size and Configuration on Cavitation in Submerged Orifice Flows". ASME Paper No. 71-FE-39 1971.

(4)   BRITISH STANDARD 1042: Part 1: 1964.
        Methods for the measurement of fluid flow in pipes. Part 1
        Orifice Plates, Nozzles and Venturi Tubes. Appendix E. Fig 62.

(5)   AU S B. Private Communication.

(6)   BOCCADORO Y. Private Communication - to be published.

(7)   GUERRERO J LOBO. Private Communication - to be published.

(8)   TULLIS J.P, Choking and Supercavitating Valves. ASCE December 1971, Hydraulics Division pp 1931-1944.

Derivation of loss coefficient in terms of orifice plate parameters.
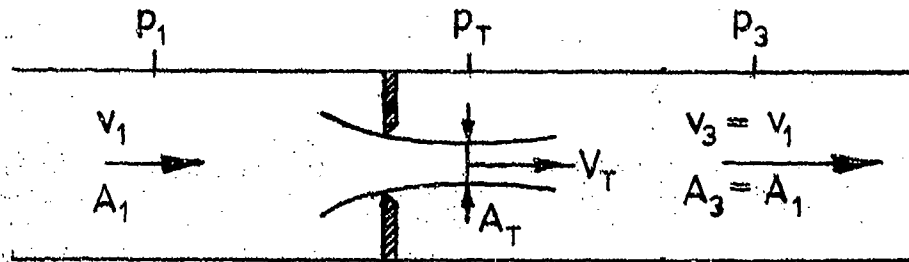
It is assumed that the velocity distribution is uniform in each section.

Applying Bernoulli's equation between location 1 and T assuming negligible losses:

$$p_1 + \tfrac{1}{2}\rho v_1^2 = p_T + \tfrac{1}{2}\rho v_T^2$$

or with $\dfrac{v_1}{v_T} = \dfrac{A_T}{A_1} = m = M_o C_o$

$$p_1 - p_T = \tfrac{1}{2}\rho v_1^2 \cdot \frac{1 - m^2}{m^2}$$

Using Borda's equation

$$p_3 - p_T = 2\left(\tfrac{1}{2}\rho v_T^2\right) m (1-m)$$

or

$$p_3 - p_T = 2\,\frac{1 - m}{m} \cdot \left(\tfrac{1}{2}\rho v_1^2\right)$$

and

$$p_1 - p_3 = \left(\frac{1 - m}{m}\right)^2 \cdot \tfrac{1}{2}\rho v_1^2$$

defining the loss coefficient

$$\xi = \frac{p_1 - p_3}{\tfrac{1}{2}\rho v_1^2} = \left(\frac{1 - m}{m}\right)^2 \qquad\qquad (1)$$

However in the use of orifice plates it is p_T which is often measured and not p_3. Hence for comparison with experimental data one should use

$$\xi' = \frac{p_1 - p_T}{\frac{1}{2}\rho v_1^2} = \frac{1 - m^2}{m^2} \qquad (1)'$$
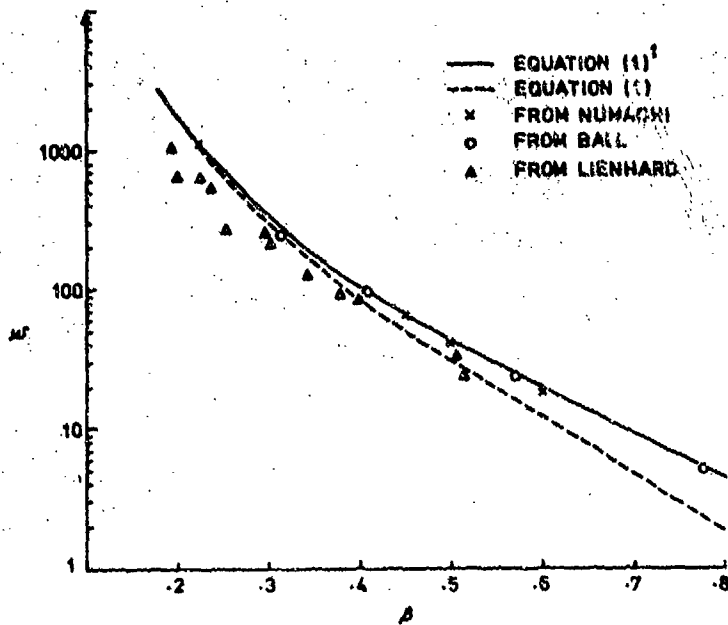
<u>FIGURE 1</u>.   LOSS COEFFICIENT FOR ORIFICE PLATE
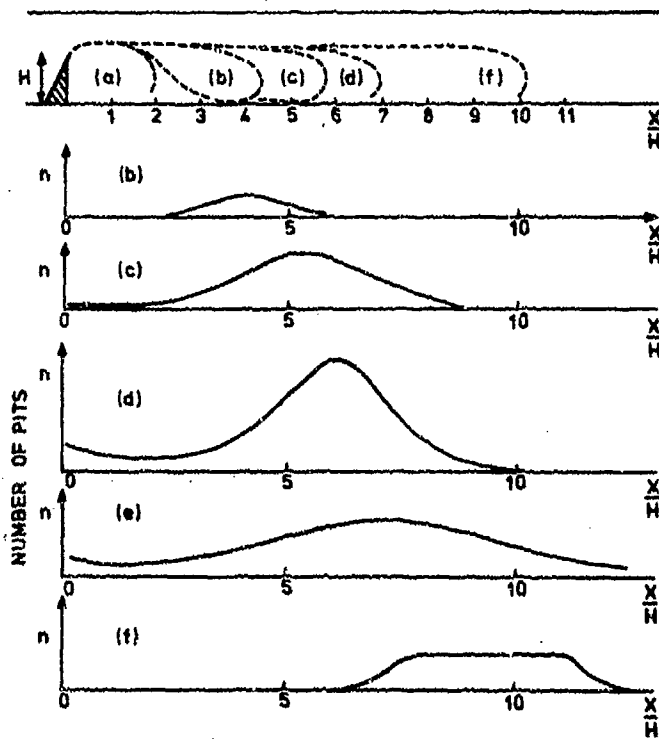
<u>FIGURE 2</u>.   DAMAGE DISTRIBUTION BEHIND A CAVITATING ORIFICE PLATE
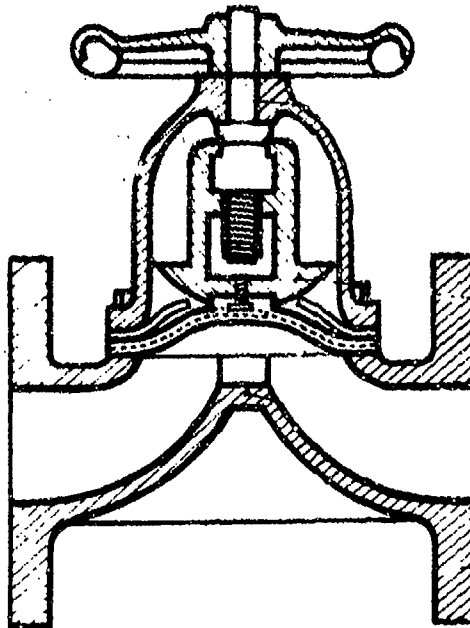
FIGURE 3.   SECTIONED VIEW OF DIAPHRAGM VALVE
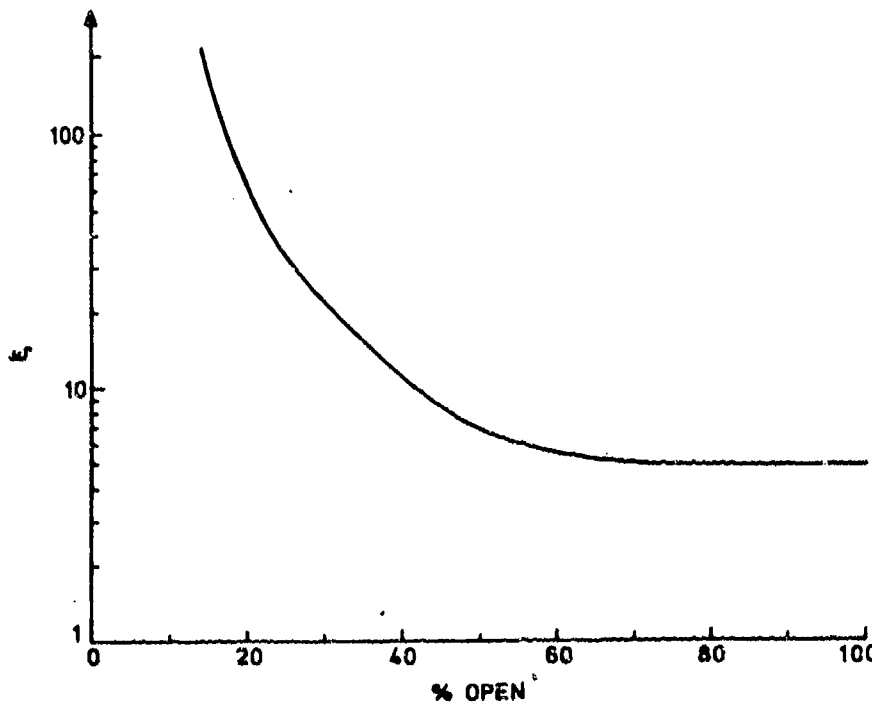
FIGURE 4.   LOSS COEFFICIENT FOR A 50 mm DIAPHRAGM VALVE
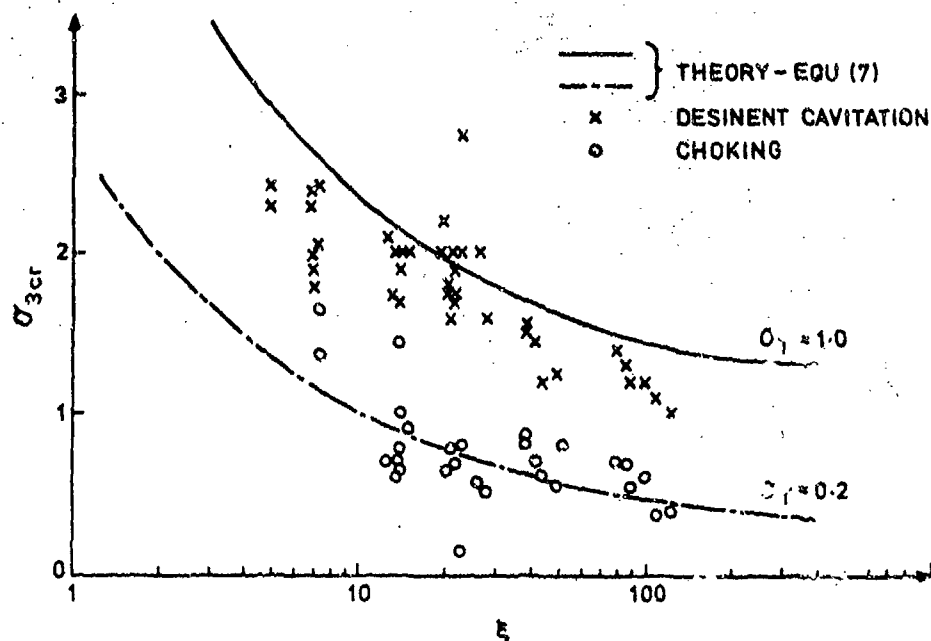
FIGURE 5. CRITICAL CAVITATION NUMBERS VERSUS LOSS COEFFICIENT FOR A 50 mm DIAPHRAGM VALVE
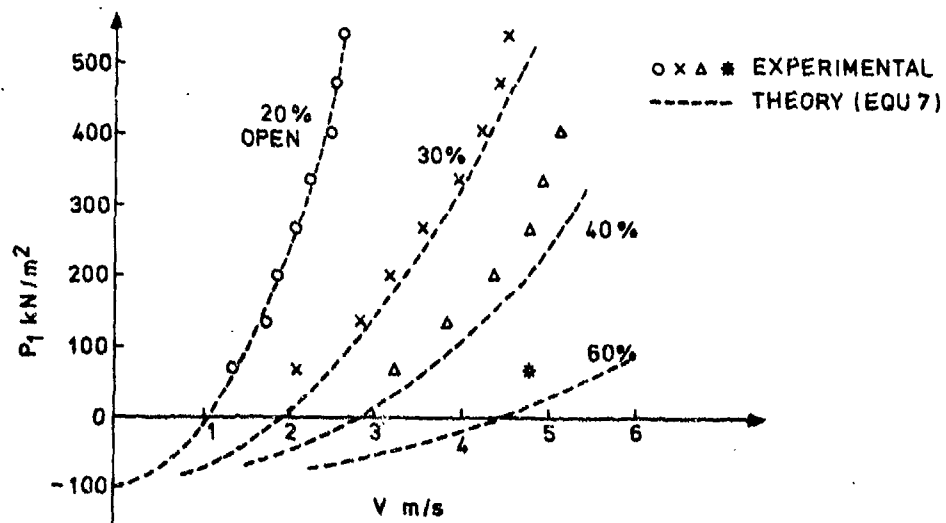
FIGURE 6. EXPERIMENTAL RESULTS FOR CAVITATION INCEPTION COMPARED WITH THEORY FOR A 38 mm DIAPHRAGM VALVE

FEASIBILITY STUDIES OF CORROSION MONITORING IN SEAWATER
SYSTEMS

by

J C Rowlands

Admiralty Materials Laboratory, Holton Heath, Poole, UK.

S U M M A R Y

Possible techniques for detection of the occurrence of cavitation erosion and
impingement attack in ships' seawater systems have been investigated. If these
forms of corrosion can be monitored, remedial action can be taken thereby achieving
improved reliability and ship availability. Development of prototype
instrumentation for ship trials of a cavitation monitoring system are under way
and instrumentation for research on the mechanism of impingement attack is
proposed.

INTRODUCTION

Considerable success has been obtained using the corrosion meter developed for the measurement of corrosive environments[1,2], its principal Naval application being the control of inhibitor injection to combat polluted estuarine water corrosion during ship construction[3] and one UK shipbuilder has used the same procedure for giant tanker and Atlantic container ship construction. Interest has also been expressed by the German and Royal Netherlands Navies for similar applications. Unfortunately, the polarisation resistance measurement utilised with this instrument only determines the corrosion rate on test electrodes and not elsewhere in the system.

Current research is aimed at developing corrosion monitoring instruments for improving the reliability of ships' seawater systems. In such systems the two principal failure mechanisms are impingement attack and cavitation erosion. In order to develop instrumentation, it is first necessary to establish the mechanisms of deterioration in order to define a parameter characteristic of the failure mode which is capable of physical measurement. It is also desirable to determine when and where the attack is occurring in the system, while it is actually happening rather than how deep or extensive it is by post-mortem examination after it has occurred as with conventional non-destructive testing methods. With the availability of appropriate corrosion monitoring instrumentation it would be possible to use existing materials more effectively within their capabilities, which is an important aspect of value engineering in large, expensive structures. The effective use of appropriate instrumentation would improve the availability and reliability of ships and reduced maintenance cost by preventing costly and inconvenient failures.

FAILURE MECHANISMS IN SEAWATER SYSTEMS

The effect of both cavitation erosion and impingement attack in seawater systems is the wastage of metal, which in the case of seawater systems is of copper based alloys and predominantly cupro-nickels. Consequently, the results of these corrosion mechanisms is the dissolution of a copper-based alloy giving rise to an excess of the corroding metal ion species in the system, and one approach to corrosion monitoring would be the chemical detection of metal ions at selected positions in the seawater system using physical analytical techniques. For other approaches it is necessary to consider the mechanisms of the corrosion processes involved.

Cavitation involves the formation of vapour bubbles caused by a local reduction in pressure below the saturated vapour pressure in a liquid system. These bubbles grow rapidly, and when they move into an area of higher pressure rapid collapse occurs in which energy is released. If this occurs adjacent to a solid surface, the energy may be sufficient to cause mechanical damage possibly by a mechanism similar to fatigue, and may occur both on metals and non-metals. Lower energy levels of bubble collapse, while insufficient to cause mechanical damage, may create areas of local high turbulence at the metal surface and result in cavitation corrosion, which is attributed to an electrochemical mechanism akin to impingement attack. The energy release of the bubble collapse causes the metal component to vibrate, transmitting sound or ultrasonic waves, which it was considered could be a parameter which would be measurable as a cavitation

monitoring technique. It is the cavitation corrosion mechanism which is responsible for the rapid deterioration of ships' components, such as pipes downstream of orifice plates, valve seats and bodies, pump impellers and seals.

Impingement attack is accelerated corrosion due to removal of protective corrosion product films and/or access of reactants by turbulent water flow, thereby continually exposing an active metal surface, which forms the anode site. The rate of attack is controlled by the hydrodynamics and geometry of the system, which determines the area of the anode of impingement site and the surrounding cathode, the greatest rate of attack being when the anode is small and the cathode is large[4]. Thus, the rate of attack is determined by the anode current density, and the detection of this current could be a means of determining the occurrence of impingement attack in a practical system. Alternatively, in conjunction with hydrodynamic studies on seawater systems, currently being investigated there is promise that it will be possible to define the situations in a seawater system where attack is likely to occur and it would be possible to simulate the worst conditions likely to occur and design electrode assemblies capable of detecting the conditions for impingement attack to arise.

CORROSION MONITORING TECHNIQUES

Chemical Monitoring

Consideration has been given to the use of analytical techniques for the determination of metal ion concentrations in seawater systems for the detection of localised corrosion. Since seawater systems are constructed of copper-based alloys, the major metal ion concentration resulting from corrosion would be copper. The feasibility of using copper estimations was examined on a 'once-through' experimental seawater facility. The amount of corrosion in an experimental 5" diameter pipe system shown diagrammatically in Fig. 1 was determined after a 5,000 hour run, with water velocity 4.5 m/s. This pipe system was 15 metres in length and had twelve cavitation corrosion or impingement attack sites. The extent of the corrosion at each site is given in Table 1. From this survey, the copper ion concentration in the seawater, assuming that all the copper is retained in solution as copper ions, would be of the order 0.13 μg/l. In a ship's seawater system this concentration of copper ions would be required to be determined on a background concentration of up to 100 μg/l mainly arising from cavitation erosion in the seawater pumps and general corrosion of the seawater system components, and the variable natural copper content of seawater. In the particular system examined the copper ion concentration at the inlet of the test section was 36 μg/l. At the present time it is not thought practical to determine such small copper ion concentration differences. Additionally, as a complicating factor, it would be necessary to allow for changes of the general corrosion of the pipe system components with age. An idea of the change in general corrosion rate with time can be seen in Table 2, where the change of corrosion rate of copper in seawater with time is given.

It has also been assumed that all the copper removed by corrosion and the selective corrosion processes is lost into solution as copper ions, whereas in practice the processes involved in corrosion are extremely complex, one of the suggested sequences of reactions following the dissolution of copper in seawater being as follows[5]:-

$$Cl^- \text{ ions} \longrightarrow CuCl_2^- \rightleftharpoons CuCl_3^{--}$$

$$Cu \longrightarrow Cu^+ + \epsilon \longrightarrow Cu^{++} + \epsilon$$

reduction of oxygen   reduction of oxygen

basic cupric carbonate $\longleftarrow$ OH^- and HCO_3^- ions
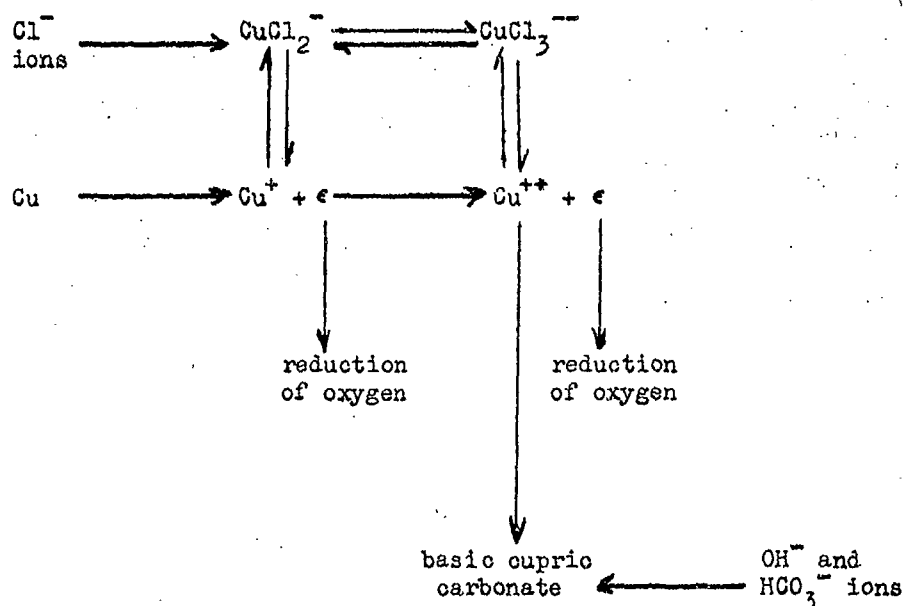
In view of the practical difficulties of accurate chemical monitoring on board ship, it is considered that chemical analytical techniques are not feasible at present for the detection of localised corrosion in ships' seawater systems.

Cavitation Monitoring

The fact that cavitating components vibrate is a well-known phenomenon. In the first instance the noise emitted by a cavitating diaphragm valve was determined by clamping a biceramic transducer to a flat area prepared on the underside of the valve body as shown in Fig. 2. On displaying the output signal from the transducer on an oscilloscope it was observed that when the valve was cavitating, as determined by a loss in valve throttling efficiency, there was a significant high frequency component.

The frequency spectrum of a variety of components including a Saunders diaphragm valve, pipework downstream of a Saunders valve, a G & K gate valve, and a Worthington Simpson pump, were determined under both cavitating and non-cavitating conditions. The transducer probe used for these experiments had a resonant frequency of 2.5 MHz and an impedance of 2 k ohms over the frequency range 5-100 kHz. A high resonant frequency probe was chosen to give a linear frequency response over the range 100 Hz to 100 kHz. The signal from this

probe was fed into a Waverley Electronics selective detector type SD466/1 which had an input impedance of 1 M ohm. The selective detector had a switched $\frac{1}{3}$ octave bandpass filter with better than 50 dB/octave roll off. The results of the frequency spectrum analyses on the various components are shown in Figs. 3-6. The significant difference in the systems between the cavitating and non-cavitating conditions is in the 6 kHz-30 kHz region, where there is a high output response due to the cavitation.

It was questionable whether the high frequency response due to cavitation was a function of bubble collapse resonant frequency or the resonant frequency of components in the seawater system. To elucidate these factors a transducer was attached to a length of water-filled pipe and fed with a variable fixed frequency signal from a signal generator. Using a matching transducer as a pickup, fed into an oscilloscope, it was intended to sweep the appropriate frequency spectrum and determine the resonant frequency of the pipe system. In practice, as the transmitting transducer was effectively a point source, nodes and anti-nodes of the longitudinal and transverse waves in the pipe, and the waterborne transmissions were detected, and consequently the resultant signal was very dependent on the particular position of the receiving probe. In the practical situation of a cavitating component this difficulty is not so obvious as the cavitation occurs over an area in the system and over a band of frequency emissions, which has the effect of flattening out the nodes and anti-nodes.

For a cavitation monitor to be used on board ship it would be necessary to detect which component in the system was cavitating, and if signals were transmitted extensively through the system, this would not be possible. Using cavitating valves as the signal source, it was found that with the conventional flange in pipelines of $1\frac{1}{2}$"-6" bore there was an attenuation due to the flange of 4-6 dB. This attenuation can be further increased to 9 dB by inserting a Perspex coupling piece 1" thick between the mating flange surfaces. Long lengths of 90/10 cupro-nickel pipe, either in the straight condition or with bends showed no significant attenuation of signal along the length. This gives rise to problems of probe positioning in a practical ship's system, but it is considered that as the likely cavitating components are easily recognised, it would be simple to insert appropriate coupling attenuators between cavitating components.

The optimum positioning of the transducer probes in a practical seawater system has been considered. For ease of operation the most convenient position would be on a flange face. The signal attenuation on the flange was variable according to the flange size and the material, but as a general observation it was found that there was a 6 dB fall off on the flange bolt heads, a 4 dB fall off on the rim of the flange, but on 1 dB fall off on the flange back face. From these results it would appear that it might be very convenient to attach the transducer to the back face of a flange coupling to seawater pipe components likely to cavitate. Various coupling fluids between the transducer and component under test were investigated but no significant improvement on the mechanical air coupling was found.

Having assessed the problems of cavitation monitoring using cavitation frequency emissions, it remained to develop suitable instrumentation for practical ship applications. It appeared that the requirement was for a ceramic transducer operating at around 10 kHz, preferably resonant at that frequency, with a low response to lower frequency transmission. For this purpose a piezoelectric transducer was preferred to the resistance type in order to avoid the requirement for bridge balancing in the electronic instrumentation. The development of a suitable probe for this purpose is being undertaken by the Electroceramics Section at AML, and will be reported separately. Considerable success has been achieved with prototype probes which ve been fed into a prototype instrument comprising of a narrow band ampli'' r operating at 10 kHz with 3 dB cut off points at 7 kHz and 20 kHz, and a minimum of 12 dB/octave roll off. The circuit diagram of this instrument is shown in Fig. 7. Depending upon the characteristics of the final design of probe the input stage of the narrow band amplifier may require to be altered to achieve matching.

The Hall Probe

When impingement attack occurs on the wall of a seawater pipe system the pitted or attack site is acting as the anode and the surrounding area behaves as the cathode. The current flowing between the anode and cathode sites is the parameter which determines the rate of attack. The magnitude of this current can be estimated using Faraday's Law and if a rate of impingement attack of 2.5 mm/year is assumed this gives a current density of 1-2 mA/mm^2, according to whether it is assumed the copper is ionised as the cuprous or cupric ion. This order of magnitude is in agreement with that determined in electrochemical investigations of the mechanism of impingement attack[4].

The Hall probe is a semiconductor device which, when placed in a magnetic field and excited with a constant current at right angles, produces a Hall voltage in the third plane, as illustrated in Fig. 8. The Hall voltage is given by the equation $V_H = \dfrac{R_H i B}{d}$ where V_H = Hall voltage, R_H = Hall coefficient of semiconductor used, d = thickness of semiconductor, i = current and B = magnetic induction. Commercial gausmeters are available with a **sensitivity** of 10^{-5} T FSD. One such instrument uses a carrier square wave at 5 kHz excitation current and indium arsenide (InAs) probes. This instrument has three cascade stages of 46 dB amplification with about 40 dB of negative feedback, which results in a stable gain overall of approximately 80,000. The amplifier uses very narrow bandwidth and phase lock techniques by taking the square wave from the probe's supply oscillator and phase witching each amplifier block. The square wave is used to switch a synchronous demodulator to enable fields of either polarity to be detected. The electronics used are sophisticated and, although not sensitive enough for the present purpose, it may be used as the basis of a more sensitive system. Using this instrument and models of a corroding system, such as the current flowing in the long straight conductor, or the current flowing in a circular plate from a central contact to the circumference, it has been established that the field strength falls off inversely as the distance squared of the probe from the conductor, and is in inverse proportion to the distance from the anode point simulated at the

centre of the circular plate conductor. The instrument was insufficiently sensitive to use in conjunction with impingement attack on a specimen subject to jet impingement attack in seawater.

By the use of ferrite collectors made as two quarter segments of a circle with the Hall probe at the centre, the segment being 40 mm in diameter, the sensitivity of the probe could be increased by a factor of 10. Attempts were made to use indium antimonide (InSb) which has a sensitivity of 1.5 volts/Wb field, which is an order of magnitude above that for InAs, in conjunction with a specially made high gain low noise amplifier. However, this was not satisfactory, due to the high temperature coefficient ($1.5\%/°C$) of the InSb material and the inherent noise of the device at low output. The amplifier used was tuned to a frequency of 76 Hz as a minimum harmonic of mains frequency.

It would appear that the most promising course for future work would be the building of a preamplifier with a further 40 dB of amplification and a correlator lacked to the internal 5 kHz square wave of the gausmeter.

Zero Resistance Ammeter

Since impingement attack is a corrosion reaction it involves a current flow between the anode which is the impingement site and the surrounding cathode. If the impingement site can be separated electrically from the surrounding area and a zero resistance ammeter (ZRA) inserted in the external circuit, the current reading given by the ZRA is proportional to the rate of impingement attack.

A possible design of zero resistance ammeter has been published by Henry and Wild[6]. This basic circuit has been modified to utilise non-proprietary components which are readily available in the UK, and the circuit diagram is shown in Fig. 9. The instrument is capable of measurement of currents from 1 μA to 10 mA with an accuracy better than 1% to the limits of $\pm$ 1 μA. To compensate for thermal drift on the microamplifier occasional checking of the offset zero is required, particularly during the instrument warm-up stage. The final read-out is conveniently displayed on a digital voltmeter. The theoretical considerations of using a high gain operational amplifier for this purpose have been published by Lauer and Mansfield[7].

It is now intended to use this instrument in conjunction with research on the mechanism of impingement attack, in which it is hoped to relate laminar sub-layer thickness for turbulent seawater flow in a pipe to the rate of impingement attack. From this investigation and theoretical considerations of the hydrodynamics of water flow in seawater systems it is proposed that an electrode assembly be installed in a ship's seawater system to relate the worst operating conditions to the onset of risk of impingement attack.

CONCLUSIONS AND RECOMMENDATIONS

Arising from the investigations of possible corrosion monitoring techniques, the following conclusions and recommendations are made:-

(a) The use of analytical techniques to determine corroding ions in solution would not appear a practical proposition for use in seawater systems, as even if the required sensitivity could be obtained the signal to noise ratio would be too low.

(b) The measurement of noise arising from cavitating systems as a monitoring technique appears very promising, and no difficulties are anticipated in the development of equipment for this purpose. It is suggested that in the near future it will be appropriate for ship trials to be organised. In the first instance it is desirable for equipment to be built for a short trial in which possible error sources such as sonar transmissions and worn ball and roller bearings can be investigated. Subject to this trial being satisfactory, a further more prolonged trial would be required in which the co-operation of ship's staff would be required to set up a non-cavitating ship seawater system. Subject to satisfactory completion of these trials, production equipment could be developed in the form of either a mobile hand monitoring instrument, or an instrumented control system possibly with read-out in the engine control room.

(c) For detection of impingement attack, the Hall probe technique would have the advantage of ease of operation under ship conditions. At the present stage of development difficulties are foreseen in producing the required level of sensitivity for this particular application. However, the technique has other applications, particularly as a corrosion research tool and it is recommended that the present investigations to obtain the maximum sensitivity on commercially available Hall probe devices should be pursued.

(d) A satisfactory zero resistance ammeter has been developed, and it now remains to pursue the electrochemical aspects of using this instrument to produce an impingement monitoring technique. The next development stage is to use the zero resistance ammeter for research on mechanism of impingement attack before offering the device as a practical ship technique. The zero resistance ammeter has, however, other applications, and at present it is proposed to use the AML instrument for studies of bimetallic corrosion problems.

ACKNOWLEDGEMENTS

ammeter. The author is also grateful to Mr E D G Brown for arranging the
construction of instrumentation and the co-operation of Mr H G Brown and
Mr W Ford of Waverley Electronics Ltd.

This paper is published with the permission of the Procurement Executive,
Ministry of Defence, but any opinions expressed are personal to the author.

REFERENCES

(1) Rowlands, J C and Bentley, M N: Br. Corros. J. 1972, 7, p. 42-46.

(2) Rowlands, J C and Bentley, M N: Brit. Patent 1,150,416.

(3) Pearson, R: J. Naval Eng. 1970, 19, p. 291-298.

(4) Rowlands, J C: Proc. Localised Corrosion Conference, Williamsburg 1971.

(5) Marine Fouling and Its Prevention, Chapter 15, Woods Hole Oceanographic
     Institute.

(6) Henry, W D and Wilde, B E: Corrosion 1971, 27, p.479-482

(7) Lauer, G and Mansfeld: Corrosion 1970, 26, p. 504-506.

TABLE 1

LOCALISED CORROSION SITES IN AN EXPERIMENTAL SEAWATER SYSTEM

Component Number (Referred to Fig. 1)	Reason for Localised Corrosion	Form of Corrosion	Estimated Loss of Metal (mm^3)
21	Cavitation corrosion	Pitting on gun metal ball	920
1	Cavitation corrosion	Ring of shallow pits	60
2	Impingement attack	Scattered shallow pitting	20
4	Impingement attack	Inside of bend attacked	110
5	Impingement attack due to flow straightening vanes	Grooves adjacent to vanes	50
8	Impingement attack downstream of bend	Isolated shallow pits	2
10	Heat affected zone corrosion	Ring of preferential corrosion	12
15	Impingement attack downstream of T-piece	Inside of bend attack	380
16	Impingement attack due to flow straightening vanes	Grooves adjacent to vanes	4
17	Impingement attack downstream of T-piece	Inside bend attack	10
20	Impingement attack downstream of T-piece and 1D bend, and heat-affected zone corrosion	Impingement inside bend attack HAZ - ring of pitting	360
		TOTAL	1928

TABLE 2

EFFECT OF EXPOSURE PERIOD ON THE CORROSION RATE OF COPPER

Exposure time – months	1	2	3	6	12	24	48
Average corrosion rate for period $\mu m/y$	115	112	108	96	34	19	18

NOTE: 1 $\mu m/y \cong$ 0.039 thou/year
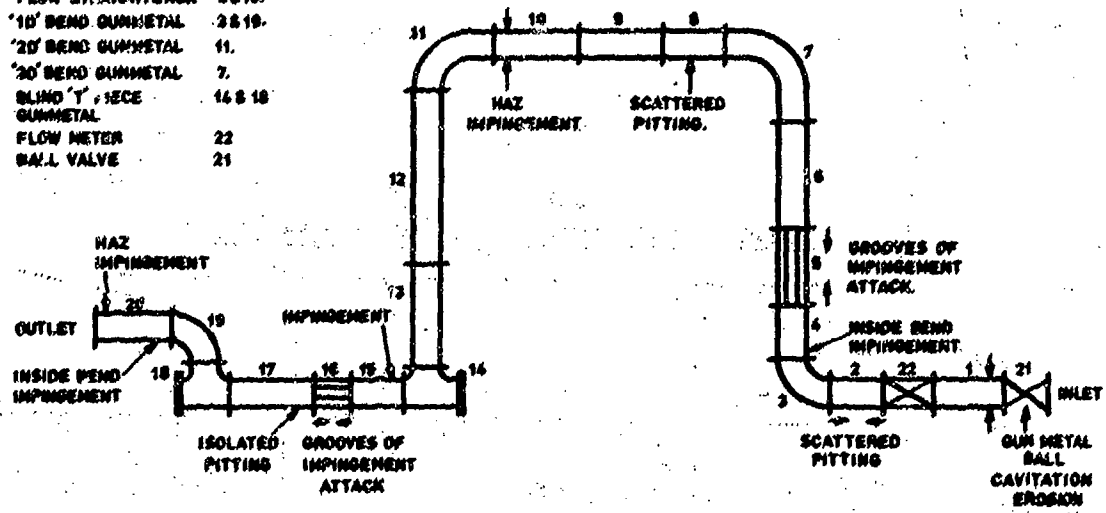
FIG.1   LOCALISED CORROSION SITES IN AN EXPERIMENTAL SEA WATER SYSTEM.
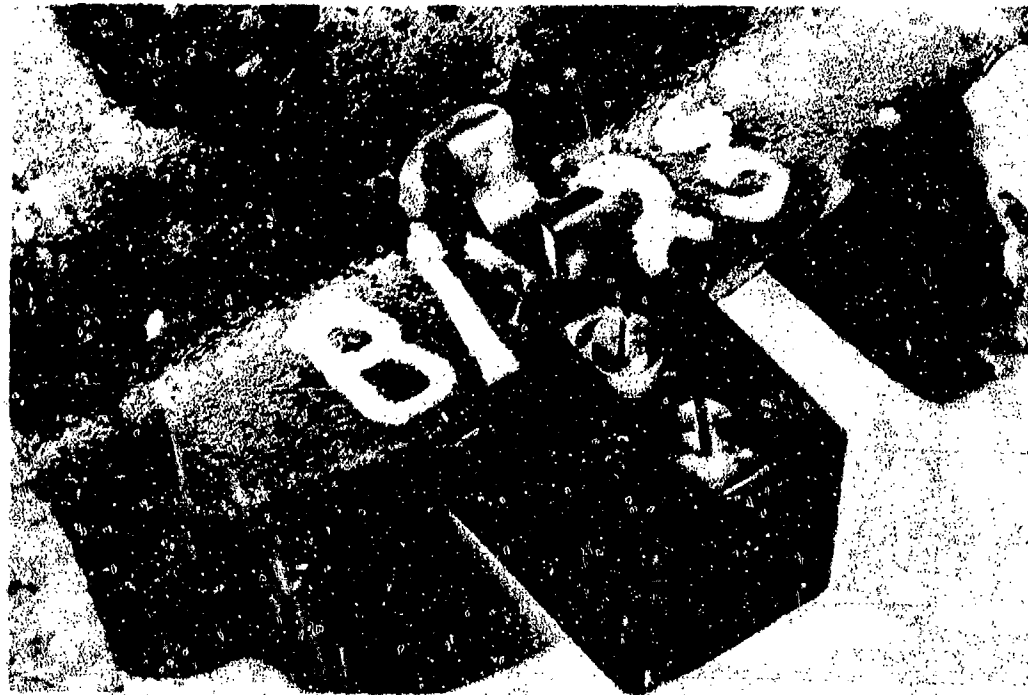
FIG.2   MOUNTING OF TRANSDUCER ON UNDERSIDE OF WEIR DIAPHRAGM VALVE.
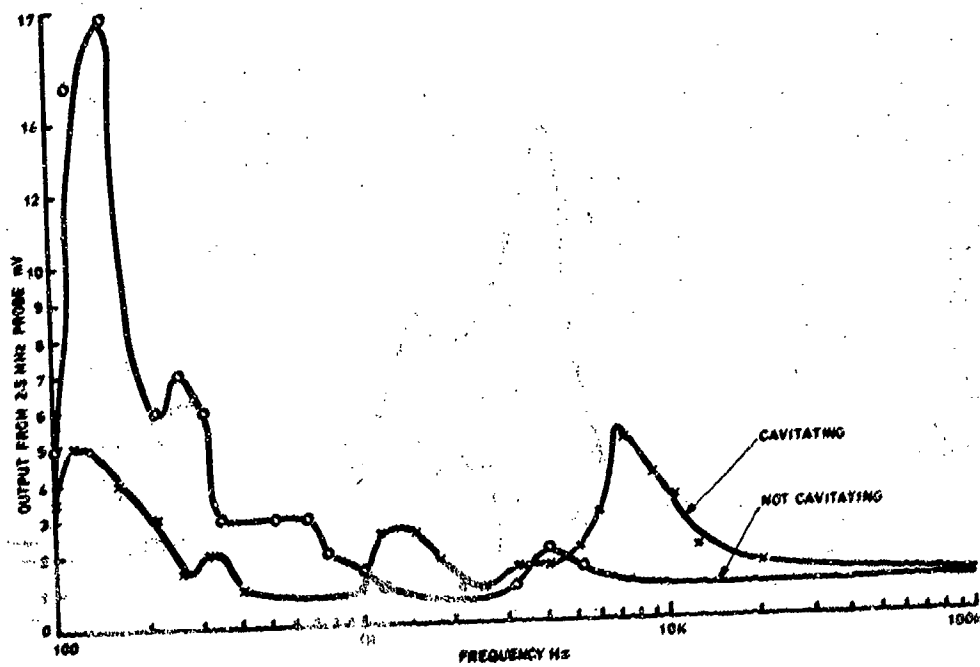
FIG.3 FREQUENCY SPECTRUM OF SAUNDERS DIAPHRAGM VALVE.
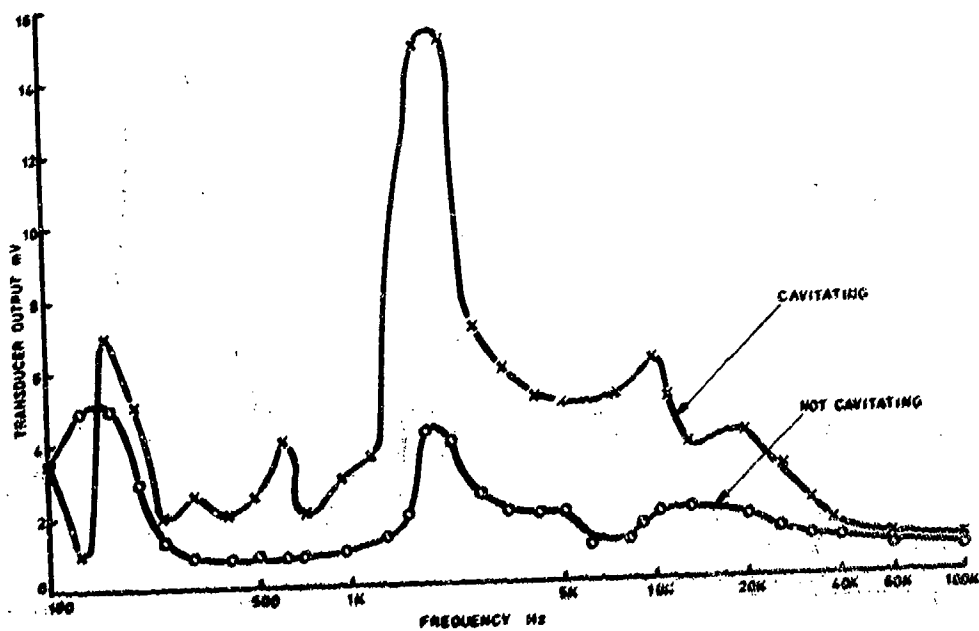
FIG.4 FREQUENCY SPECTRUM OF PIPE 4INS. DOWNSTREAM OF SAUNDERS VALVE.

171
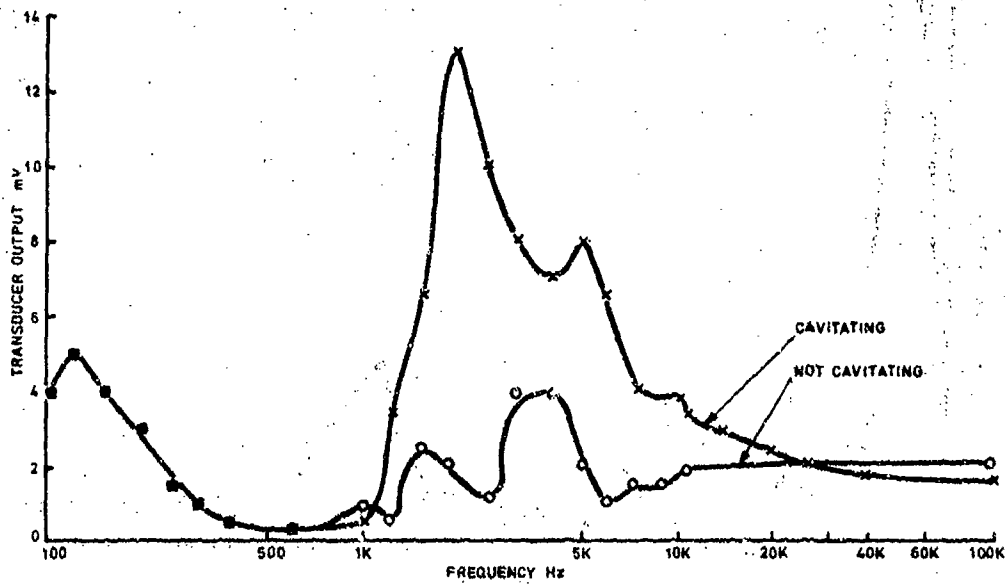
FIG.5 FREQUENCY SPECTRUM FOR G & K GATE VALVE.
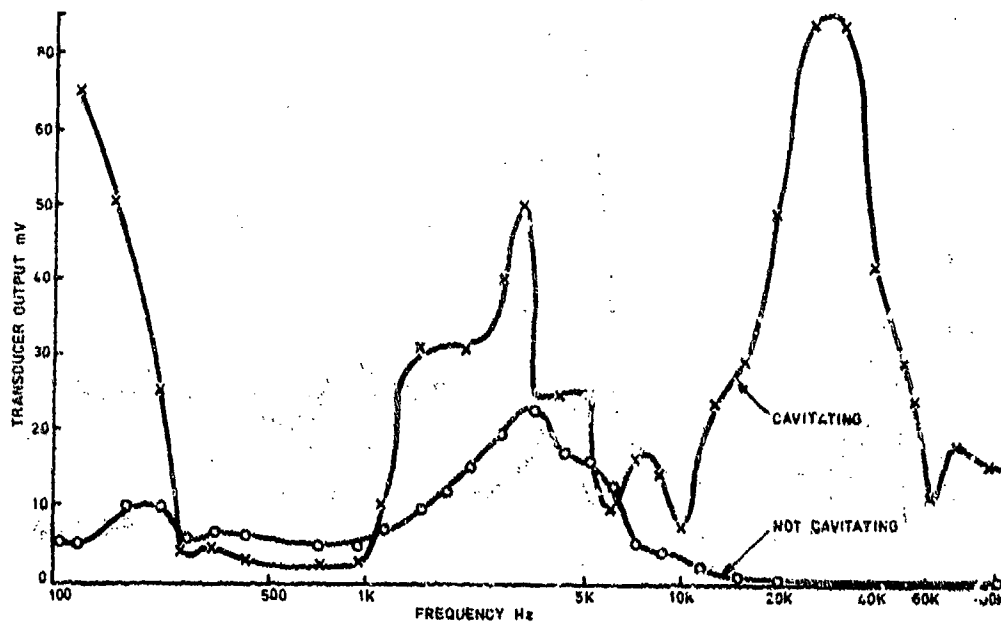
FIG.6 FREQUENCY SPECTRUM OF WORTHINGTON SIMPSON PUMP.

172
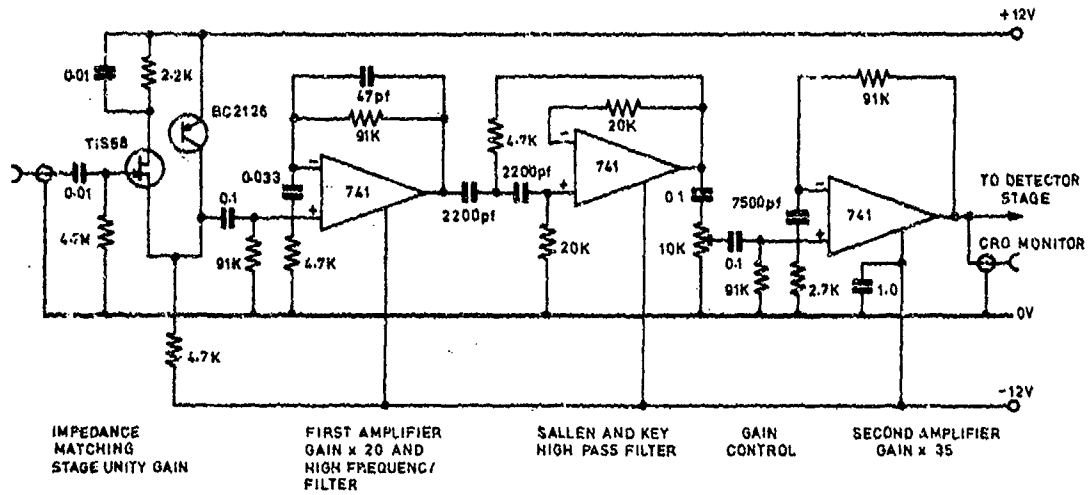
FIG.7a   CAVITATION MONITOR AMPLIFIER STAGE.
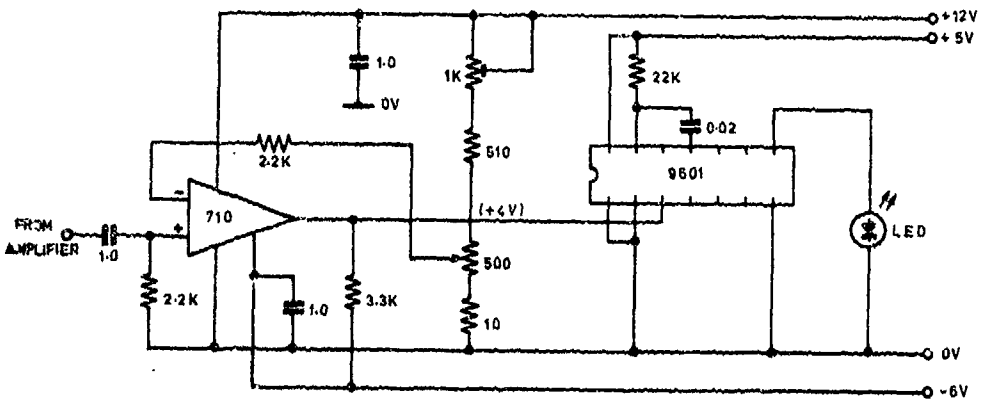
FIG.7b   CAVITATION MONITOR LEVEL DETECTOR AND LAMP LOGIC.
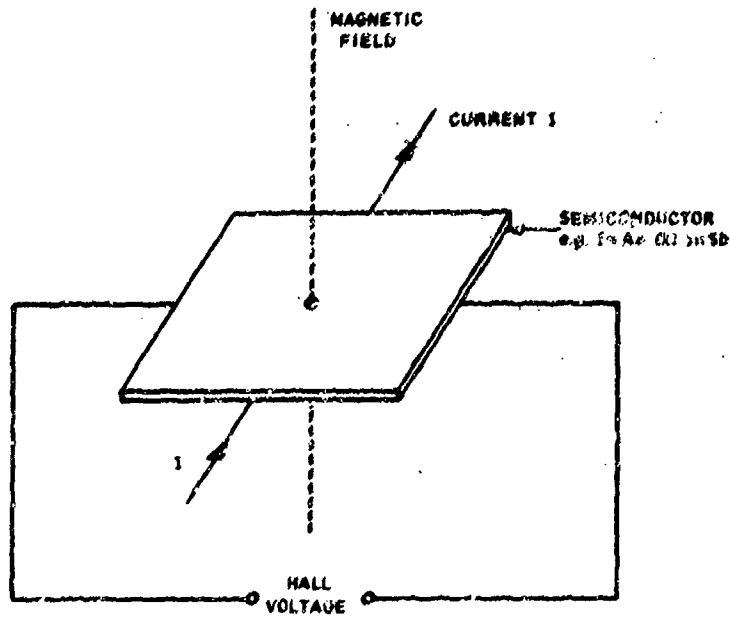
FIG.8   HALL PROBE FOR MEASUREMENT OF MAGNETIC FIELDS.
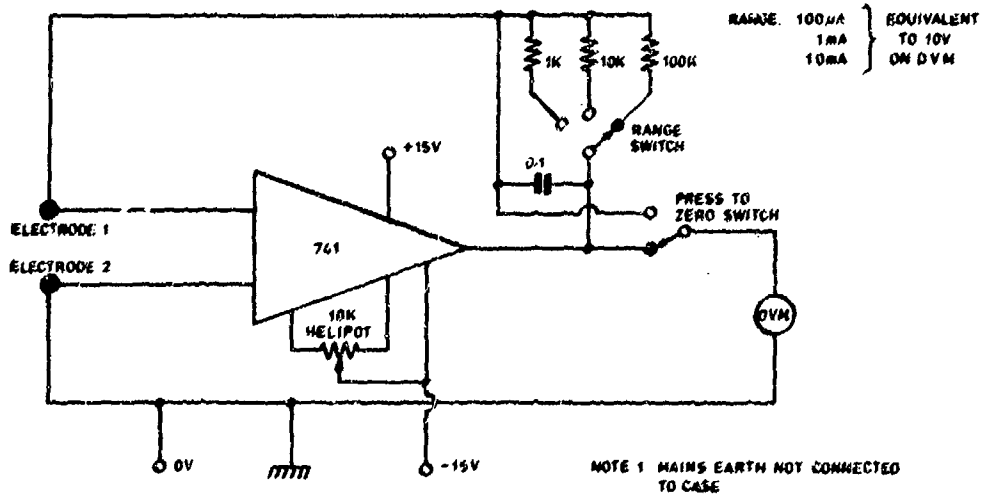
FIG.9   CIRCUIT DIAGRAM OF ZERO RESISTANCE AMMETER.

SESSION VI

CORROSION TEST METHOD STANDARDS DEVELOPMENT

Stress Corrosion Cracking of High Hardness Steel Armour

D.B. Dawson, M. Levy and D.W. Seitz Jr
U.S. Army Materials and Mechanics Research Center

SYNOPSIS

A stress corrosion cracking test has been developed for use with armor alloys. It is self-loaded, and it can be used to test armor plate of any thickness. K_{ISCC} values can be determined with a single specimen of the crack arrest, decreasing K type. High hardness XAR-30 plate from two sources has been tested and found to be very susceptible to stress corrosion cracking if a sharp crack is present: K_{ISCC} values ranged from 11 to 19 ksi $\sqrt{}$ inch, despite good fracture toughness performance. There were no significant differences in stress corrosion susceptibility between plate from different manufacturers, or different specimen orientations. Distilled water is observed to be as aggressive as seawater in K_{ISCC} determinations.

INTRODUCTION

High-strength materials are frequently found to have poor resistance to stress corrosion cracking (SCC). In particular, high-strength steels (yield strength over 200 ksi) which contain a crack or a sharp notch are often susceptible to SCC in water, or even in humid air(1). Several failures of high-hardness armour plate in Army weapons systems have recently been attributed to stress corrosion(2).

The present study was undertaken to develop a stress corrosion cracking test which could be used to evaluate armour plate of varying thicknesses, and to provide engineering data on the SCC resistance of high-hardness XAR-30 steel armour obtained from several producers.

BACKGROUND

There is no universally acceptable test method for susceptibility to stress corrosion cracking. Until the recent development of SCC specimens designed using fracture mechanics principles, the most common types of SCC tests used smooth, uncracked specimens (e.g., tensile, U-bend, and bent beam specimens). However, in certain alloy systems, tests using unnotched specimens are not sufficiently discriminating. For instance, some high-strength steels in humid air or water environments(1), and some titanium alloys in aqueous chlorides(3), are susceptible to SCC if a sharp crack is present, but are not susceptible in the absence of such a crack.

The Charpy test has traditionally been used to evaluate the toughness of materials, but it has certain limitations when applied to the high-strength materials which have been developed in recent years. For these materials, fracture-toughness tests provide a much better measure of resistance to flaw strength in noncorrosive environments, but the resultant values of K_{IC} are still not an adequate measure of resistance to SCC. For example, in a recent study for the Army Tank Automotive Command, Mostovoy and Ripling(2) have studied the SCC behaviour of several plates of high-hardness armour steel. Of the four plates studied, two had cracked in service, one had cracked in storage, and one was procured direct from the producer (having been picked as representative of "good" material). The three failures had all occurred in circumstances indicative of stress corrosion cracking, even though measured values of fracture toughness were considered adequate in all three cases. However, stress corrosion tests of all four plates, using precracked specimens, showed that the good plate had a threshold SCC stress intensity (K_{ISCC}) of approximately 40 ksi $\sqrt{\text{inch}}$, whereas the three failed plates exhibited K_{ISCC} values of 10 ksi $\sqrt{\text{inch}}$ or less(2). It is evident that fracture toughness tests alone are not a good measure of resistance to SCC for high-hardness armour alloys, and the results of the present investigation confirm this view.

In summary, it may be concluded that SCC resistance of high-strength armour alloys cannot be adequately measured by mechanical properties tests such as impact toughness or fracture toughness tests, or by the traditional SCC tests using smooth specimens. Stress corrosion testing should be conducted with precracked fracture mechanics-type specimens in a corrosive atmosphere representative of actual service environments (such as moist air or aqueous solutions). The threshold stress intensity below which a crack will not propagate in a corrosive environment is commonly referred to as K_{ISCC}. It is this value which should be of primary interest when considering the SCC behaviour of armour alloys.

SPECIMEN DESIGN

Design Considerations

In designing a fracture mechanics-type test for armour alloys, there are several factors of primary importance as well as several secondary considerations. The following were considered to be primary factors:-

(i) XAR-30 high-hardness steel armour and dual-hardness steel armour are difficult to machine by conventional techniques. Therefore, SCC specimens of these materials must be capable of being produced using electric discharge machining (EDM) and grinding.

(ii) Armour is used in a wide range of thicknesses. Either a single SCC specimen configuration must be found which is applicable to any thickness, or several tests may be used, each useful for a particular range of plate thicknesses. For obvious reasons a single test is preferable.

Secondary factors, which are nonetheless important, include:

(i) The specimen should be self-loaded. Self-loading enables a large number of specimens to be loaded and placed in corrosive environments, without requiring the continuous use of loading equipment (particularly such items as tensile and/or fatigue test machines) during the course of a test. Only the self-loading fixtures are in continuous use.

(ii) The specimen should be of the crack-arrest type. As described in the following section, in a crack-arrest specimen, the crack opening displacement at the load line is held constant. As the crack propagates, the load (and hence the stress intensity) decreases, and the crack will stop when the stress intensity decreases to K_{ISCC}. Thus K_{ISCC} can be determined from a single specimen, whereas other methods require numerous specimens (5).

Stress Corrosion Cracking Specimen Designs

Two fracture mechanics specimens have been used extensively for SCC testing, and several others have seen more limited applications. Brown(5) was the first to propose use of fracture mechanics in stress corrosion testing, and his cantilever beam specimen has been used to generate a large proportion of the K_{ISCC} data available today. For armour applications, however, it has two drawbacks. First, it is a constant load rather than a constant displacement (crack-arrest) specimen. More important, it is not applicable to thin plate.

Novak and Rolfe(4) proposed a modification of the WOL-T crack-line-loaded specimen geometry for SCC testing. It is a self-loaded specimen (bolt loaded) of the crack-arrest type. The bolt loading method has two serious drawbacks for our application, in that the necessity for producing the bolt hole requires a thickness of one inch or more, as well as drilling and tapping the hole. However, despite the difficulties inherent in the loading method, the basic principles of the self-loaded crack-arrest specimen put forward by Novak and Rolfe have been utilized in the specimen configuration selected for armour SCC testing.

The WOL-T geometry belongs to a large class of fracture specimens, frequently referred to as "crack-line-loaded" (CLL) or "double cantilever beam" (DCB) specimens. They are distinguished chiefly by (1) their method of loading, and (2) their H/W is a geometrical factor relating H, the half-height of the specimen, and W, the distance from the load line to the end of the specimen (see Figure 1 for an explanation of how these dimensions relate to the WOL-T geometry, where H/W = 0.486). For a given H/W ratio, the compliance of a specimen should be unchanged regardless of the choice of the actual H and W dimensions(6).

The specimen geometries belonging to the CLL or DCB class include:-

(i) Wedge-Open Loading, WOL-T (H/W = 0.486). This is the geometry used by Novak and Rolfe for their crack-arrest specimen(4). Scaling the H and W dimensions by a factor of two, this geometry was used for the initial armour SCC specimens reported here. This specimen is referred to as a WOL-2T geometry, despite the fact that a true WOL-2T has a thickness of 2 inches.

(ii) Compact Tension, CT (H/W = 0.60). In its pin-loaded variation, the compact tension geometry is widely used today for the measurement of fracture toughness. Because of crack curvature problems with the WOL-T geometry, the CT geometry has now been adopted for armour SCC testing.

(iii) Contoured DCB or Ripling Specimen (H/W = variable). The tapered test section of the contoured DCB keeps the stress intensity at the crack tip constant(7). It is useful for measuring stress corrosion crack velocities as a function of stress intensity, but it is not applicable to K_{ISCC} measurements of the crack-arrest type.

(iv) Small H/W specimens. Several investigators have reported SCC tests using CLL specimens where H/W is quite low. Mostovoy and Ripling(2) report the use of a specimen where H/W is approximately 0.2, and Hyatt(8) uses a specimen where H/W is approximately 0.1. The advantages and disadvantages of using a low H/W specimen are discussed below.

The choice of a specimen with a given H/W ratio entails several considerations. In a crack-arrest specimen, where stress intensity at the crack tip decreases with crack growth, the stress intensity which is reached as the crack grows completely through the specimen will depend on the initial stress intensity (which is a function of the initial crack opening displacement) and the specimen geometry. For a given initial stress intensity K_{IO}, this minimum, measurable stress intensity will decrease with decreasing H/W ratio. On this basis, a low H/W (long, thin) specimen would be preferable, since a greater range of stress intensities can be evaluated with a single specimen.

However, the low H/W geometry has an inherent disadvantage. As the crack propagates through the specimen, the stress at the crack tip has an increasing tendency to deviate from the specimen mid-plane, making K_{ISCC} measurements impossible if the deviation is sufficiently pronounced. In a low H/W specimen, this deviation will occur unless there is some external force keeping the crack on or near the specimen mid-plane. Mostovoy and Ripling(2) used face notching for their specimen, while Hyatt(8) made use of the fact that the driving force for SCC of aluminium is much greater for stressing normal to the short transverse direction.

In choosing the WOL-T and CT geometries for the armour SCC program, it was felt that the possible advantages to be gained by choosing a low H/W specimen were outweighed by the disadvantages of face grooving specimens, and it is unlikely that there would be any possibility of using Hyatt's technique (e.g., anisotropic SCC susceptibility) to keep the cracks on the mid-plane. It should be noted that the WOL-T geometry is borderline with regard to suppression of crack deviation*. As will be discussed, it is for this reason that it has been found necessary to switch to the CT geometry.

Wedge-Loading of Crack-Line-Loaded Specimens

The specimen design chosen for initial SCC trials was the WOL-2T geometry (Figure 1). As noted, the compact tension (CT2) geometry has now been adopted. The only difference between the CT2, and the WOL-2T shown in Figure 1, is the W dimension as shown in Table 1.

* McCABE, D.E., private communication.

The disadvantages inherent in Novak and Rolfe's bolt-loaded WOL-T specimen were overcome by using the wedge-loading system devised by Heyer and McCabe(9),(10). This system, which is applicable to both the WOL-T and CT geometries was originally devised for plane-stress testing of thin sheet materials(9). However, it is also applicable to stress corrosion testing, where it posseses several distinct advantages over other SCC test methods. It is a self-loaded crack-arrest-type specimen, which can be applied to any thickness of armour plate, from thin sheet to thick plate. And it is capable of being produced using only EDM and grinding.

Instead of pin-loading or bolt-loading the specimen at the load line, the specimen is loaded by forcing a wedge between two semicircular segments, which have been inserted in a 1.5-inch-diameter hole (see Figures 1, 2, and 3). Figure 2 is a photograph of the loading set-up, and Figure 3 shows a section through the loading set-up located at the load line. The essential features of the loading process are shown in Figure 3. Both the wedge and the split segments have matching 3° tapers. The wedge is driven between the segments by the descending head of a Wiedemann-Baldwin tensile test machine, and the segments in turn force the crack in the specimen open. Because of the stick-slip nature of the motion of the wedge between the segments, it is essential that some form of displacement control rather than load control be employed on the machine being used to load the wedge.

The specimen rests on a loading block or fixture, with a thin Teflon sheet between them to allow free opening of the crack as the wedge is inserted. To prevent the segments from being pushed through the hole during insertion of the wedge, there are two support blocks which rest in a channel in the loading block. Their only purpose is to position the segments, and they are free to slide if pushed sideways by the descending wedge. Several hold-down clamps are provided to keep the specimen in place during loading. Their necessity is doubtful during loading of 1/2-inch-plate specimens as reported here, but they become increasingly important as specimen thickness decreases, since buckling of the specimen becomes more likely.

A loaded specimen is shown in Figure 4, with wedge and segments in place. Once the specimen is loaded, friction holds the wedge and segments in place, and the assembly may be placed in a corrosive bath to propagate a stress corrosion crack.

Prior to loading, the specimen is notched to a distance 1.5 inches from the load line, and a fatigue crack is grown from the end of the notch for another 1/4 inch, for a total initial crack length (a_0) of approximately 1.75 inches. In the plane-stress specimen designed by Heyer and McCabe(9), it was possible to produce fatigue cracks in the thin sheet by loading split inserts which were placed in the 1.5-inch hole. For armour specimens, this was not possible because of the greater specimen width and greater loads required. Because of geometrical considerations, it was not possible to design similar fixtures which would not have suffered fatigue fracture after very few stress cycles. For this reason, two 0.625-inch-diameter holes were added to the specimen for the specific purpose of fatigue precracking the stress corrosion specimens. Since the location of the holes does not correspond to the load line of any standard specimen geometry, it was necessary to estimate loads for desired fatigue crack growth rates, based on the data in the Srawley and Gross paper(6) for arbitrary H/W ratios. This was necessary only for the first attempt at fatigue precracking, since later efforts could be based on the actual crack growth rates in the first specimen.

The procedure for determining the loading conditions, and measuring stress intensities, is reported by Novak and Rolfe(4). The stress intensity may be given by:-

$$K_I = \frac{P}{B\sqrt{a}} \; C_3 \left(\frac{a}{w}\right) \tag{1}$$

where
        P is the load along the load line

        B is the thickness of the specimen

        a is the crack length (measured from the load line)

        $C_3 (a/w)$ is a function of a/w based on the specimen geometry.

Compliance calibrations are usually plotted as $(K_IBW)/(Pa^{1/2})$ versus (a/w), and are available for both the WOL-T and compact tension geometries. Equation 1 for K_I is merely a rearrangement of this relationship; however, note that for a wedge-loaded system the load, P, is not known. P must be found from a second relationship, which is based on measurements of the load necessary to produce a given crack opening displacement (COD) at a given value of a/w. Novak and Rolfe express this in the form:-

$$P = EBV/C_6(a/w) \qquad\qquad (2)$$

where   V is the COD at the load line

            $C_6(a/w)$ is another function of a/w based on the specimen geometry.

In practice, determination of the initial COD necessary to produce a given initial stress intensity, K_{10}, is made as follows:-

     (i)   Knowing a_0 (the initial crack length), and hence $C_3(a/w)$, calculate P_0 for the desired K_{10} from Equation 1.

     (ii)   Using this value of P_0, and knowing $C_6(a/w)$ for the initial crack length a_0, calculate the required COD (V_0) from Equation 2.

Once the crack starts to grow, the procedure is reversed. V_0 is fixed, and crack length, a, is measured. Knowing $C_3(a/w)$ and $C_6(a/w)$, P can be calculated from Equation 2. Using this value of P, K_I can be calculated from Equation 1. Combination of Equations 1 and 2 gives the expression:-

$$K_I = \frac{EV_0}{\sqrt{a}} \quad \frac{C_3 \frac{a}{w}}{C_6 \frac{a}{w}} \qquad\qquad (3)$$

Since $C_6(a/w)$ increases faster than $C_3(a/w)$ with increasing crack length(4), it can be seen that the stress intensity at the crack tip will drop as the crack grows. When the stress intensity decreases to the threshold stress intensity K_{ISCC}, the driving force for crack growth will disappear, and the crack will stop. A possible complication can occur in systems where the stress corrosion crack velocity decreases gradually as the stress intensity approaches K_{ISCC}, as opposed to a discontinuous drop in crack velocity. With a gradual decrease in crack velocity, the time for the stress intensity to fall to K_{ISCC} may be quite long. Stress corrosion cracking of steel alloys, including armour steels, is typical of this type of behaviour.

For this program, values of $C_3(a/w)$ and $C_6(a/w)$ for the WOL-T geometry were taken from Novak and Rolfe(4), while for the compact tension geometry, $C_6(a/w)$ values were obtained from a paper by Brown(11), and $C_3(a/w)$ from ASTM E399-70T(12). It should be noted that, for Equation 2 to be independent of specimen size, the crack opening displacement V_y must be measured at the load line. Since V_y cannot be measured directly, it must be measured at some other point and a linear correction applied (see Novak and Rolfe(4), Figure 7). The same linear correction must then be applied to $C_6(a/w)$ values which are based on V_y. This must be done whenever there is a change in the position at which V is measured. In the case of the WOL-2T armour specimen, this meant extrapolation of $C_6(a/w)$ values from Novak and Rolfe, Table V in Reference 4, back to V_y, and then extrapolation from V_y to the edge of our specimen, 1.5 inches from the load line. Brown's data(11) for the compact tension specimen already applies to load line V_y position.

EXPERIMENTAL

Materials

The 0.500 inch thick XAR-30 high-hardness steel armour tested in this program was obtained from two different manufacturers. The two plates for which data is presented here are identified as J13 and G11. Stress corrosion specimens were obtained from 2 ft by 2 ft plates which had been cut from the 4 ft by 8 ft plates supplied by the manufacturers. Other 2 x 2 plates were used simultaneously to obtain ballistic and mechanical property data in companion programs. The chemical

analysis of these two plates is given in Table II. Mechanical properties and plane strain fracture toughness values, which were obtained in another program (Reference 13), are listed in Tables III and IV.

Test Procedure

For each material source, specimens were obtained for both the WR and RW orientations (crack growing in the rolling direction and width direction, respectively). All specimens from J13 were WOL-2T geometry, while specimens from G11 were CT type. Crack opening displacement was measured initially by micrometer, and later by clip gauge. Both 3.5% NaCl solution and distilled water were used as test environments, but the addition of NaCl was not found to cause any discernable lowering of the already-poor K_{ISCC} values obtained in distilled water. Crack lengths were measured with a Gaertner travelling microscope after removing the specimens from the environment. Crack length measurements were made at irregular intervals: usually daily at first, then with decreasing frequency as crack growth slowed.

Specimen Performance

The performance of the wedge-loaded crack arrest specimens was generally satisfactorily, although several minor problems were encountered. The most immediate problem was that of crack deviation from the specimen mid-plane in the WOL-2T specimens cut from plate J13.

Since the stress corrosion characteristics of this material were not known, the first specimen (J13-1WR) was loaded to an initial stress intensity (K_{I0}) of 49 ksi$\sqrt{inch}$. As shown in Figure 5, the crack grew fairly straight. However, because of the low SCC threshold of this material, the crack grew beyond the point where a valid stress intensity could be calculated. At this point (Figure 5, point A), the stress intensity was about 23 ksi$\sqrt{inch}$. Subsequent specimens were loaded to K_{I0} values between 23 and 27 ksi$\sqrt{inch}$ to obtain crack arrest within the valid range (crack length less than 80% of width, W). Despite the fairly straight path of the crack in J13-1WR, subsequent specimens from J13 showed an increased tendency or crack deviation from the specimen mid-plane. J-13-2WR showed a moderate degree of crack curvature, but crack length measurements are still believed to give good K_{ISCC} values. However, the crack curvature exhibited by J13-4WR (Figure 6) and -3WR was so pronounced that valid stress intensities could not be calculated. Crack curvature was much less pronounced in the four RW-orientation specimens, indicating a certain degree of anisotropy in the preferred direction of stress corrosion crack propagation.

Because of the crack curvature problem in WOL-2T specimens, a decision was made to switch to the compact tension CT2 geometry, which has inherently higher resistance to crack deviation from the mid-plane. As a result, the specimens obtained from plate G11 showed substantially less crack curvature in both WR and RW orientations, and all specimens were considered to give valid K_{ISCC} values.

A second problem which is not so easily resolved is the fact that the stress corrosion cracks never did arrest completely, even for exposures over 4000 hours. The problem of slow crack growth near K_{ISCC} for steels has already been noted by Novak and Rolfe (Reference 4), and is not restricted to crack arrest-type SCC specimens. The comparable problem in K_{ISCC} determination using the cantilever beam specimen is knowing whether or not crack growth is occurring for stress intensities close to the expected threshold. The closer the initial K_{ISCC} in a cantilever beam specimen, the longer the time necessary to observe detectable stress corrosion crack growth or the lack of same. For crack arrest specimens, an exposure time of 1000 hours has been recommended (Reference 4) as necessary to obtain a good value of K_{ISCC}, even though some further crack growth will occur beyond this time. The data from this program bear out this contention, although it can be seen from Figures 7 and 8 that a fair estimate of K_{ISCC} could be obtained in times as short as 300 to 600 hours.

In a previous SCC study of high-hardness steel armour by Mostovoy and Ripling (Reference 2), the authors propose that an approximate indication of stress corrosion susceptibility can be obtained by observation of the rate of crack propagation in the first few days of the test. However, it would seem that this would not be a useful test method in most cases, because of the existance of an incubation period prior to initial crack growth (Reference 14, 15). From the data presented by

Wei et al (Reference 15), it would appear that the differences in initial crack growth observed by Mostovoy and Ripling for their "good" and "bad" material were at least partially due to differences in incubation time. Incubation time is related to the ratio K_{IO}/K_{ISCC} (Reference 15), as well as environmental factors (Reference 14), and could vary considerably depending on such factors as methods of loading and exposure to the environment, and initial applied stress intensity. In the armour SCC program reported here, incubation times ranged from less than one hour for $K_{IO} \approx 49$ ksi $\sqrt{inch}$, to between one and three days for K_{IO} in the range 20 to 27 ksi $\sqrt{inch}$. Because of this complicating factor, it appears necessary to wait at least 600 to 1000 hours for the crack arrest specimen to reach some relatively stable crack growth pattern before attempting to estimate K_{ISCC}. An attempt to obtain anything more than very rough rankings of SCC susceptibility before this time runs the risk of being influenced by factors having at best a second-order effect on the stress corrosion threshold, K_{ISCC}. The conclusion of Wei et al (Reference 15) is that the crack arrest-type specimen may have the best chance for circumventing these secondary factors, so long as sufficient time is available to determine crack arrest.

Armour Stress Corrosion Cracking Data

The results of SCC testing of high-hardness steel armour plates G11 and J13 are presented in Table V. From these results, it can be seen that most of the variables tested had little or no effect on the measured stress corrosion threshold, K_{ISCC}. Distilled water is observed to be as aggressive as 3.5% NaCl solution in causing SCC, as evidenced by the fact that specimens G11-4WR and -4RW do not show any lowering of K_{ISCC} when tested in salt solution. Specimen orientation appears to have no significant effect on susceptibility for plate G11. Any speculation about the higher K_{ISCC} for J13-2WR compared with RW specimens should be tempered by the fact that it was the only WR specimen for which valid results were obtained, and the apparent K_{ISCC} is not appreciably higher; it is in fact comparable to the upper limit values for both RW and WR specimens from G11. Furthermore, there appears to be no difference in SCC behaviour between plates G11 and J13, which come from two different manufacturers and have different chemistries (Table II) and mechanical properties (Tables III and IV).

Nearly all valid stress corrosion test results fall in the K_{ISCC} range from 14 to 19 ksi $\sqrt{inch}$. The one exception is specimen G11-3WR, which for unexplained reasons exhibited a greater degree of susceptibility. K_{ISCC} values in this range represent poor resistance to stress corrosion, which could pose severe limitations on service behaviour of this material in wet or humid environments. This is particularly important when comparison is made to the excellent fracture toughness data for these plates as tabulated in Table IV. Depending on orientation, fracture toughness for plate G11 averaged from 78 to 89 ksi $\sqrt{inch}$, and for plate J13 averaged from 94 to 104 ksi $\sqrt{inch}$. Since the stress corrosion threshold is only of the order of 15% of the fracture toughness, designing to the fracture toughness with a factor of safety of even two or three would still result in the possibility of stress intensities being substantially above K_{ISCC} for this material. Since the necessary corrosive environment, water, is certain to be encountered in nearly all potential armour applications, the possibility of catastrophic stress corrosion cracking failure of this material in service is a very real possibility. Because of the poor stress corrosion resistance of high-hardness steel armour, load-bearing applications would appear to be precluded; indeed, even stress corrosion failure due to residual processing stresses would seem to be a distinct possibility, as has already been demonstrated (Reference 2).

CONCLUSIONS

At this point in the armour stress corrosion cracking program, the following conclusions can be made:

(i)   The wedge-loaded crack arrest specimen appears to be the best choice for stress corrosion testing of armour steels.

(ii)   Where face grooving is not desired, the compact tension specimen geometry should be used to prevent crack deviation. Where face grooving is used to suppress crack deviation, lower H/W ratio specimens can be used to extend the range of stress intensities obtained with a given specimen.

(iii) A good measure of K_{ISCC} can be obtained in 600 to 1000 hours, despite some very slow crack growth beyond this time. Attempts to shorten this time do not appear fruitful at the present time, because of certain kinetic features of stress corrosion crack growth in steels.

(iv) XAR-30 high-hardness armour plate from two manufacturers was tested using crack arrest SCC techniques. K_{ISCC} values were nearly all in the range 14 to 19 ksi $\sqrt{inch}$, indicating very poor SCC behaviour.

(v) There were no significant differences in SCC behaviour of plates from different sources, nor was specimen orientation significant.

(vi) Distilled water produced stress corrosion threshold levels at least as low as aqueous 3.5% NaCl (seawater concentration).

(vii) Plane strain fracture toughness measurements will not provide useful information about SCC susceptibility, as evidenced by a comparison of K_{IC} and K_{ISCC} results obtained here for high-hardness steel armour.

TABLE I

Dimensions of Crack-Line-Loaded Specimens

Specimen Type	Wedge-Open-Loaded (WOL-2T)	Compact Tension (CT2)
H/W	0.486	0.600
H	2.48"	2.48"
W	5.10"	4.13"
thickness	(thickness of armour plate)	

183

REFERENCES

1. JOHNSON, H.H. and WILNER, A.M. "Moisture and Stable Crack Growth in a High-Strength Steel". *Applied Materials Research, January 1965, p 34.*

2. MOSTOVOY, S. and RIPLING, E.J. "The Feasibility of Using Fracture Mechanics for Evaluating High-Hardness Armour Steel". *US Army Tank Automotive Command, Warren, Michigan, Technical Report No. 10580, 19 June 1969.*

3. PIPER, D.E., SMITH, S.H. and CARTER, R.V. "Corrosion Fatigue and Stress Corrosion Cracking in Aqueous Environments". *Metals Engineering Quarterly, v. 8, August 1968, p 50.*

4. NOVAK, S.R. and ROLFE, S.T. "Modified WOL Specimen for K_{ISCC} Environmental Testing". *J. of Materials, v. 4, no. 3, 1969, p 701.*

5. BROWN, B.F. "A New Stress-Corrosion Cracking Test for High-Strength Alloys". *Materials Research and Standards, v. 6, no. 3, 1966, p 129.*

6. SRAWLEY, J.E. and GROSS, B. "Stress Intensity Factors for Crack-Line-Loaded Edge-Crack Specimens". *Materials Research and Standards, v. 7, no. 4, 1967, p 155.*

7. MOSTOVOY, S., CROSLEY, P.B. and RIPLING, E.J. "Use of Crack-Line-Loaded Specimens for Measuring Plane-Strain Fracture Toughness." *J. of Materials, v. 2, no. 3, 1967, p 661.*

8. HYATT, M.V. "Use of Precracked Specimens in SCC of High-Strength Aluminum Alloys". *Boeing Document D6-24466, November 1969.*

9. HEYER, R.H. and McCABE, D.E. "Plane-Stress Fracture Toughness Testing Using a Crack-Line-Loaded Specimen". *Engineering Fracture Mechanics, v. 4, 1972, p 393.*

10. HEYER, R.H. and McCABE, D.E. "Crack Growth Resistance in Plane-Stress Fracture Testing." *Engineering Fracture Mechanics, v. 4, 1972, p 413.*

11. BROWN, W.F., Jr. "Effects of Some Dimensional Variables for Compact Tension Specimens". *Note for ASTM E-24 Sub I, September 23, 1969.*

12. "Tentative Method of Test for Plane-Strain Fracture Toughness of Metallic Material". *ASTM Specification E399-70T, March 1970.*

13. HICKEY, C.F., Jr. "Toughness Data from Monolithic High Hardness Armour Steel". *AMMRC, Watertown, Mass., PTR 72-3, July 1972.*

14. BENJAMIN, W.D. and STEIGERWALS, E.A. "An Incubation Time for the Initiation of Stress-Corrosion Cracking in Pre-Cracked 4340 Steel". *Trans. ASM, v. 60, no. 4, 1967, p 547.*

15. WEI, R.P., NOVAK, S.R. and WILLIAMS, D.P. "Some Important Considerations in the Development of Stress Corrision Cracking Test Methods". *Materials Research and Standards, v. 12, no. 9, 1972, p 25.*
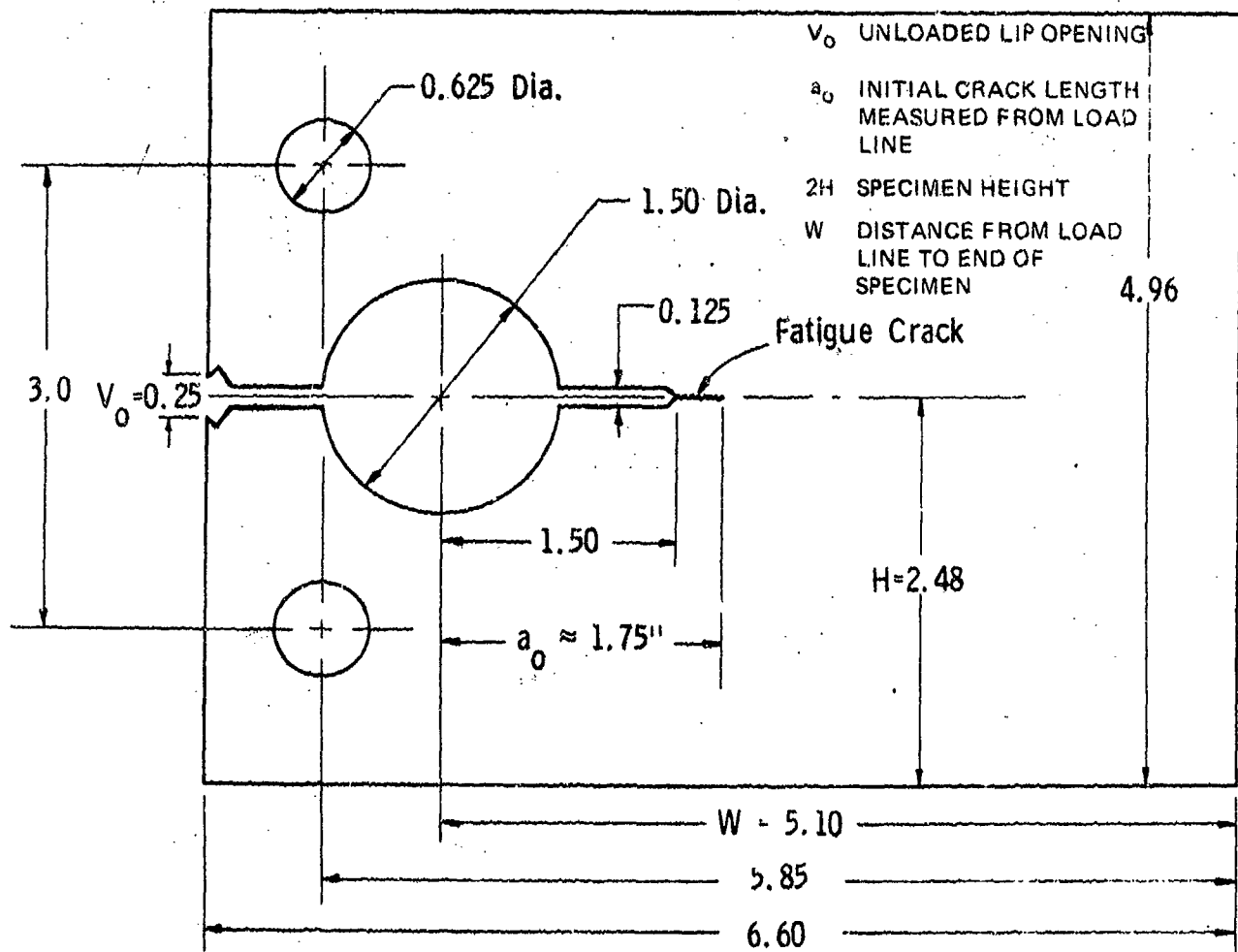
Figure 1. MODIFIED WOL-2T STRESS CORROSION SPECIMEN
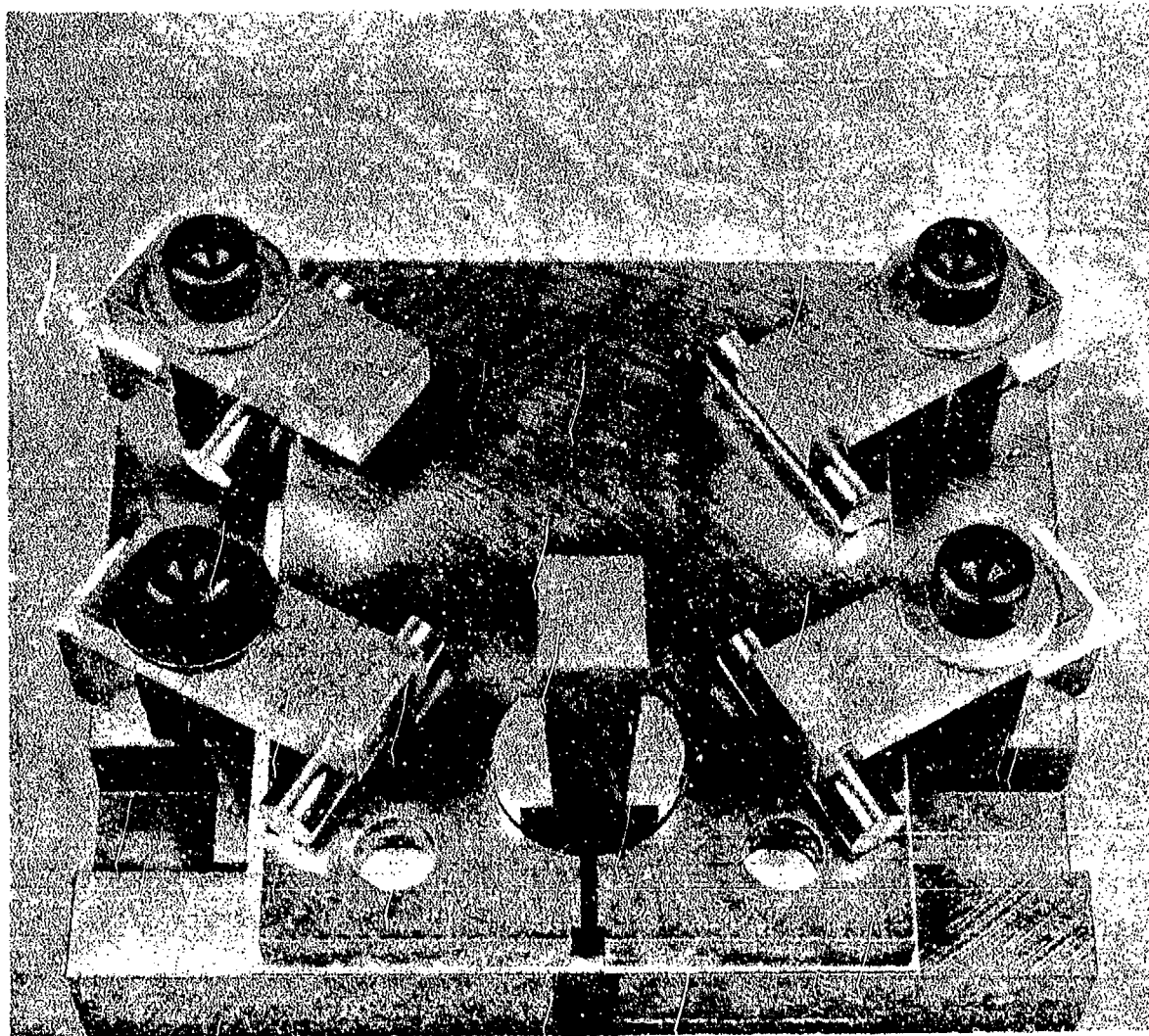
Figure 2. LOADING FIXTURE FOR WEDGE-LOADED TYPE SPECIMENS

SECTION X-X

Threaded holes for
hold-down clamps
(Clamps not shown)

Load

Slot in 1-1/2 loading plate
for support blocks ⒟

1/16" Teflon sheet

1-1/2"

1-1/2" dia. hole in loading
plate for wedge clearance

Key:

ⓐ SPECIMEN (WOL-2T SHOWN)
ⓑ TAPERED WEDGE
ⓒ TAPERED SEMI-CIRCULAR SEGMENTS
ⓓ SEGMENT SUPPORT BLOCKS
ⓔ 1½" THICK LOADING BACKUP PLATE
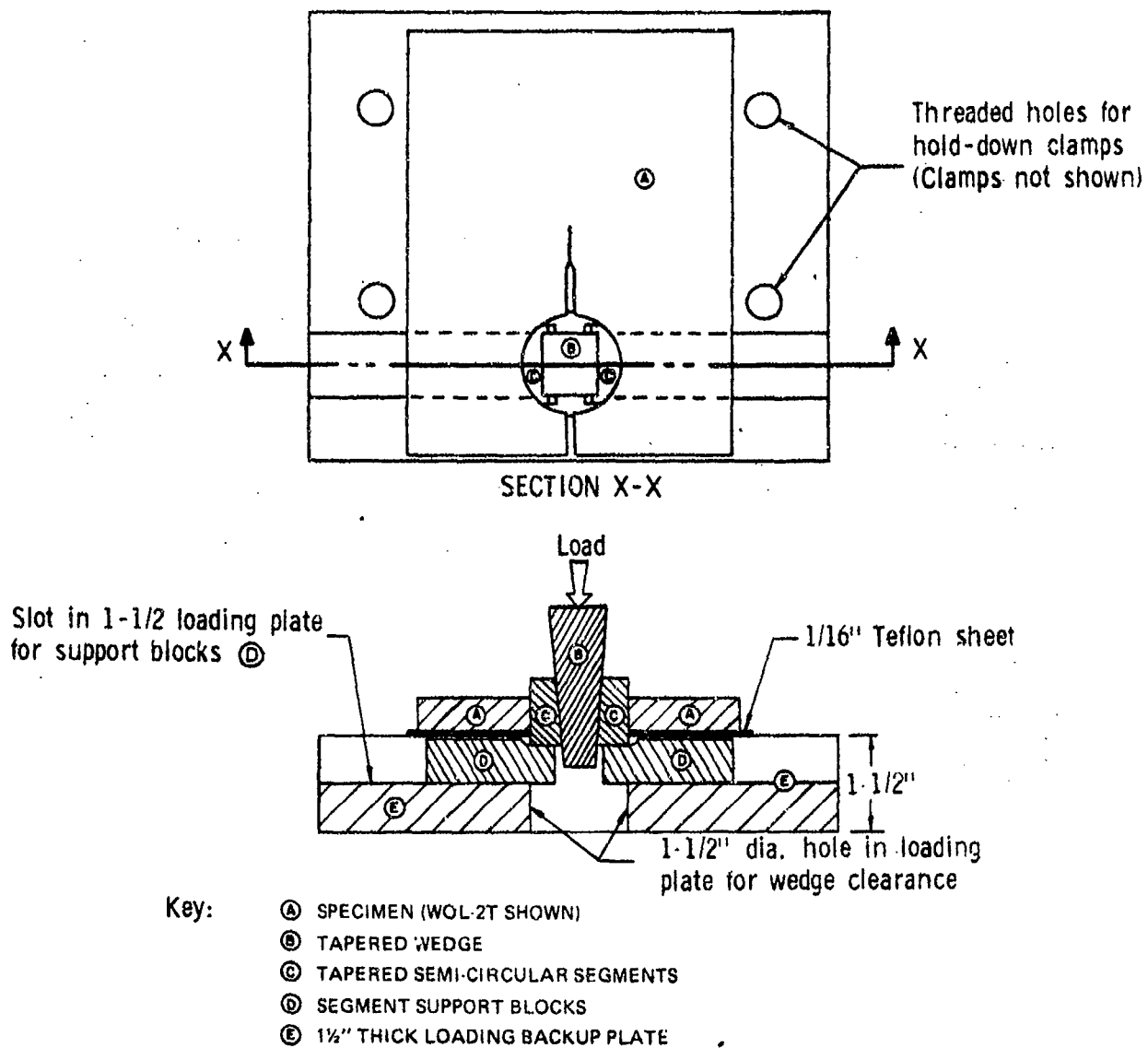
Figure 3. SCHEMATIC DRAWING OF LOADING SYSTEM

Figure 4. WEDGE-LOADED WOL-2T SPECIMEN
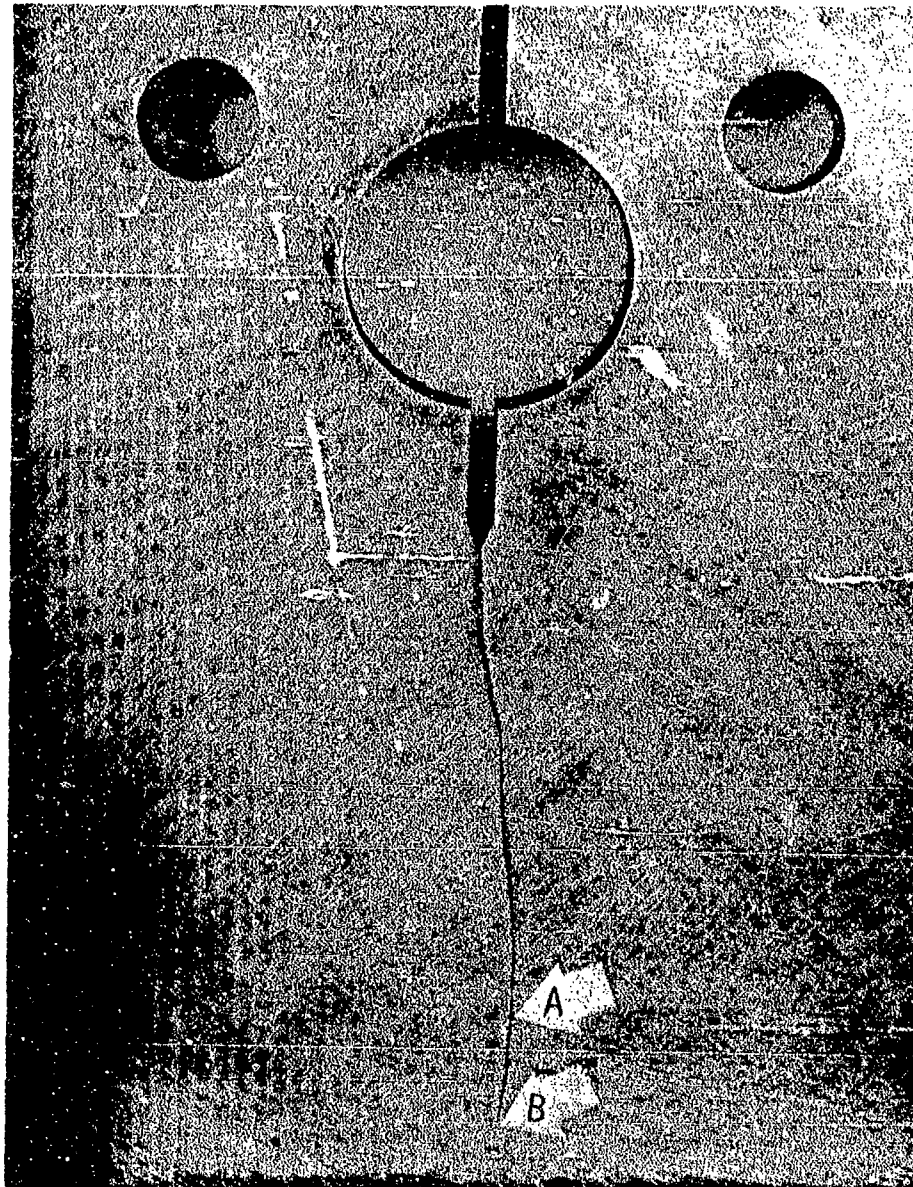
Figure 5. STRESS CORROSION CRACK IN WOL-2T SPECIMEN J13-1WR
(A. LIMIT FOR VALID MEASUREMENT OF STRESS INTENSITY
$\left(\dfrac{a}{W} = 0.08\right)$ B. CRACK TIP)
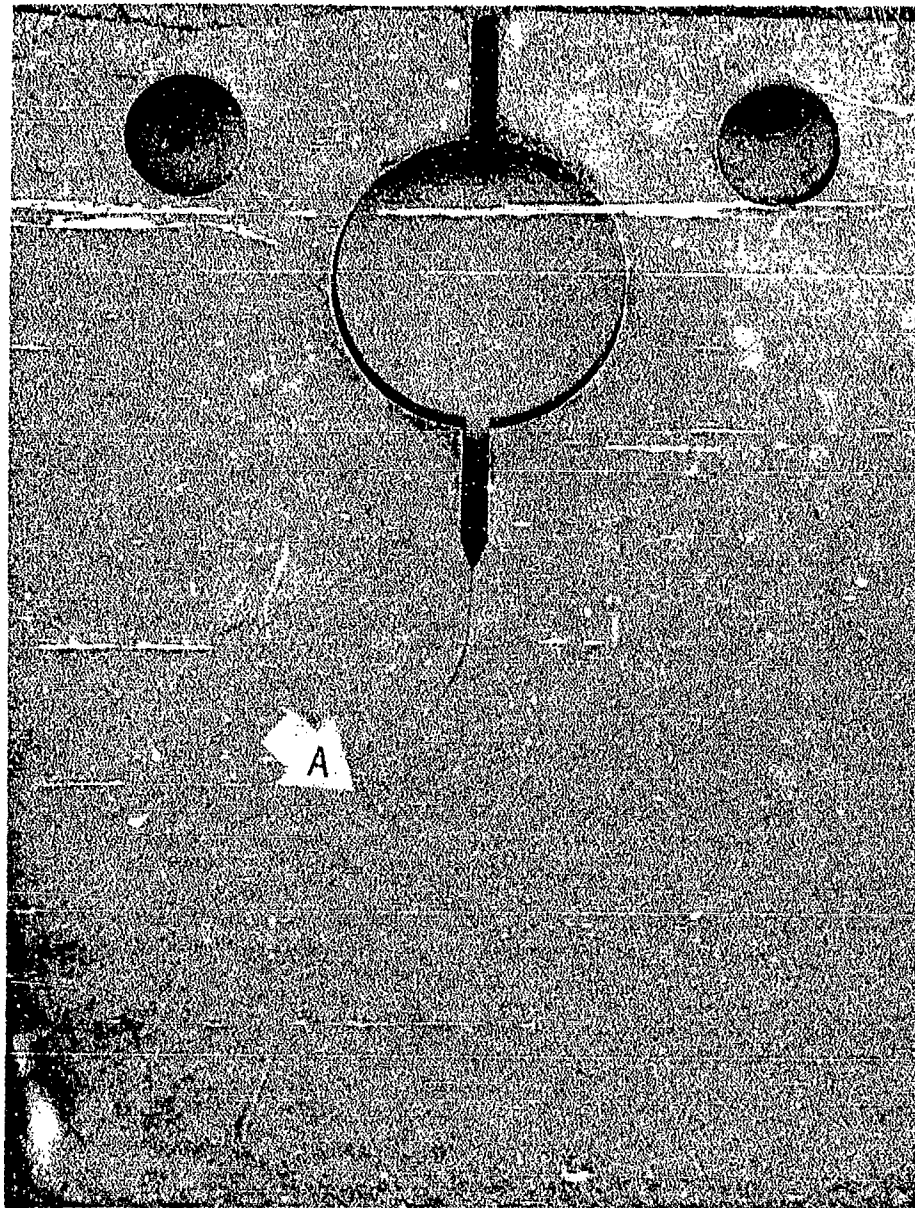
Figure 6. STRESS CORROSION CRACK IN WOL-2T SPECIMEN J13-4WR
(A. CRACK TIP)
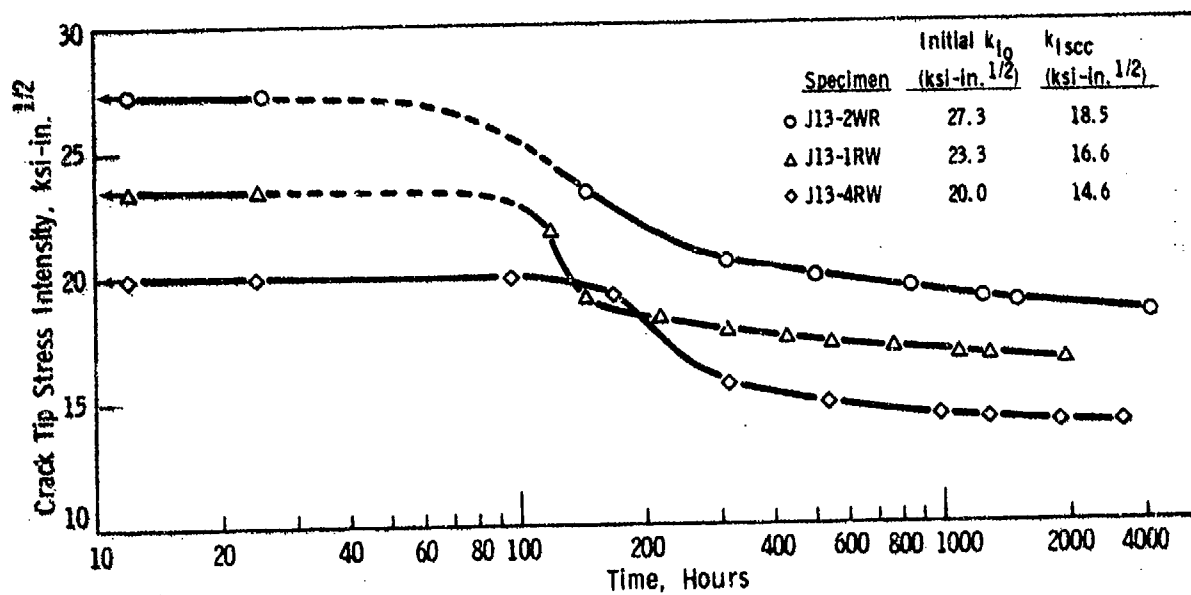
Figure 7. TYPICAL STRESS INTENSITY VERSUS TIME FOR STRESS CORROSION CRACKING OF WOL-2T SPECIMENS FROM PLATE J13
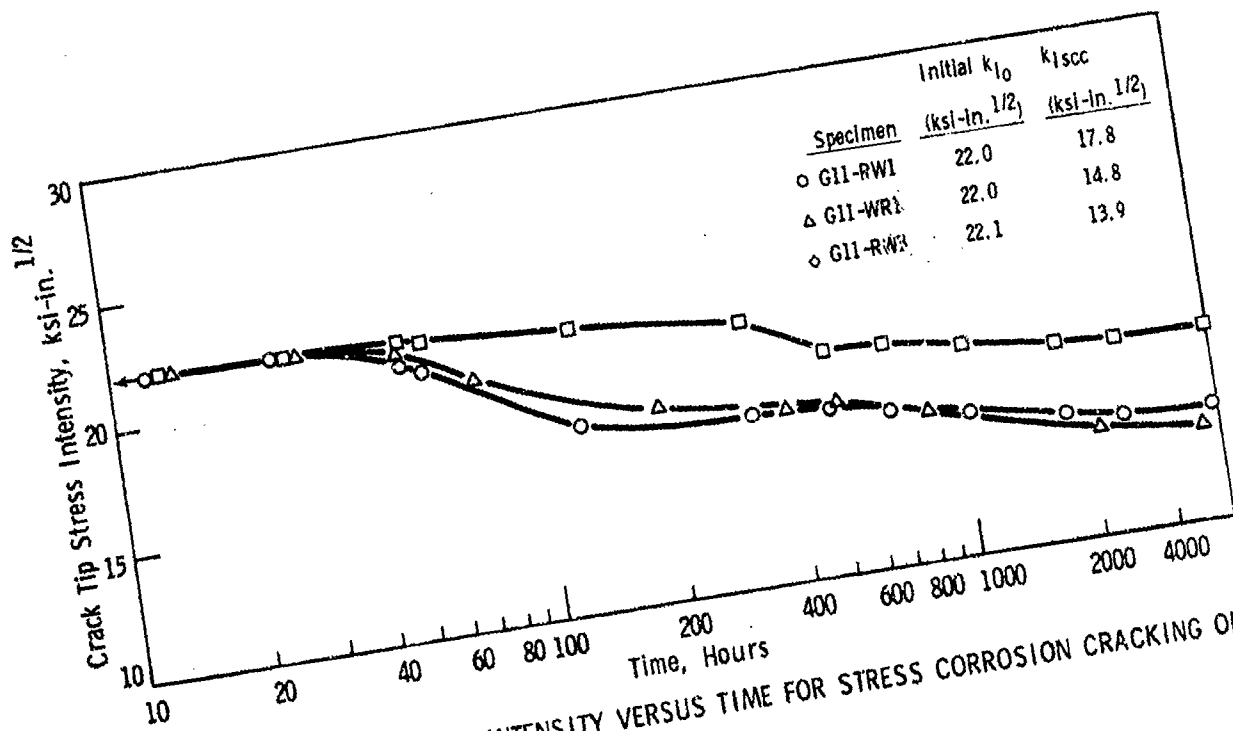
Figure 8. TYPICAL STRESS INTENSITY VERSUS TIME FOR STRESS CORROSION CRACKING OF CT2 SPECIMENS FROM PLATE G11

ALUMINUM ASSOCIATION TASK GROUP EXFOLIATION AND
STRESS CORROSION TESTING OF ALUMINUM ALLOYS FOR BOAT STOCK

By

T. J. Summerson

INTRODUCTION

In March, 1968, the Aluminum Association organized an Ad Hoc Committee which appointed a task group to answer the U. S. Navy's request for a test to detect susceptibility to exfoliation corrosion. This request came after exfoliation corrosion was encountered in the bilge areas of aluminum hulled (5456-H321) patrol boats used in Vietnam. (See Figures 1 and 2)

This task group consisted of representatives of Alcoa, Kaiser, and Reynolds. A test program was conducted in which metals supplied by the three producer members, as well as corroded hull plates from boats which had been in service, were evaluated by each of the three producers' laboratories. In this evaluation program, two acidified salt spray tests were compared. Results indicated that the 2 hour cycle acetic acid-salt spray test (SWAAT) most effectively detected exfoliation corrosion of the type which had occurred on service boats. This evaluation also clearly revealed that exfoliation susceptibility in 5456-H321 was related primarily to an elongated grain structure with relatively continuous precipitation of an Al - Mg phase along these grain boundaries. (See Figure 3)

193

The U. S. Navy incorporated the SWAAT Test into Federal Spe-
cifications QQ-A-00250/19&20 dated December 31, 1968. While
the problem was related strictly to 5456 -H321, the Navy decided
that a similar test should be required for the lower alloyed
5086 plate, even though this material had not exfoliated. In
addition, the Navy included a second corrosion test, recommended
to the Navy by Alcoa, for weldments which had not been evaluated
by the Task Group. Finally, metallographic evidence was re-
quired to characterize resistant material.

Meanwhile, the aluminum producers developed new exfolia-
tion resistance tempers for both 5456 and 5086 alloy boat hull
plate materials. The temper designations are referred to as
-H116 and -H117. Examination of typical photomicrographs of
these tempers reveal that the highly directional grain struc-
ture with continued grain boundary precipitation has been
eliminated. (See Figures 4 and 5)

Further round robin tests were initiated in late 1968
in order to test weldments, which the Navy had unilaterally
added to the specifications, and to evaluate the two new ex-
foliation resistance tempers by the new test methods. The
membership in the Task Group was expanded to include Alcan,
Amax, Dow, Martin-Marietta, Olin and Revere. Commercially pro-
duced samples of the -H116 and -H117 tempers of 5086 and 5456
plate, as well as control samples, were supplied. Results of
these round robin tests verified earlier tests indicating that

the SWAAT (2 hour cyclic acetic acid salt-spray) test could clearly detect exfoliation susceptible material. The new -H116 and -H117 Tempers were shown to be resistant to exfoliation corrosion. In addition, a continuous immersion test, ASSET, appeared to require supplemental metallographic examination because of pit-blistering encountered.

A nitric acid weight loss test was proposed in June, 1970. It and a modified ASSET test were also studied by Round Robin.

The ASSET test was preferred over the SWAAT (as a result of these Round Robin tests) because ASSET gave more rapid results. The commercially produced plates in each of the -H116 and -H117 tempers were found immune to intergranular corrosion as well as exfoliation corrosion. Finally, it was determined that the weldments and the associated heat affected zones were not susceptible to exfoliation corrosion. The 24-hour nitric acid weight loss test showed promise as a means of detecting susceptibility to both intergranular corrosion and exfoliation corrosion. On the basis of these tests, the Task Group recommended that the ASSET test replace the SWAAT test in Federal Specification QQ-A-00250/19 and 20. In addition, it was recommended that testing of weldments be deleted because it was clearly obvious that neither the weld metal nor the heat affected zone was susceptible to exfoliation corrosion. The ASSET test is described in Appendix A.

These conclusions and recommendations were reported to the Navy. In early 1974, the Navy advised the Aluminum Association

that these recommendations were accepted and would be incorporated into specifications.

Meanwhile, in the spring of 1972, a second corrosion problem arose in the Navy. This problem pertained to aluminum bulkhead and deck plate weldments. In April of 1972, the Naval Research Laboratory reported this to be stress corrosion susceptibility in thin sheet-plate material, and recommended a wedge type test specimen to detect stress corrosion cracking susceptibility. Erickson at the U. S. Navy's Mare Island Laboratory carried out more extensive work on the LST bulkheads and structures. He confirmed stress corrosion cracking had occurred in the 5456 -H321--thin bulkhead and deck plate. He recommended the Navy switch from the -H321 temper to the -H116 or -H117 tempers and suggested that the NRL developed wedge sample be used to test stress corrosion susceptibility in the -H321 temper. (His tests with wedge samples showed that the -H116 and -H117 tempers were not susceptible.)

Two months later, in July, the Naval Engineering Center, Sec. 6101D, asked the Aluminum Association Task Group for advice and recommendations on the cause and preventative measures relative to cracking of these welded 5456-H321 deck plates and bulkhead sheets. In addition, the Navy asked for a pre-production stress corrosion test to assure that aluminum alloys possess adequate stress corrosion resistance and, finally, they asked for documentation from producers that currently produced

196

5XXX aluminum alloy boat stock materials did meet desired exfoliation corrosion and stress corrosion resistance criteria. From earlier work on exfoliation tests, an explanation for stress corrosion cracking was quite obvious. For example, one of the hull plate samples tested in 1968 showed intergranular corrosion in an equiaxial, recrystallized grain structure. To the naked eye this appears to be a pitting, but as the Figure 6 shows, this is intergranular corrosion.

Figure 7 shows a typical crack in a welded bulkhead structure. Samples of the cracked 5456 -H321 decking and bulkhead plates were provided from the Navy for control purposes. The Task Group and various producer members provided samples of their current production on 5086, 5083 and 5456 in appropriate tempers for an evaluation. A round robin test program was begun in late 1973 with sets of test plates sent to 8 different laboratories. The materials being tested are described in Table I. The test methods are described in Table II. The eight laboratories included two of the Navy testing facilities-- Mare Island and the Naval Research Laboratories. (See Table III)

Stress corrosion resistance and intergranular corrosion susceptibility of each material was evaluated, with exception of the control material, in four conditions: 1) as received, 2) heated one week at 212°F, 3) heated 6 days at 300°F, and 4) heated one hour at 450°F.

The sheared sample test involved samples that were 2"
wide and 4" long. In some laboratories, two of the edges were
sheared before thermal treatment and two edges were sheared after
the desired thermal treatment. (Some laboratories sheared all
edges after thermal treatment.) The shearing was done at room
temperature. Each laboratory was to advise the amount of offset
between blade and table, since the amount of cold work or defor-
mation would be dependent upon that offset. (The sheared edges
contain residual tensile stresses in a short transverse direc-
tion and this enables determining susceptibility to SC cracking.)

From our past work, we found that intergranular corrosion
susceptibility, a requirement for stress corrosion cracking in
aluminum alloys, could be determined by the 24-hour immersion
(NAWLT) in concentrated nitric acid, providing immersion tem-
perature is controlled. Samples were carefully weighed before
and after immersion in the nitric acid. The weight loss is in-
dicative of the degree of intergranular susceptibility; i.e.
high weight losses indicate IG susceptible, low weight losses
are not susceptible. The standard specimen measures a 1/4"
width of 2" of length in rolling direction and full thickness
of sheet or plate. The NAWLT is described in Appendix B.

A third test used was the preform test. This involves
machining specimens from sheet or plate surface, cold bending
them to a 90° permanent set, and then springing each sample
into fixture having a 2-1/2" span. (See Figure 8) These were

then subjected to a 3.5% NaCl continuous immersion test for a 30-day period.

At the Navy's request, further attempts were made to evaluate these materials by the NRL wedge test specimen. The NRL specimen is 1" square by full thickness. The sample is notched or saw slotted and then a wedge driven in to initiate a mechanical crack. Specimens were to be tested in 3.5% salt solution for at least one day before being examined to see if the crack had propogated.

SUMMARY

All of the producer-provided 5086, 5083, and 5456 plates in the as-received condition exhibited good resistance to stress corrosion cracking and showed a low susceptibility to intergranular corrosion. As expected, the 5456 -H321 control materials (Navy Sample 345A) stress corrosion cracked in the shear cracking test, as well as in the preform test. This confirms service performance. Figure 11 illustrates the sheared edges of 5456 -H116 material in the four conditions after ASSET. Sensitizing treatments at 212°F and 300°F caused intergranular corrosion and stress corrosion cracking. The 6-day/300°F treatment was more severe than the 7-day/212°F treatment, causing sensitization in all alloys. The 212°F sensitized only the 5450 alloy. The other thermal treatment, 1 hour at 450°F, did not "sensitize" any material except 5456 -H117 and one of the two samples of 5456 -H116. (See Figure 9 and Figure 10)

In the shear crack-ASSET test, cracking was markedly reduced by the thermal stress relieving resulting from shearing two edges before the thermal treatment as opposed to shearing after thermal treatment.

The preform stress test in 3.5% salt continuous immersion proved less severe than the shear crack-ASSET test. However, good correlation between the preform test and 2 months' marine atmospheric exposure has been observed.

The nitric acid weight loss (NAWLT) continues to provide a good means of detecting intergranular corrosion and stress corrosion susceptibility. However, some care must be taken to maintain constant temperature control, otherwise results may not be reproducible because weight loss increases as the heat of the reaction causes the temperature to rise.

Atmospheric tests were started on shear crack specimens and preform sheet specimens at the marine test site near Daytona Beach, Florida, in January 1974. (See Figure 11) (Sheared samples are planned to be treated at a marine atmospheric site, Point Judith, Rhode Island.)' In the Daytona Beach atmospheric tests, the preform sheet samples of 5456 -H321 controls failed in less than one month as received, while the 5456 -H117 samples, which had been sensitized in one week at 300°F, failed in less than 2 months. All the other preform sheets continue to perform satisfactorily with no cracks. Moreover, there has been no cracking reported on any of the sheared edge specimens.

RECOMMENDATIONS

Although these results are of an interim nature, a recommended practice should be prepared for the nitric acid weight loss test method (NAWLT), which is suitable for detecting intergranular corrosion, as well as exfoliation corrosion and stress corrosion susceptibility in the 5000 Series alloy. (In 1968 and 1970 tests, this task group evaluated the NAWLT exfoliation tests.

Recommended practices should be prepared for the shear crack-ASSET test and for the preform stress test in 3.5% salt continuous immersion.

Considerable difficulty was encountered by members of the Task Group in trying to crack NRL's wedge specimens in the -H116 and -H117 resistant tempers. (Wedges would slip and the material was difficult to crack.) This bears out Erickson's earlier work at Mare Island when he reported that it was difficult to pop in cracks in these resistant tempers. More study is needed before this method could be suggested as a means of evaluating stress corrosion resistance.

The Aluminum Association Task Group members wish to express their appreciation for cooperation received from various Navy agencies in providing materials and background information. They believe that this cooperative spirit has been most helpful in establishing reliable and meaningful standard corrosion test methods for these alloys.

APPENDIX A

METHOD OF TEST FOR VISUAL ASSESSMENT OF EXFOLIATION CORROSION SUSCEPTIBILITY OF 5XXX ALUMINUM ALLOYS WITH 2.0-5.5% Mg.

ASSET
(Ammonium-Salt Solution Exfoliation Test)

1. ### SCOPE

   1.1 This method describes a procedure for constant immersion exfoliation* corrosion testing of aluminum-magnesium alloys with 2.0-5.5% Mg.

   1.2 This method applies only to wrought products such as sheet, plate and extrusions.

2. ### SUMMARY OF ASSET IMMERSION TEST METHOD

   2.1 This test involves continuous immersion of the specimens for 24 hours at $150^{\circ}F \pm 2^{\circ}F$ ($66^{\circ}C$) in a corrosion solution containing 1.0 molar Ammonium Chloride, 0.25 molar Ammonium Nitrate, 0.01 molar Ammonium Tartrate, and 3 g/1 Hydrogen Peroxide (10 ml of 30% stock solution per liter.) The solution has a pH of 5.2 to 5.4.

3. ### SIGNIFICANCE

   3.1 Use of this method provides a reliable prediction of the exfoliation corrosion behavior of alloys 5086 and 5456 for all types of marine environment service.

4. ### APPARATUS

   4.1 Any suitable glass or plastic container can be used to contain the solution and specimens during the test period. Depending upon the shape and size of the specimens, rods or racks of glass, plastic, or other inert substance shall be used to support the specimens above the bottom of the con-

---

*The term exfoliation is used to describe that form of corrosion which proceeds laterally from the sites of initiation along planes, generally grain boundaries, parallel to the surface. The resulting corrosion products force the metal upwards giving rise to a layered appearance to the surface.

tainer. The container should be fitted with a removable cover to reduce evaporation.

5.   CORROSION SOLUTION

5.1 All chemicals shall be of reagent grade and the distilled or deionized water shall conform to the latest issue of ASTM D 1193-70 - Type II reagent water.

5.2 The corrosive solution shall be prepared by dissolving in distilled or deionized water, chemicals in the following concentrations:

> 1.0 M ammonium chloride
> 0.25 M ammonium nitrate
> 0.01 M ammonium tartrate
> 3 g/l hydrogen peroxide (10 ml of 30% stock
> solution per liter)

The solution has a pH of about 5.2 to 5.4.

Note: If a stock solution of the above chemicals is to be stored, the hydrogen peroxide should not be added until the solution is actually used for the test.

5.3 Solution shall be used in sufficient quantity so as to provide a minimum volume to exposed specimen surface area ratio of 50 ml/sq. in.

5.4 The temperature of the solution shall be maintained at $150°F \pm 2°F$ ($66°C$).

5.5 Method of exposing specimens
5.5.1 Specimens shall be exposed in the vertical position with the top edge of the specimens being at least one inch below the surface of the solution.

6.   DURATION OF TESTS

6.1 The specimens shall be immersed continuously for 24 hours except for permissible momentary interruptions for visual inspections. There shall be no removal of the corrosion products or other disturbance to the metal surface during the test. The solution shall not be changed or additions made during the test.

7.   SAMPLING

7.1 Base metal specimens 1-1/2" by 4" by gauge shall be tested with the rolling direction in the 1-1/2" dimension. The specimens should be sawed or machined to minimize introducing residual stresses

during preparation of the specimens.

7.2 Preparation of specimen

    7.2.1 The samples shall be degreased with a suitable
solvent. After degreasing, they shall be given
the following preparation:

        Etch 1 minute in 5% by weight sodium
hydroxide at $180^{\circ}F$ ($82^{\circ}C$), rinse in
water, desmut 30 seconds in concen-
trated nitric acid at room temperature,
rinse with distilled or deionized water,
air dry. If specimens are not to be im-
mersed in the test solution immediately,
they should be stored in a desiccator
maintained at less than 1% relative
humidity.

8.   CLEANING OF EXPOSED SPECIMENS

8.1 Immediately upon removal from the solution, the specimens
shall be rinsed in running tap water, then soaked in concen-
trated nitric acid at room temperature until clean. They will
then be rinsed in water and air dried.

9.   INTERPRETATION OF RESULTS

9.1 The following codes and classifications shall be used for re-
porting the visual examination of corroded specimens.

Code	Classification
N	No appreciable attack
P	Pitting
E	Exfoliation

9.2 Description of the various classifications, which are illustrated
in Figures B1 and B2, are as follows:

    9.2.1 N - No appreciable attack: Surface may be
etched or discolored.

    9.2.2 P - Pitting: Includes discrete pitting or pit-
blistering. In the latter case, attack re-
sults in a slight undercutting of the sur-
face. With this test such attack, pitting,
or pit-blistering, is to be expected on this
type of material. This type of attack can
occur in varying degrees of severity, as

shown in Figure 1, and should not be con-
strued as exfoliation.

9.2.3 E - Exfoliation: Visible lifting of the surface
A range of exfoliation can occur in varying
degrees of severity, as shown in Figure 2.

10. REPORT

10.1 The report should contain the following essential information:

10.1.1 Alloy Identification

10.1.2 Product and temper of material tested, including
reference to applicable product specification.

10.1.3 Sampling procedure if other than that specified in
referenced product specification.

10.1.4 A rating of the test specimens using the "Code"
and "Classifications" given in paragraph 9.

10.1.5 Notation of any deviation in test procedure from
that set forth in preceding paragraphs.

10.2 Where specifically required, the following additional information
shall be reported:

10.2.1 Size, type, and number of replicate specimens;
method of edge preparation.

10.2.2 Volume to surface ratio.

APPENDIX B

PROCEDURE FOR CONDUCTING
NITRIC ACID WEIGHT-LOSS TEST

1. Prepare specimens measuring 2.000" x .250" x thickness with the 2" dimension parallel to the rolling direction. If the thickness exceeds 1", reduce the thickness by 1/2 or to 1", whichever is less, while retaining one original surface. Machine all sawn surfaces.

2. Smooth all edges wit a fine file or fine emery cloth.

3. Measure all three dimensions to the nearest .001" with a micrometer. Calculate the total surface area.

4. Immerse the specimen in 5% NaOH solution at 180°F for one minute followed by a distilled water rinse, a 30-second immersion in concentrated, reagent-grade nitric acid, and a distilled water rinse.

5. Allow the specimen to air dry completely. Do not wipe dry with a rag or paper towel. From this point on, in the procedure, handle the specimens with tongs or tweezers.

6. Weigh the specimens to the nearest .1 milligram.

7. Fully immerse each specimen in 80 ml. of concentrated nitric acid[1] contained in a 100 ml beaker.[2] It is suggested that beakers without spouts be used with watch glasses as covers. Place the beaker in water bath controlled to $30 \pm 0.1°C$.

8. After 24 hours, remove the specimens, rinse in distilled water and brush with a stiff nylon bristle toothbrush to remove loosely adhering particles, then allow to dry.

9. Weigh the specimens and determine the weight losses.

10. Determine the weight loss per unit area and express it in terms of Mg/in^2.

(1) Reagent Grade, 70% by weight. Fresh acid should be used for each test.
(2) Beaker, Brezelius (Corning #1040).

Figure 1 (68-1457)

Exfoliation Corrosion - 5456-H321

Figure 2 (68-1455)

Exfoliation Corrosion of 5456-H321

Hull Plate in Bilge Area
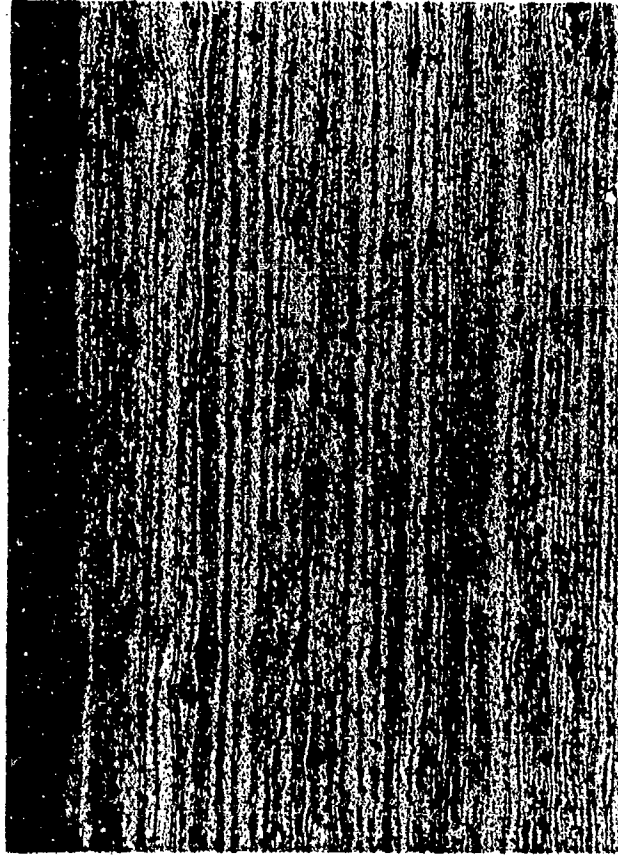
Figure 3 (M 38832)

Microstructure of Exfoliation Corrosion Susceptible 5456-H321 Hull Plate

The highly directional structure and continuous, selective grain boundary precipitate characterize exfoliation corro-
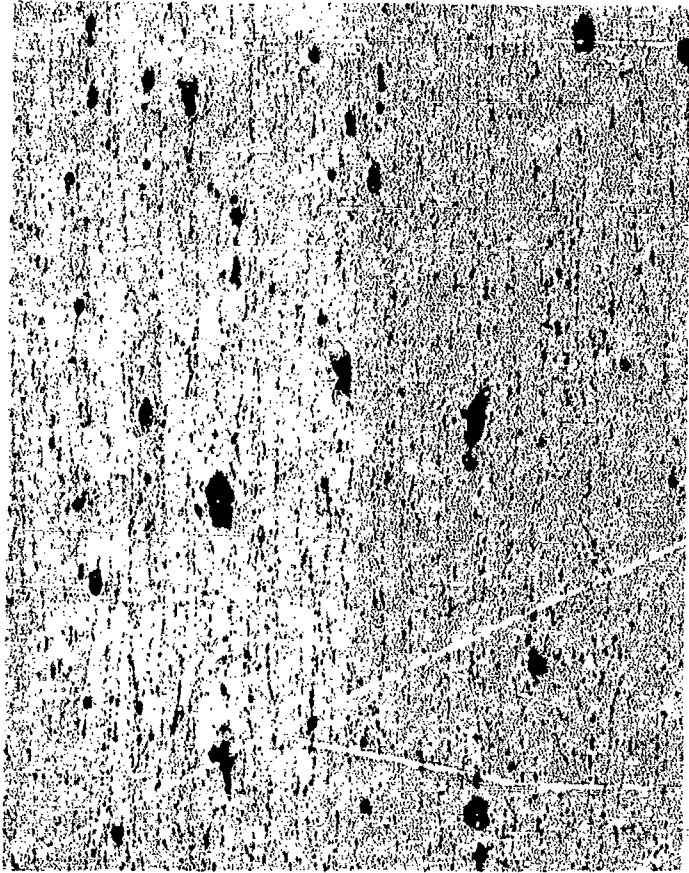
Figure 4 (M 52379)

Exfoliation Resistant 5456-H116 Hull Plate
500X
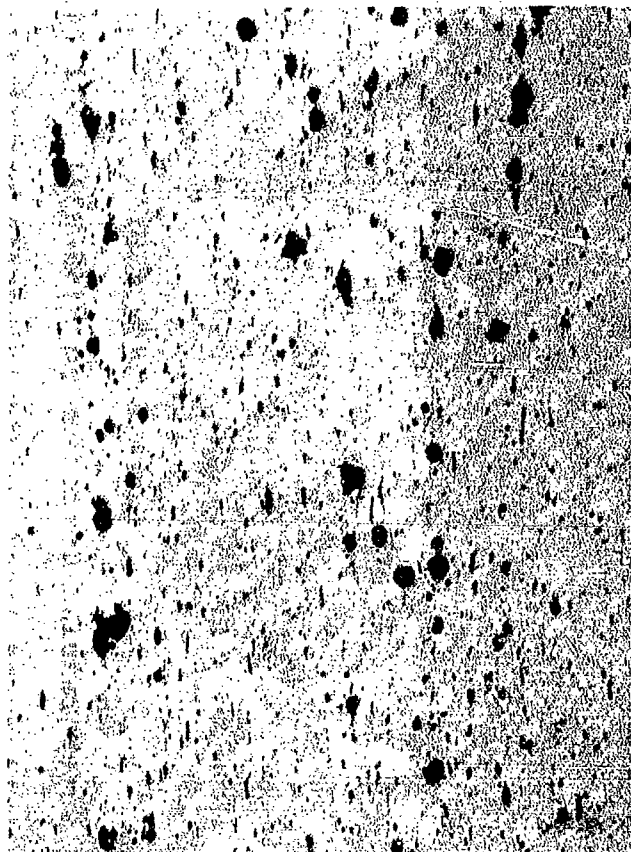
Figure 5 (M 52383)

Exfoliation Resistant 5456-H117 Hull Plate

500X

Figure 6 (74-2848)

Intergranular Corrosion in 5456-H321 Hull Plate

A recrystallized, equiaxial grain structure with
continuous grain boundary precipitation

200%, H_3PO_4 etch

212
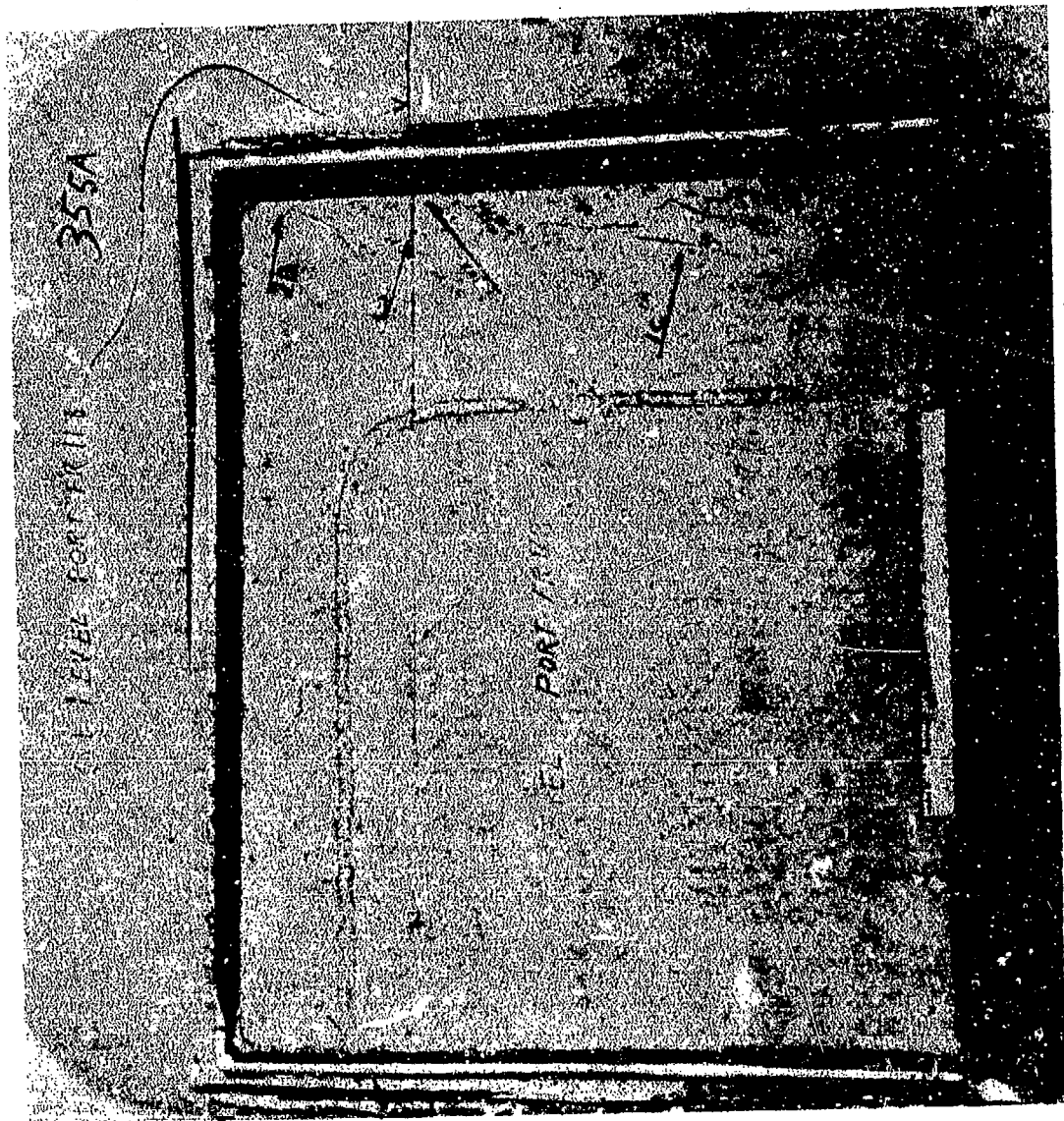
Figure 7 (74-2048)

Stress Corrosion Cracks in 5456-H321 Bulkhead Sheet

ALUMINUM ASSOCIATION
ROUND ROBIN STRESS CORROSION TESTS 5XXX ALLOYS

Test Materials

5456-H321 (control S/N 345A & 346A)

5086-H116 (Alcan, Kaiser, Martin Marietta, Reynolds)
     -H117 (Alcoa)

5083-H321 (Alcan)

5456-H116 (Alcan, Reynolds)
     -H117 (Alcoa)
     -H343 (Alcoa)

Table I (74-2272)

ALUMINUM ASSOCIATION
ROUND ROBIN STRESS CORROSION TEST METHODS FOR 5XXX ALLOYS

A. NAWLT - HNO$_3$ Weight Loss

B. Shear Crack - ASSET

C. Preformed SC - 3.5% NaCl, 90 Days

D. NRL Wedge SC - 3.5% NaCl, 5 Days

Table II (74-2273)

215

ALUMINUM ASSOCIATION
ROUND ROBIN STRESS CORROSION TESTS, 5XXX ALLOYS

Test Laboratories

Alcan
Alcoa
Kaiser
U.S. Navy, Mare Island

Martin Marietta
Naval Research Lab.
Olin
Reynolds

Table III (74-2274)

216
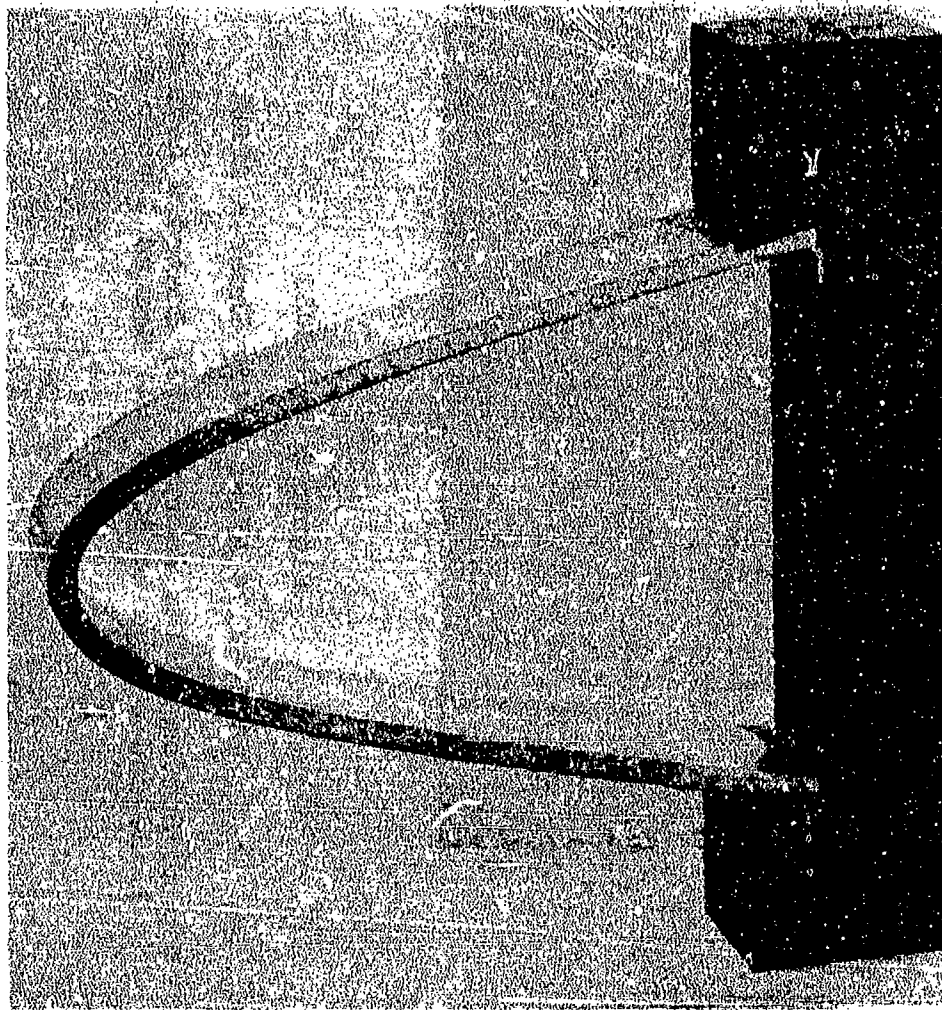
Figure 8 (60-1158)

Preform Stress Corrosion Test Specimen

Specimen is cold formed to 90 degree permanent set,
then sprung into the micarta fixture to provide a high, elastic strain.
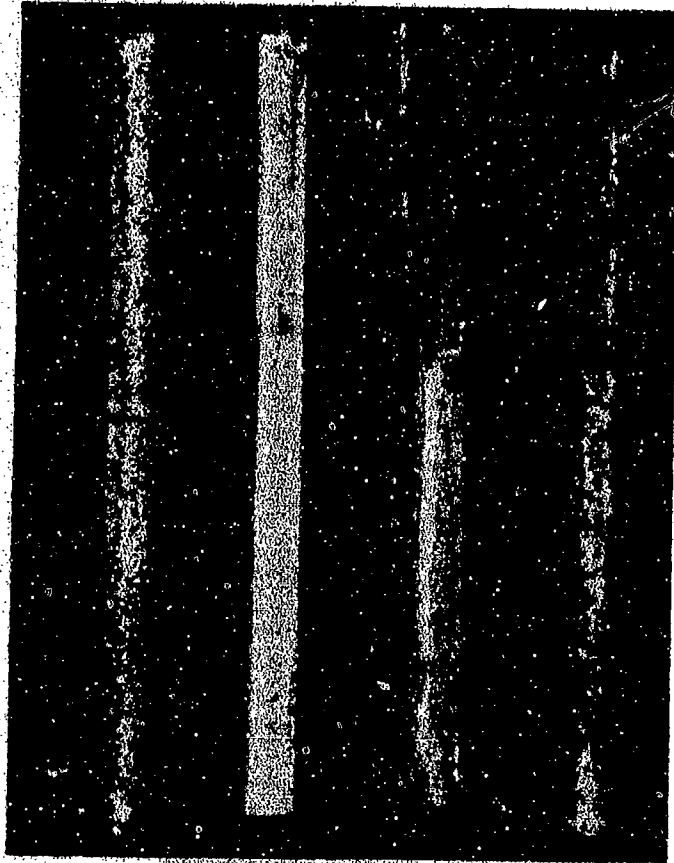
Figure 9 (73-2052)

5456-H116 After 1 Day Shear - ASSET

Top to Bottom - 1) As Received, 2) Heated 7 days at 212°F,
3) Heated 6 days at 300°F, 4) Heated 1 hour at 450°F
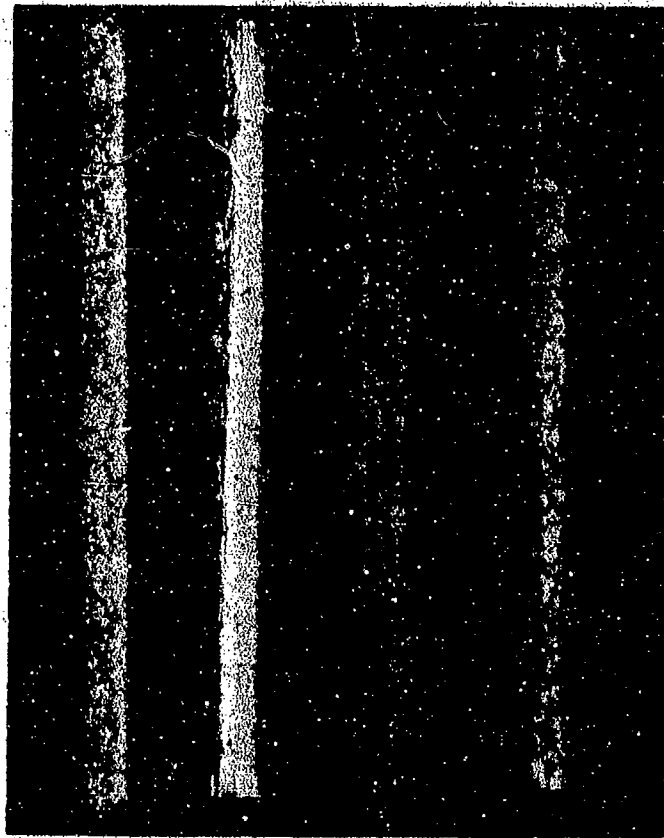
Figure 10 (73-2053).

5456-H117 After 1 Day Shear - ASSET

Top to Bottom – 1) As Received, 2) Heated 7 days at 212°F,
3) Heated 6 days at 300°F, 4) Heated 1 hour at 450°F

Figure 11 (74-1054)

Daytona Beach, Florida Marine Atmospheric
Exposure of Sheared 5XXX Aluminum Alloys

AN AUTOMATED METHOD FOR EVALUATING RESISTANCE TO STRESS-CORROSION CRACKING WITH RING LOADED PRECRACKED SPECIMENS

By

J. G. Kaufman, J. W. Coursen and D. O. Sprowls

ABSTRACT

This paper describes a ring-loading method for evaluating stress-corrosion resistance with precracked compact tension specimens and presents representative data for some high strength aluminum alloys. The ring can be designed to produce different test conditions. In the tests presented, however, the deflection of the ring was large relative to that of the specimen, simulating dead weight loading. This method provides several advantages over techniques previously used. Unlike the constant displacement type loading, the load and crack length and thus the stress intensity are known accurately throughout the life of each test, and the initiation and growth of stress-corrosion cracking provides a definitive end point (failure). Also, the effects of corrosion product wedging are minimal. The ring loading system is more compact than most dead weight systems, and because it is readily automated, more data can be collected with the expenditure of few man-hours.

INTRODUCTION AND OBJECT

Fracture mechanics principles and precracked specimens have been used to advantage in recent years in evaluating the stress-corrosion resistance of metallic alloys[1]. Although the presence of the mechanical precrack does not necessarily eliminate the incubation period as first thought, the fracture mechanics approach does provide some additional screening and design tools such as crack growth rate (da/dt) data and threshold stress intensity (K_{Ith}) values.

The specimens used by various investigators have included compact-tension, cantilever beam, double cantilever beam and center slot. The principal methods of loading have been constant displacement and constant load (dead weight). Constant displacement loading provided by bolt or wedge loading is useful for screening tests in either accelerated or atmospheric environments. Systems employing this technique are compact and self-contained and, theoretically at least, each specimen can provide an arrest or threshold stress intensity value in addition to crack growth rate (da/dt) data. However, with this method the applied load and stress intensity are inferred and are not known precisely even at arrest. An additional problem is the wedging effect caused by corrosion products which can prevent arrest[2]. The dead weight loading systems are usually bulky and better suited to accelerated environmental testing, and several tests are required to establish threshold values. However, the applied loads, and therefore stress intensities, are known more precisely and corrosion product wedging is not a significant problem.

The ring-loading method described in this paper provides a bridge between the extremes of dead weight and constant displacement loadings. For instance, with proper design of the specimen and ring, a constant stress intensity test can be conducted. Or, as was the case in this investigation, the spring constant of the ring can be made large in comparison with that of the compact-tension specimens, thus simulating a dead weight loading. The ring-loading system, however, is much more compact than most dead weight loading systems, and with the ability for direct recording of both load (from ring stress) and crack opening displacement (COD), offers advantages over all of the other systems[a]. It is the purpose of this paper to describe this automated method of evaluating resistance to stress-corrosion cracking (SCC) utilizing the ring-load method.

---

[a] Some ring-loading-type tests were made by E. P. Dahlberg in the ARPA Coupling Program on Stress-Corrosion Cracking (Ref. 1), but without the automated features described in this paper.

MATERIAL

All of the samples for which data are presented were 2.0 or 2.5-in. thick aluminum alloy plate. The alloys and chemical compositions are shown in Table I. The tensile properties, determined in the long-transverse and short-transverse directions in accordance with ASTM Methods E8[3] and B557[4], are shown in Table II. Both the compositions and tensile properties were within the applicable limits for these alloys.

Ambient fracture toughness tests were conducted with 0.75 or 1.0-in. thick short-transverse (S-L) compact-tension specimens in accordance with ASTM Method E399[5]. The results of these tests are also shown in Table II.

EQUIPMENT AND PROCEDURE

Load-deflection calibration data were obtained for the compact-tension specimens over a crack length-to-specimen width (a/W) range of 0.45 to 0.80, so that the crack lengths could be monitored throughout the ring load tests. This was accomplished by making successively longer saw cuts in the specimens, and with each length, loading the specimen in a testing machine utilizing a clip gage in the crack opening at the edge of the specimen to measure displacement. Using a least squares analysis, a series of polynomial equations were fit to the load-displacement-crack length data. The equation providing the best fit is as follows:

$$a = W \left[0.18728 + 8.0737 \times 10^{-3} \frac{VEB}{P} - 4.8716 \times 10^{-5} \left(\frac{VEB}{P} \right)^2 + 1.410 \times 10^{-7} \left(\frac{VEB}{P} \right)^3 \right.$$

$$\left. - 1.5267 \times 10^{-10} \left(\frac{VEB}{P} \right)^4 \right] \tag{1}$$

Where: a = crack length, in.
W = specimen width, in.
V = crack opening displacement (COD), in.
E = modulus of elasticity, psi
B = specimen thickness, in.
P = load, lbs.

All of the tests were conducted with short-transverse (S-L) compact-tension specimens. The specimens were either 0.75 or 1.0 in. thick and were precracked in fatigue at a stress intensity of about 12 ksi√in. prior to testing. The crack length after precracking was estimated from measurements made on the sides of the specimens. The loads required to provide the desired initial stress intensity levels were calculated using the equation for the compact specimen shown in ASTM Method E399[5].

A typical ring-load setup is shown in Fig. 1. The rings and tension bolts are constructed from high-strength aluminum alloys. The nuts on the ends of the tension bolts are spherically seated to provide self-alignment. The clip gage is a single piece keyhole-shape construction. Both the load rings and the clip gages are instrumented with strain gages, and the readings are monitored with the multi-channel digital strain indicator.

In the loading procedure, the clip gage is mounted on the specimen and the load is applied by tightening one of the spherically seated nuts. The applied load is read from the meter on the multichannel strain indicator, and the specimens are immediately immersed in the corrodent. The corrodent used was a corrosion inhibited and buffered 3.5% NaCl solution of the formula: $0.6M(3\ 1/2\%)$ NaCl $+ 0.02M\ Na_2Cr_2O7 + 0.07M\ NaC_2H_3O_2$ to a pH of 4. This solution was found to be more effective in developing SCC than the standard 3.5% NaCl solution[2].

Load and COD readings from up to 15 tests can be logged simultaneously with the equipment shown in Fig. 2. The load and COD readings are taken automatically every 8 hours (the reading interval can be varied), and these readings are printed on a teletype and punched on paper tape for subsequent computer analysis.

Computer programs were developed to sort the data by test, plot the load and COD data against time, and fit polynomial equations to these data. A typical plot of the data and best fit curves is shown in Fig. 3. Using these best fit equations, equation 1, and the equation for K for the compact-tension specimens[5], the crack lengths and stress intensities were evaluated at selected time intervals throughout the life of each test. The crack growth rate was also determined by differentiating the equation developed for crack length versus time. A typical computer printout of these data is shown in Table III.

RESULTS AND DISCUSSION

The results of the ring-load stress corrosion tests are summarized in Table IV. The applied loads were calculated based on the target stress intensity values and the crack lengths measured on the sides of the specimens. When the loads were applied, the crack lengths calculated from the load and COD measurements often differed from those measured on the sides of the specimens. Thus, the calculated initial stress intensities differed somewhat from the target values. The initial crack lengths calculated from load and COD measurements provide an integrated average crack length as opposed to an estimated value based on side measurements and were found to be more accurate. General corrosion of the crack faces usually destroys the definition of the end of the fatigue crack but in the few instances where the precrack lengths could be discerned after fracture, the initial crack lengths were very close to the calculated values. The crack lengths at fracture, which would normally be the end of environmental crack growth, were also reasonably close to the calculated values in most instances.

A decided advantage of the ring-load test is that the initial load and crack length, and thus stress intensity, are known accurately. The load can be adjusted to provide the desired initial stress intensity, as was done in two of these tests, but in most instances it seemed sufficient to know the initial values without making minor load adjustments. The stress intensity at fracture (K_{If}) was usually equal to or greater than the ambient K_Q value.

Many of the tests demonstrated a period of incubation before the initiation of environmental crack growth. As might be expected, the length of the incubation time generally increased with decreasing initial stress intensity. Also, some of the 2000 series alloys, particularly alloy 2219-T37, demonstrated temporary arrest during the test. This is illustrated by the data for one of the specimens of 2219-T37 shown in Fig. 4. The specimen experienced a short incubation period, followed by rapid crack growth and then an arrest of about 100 hours duration before accelerated crack growth to failure[b].

Metallographic examinations reveal that the probable cause of these temporary arrests is crack branching, which may delay the forward progress of the crack on its final path to failure. Evidence of such branching is shown in the photomicrograph of a fractured specimen of 2219-T37 shown in Fig. 5.

DATA ANALYSIS

One method of analyzing these data and comparing different alloys is by plotting crack growth rates (da/dt) as a function of instantaneous stress intensity. A plot of such data for 7075-T651 is shown in Fig. 6. A close look at the data indicates that because of the incubation periods and slow development of crack growth at the beginning of these tests, a family of curves may be developed showing low da/dt rates at the initial stress intensity level (regardless of what that level is) but with a tendency for the da/dt rates to converge somewhat at stress intensity levels approaching K_{IC}[6]. Also, it may be observed that two of the individual tests demonstrate an intermediate period of constant crack growth rate (or plateau value) and one test demonstrates a steadily increasing crack growth rate.

These idiosyncrasies, plus the intermediate arrests previously mentioned, make da/dt data difficult to analyze; nevertheless, some information can be gained by observing the upper limit of maximum crack growth rates developed by all of the tests of a given alloy as shown by the line in Fig. 6. The upper boundary lines for several alloys are shown in Fig. 7. This comparison of crack growth rates indicates that alloys 7075-T651 and 7039-T6351 are clearly the most susceptible to

---

[b] Fig. 4 also illustrates that the load readings can be used as a secondary indication or check on crack growth. The clip gage readings were more sensitive to temperature effects and sometimes evidenced long term drift; however, the load readings were extremely stable and a decrease in load of only 1 or 2 per cent is indicative of an event.

stress-corrosion cracking and alloys 2021-T81, 2219-T87 and 7075-T7351 are very resistant to stress-corrosion cracking. Alloys of low and intermediate resistance to SCC develop a "plateau velocity" which has often been observed in constant displacement (bolt load) type tests. Alloys of relatively high resistance to SCC, such as 2024-T851 and 2021-T81, experience crack growth only at K_I levels close to their K_{Ic} values and do not demonstrate a clearly defined plateau value[c].

Data for alloys 2219-T87 and 7075-T7351 are shown as points on axes of Fig. 7. Two specimens of 2219-T87 failed, but at levels above the ambient K_{Ic} value, and metallographic examination indicated that the fractures were of a tensile nature and not SCC. Creep may be responsible for the failure of these specimens. Some slight crack growth was detected for a specimen of 7075-T7351, but it was so small that the growth rate is below the limits of Fig. 7, and the fact that SCC growth occurred had to be confirmed by metallographic examination.

As Fig. 7 demonstrates, crack growth rate data may be used to compare the relative resistance of various alloys and, theoretically, these data can be extrapolated to a very low rate to establish a threshold stress intensity factor (K_{Ith}). However, a more straightforward method of determining threshold values with ring load test data is to plot initial or applied stress intensity versus time to failure as shown in Figs. 8 and 9. For both high and low resistance alloys, a near threshold level was reached within 1000 hours of exposure in this accelerated test environment. An exposure of about 2000 hours, coupled with no significant indication of crack growth or drop in load, was considered sufficient to establish threshold values. Metallographic examinations of the "run-out" specimens showed no evidence of stress-corrosion cracking except in those of 7075-T651 and T7351.

The data in Figs. 8 and 9, tempered by the metallographic evidence, were used to establish the following threshold stress intensity levels:

ESTIMATED THRESHOLD STRESS INTENSITY FACTORS

Resistant Alloys			Susceptible Alloys		
Alloy & Temper	K_{Ith}		Alloy & Temper	K_{Ith}	
	ksi $\sqrt{in}$.	%K_{Ic}		ksi $\sqrt{in}$.	%K_{Ic}
2219-T87	>20	100	2024-T351	11	50
2021-T81	17	85	2219-T37	12	45
7075-T7351	18	85	7039-T6351	6	30
2024-T851	13	80	7075-T651	4	20

[c] Reference[1], page 9

Another alloy comparison is shown in Fig. 10 where the K_{Ith} values (in the salt-dichromate-acetate solution) are shown as a percentage of their respective ambient K_{Ic} values along with the percentage of yield strength data determined with smooth tensile specimens in a 3.5% NaCl solution, alternate immersion test. Although the percentages are sometimes quite different, the data from both types of tests rate these alloys in the same order with respect to resistance to SCC.

Although the data for precracked and smooth specimens are usually in agreement with respect to alloy ratings, a question arises as to how these data can be used for design purposes. If the applied stress and the size of an existing flaw are known, then the stress intensity level can be calculated and compared with the threshold stress intensity for the material to predict whether or not SCC will occur. On the other hand, we know that smooth specimens containing no initial flaws (in which case the stress intensity is zero) fail under relatively low stresses if the alloy is susceptible to SCC.

This has led to a proposal[2] which considers both threshold stress and threshold stress intensity values for determining the design stresses, as illustrated in Fig. 11. The "safe" region (no SCC expected) is below the threshold stress line and to the left of the threshold stress intensity line. For alloy 7075-T651, a stress of 10 ksi would apply in the absence of flaws. If flaw sizes larger than that occurring at the intersection of the threshold lines (≈ 0.04 in. for 7075-T651) are expected, then the design would be goverened by fracture mechanics concepts and the gross-section design stress would have to be reduced in proportion to the flaw size. Obviously, resistant alloys, such as 2219-T87, would have safe regions encompassing higher stresses than susceptable alloys, such as 7075-T651.

SUMMARY

The ring-loading method used in conjunction with automatic data logging equipment has proven to be a reliable method of determining stress-corrosion resistance using a fracture mechanics approach. Alloy rankings developed with ring-load data are about the same as those developed with smooth tensile specimen data and a proposal has been made for combining these two types of data for design purposes.

The ring-loading method has the following advantages over other techniques used for tests of precracked specimens:

1. The applied load, initial crack length and the applied stress intensity are known more accurately than in the constant displacement type test.

2. The progress of the test is monitored automatically with the data logging equipment and is in a form amenable to computer analysis. Thus more data can be collected with the expenditure of fewer man-hours. This facilitates the determination of incubation periods and temporary arrests and can indicate instances in which metallographic examination may provide more information.

3. Because the stress intensity increases if crack growth developes, the test has a definite end point (fracture), and since the crack is opening, there are no apparent problems with corrosion product wedging effects.

4. The ring load system is more compact and less cumbersome to operate than most dead weight systems.

REFERENCES

1. Brown, B. F., "Stress Corrosion Cracking in High Strength Steels and in Titanium and Aluminum Alloys," Naval Research Laboratory, Washington, D.C., 1972. (Sponsored by the Advanced-Research Projects Agency ARPA Order No. 878).

2. Sprowls, D. O., Shumaker, M. B., Walsh, J. D. and Coursen, J. W., "Evaluation of Stress-Corrosion Cracking Susceptibility Using Fracture Mechanics Techniques," Final Report of Government Contract NAS 8-21487-Part I, May 31, 1973.

3. Standard Methods of Tension Testing of Metallic Materials (Designation: E8-69), 1974 Annual Book of ASTM Standards, Part 10, pp. 90-110.

4. Standard Methods of Testing Wrought and Cast Aluminum and Magnesium Alloy Products (Designation: B557-73), 1974 Annual Book of ASTM Standards, Part 7, pp. 535-538.

5. Standard Method of Test for Plane-Strain Fracture Toughness of Metallic Materials (Designation: E399-74), 1974 Annual Book of ASTM Standards, Part 10, pp. 432-451.

6. Wei, R. P., Novak, S. R., and Williams, D. P., "Some Important Considerations in the Development of Stress-Corrosion Cracking Test Methods," AGARD-CP98, AGARD Conference Proceedings, No. 98, October 4-8, 1971.

TABLE I

CHEMICAL COMPOSITIONS OF SOME SAMPLES
OF ALUMINUM ALLOY PLATE

Alloy & Temper	Thickness, in.	Si	Fe	Cu	Mn	Mg	Zn	Cr	Ni	Ti	Be	V	Sn	Zn	Cd
2021-T87	2.5	0.06	0.14	6.30	0.31	0.01	0.02	0.00	0.01	0.06	--	0.08	0.05	0.13	0.13
2024-T351	2.5	0.09	0.33	4.78	0.66	1.37	0.04	0.00	0.00	0.02	0.001	--	--	--	--
2024-T851	2.5	0.09	0.33	4.81	0.65	1.39	0.04	0.00	0.00	0.02	0.001	--	--	--	--
2219-T37	2.0	0.10	0.21	6.35	0.26	0.00	0.05	0.00	0.01	0.06	--	0.09	--	0.15	--
2219-T87	2.0	0.10	0.21	6.35	0.26	0.00	0.05	0.00	0.01	0.06	--	0.09	--	0.15	--
7039-T6351	2.5	0.13	0.25	0.04	0.25	2.93	4.30	0.21	0.00	0.03	0.000	--	--	--	--
7075-T651	2.5	0.12	0.26	1.80	0.07	2.42	6.07	0.19	0.00	0.03	0.002	--	--	--	--
7075-T7351	2.5	0.12	0.26	1.82	0.07	2.41	6.09	0.19	0.00	0.03	0.002	--	--	--	--

Composition, %

TABLE II

RESULTS OF TENSILE AND FRACTURE TOUGHNESS TESTS OF SOME ALUMINUM ALLOY PLATE

Alloy & Temper	Long-Transverse(1)			Short-Transverse(2)			Short Transverse (S-L)		
	Tensile Strength, ksi	Yield Strength, ksi	Elongation in 4D, %	Tensile Strength, ksi	Yield Strength, ksi	Elongation in 4D, %	Specimen Thickness, in.	K_Q, ksi√in.	Valid K_{Ic}
2021-T81	68.8	59.5	4.8	68.6	59.1	5.0	1.00	19.6	yes
2024-T351	67.5	47.1	17.0	55.4	42.4	3.5	1.00	21.0	yes
2024-T851	68.6	62.2	7.5	63.9	61.8	1.0	1.00	16.7	yes
2219-T37	58.7	42.5	17.5	57.9	42.1	12.0	0.75	27.1	nc(3)
2219-T87	71.6	58.2	9.5	69.1	57.7	5.5	0.75	19.6	yes
7039-T6351	64.4	55.1	12.0	62.6	54.2	6.0	1.00	20.4	yes
7075-T651	81.9	71.9	8.5	75.3	66.7	2.0	1.00	19.5	yes
7075-T7351	69.7	58.6	10.0	65.0	55.1	4.0	1.00	21.0	yes

(1) Duplicate 0.500 in. diam. specimens taken at quarter - plane per ASTM Standards
(2) Duplicate 0.125 in. diam. specimens centered in plate thickness.
(3) Did not meet ASTM criteria for specimen thickness or plastic deformation.

TABLE III

STRESS CORROSION FRACTURE TOUGHNESS DATA FOR RING LOADED COMPACT TENSION SPECIMENS

ALLOY – TEMPER 7075-T651
SAMPLE NUMBER 366209
SPECIMEN THICKNESS 1.000 in.
RING CONSTANT 0.500 in./hr

PRODUCT PLATE
SPECIMEN NUMBER S-L-1
SPECIMEN WIDTH 2.000 in.
GAGE CONSTANT 180000. in./in.

SIZE in. 2.5 THICK
MECH. TEST NUMBER 092768A
INITIAL CRACK LENGTH 0.990 in.
MODULUS; ksi 10 0.

SPEC. LOADED 03-23-71
TYPE TEST T1
TYPE PRE-CRACK FC
INT. K_i 14660 psi-in. 1/2

TIME hrs	LOAD(P) lbs	COD(V) in.	CRACK LENGTH (A), in.	CRACK GROWTH RATE (ADOT), in./hr	STR. INT. FACTOR (KI) psi-in. (1/2)	REMARKS CGR DIFF.
0	2191.	0.00864	0.888	0.1216E-03	12715.	0.0000E-00
10	2190.	0.00877	0.893	0.7000E-03	12808.	0.5784E-03
20	2188.	0.00895	0.902	0.1011E-02	12943.	0.3116E-03
30	2185.	0.00918	0.912	0.1131E-02	13108.	0.1199E-03
40	2181.	0.00942	0.923	0.1125E-02	13288.	-0.5765E-05
50	2178.	0.00966	0.934	0.1050E-02	13469.	-0.7545E-04
60	2175.	0.00989	0.945	0.9507E-03	13642.	-0.9970E-04
70	2171.	0.01011	0.954	0.8614E-03	13802.	-0.8933E-04
80	2168.	0.01030	0.962	0.8063E-03	13948.	-0.5503E-04
90	2165.	0.01048	0.970	0.7993E-03	14088.	-0.7024E-05
100	2161.	0.01067	0.978	0.8446E-03	14229.	0.4527E-04
110	2157.	0.01087	0.987	0.9382E-03	14385.	0.9362E-04
120	2153.	0.01110	0.997	0.1069E-02	14566.	0.1312E-03
130	2148.	0.01138	1.008	0.1222E-02	14783.	0.1534E-03
140	2144.	0.01170	1.021	0.1380E-02	15043.	0.1573E-03
150	2138.	0.01208	1.036	0.1523E-02	15349.	0.1428E-03
160	2133.	0.01250	1.052	0.1636E-02	15700.	0.1129E-03
170	2127.	0.01295	1.069	0.1709E-02	16088.	0.7361E-04
180	2121.	0.01344	1.086	0.1744E-02	16504.	0.3448E-04
190	2114.	0.01394	1.103	0.1753E-02	16941.	0.9201E-05
200	2106.	0.01445	1.121	0.1769E-02	17396.	0.1569E-04
210	2097.	0.01499	1.135	0.1845E-02	17884.	0.7654E-04
220	2086.	0.01560	1.158	0.2064E-02	18445.	0.2193E-03
230	2074.	0.01638	1.181	0.2541E-02	19164.	0.4769E-03
240	2059.	0.01745	1.211	0.3429E-02	20184.	0.8880E-03
248	2045.	0.01868	1.242	0.4567E-02	21362.	0.1137E-02

CALCULATED SIF BASED ON
MEASURED (A) AFTER FRACTURE 1.278   23089.

STANDARD ERROR = 0.4214052

LOAD= 0.1095E 04+ 0.3124E-01T+ -0.7680E-02T**2+ 0.1433E-03T**3+ -0.1393E-05T**4+ 0.7107E-08T**5
+-0.1822E-10T**6+ 0.1815E-13**7+

COD = -0.8648E 03+ 0.8799E 00T+ 0.3715E-01T**2+ -0.9484E-04T**3+ -0.7191E-05T**4+ 0.8756E-07T**5
+-0.3743E-09T**6+ 0.5561E-12T**7+

A = 0.8882E 00+ 0.1216E-03T+ 0.3694E-04T**2+ -0.5819E-06T**3+ 0.3601E-08T**4+ -0.5193E-11T**5
+-0.2498E-13T**6+ 0.6918E-16T**7+

TABLE IV

RESULTS OF TESTS OF RING-LOADED SHORT TRANSVERSE (S-L) COMPACT TENSION SPECIMENS FROM SOME ALUMINUM ALLOY PLATE

| Alloy & Temper	Target K_Ii ksi√in.	Target %K_Ic	Initial Crack Length, in.	Initial Load, lbs.	Initial K_Ii ksi√in.	Final Crack Length, in.	Final Load, lbs.	Final K_If ksi√in.	Incubation Time, hrs.	Time to Failure, hrs.
High Resistance Alloys										
2021-T87	17.7	90	1.030	2490	17.7	1.141(1)	2440	20.9(1)	200(5)	392
	15.0	76	1.054	2210	16.3	1.112(1)	2206	17.9(1)	--	OK 2328
2024-T851	15.0	90	0.962	2270	14.6	1.137(1)	2190	18.6(1)	80	240
	12.0	72	0.939	1810	11.3	0.979(1)	1810	11.9(1)	--	OK 2400
2219-T87	19.0	97	0.782	1820	20.4	0.840	1790	22.7	0(5)	16
	18.6	95	0.809	1800	21.3	0.871(1)	1760	24.1(1)	--	504
	17.7	90	0.758	1730	18.4	0.803(1)	1720	20.1(1)	--	OK 1816
7075-T7351	21.0	100	0.909	3180	18.7	0.926	3120	19.1	--	OK 2780
Low Resistance Alloys										
2024-T351	15.8	75	0.882	2360	13.6	1.323	2140	26.8	50	664
	12.0	57	0.958	1900	12.1	--(2)	1865	--(2)	150	1192
	10.5	50	0.870	1570	8.9	--(2)	--	--(2)	--	OK 3980
2219-T37	13.5	50	0.767	1311	14.2	1.118	1040	31.1	50(5)	376
	13.5	50	0.760	1330	14.2	1.199	900	36.5	200(5)	1280
	12.0	44	0.779	1160	12.9	1.201	810	33.3	0(5)	560
7039-T6351	15.3	75	0.886	2300	13.3	1.286	2110	24.2	0	320
	10.2	50	0.972	1470	9.6	1.438	1250	21.0	0	600
	8.2	40	1.000	1190	8.2(4)	--(3)	660	--(3)	1300	1872
	7.0	34	0.888	1200	7.0(4)	--(3)	870	--(3)	0	2376
7075-T651	14.7	75	0.888	2190	12.7	1.242	2040	21.4	0	248
	9.8	50	0.910	1490	8.9	1.338	1350	17.5	200	400
	7.0	36	0.852	1200	6.6(4)	1.456	980	17.2	350	824
	5.9	30	0.826	880	4.7	0.865	870	4.9	--	OK 2208

(1) Apparent increase in crack length and stress intensity due to long term drift in clip gage. There was no significant decrease in load.

(2) Clip gage failed during test.

(3) Rapid fracture. Cracks too long for meaningful calculation.

(4) Load was adjusted at beginning of test to obtain target K_Ii level.

(5) Temporary arrest occurred during the test.
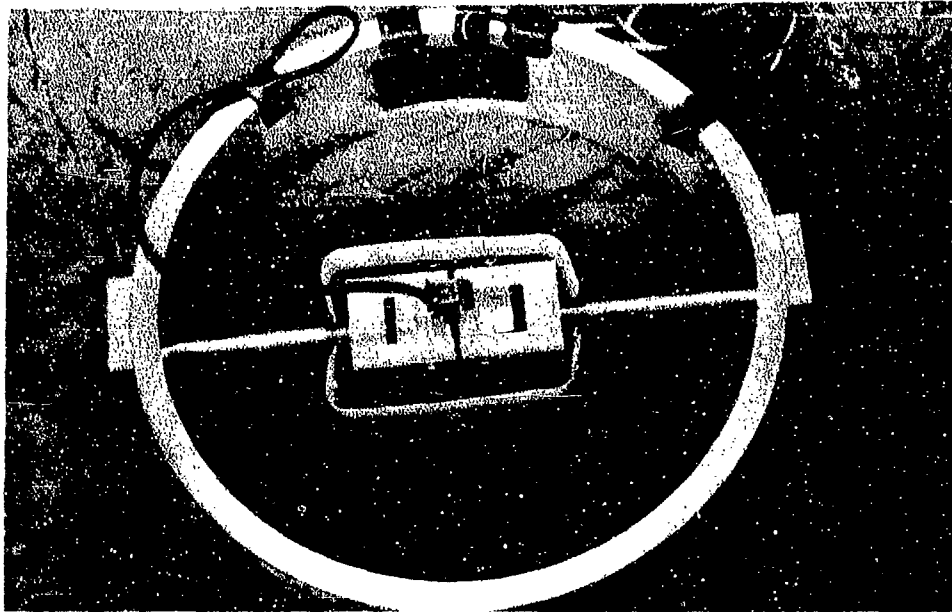
RING LOADED COMPACT SPECIMEN

**Fig. 1**
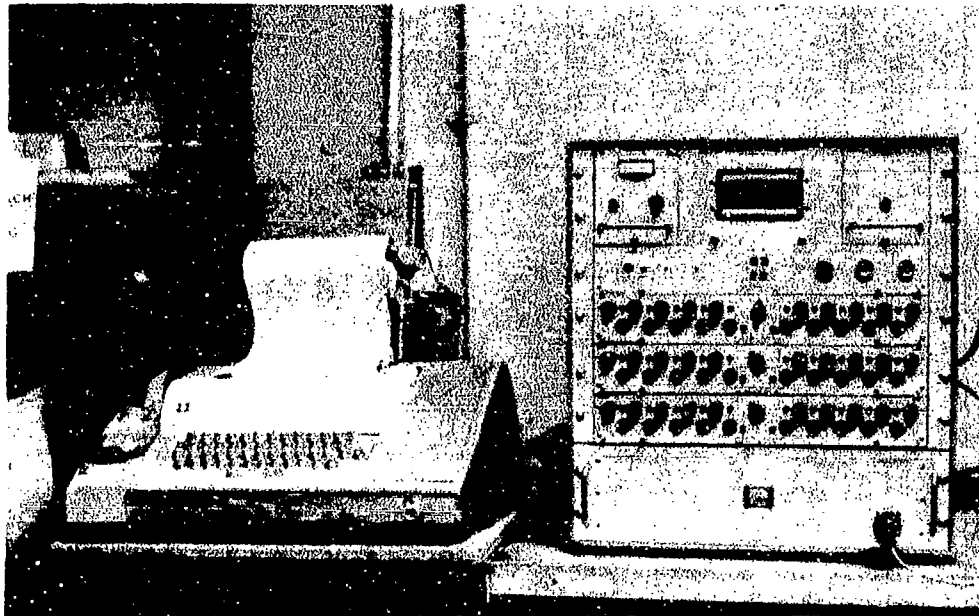
**MULTI-CHANNEL DIGITAL
STRAIN INDICATOR AND TELETYPE**

Fig 2
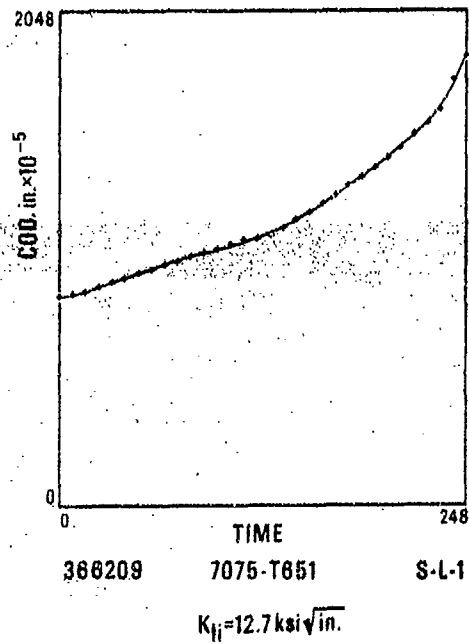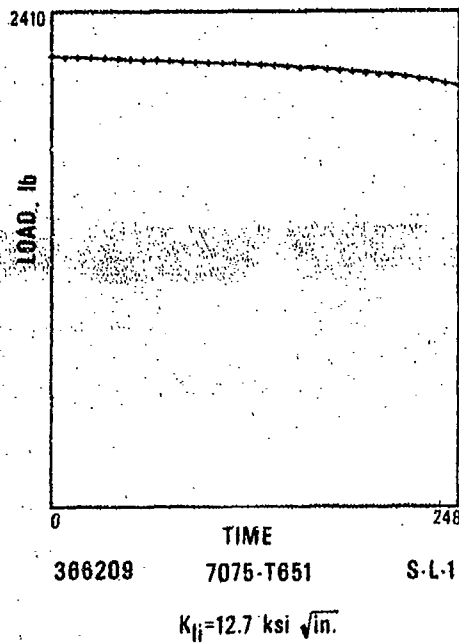
TYPICAL COMPUTER PLOT OF LOAD AND COD DATA WITH "BEST-FIT" CURVES

FIG. 3
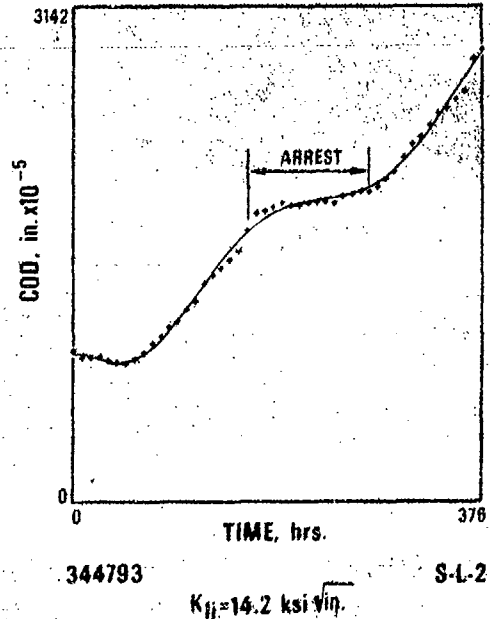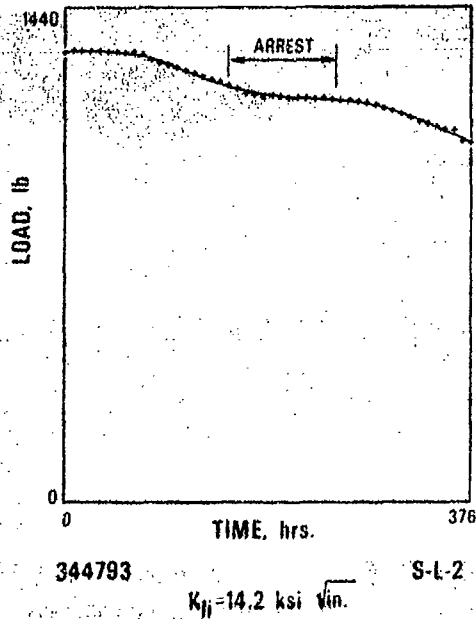
RING LOADED COMPACT TENSION SPECIMEN OF 2219-T37
EXPOSED IN A SALT DICHROMATE SOLUTION

FIG. 4

235
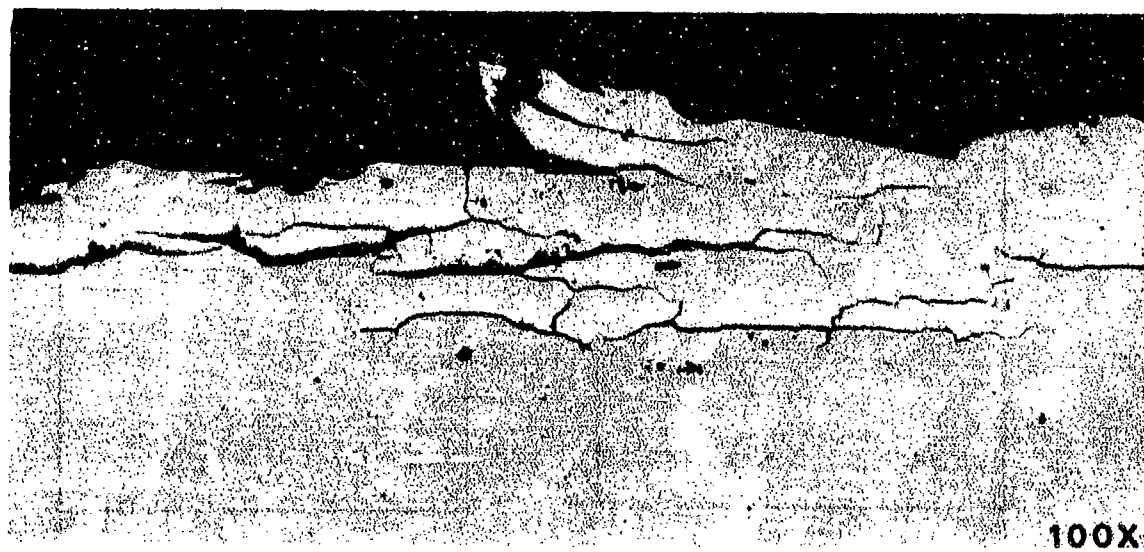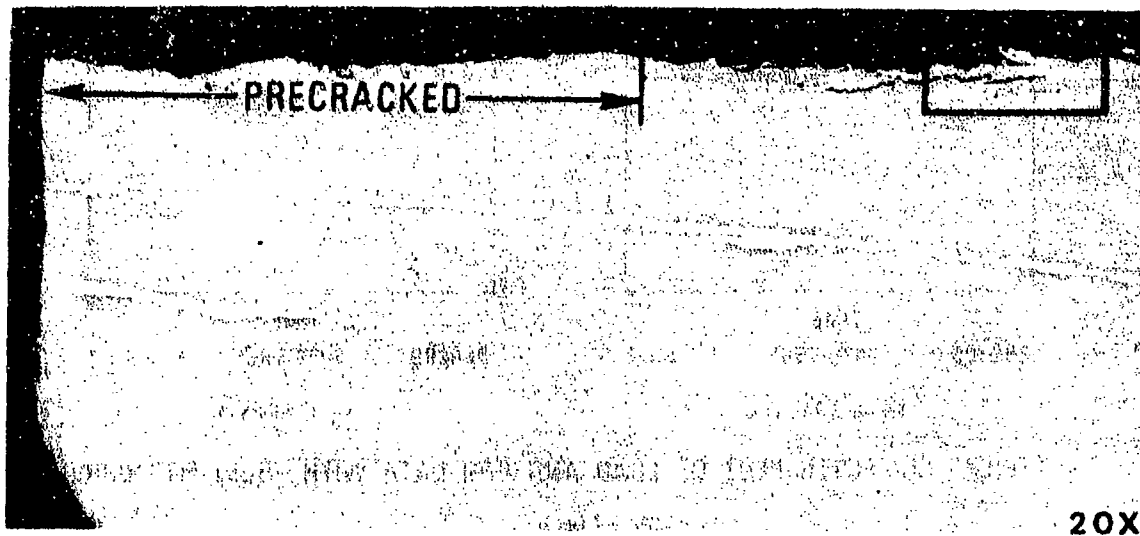
MICROGRAPHS SHOWING BRANCHING OF SCC IN RING LOADED COMPACT TENSION SPECIMEN OF 2219-T37 EXPOSED TO SALT-DICHROMATE-ACETATE SOLUTION

Fig. 5

CRACK GROWTH RATE VS STRESS INTENSITY
FOR S-L COMPACT SPECIMENS OF 7075 -T651 PLATE
EXPOSED IN A SALT-DICHROMATE-ACETATE SOLUTION

Fig 6
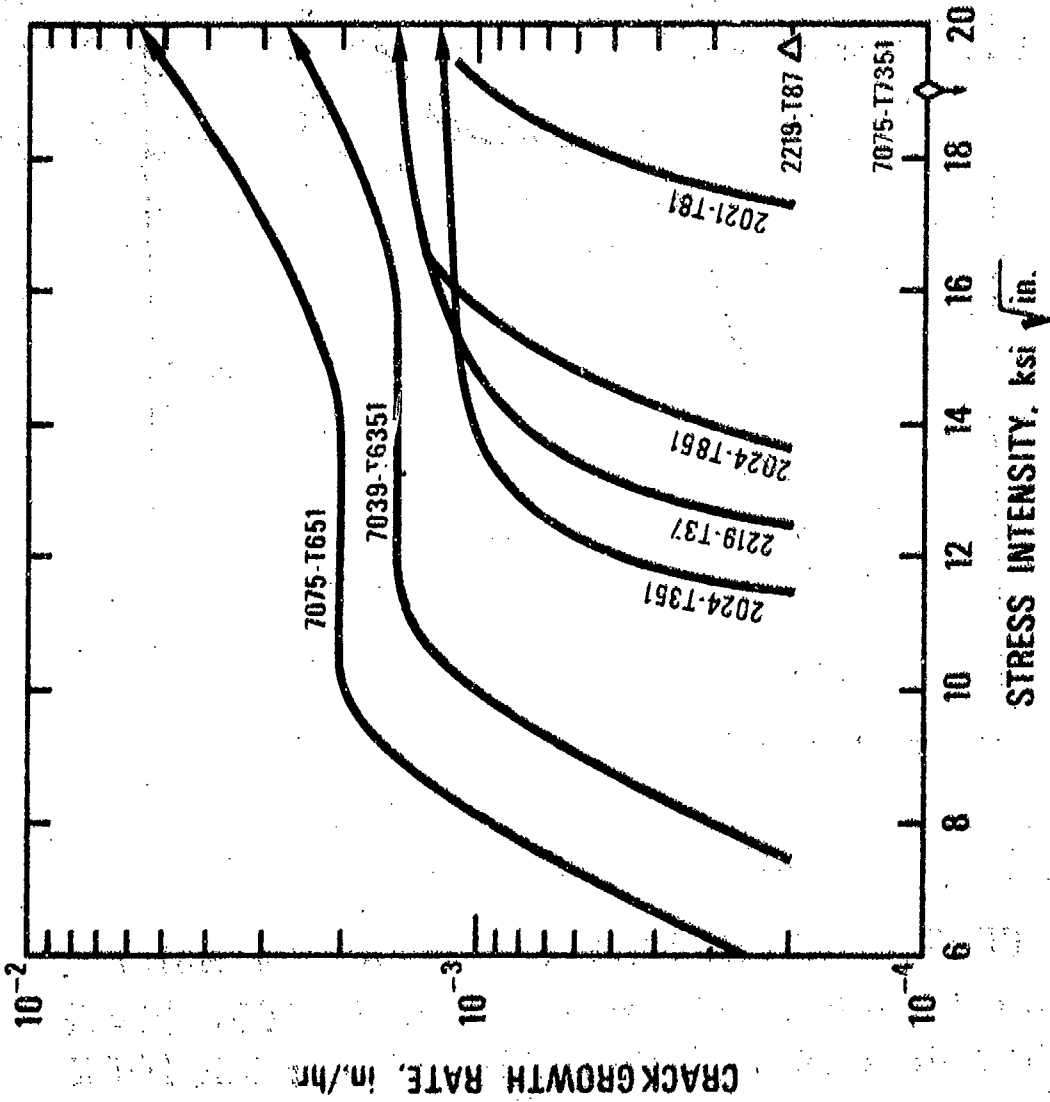
CRACK GROWTH RATE vs STRESS INTENSITY FOR
S-L COMPACT SPECIMENS OF SOME ALUMINUM ALLOYS
EXPOSED IN A SALT-DICHROMATE-ACETATE SOLUTION

FIG. 7
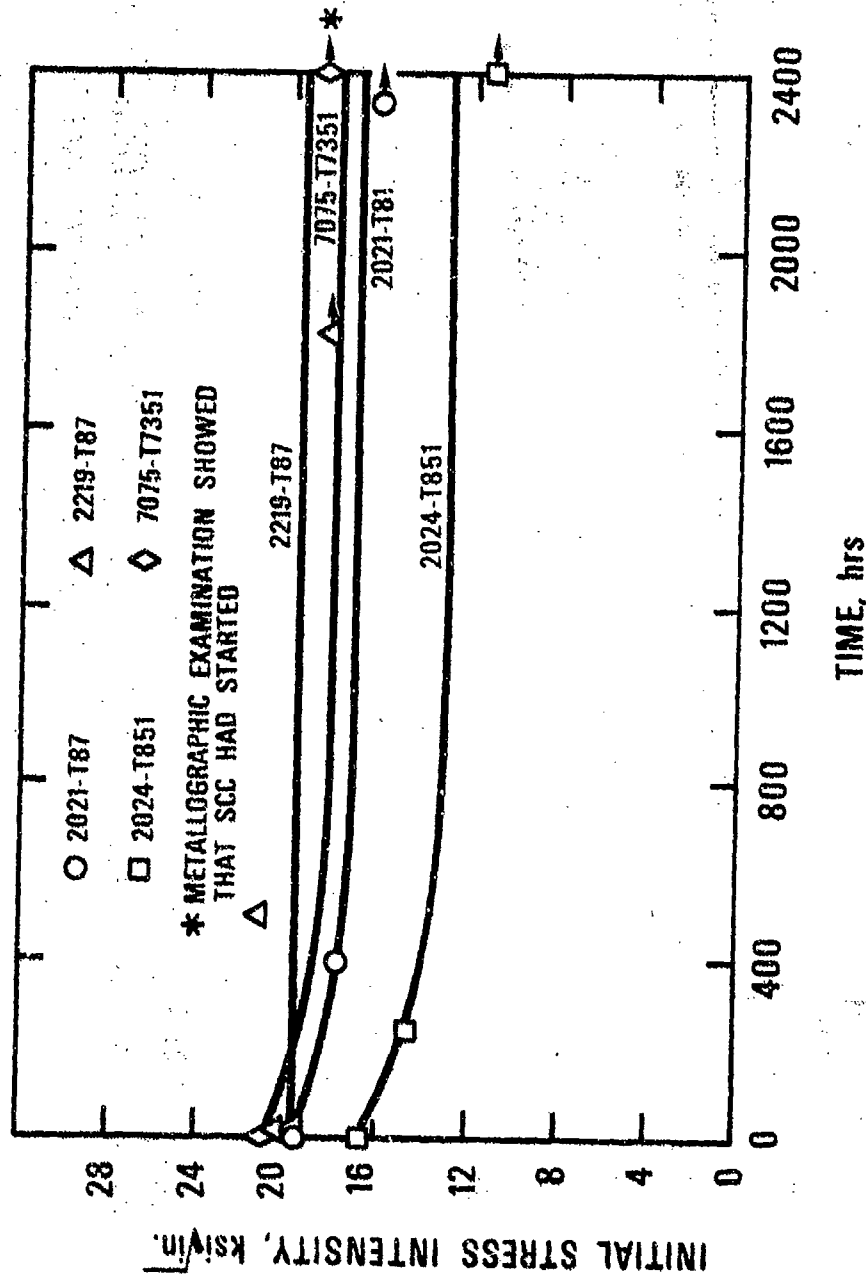
INITIAL STRESS INTENSITY VS TIME TO FAILURE FOR SOME S-L COMPACT SPECIMENS OF RESISTANT ALUMINUM ALLOYS EXPOSED IN A SALT-DICHROMATE-ACETATE SOLUTION

FIG 8
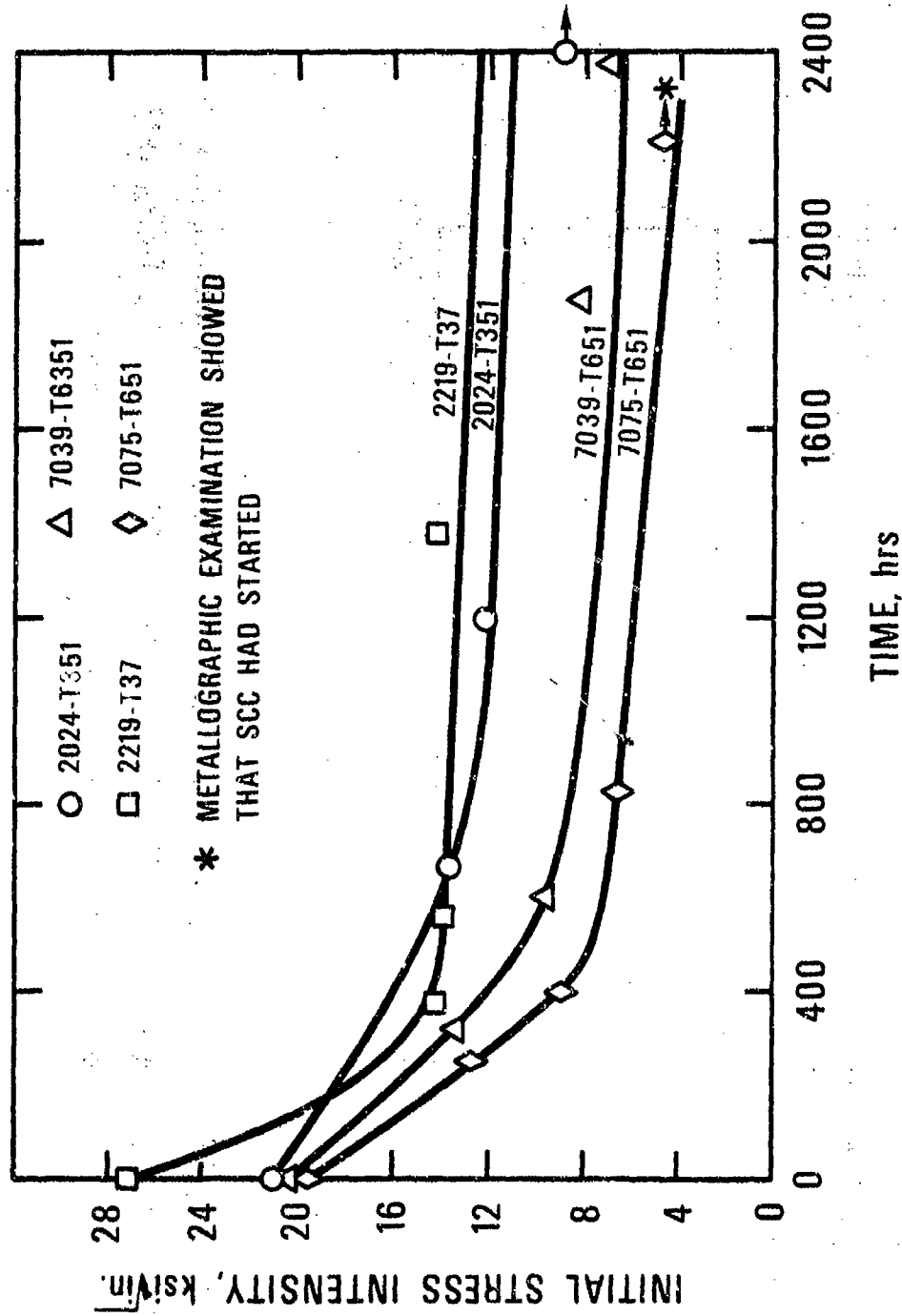
INITIAL STRESS INTENSITY VS TIME TO FAILURE FOR SOME S-L COMPACT SPECIMENS OF LOW RESISTANCE ALUMINUM ALLOYS EXPOSED IN A SALT-DICHROMATE-ACETATE SOLUTION

FIG 9
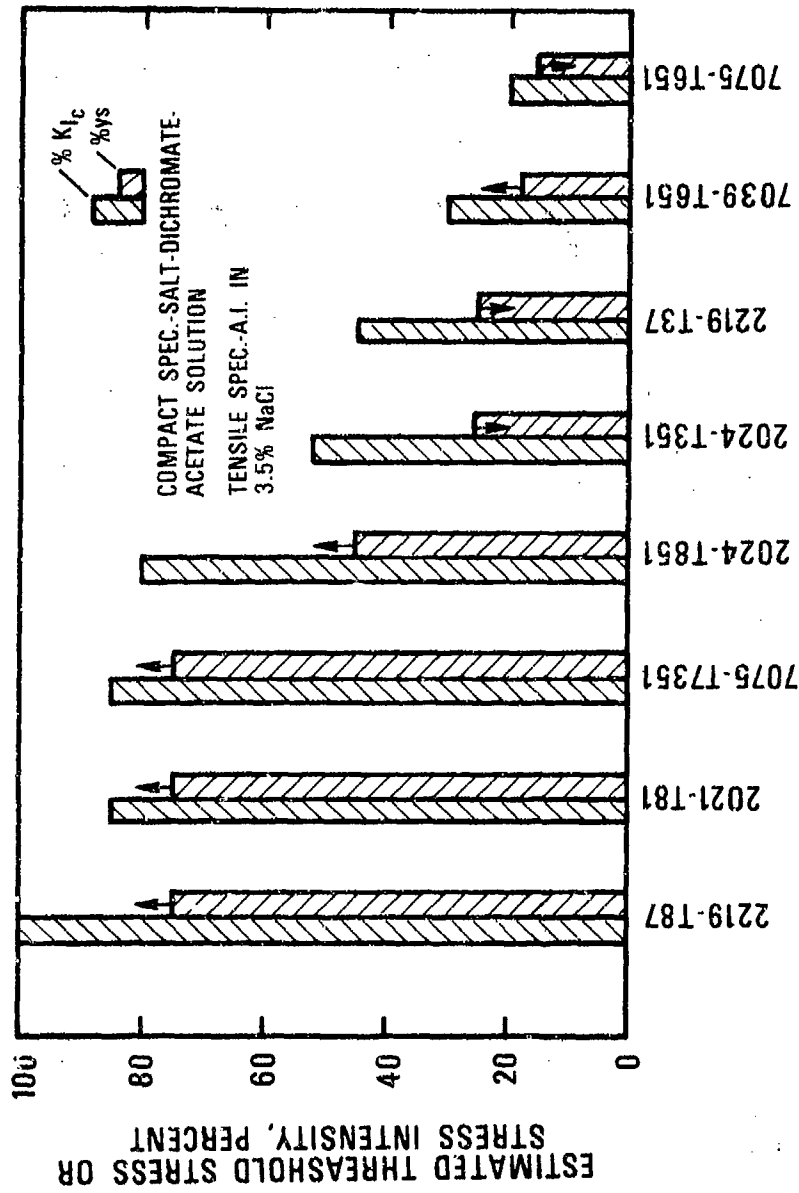
COMPARISON OF SCC RANKINGS OF SOME ALUMINUM ALLOYS
DETERMINED WITH RING LOADED COMPACT SPECIMENS AND
SMOOTH TENSILE SPECIMENS

FIG. 10

FLAW DEPTH, in.
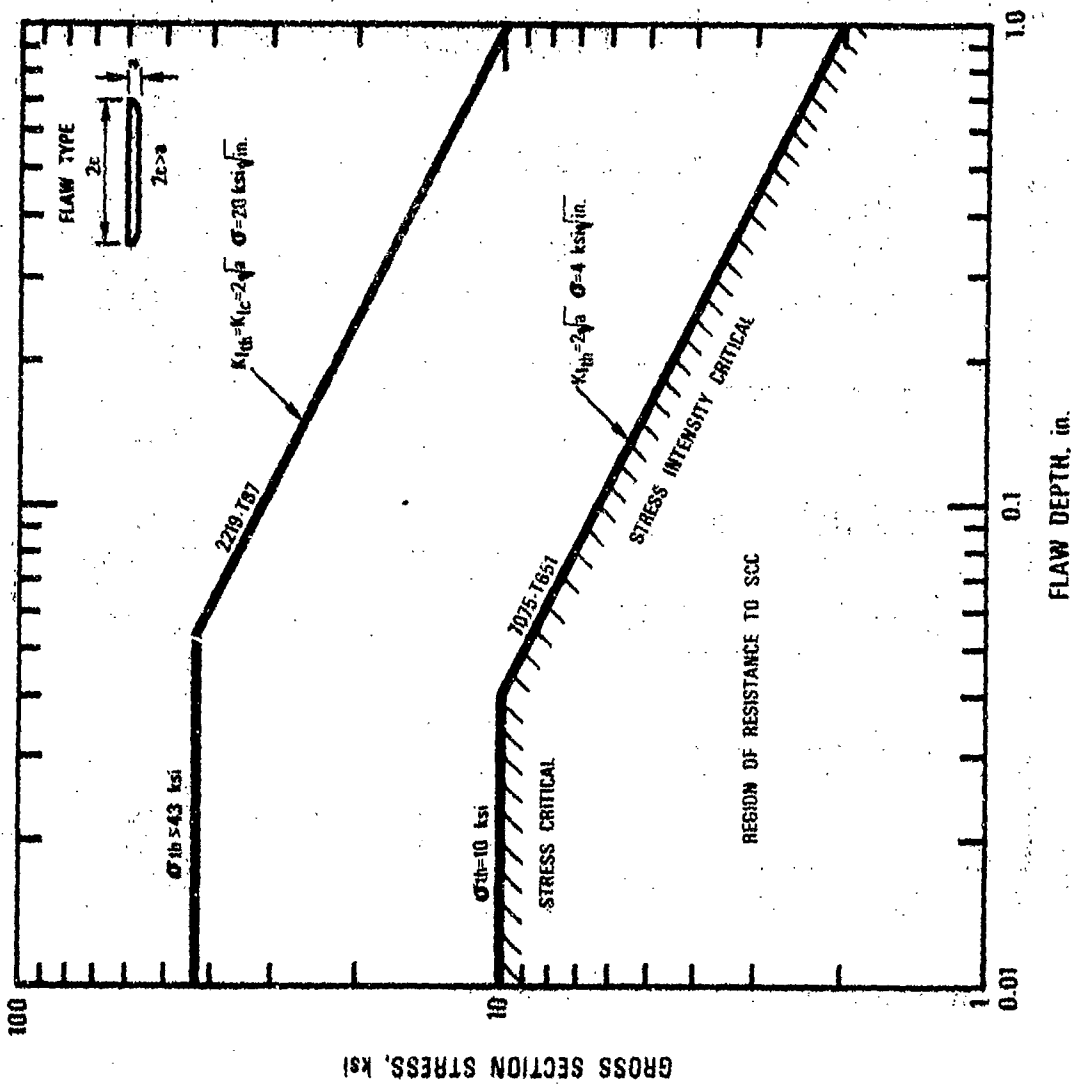
COMPOSITE STRESS-STRESS INTENSITY SCC THRESHOLD
CHARACTERIZATION FOR TWO ALUMINUM ALLOYS EXPOSED
IN A SALT-DICHROMATE-ACETATE SOLUTION

FIG. 11

ELECTROCHEMICAL TESTING OF GALVANIC CORROSION

by
Florian Mansfeld and J. V. Kenkel

Science Center, Rockwell International
Thousand Oaks, California 91360

ABSTRACT

In a systematic study of galvanic corrosion of Al alloys the effects of the dissimilar metal, the solution composition and area ratio have been studied using galvanic current and weight loss measurements. In 3.5% NaCl, galvanic corrosion rates of the Al alloys 1100, 2024, 2219, 6061 and 7075 decrease with the nature of the dissimilar metal in the order Ag>Cu>4130 steel $\gg$ stainless steel$\approx$ Ni> Inconel 718> Ti-6Al-4V $\approx$ Haynes 188>Sn>Cd. Coupling to zinc did not lead to cathodic protection of the Al alloys as shown by weight loss data although the Al alloys were the cathode in the Al/Cu couple. The potential difference of uncoupled dissimilar metals has been found to be a poor indicator of galvanic corrosion rates. Dissolution rates of Al alloys coupled to a given dissimilar material are higher in 3.5% NaCl than in tapwater and distilled water where they are found to be comparable. The effect of area ratio $\frac{A^C}{A^A}$ has been studied in 3.5% NaCl for area ratios of 0.1, 1.0 or 10. The galvanic current was found to be independent of the area of the anode, but directly proportional to the area of the cathode. The galvanic current density i_g^A with respect to the anode has been found to be directly proportional to the area ratio $(i_g^A = k_1 \frac{A^C}{A^A})$, while the dissolution rate r_A of the anode was related to area ratio by $r_A = k_2 (1 + \frac{A^C}{A^A})$. The results obtained have been explained based

on mixed potential theory. It is shown that both the relative and the absolute increase of the dissolution rate of the anode due to coupling can be claculated from the same electrochemical measurement, thus eliminating the need for weight loss data.

INTRODUCTION

Accelerated corrosion of dissimilar metals which are electrically coupled and exposed to a corrosive environment is one of the most common and most severe forms of corrosion. Although the danger of galvanic corrosion has been recognized generally, very little work has been done to quantitatively measure the extent of corrosion of various galvanic couples and use such measurements as a basis for a ranking of galvanic couples. Usually uncoupled metals and alloys, instead of actual galvanic couples, are ranked in a galvanic series according to their corrosion potentials in a given environment; e.g., seawater (1). While this type of classification of metals and alloys might be quite useful as an indication of general trends in galvanic corrosion, it cannot give an indication of the actual extent of galvanic corrosion when dissimilar metals are coupled. As pointed out recently (2,3), the magnitude of galvanic corrosion depends not only on the potential difference of dissimilar metals, but also on kinetic parameters such as corrosion rates or exchange current densities of the uncoupled materials and Tafel slopes, and on area ratios.

In light of the rather complicated interaction of reduction and oxidation reactions on coupled metals, it is important to measure directly the extent of galvanic corrosion of those materials which may come in electrical contact in various structures rather than rely on measurements of only one of the parameters involved; e.g., potential differences. Various methods for measurements of galvanic current have been discussed recently (12). The authors have been using the zero impedance ammeter described by Lauer and Mansfeld (4) and have developed an electrochemical test which has been used to evaluate inorganic conversion coatings on Al alloys (5) and to study the effect of metallic coatings on PH13-8Mo on galvanic corrosion of Al alloys in NaCl (6).

This paper summarizes results of a systematic investigation of galvanic corrosion in which the galvanic interaction of 20 metals and alloys have been measured in order to establish a galvanic series based on quantitative measurements of dissolution rates of the metals in a galvanic couple. Results for the 95 galvanic couples in which an Al alloy is one of the two dissimilar metals are summarized here for immersion in air-saturated 3.5% NaCl (7). Also included are results of galvanic corrosion tests in tapwater and distilled water for some selected couples (8), and of studies of the effect of area ratio (9).

EXPERIMENTAL

Materials and Test Methods

Table I lists the materials studied. The test specimens were flat coupons (1" x 3" x variable thickness). They were degreased for 5 min. in boiling benzene, cleaned by conventional chemical methods, if necessary, and weighed to 0.1 mg. The test specimens to be coupled were then placed into a lucite holder with a 1/2" x 1/2" x 1/8" lucite spacer between the specimens as described earlier (ref. 5,6). About 20 cm^2 of each specimen were exposed to the electrolyte.* After assembly, the holder containing the specimens was placed in a solution of air-saturated 3.5% NaCl and the corrosion potential of the two uncoupled materials followed for 15 min. immediately after immersion (all potentials refer to the saturated calomel electrode (SCE)). The specimens were then connected to the zero impedance ammeter (4) (Fig. 1). The output of this instrument, which is proportional to the galvanic current I_g, was connected to a two-pen strip-chart recorder. The potential ϕ_g of the couple was also recorded continuously for 24 hours. From plots of galvanic current I_g vs time t,

---

*In studies of the effect of area ratio, this holder was not used.

the average galvanic current density (c.d.) $\bar{i}_g = I_g/A$, where A is the area of the Al alloy tested, was calculated by graphical integration.

Table I. List of Materials Studied

Ag (99.9%)	SS304L	Ti-6Al-4V
Cu (OFHC)	SS347	Al 1100-0
Ni 270	PH13-8Mo	Al 2024-T851
Sn (99.9999%)	A286	Al2219-T87
Cd (99.98%)	4130 Steel	Al 6061-T651
Zn (99.9%)	Haynes 188	Al 7075-T76
SS301	Inconel 718	

After the 24-hour test, the Al alloys were deoxidized using a commercial cleaner (AMCHEM), washed, dried, and weighed again. The weight loss caused by the deoxidizing treatment was also measured using separate uncorroded Al specimens, and this correction was applied to the weight loss of the corroded specimen. If necessary, the other materials were freed of corrosion products using standard techniques (NACE Standard TM-01-69). The corrected weight loss, the duration of the test and the specimen area were used to calculate the dissolution rate r of the test specimen in mdd (mg/dm^2 day). Further details concerning the experimental procedure can be found in Ref. (5-10).

RESULTS

I. The Effect of the Dissimilar Metal (Ref. 7)

A. Corrosion Parameters of Uncoupled Al Alloys

All galvanic couples studied include one Al alloy. In order to relate galvanic couple data to corrosion parameters of Al alloys,

the corrosion rates of uncoupled Al alloys were determined in 24-hour immersion tests. Table II shows corrosion potentials ϕ_{corr} (average of 19 tests, 15 min. exposure) and corrosion rates r_o (average of 3 tests, 24 hours).

Table II.   Corrosion Potentials and Corrosion Rates of Uncoupled Al Alloys 3.5% NaCl, 22 + 1°C

Al Alloy	ϕ_{corr} (mV vs SCE)	r_o (mdd)
1100-0	-756 ± 39	0.24
2024-T851	-733 ± 4	5.25
2219-T87	-724 ± 6	4.62
6061-T651	-756 ± 28	0.56
7075-T76	-814 ± 18	0.95

B. Galvanic Current Data

Typical galvanic current data are shown in Fig. 2 and 3. Fig. 2 shows that the galvanic current I_g is appreciably higher when Al 7075 is coupled to Cu than when it is coupled to stainless steel type 304 or Ti-6Al-4V. When coupled to Zn, the galvanic current is negative with respect to Al, because Zn was the anode in the galvanic couple. After an initial period of 2 hours, the galvanic current stayed more or less constant except for the couple involving Cd, where the current increased constantly.

Despite the appreciable initial potential differences between the Al alloy and Cu, SS304 or Ti-6-4, respectively, the galvanic potentials of the corresponding couples with Al 7075 have similar values which are only slightly more noble than the corrosion potential of the uncoupled Al alloy (Ref. 7). This is probably due to the fact that the pitting

potential is also only slightly more noble than the corrosion potential of the Al alloys and the fact that the Al alloys cannot be polarized more noble than to the pitting potential.

Fig. 3 shows that similar results are obtained when the five Al alloys are coupled to the same, more noble material, 4130 steel. A comparison of the curves in Fig. 3.with those in Fig. 2 shows that coupling of Al alloys to Cu leads to higher galvanic currents than coupling to 4130 steel which, in turn, produces higher galvanic currents than the stainless steel and the Ti alloy.

Based on the galvanic current I_g- time t traces the galvanic current density $\bar{i}_g$ with respect to the Al alloy in a galvanic couple has been calculated. Tables have been prepared (7) for each of the Al alloys studied in which the galvanic couples have been ranked according to the value of $\tilde{i}_g$. Table III is an example for such a galvanic series; in this case Al 6061 has been coupled to 19 dissimilar metals and alloys. Also listed in Table III are the corrosion potential differences $\Delta\phi^S$ of the two uncoupled metals before the start of the galvanic current test and the dissolution rates r_A based on weight loss data (see below). The overall ranking in the last column of Table III is obtained by a ranking of all 95 couples studied (for details see Ref. 7).

C. Weight Loss Data

The dissolution rate r_A of the Al alloy in the galvanic couples as calculated from weight loss data has also been listed in Table III.

Only very small weight changes were recorded for Ag, Cu, Ni, the stainless steels, Ti-6Al-4V, Haynes 188 and Inconel 718. The 4130 steel was covered with rust after galvanic tests; after removal of corrosion product, weight gains or weight losses were found (-7 to

TABLE III. Galvanic Series for Al6061-T651 in 3.5% NaCl, r_0 = 0.56 mdd

#	Coupled To	$\bar{i}_g$ ($\mu A/cm^2$)	r_A (mdd)	$\Delta\phi^s$ (mV)	Overall No.
1	Ag	54.5	65.6	-721	2
2	Cu	43.6	47.7	-507	7
3	4130	24.3	27.0	-205	14
4	Ni	21.9	29.7	-481	16
5	PH13-8Mo	16.0	19.8	-664	25
6	A286	14.7	18.7	-704	27
7	SS347	14.1	21.2	-653	28
8	SS301	12.4	17.3	-672	36
9	SS034L	11.3	16.1	-679	42
10	Inco 718	8.1	7.0	-556	53
11	Ti-6-4	5.2	8.3	-510	59
12	Haynes 188	5.0	7.7	-543	60
13	Al2219	3.1	-0.5[†]	- 99	66
14	Al2024	1.95	$\underline{+0}$	- 6	71
15	Sn	1.59	5.9	-183	72
16	Al1100	0.66	3.7	- 68	75
17	Cd	0.28	4.0	- 95	77
18	Al7075	-0.66	-1.4[†]	+ 36	81
19	Zn	-1.51	6.6	+298	85

[†]Negative values of r_A correspond to weight gain.

+8 mdd). The dissolution rates for Zn ranged between 0 and 5 mdd, those for Cd between 5 and 22 mdd and those for Zn between 90 and 175 mdd depending on the type of Al alloy these materials had been coupled to.

D. Correlation Between Galvanic Current and Weight Loss Data

In the study reported here, galvanic current and weight loss data have been collected for all galvanic couples in order to find a correlation between the electrochemical measurements and the dissolution rate of the anode in a galvanic couple. As discussed in more detail earlier (2,3) the measured galvanic current I_g for the case of diffusion control of the cathodic reaction is equal to the cathodic current I_c^C at the cathode and the difference between the anodic metal dissolution current I_a^A and the cathodic reduction current I_c^A at the anode at the potential ϕ_g of the galvanic couple:

$$I_g = I_c^C (\phi_g) = I_a^A (\phi_g) - I_c^A (\phi_g) \tag{1}$$

Equation 1 can be written in terms of current densities (c.d.) and areas A^A and A^C of anode and cathode, respectively:

$$i_g^A \ A^A = i_c^C \ A^C = i_a^A \ A^A - i_c^A \ A^A \tag{2}$$

Considering that due to diffusion control:

$$i_c^A = i_c^C = i_{o_2}^L , \tag{3}$$

where $i_{o_2}^L$ is the limiting diffusion c.d. for oxygen reduction, Eq. 2 can be written as:

$$i_g^A = i_a^A - i_{o_2}^L . \tag{4}$$

Since also due to diffusion control:

$$i_{O_2}^L = i_{corr}^A \qquad\qquad (5)$$

where i_{corr}^A is the corrosion c.d. of the uncoupled anode, Eq. 4 can be rewritten as:

$$i_g^A = i_a^A - i_{corr}^A \qquad\qquad (6)$$

Equation 6 shows that the measured value of the galvanic c.d. i_g^A is equal to the difference between the dissolution rates of the anode when coupled (i_a^A) and uncoupled (i_{corr}^A). Galvanic current measurements, therefore, can be used to calculate the increase of dissolution rates due to coupling. Equation 6 can be converted to dissolution rates r of the anode using Faraday's law:

$$i_g^A = k (r_A - r_o) \qquad\qquad (7)$$

Figure 4 shows a plot of the average galvanic c.d. $\overline{i}_g$ with respect to the Al alloy against the difference of dissolution rates $r_A - r_o$ for coupled (r_A) and uncoupled (r_o) Al alloys determined from weight loss data for the 95 galvanic couples studied in 3.5% NaCl (7). Each data point represents a different galvanic couple. The solid line represents Faraday's law for pure Al ($1\mu A/cm^2 \simeq 0.81$ mdd). Most data points fall on a straight line which has a lower slope ($1\mu A/cm^2 \approx 1.2$ mdd). The reason for this systematic deviation might be seen in the fact that Al alloys containing Cu, Zn and other elements were tested. A correction for Al-Cu or Al-Zn alloys would move the theoretical line in the direction observed experimentally. Since five different Al alloys have been tested, no attempts for such a correction have been made.

Since a very good correlation between electrochemical measurements (i_g^A) and weight loss data ($r_A - r_o$) has been observed, it is not necessary to determine weight loss data, which eliminates the problem of removal of corrosion products, etc. The electrochemical data have also the advantage that they provide "instantaneous" corrosion rate data and allow to follow the corrosion process as a function of time which usually is not possible with weight loss data. Any changes in corrosion behavior will be immediately recognized in corresponding changes of the galvanic current.

II. The Effect of Area Ratio (Ref. 9)

All measurements during the study of the effect of the nature of the dissimilar metals (7) have been made for an area ratio $A^C/A^A = 1$. It will be shown, however, in the following that dissolution rates of the anode in a galvanic couple can be calculated for any value of A^C/A^A if they have been measured for one area ratio; e.g. of one.

A general discussion of area relationship in galvanic corrosion has been presented elsewhere (2,9). The relationship between the galvanic c.d. i_g^A and the area ratio A^C/A^A can be found from Eq. 2 considering Eq. 3 and Eq. 5 as:

$$i_g^A = i_{o_2}^L \frac{A^C}{A^A} = i_{corr}^A \frac{A^C}{A^A} = k_1 \frac{A^C}{A^A} . \tag{8}$$

According Eq. 8, the galvanic c.d. i_g^A is directly proportional to the area ratio A^C/A^A. The dissolution c.d. i_a^A of the anode can be calculated by combining Eq. 4 and Eq. 8 to give:

$$i_a^A = i_{o_2}^L (1 + A^C/A^A) = k_1 (1 + \frac{A^C}{A^A}) \tag{9}$$

Equation 9 is the so-called "catchment principle" according to which the dissolution rate of the anode in a galvanic couple is proportional to the area ratio. For large area ratios it follows from Eq. 9 using Faraday's law:

$$r_A = k_2 \frac{A^C}{A^A} \tag{10}$$

The constants k_1 and k_2 are characteristic for a given metal/electrolyte system.

In order to test the relationships in Eq. 8 and 9, the Al alloys 2024-T851 and 7075-T76 were coupled to Cu, stainless steel 304L, 4130 steel, Ti-6Al-4V, Cd or Zn in air-saturated 3.5% NaCl at 22 ± 1°C. Flat test specimens were prepared so that an area of about 2 or 20 cm^2 was exposed to the electrolyte. Area ratios used were approximately 0.1, 1.0, or 10. Weight loss data for the materials in a given couple were used to calculate dissolution rates of anode and cathode as a function of area ratio. Figure 5 shows a plot of the galvanic c.d. i_g^A with respect to the Al alloys as a function of area ratio for Al 2024/Cu. The galvanic c.d. i_g^A increases by about a factor of 10 when the area ratio A^{Cu}/A^{Al} is increased by a factor of 10 as predicted in Eq. 8. It is important to note that in order to evaluate the effect of area ratio galvanic current densities rather than currents have to be considered (9) since according to Eq. 1, the galvanic current is proportional to the area of the cathode, but independent of the area of the anode.

$$I_g = I_c^C = i_c^C A^C = i_{0_2}^L A^C = k_1 A^C, \tag{11}$$

and therefore not a measure of area ratio effects.

A plot of log i_g^{Al} vs log A^C/A^A according to Eq. 8 results in a straight line with a slope of one for both Al 2024 and Al 7075 (Fig. 6).

The data for Al 2024/Cd, Al 2024/Zn, and Al 7075/Zn have been omitted from Fig. 6 since in these couples the Al alloys were the cathodes. The different values of i_g^{Al} at a constant value of A^C/A^A are assumed to result from the fact that contrary to the normal assumption, that the limiting diffusion c.d. $i_{0_2}^L$ is independent of cathode material (Eq. 3), experimental values of $i_{0_2}^L$ are found to be dependent on the nature of the cathode. Mansfeld and Parry (5) have shown, based on potentiostatic polarization curves, that in 3.5% NaCl $i_{0_2}^L$ is larger for SS304 than for Ti-6Al-4V. The decrease of the galvanic c.d. i_g^A at a given area ratio in the order Cu>4130>SS304L>Ti-6Al-4V>Cd is then related to a corresponding decrease of $i_{0_2}^L$. Based on experimental evidence, Eq. 3 is not exactly fulfilled and Eq. 8 has to be rewritten as:

$$i_g^A = i_{0_2}^{L,C} \frac{A^C}{A^A} \tag{8a}$$

where $i_{0_2}^{L,C}$ is the material-dependent limiting c.d. for oxygen diffusion.

The dissolution rates calculated from the weight loss data for the Al alloys in galvanic couples have been plotted vs $1 + A^C/A^A$ in log-log plots in Fig 7 for Al 7075. The approximately straight line relationship with a slope of one confirms Eq. 9 since the dissolution c.d. i_a^A is related to the dissolution rate r_A by Faraday's law. The dependence of dissolution rates on cathode material at a constant area ratio has to be explained as above. For material-dependent cathodic c.d. $i_{0_2}^{L,C}$, the catchment principle has to be expressed as:

$$i_a^A = i_{0_2}^{L,A} + i_{0_2}^{L,C} \frac{A^C}{A^A} \tag{9a}$$

Based on these relationships which are confirmed by the experimental result presented here, the dissolution rate of an anode in a galvanic couple can be calculated for any area ratio if it has been measured for one area ratio; e.g., of one.

255

III. The Effect of Corrosive Environment (Ref. 8)

Having studied the effect of the dissimilar metal, it seemed also
of interest to investigate the effect of the corrosive environment (8).
From the many possible electrolytes, tapwater and distilled water were
chosen due to the obvious practical applications involving galvanic
couples. Distilled water was of additional interest since only dissolved
oxygen and the water molecule can-at least initially-react on the surface
of the dissimilar metals forming the galvanic couple. The very low
conductivity of distilled water did not lead to experimental problems;
due to the characteristics of the zero impedance ammeter (4) used,
the potential difference of coupled dissimilar metals was less than 0.1 mV,
even in distilled water. From the many experiments conducted and reported
elsewhere (8,10), Fig. 8a shows a comparison of galvanic current data in
3.5% NaCl, tapwater, and distilled water for Al2024/ 130 steel. It is
interesting to note that the steel is the anode in distilled water
and tapwater, while the Al alloy is the anode in 3.5% NaCl. Weight loss
data showed (10) that the steel was cathodically protected in NaCl, but
showed increased corrosion rate due to coupling to the Al alloy in the
other media. For the Al 2024/Cu couple, no reversals of the sign of the
galvanic current were observed (Fig. 8b). The average galvanic c.d. $\bar{i}_g$
is much higher in 3.5% NaCl than in tapwater and distilled water. In
the latter two solutions, the average galvanic c.d. values of $\bar{i}_g$ are
comparable. Note the different time behavior of the galvanic current
in tapwater and distilled water.

The average galvanic c.d. $\bar{i}_g$ with respect to the Al alloy as determined
from graphical integration of the $\bar{i}_g$-time curves and the initial potential
difference $\Delta\phi^s$ between the two dissimilar metals before coupling have been

256.

listed in tables for the five Al alloys tested in tapwater and distilled water in Ref. 8.

In assessing galvanic corrosion behavior of a given Al alloy as a function of environment, one has to consider the effect of the dissimilar metal: the dissolution rate of Al 6061 has been found, for example, to be higher in tapwater with Cu as cathode than in 3.5% NaCl with SS304 L or Ti-6Al-4V as cathode (8).

The main difference between the effect of NaCl, tapwater, and distilled water on galvanic corrosion of Al alloys seems to be the fact that due to the high chloride content in 3.5% NaCl the pitting potential of Al alloys is only slightly more noble than the corrosion potential. Potentiostatic polarization studies with IR-drop compensation in tapwater (11) have shown that the pitting potential in tapwater is much more noble than in 3.5% NaCl while in distilled water pitting does not occur. The Al alloys, can therefore, not be polarized more noble than their pitting potential in 3.5% NaCl and consequently dissolve with high rates due to pitting. In tapwater and distilled water polarization to more noble potentials is possible, and changes in polarity of the dissimilar metals in a galvanic couple are also possible as seen for Al alloy/4130 steel couples (8).

DISCUSSION

I. The Effect of Potential Difference Between Dissimilar Metals

It is often assumed that the rate of galvanic corrosion can be judged based on the difference of the corrosion potential of uncoupled dissimilar metals. For a diffusion controlled cathodic process the dissolution rate of the anode in a galvanic couple should, however, be independent of the nature of the cathode and, therefore, also independent of the potential difference between anode and cathode. As pointed out above, the diffusion c.d. $i_{O_2}^L$ has been found to be material dependent to some extent, most likely due to the formation of surface films which

257

change the ratio D/δ of diffusion coefficient D for oxygen and diffusion layer thickness δ. Due to this fact, a material dependence of the rate of galvanic corrosion could be experimentally observed, which in turn could be interpreted incorrectly as being due to the difference of corrosion potentials $\Delta\phi^S$ of the uncoupled dissimilar metals. In order to evaluate the possible effect of potential difference of uncoupled dissimilar metals on the dissolution rate of the coupled materials, the experimental galvanic current data obtained in 3.5% NaCl for 95 galvanic couples involving Al alloys have been plotted as a function of potential difference $\Delta\phi^S = \phi^{Al}_{corr} - \phi^C_{corr}$. According to Eq. 7, the galvanic c.d. i^A_g represents the absolute increase of the dissolution rate of the anode due to coupling. On the other hand, the relative increase of dissolution rates can be calculated using the same galvanic c.d. i^A_g value as:

$$\frac{r_A - r_0}{r_0} = \frac{i^A_g}{i^A_{corr}} \tag{12}$$

The experimental data of Part I of this study (7) have been plotted in Fig. 9 as i^A_g vs. $\Delta\phi^S = \phi^{Al}_{corr} - \phi^C_{corr}$ for the 95 galvanic couples studied in 3.5% NaCl. In Fig. 10 the relative increase of dissolution rates $\frac{r_A - r_0}{r_0}$ due to coupling has been plotted vs. $\Delta\phi^S$ using weight loss data.

Fig. 9, which represents the absolute increase of dissolution rates $r_A - r_0$ due to coupling and Fig. 10 which represents the relative increase of dissolution rates $\frac{r_A - r_0}{r_0}$ with respect to the corrosion rate of the uncoupled Al alloy, show that the initial potential difference $\Delta\phi^S$ of uncoupled metals cannot be used as a reliable indicator of the extent of galvanic corrosion. While one can distinguish two groups of data in Fig. 9 which show a general increase of the galvanic c.d. with increasing potential difference $\Delta\phi^S$, a measurement of $\Delta\phi^S$ alone cannot give information

258

about the rate of galvanic corrosion to be expected for a given galvanic couple. Figure 10 shows that for $\Delta\phi^S$ values between -600 and -700 mV the relative increase of dissolution rates can be between 3 and 5 for Al 2219 and 2024, but between 60 and 230 for Al 1100. One can also find a relative increase of about 46 at $\Delta\phi^S$ = -200 mV and a relative increase of dissolution rates of only 10 at $\Delta\phi^S$ = -550 mV for Al 6061. Galvanic series based on corrosion potentials of uncoupled materials have, therefore, to be considered as only very qualitative guidelines.

The effect of the dissimilar metals is shown clearly if galvanic current data, which represent the absolute increase of the dissolution rate of the Al alloy over the corrosion rate of the uncoupled alloy, are considered. The large effect of Ag, Cu and 4130 steel can be recognized in Fig. 9, where the five Al alloys studied appear in clusters at $\Delta\phi^S$ = -630 to -720 mV (Ag), at $\Delta\phi^S$ = -500 to -570 mV (Cu) and $\Delta\phi^S$ = -90 to -340 mV (steel 4130). A second group of galvanic couples ranges from couples involving zinc and Al alloys of different composition, where galvanic currents are negative with respect to the Al alloys, to couples involving the stainless steels and Ni ($\Delta\phi^S$ = -600 to -800 mV). Couples involving Ti-6Al-4V, Haynes 188, Inconel 718, tin, and cadmium fall between these two extremes.

II. Ranking of Galvanic Couples

The results obtained have shown that reliable classification of galvanic couples can only be achieved if kinetic data such as galvanic current measurements are collected for the couples of interest. The galvanic couples can then be ranked according to the absolute increase of dissolution rates ($\bar{i}_g^A$) (see Ref. 7) or the relative increase of dissolution rates ($r_A - r_o/r_o = \bar{i}_g/i_{corr}^A$). The continuous monitoring of galvanic currents has the advantage over weight loss data that dissolution rates

can be followed as a function of time with great accuracy (fractions of μA to many mA can be accurately measured). Problems of removal of corrosion products before re-weighing after the test are avoided.

III. General Classification

If the general compatibility of an Al alloy with other materials is of interest, then the relative increases of dissolution rates should be considered. In Table IV compatibility of the five Al alloys with the 15 other materials is indicated by placing the dissimilar materials in 3 classes according to relative increases of dissolution rates $r_A - r_o/r_o$ $= \bar{i}_g^A / i_{corr}^A$ below 5 (Class I), between 5 and 15 (Class II), and above 15 (Class III).

Table IV shows that under this classification Al 1100 is compatible only with Cd, Al 6061 only with the Al alloys 7075, 2219, and 2024, while Al 7075 is compatible only with zinc and the other Al alloys tested. The Al alloys 2024 and 2219 are compatible with most materials tested, borderline cases involve 4130 steel, Cu and Ag (and Ni and Zn for Al 2219); no combinations have been found to be incompatible based on the present criteria. These criteria have been arbitrarily selected and might have to be modified for special applications.

TABLE IV.   Compatibility of Al Alloys and Dissimilar Materials

Class	Al 1100	Al 2024	Al 2219	Al 6061	Al 7075
I	Cd	Cd,7075,1100 Sn, Haynes, 2219, Ti-6-4, 6061, Zn, Inco 718, PH13-8Mo SS347,A286, SS304,Ni,SS301	Cd,2024,6061 1100, Haynes 7075,Zn,PH13-8Mo,SS301, SS304,A286, Inco 718,Ti-6-4,SS347	7075,2219 2024	1100,6061, 2024, Zn, 2219
II	2024,6061	4130,Cu,Ag	Ni,Zn,4130, Cu,Ag	1100,Cd,Sn Inco 718, Zn,Haynes, Ti-6-4	Cd,Haynes, Sn,Ti-6-4, Inco 718
III	Sn, 7075, Haynes,Ti-6-4,Zn, Inco 718, A286, SS304, PH13-8Mo, SS301, 4130,Cu,Ag			SS304,SS301, A286,PH13-8Mo,SS347, 4130,Ni,Cu, Ag	SS304,SS347, SS347,PH13-8Mo,SS301, A286,Ni, 4130,Cu,Ag

FIGURE CAPTIONS

1. Zero impedance ammeter (4)

2. Time behavior of galvanic current I_g for Al 7075 coupled to Cu, stainless steel 304L, Ti-6Al-4V, Cu or Zn.

3. Time behavior of galvanic current I_g for Al alloys coupled to 4130 steel.

4. Correlation between the average galvanic c.d. $\bar{i}_g$ and the increase of dissolution rates $r_A - r_o$ due to coupling.

5. Galvanic c.d. i_g^{Al} for Al 2024/Cu in 3.5% NaCl as a function of area ratio.

6. Dependence of galvanic c.d. i_g^{Al} on area ratio A^C/A^A for Al 7075 in 3.5% NaCl.

7. Dependence of dissolution rates r_A on area ratio A^C/A^A for Al 7075 in 3.5% NaCl.

8. Galvanic current data in 3.5% NaCl, tapwater, and distilled water.

   a. Al 2024/4130 steel

   b. Al 2024/Cu

9. Average galvanic c.d. $\bar{i}_g$ as a function of difference $\Delta\phi^S$ of corrosion potentials of uncoupled materials.

10. Relative increase $r_A - r_o/r_o$ of dissolution rates of Al alloys (weight loss data) as a function of $\Delta\phi^S$.

262

References

1. F. L. LaQue, Proc. ASTM 51, 495 (1951).

2. F. Mansfeld, Corrosion 27, 436 (1971).

3. F. Mansfeld, Corrosion 29, 403 (1973).

4. G. Lauer and F. Mansfeld, Corrosion 26, 504 (1970).

5. F. Mansfeld and E. P. Parry, Corrosion Science 13, 605 (1973).

6. F. Mansfeld, Corrosion, 29, 276 (1973).

7. F. Mansfeld, D. H. Hengstenberg, and J. V. Kenkel, "Galvanic Corrosion of Al Alloys. I. Effect of Dissimilar Metals," Corrosion (in press).

8. F. Mansfeld and J. V. Kenkel, "Galvanic Corrosion of Al Alloys. II. Effect of Corrosive Environment," Corrosion Science (in press).

9. F. Mansfeld and J. V. Kenkel, "Galvanic Corrosion of Al Alloys. III. Effect of Area Ratio," Corrosion Science (in press).

10. F. Mansfeld and J. V. Kenkel, "Laboratory Studies of Galvanic Corrosion. I. Two-Metal Couples," submitted to Corrosion.

11. F. Mansfeld, R. L. Myers, and G. Lauer, Technical Report, Science Center, Rockwell International, 1973.

12. F. Mansfeld and J. V. Kenkel, "Laboratory Studies of Galvanic Corrosion of Al Alloys," ASM Congress, 1974.
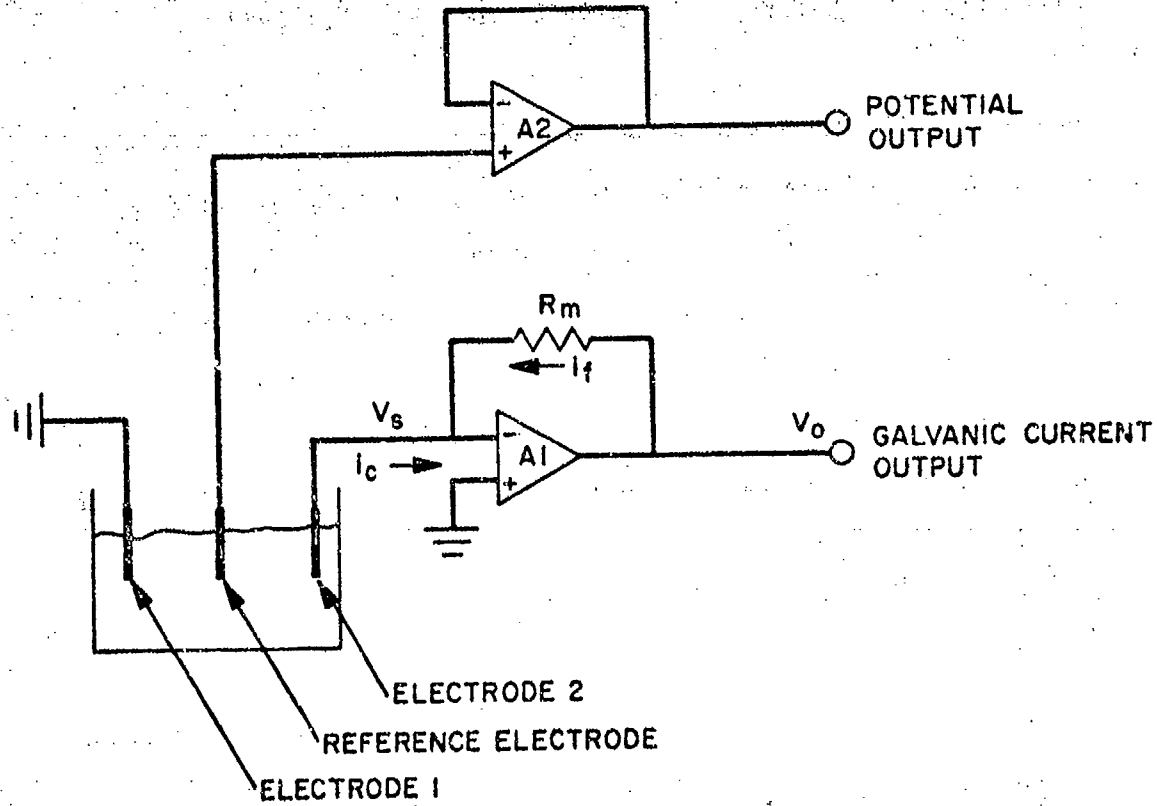
Figure 1
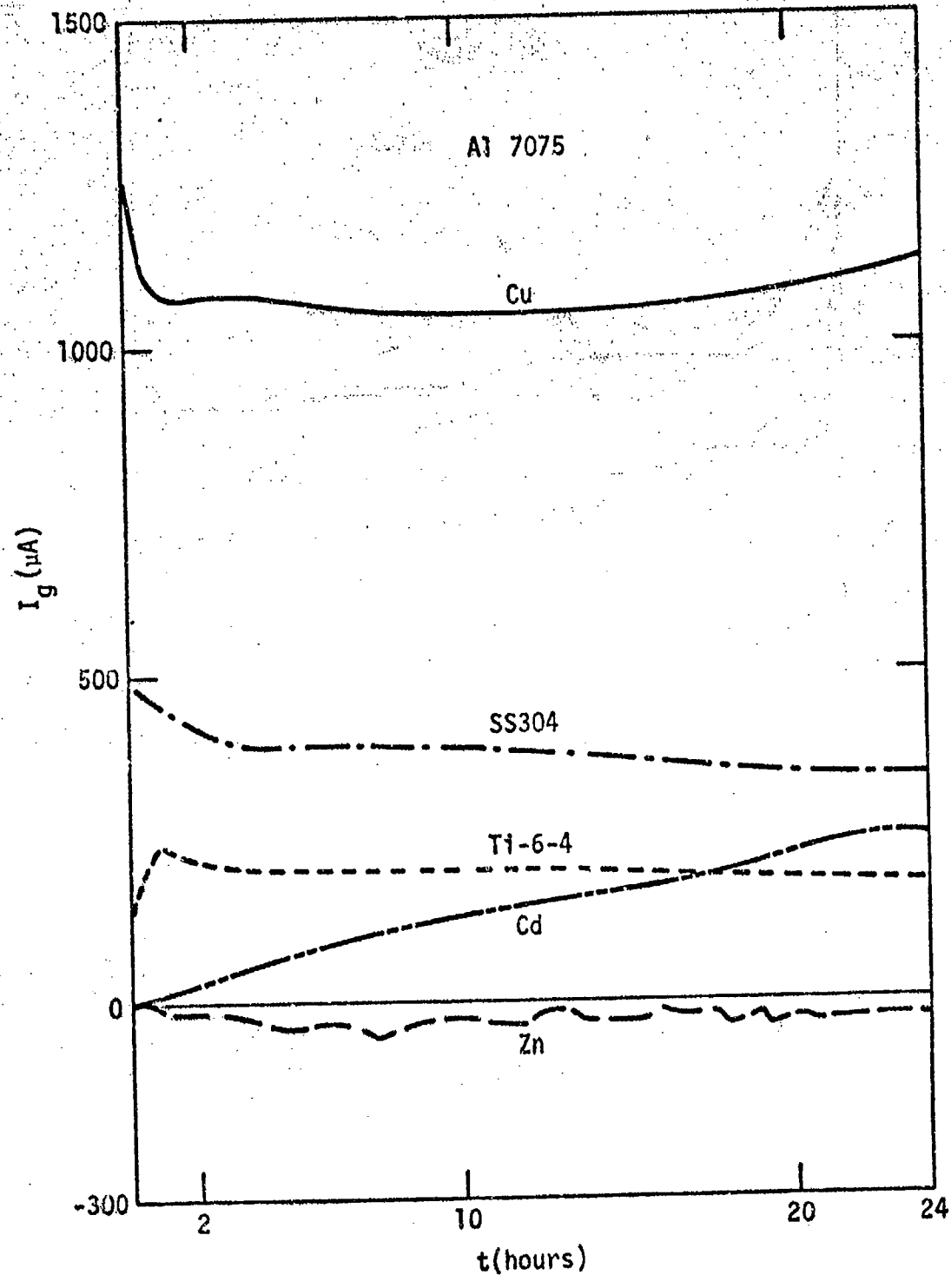
Figure 2
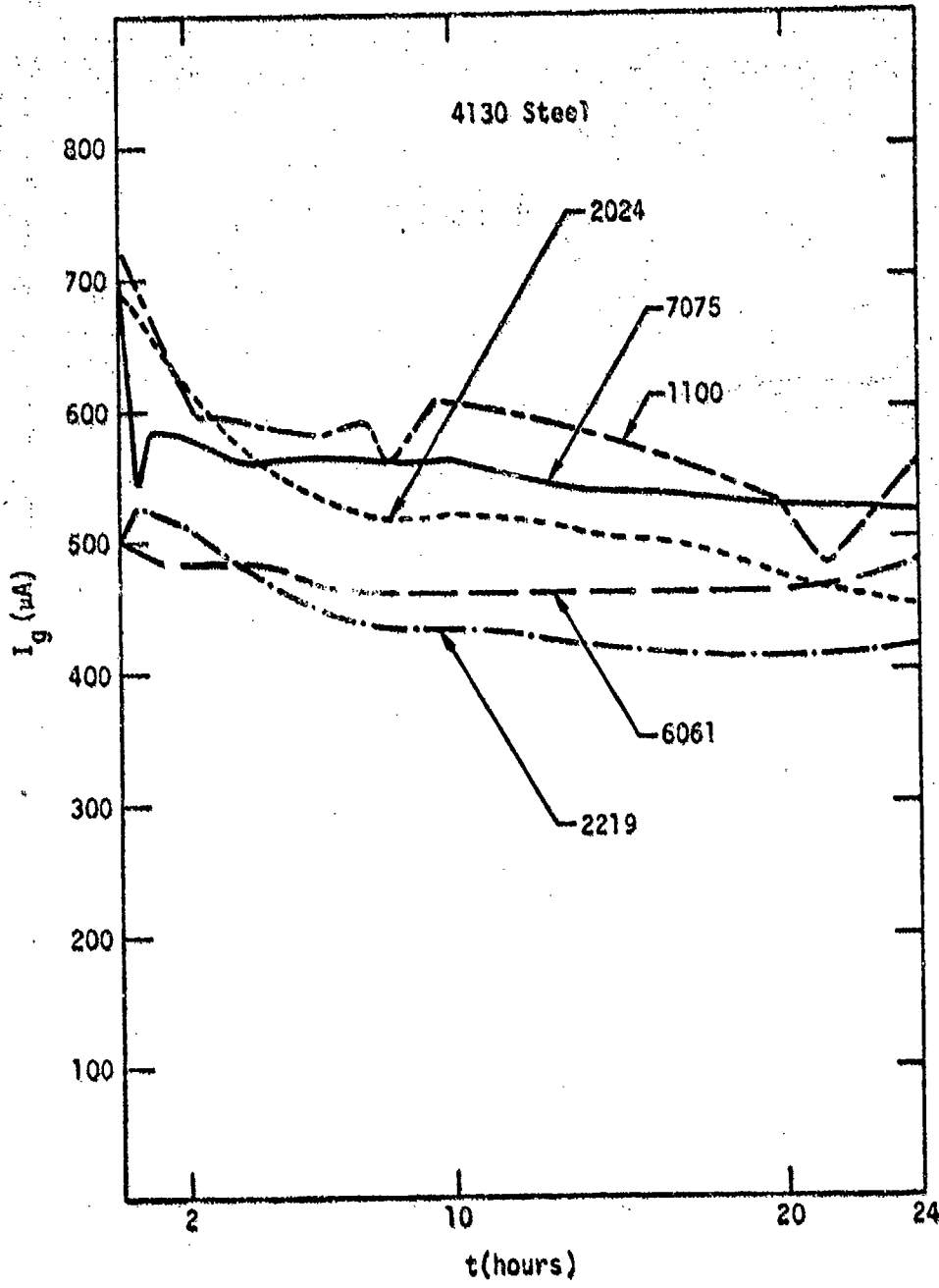
Figure 3

Figure 4

Figure 5

Al 2024 / 3.5% NaCl

i_g Al $(\mu A/cm^2)$

$\frac{A_C}{A_A}$

Figure 6

269

Figure 7

A1 2024/4130 Steel
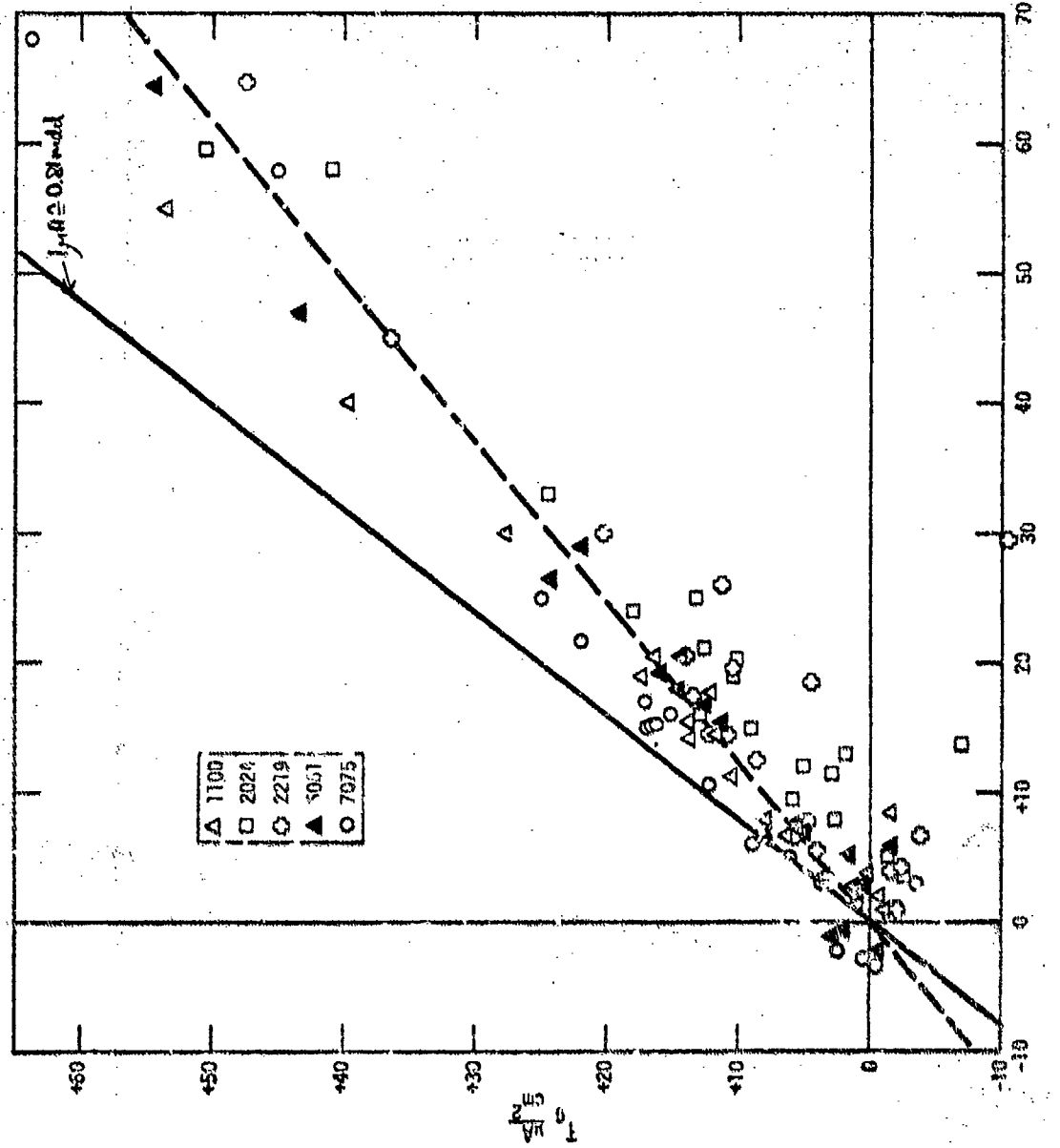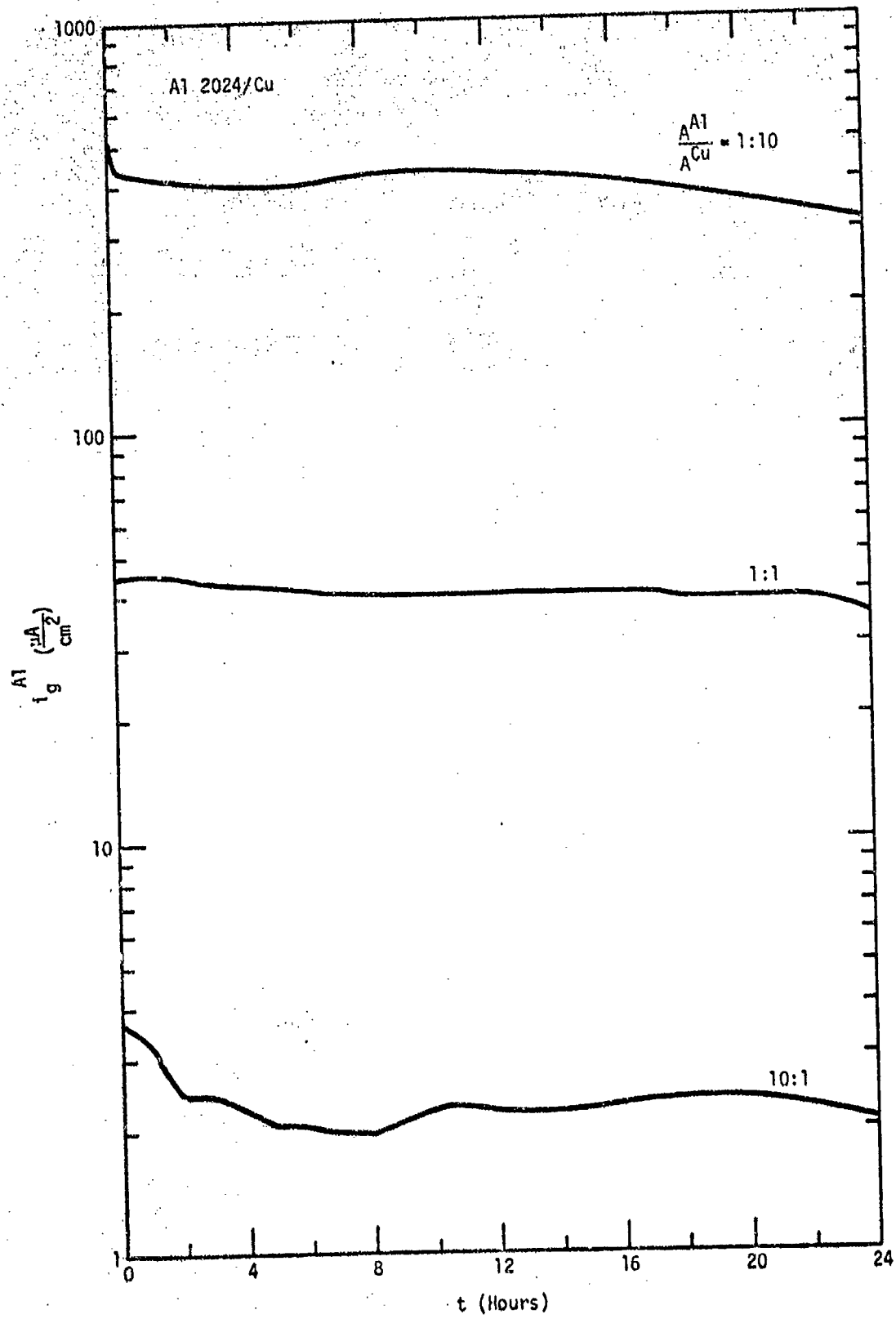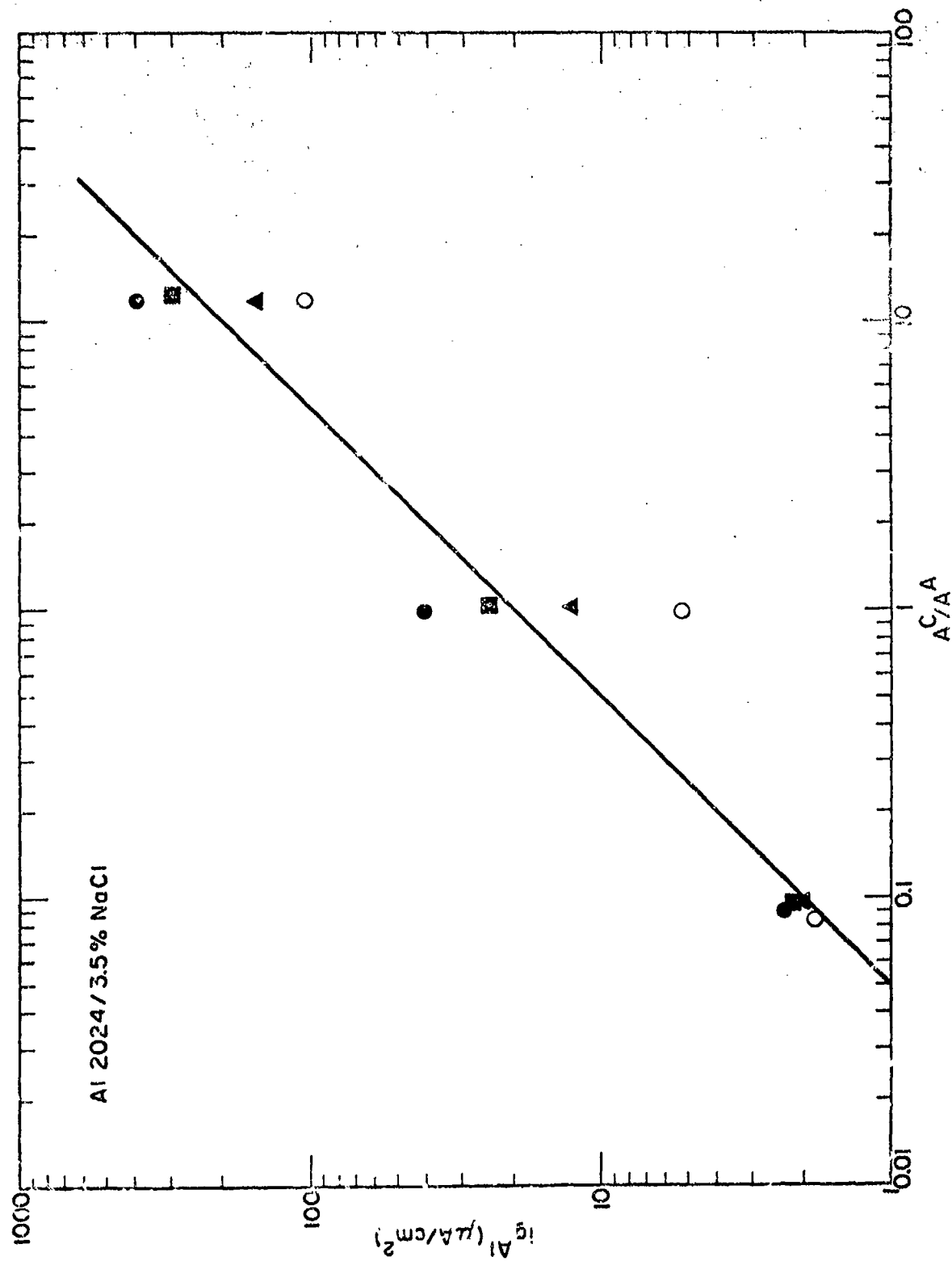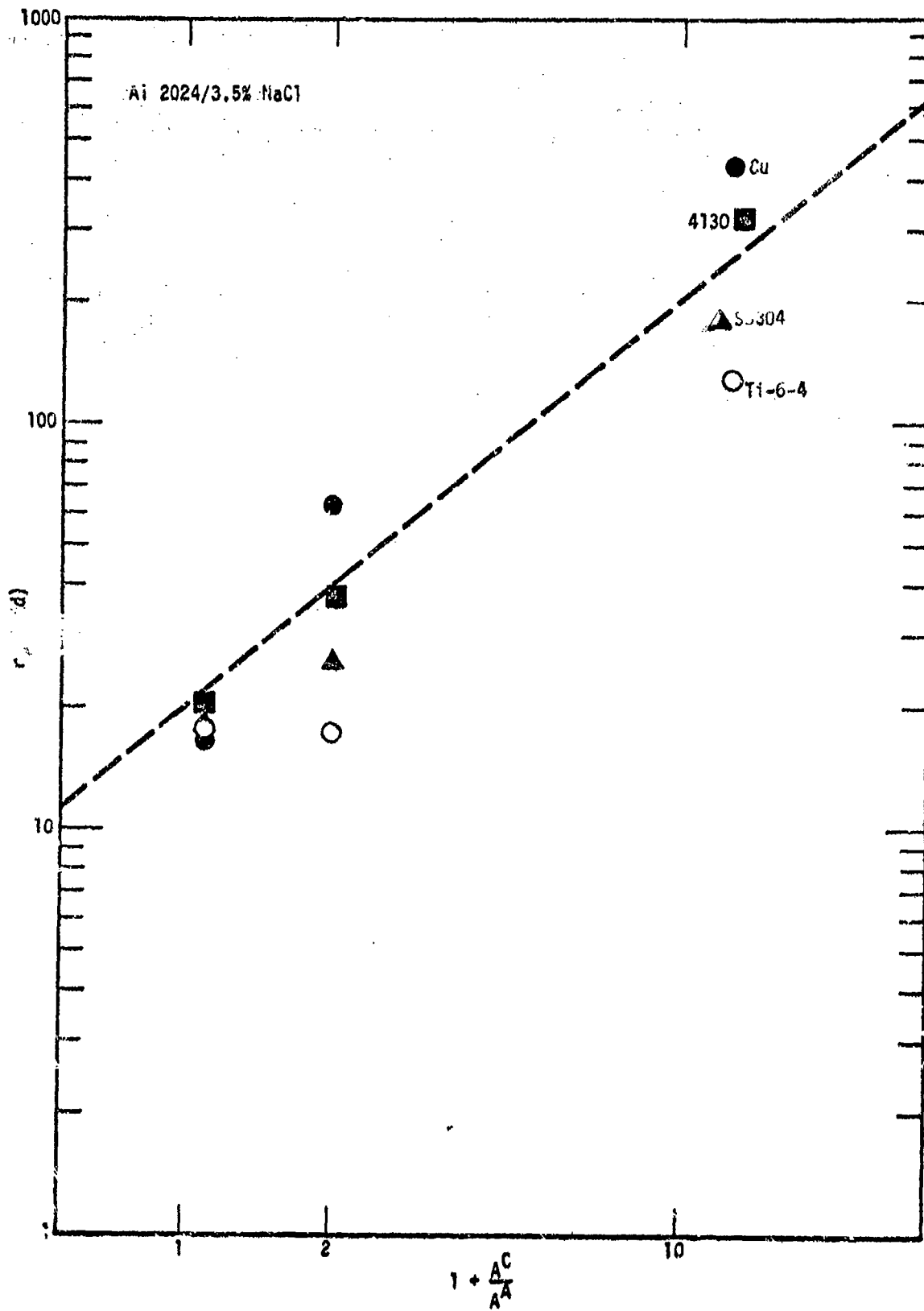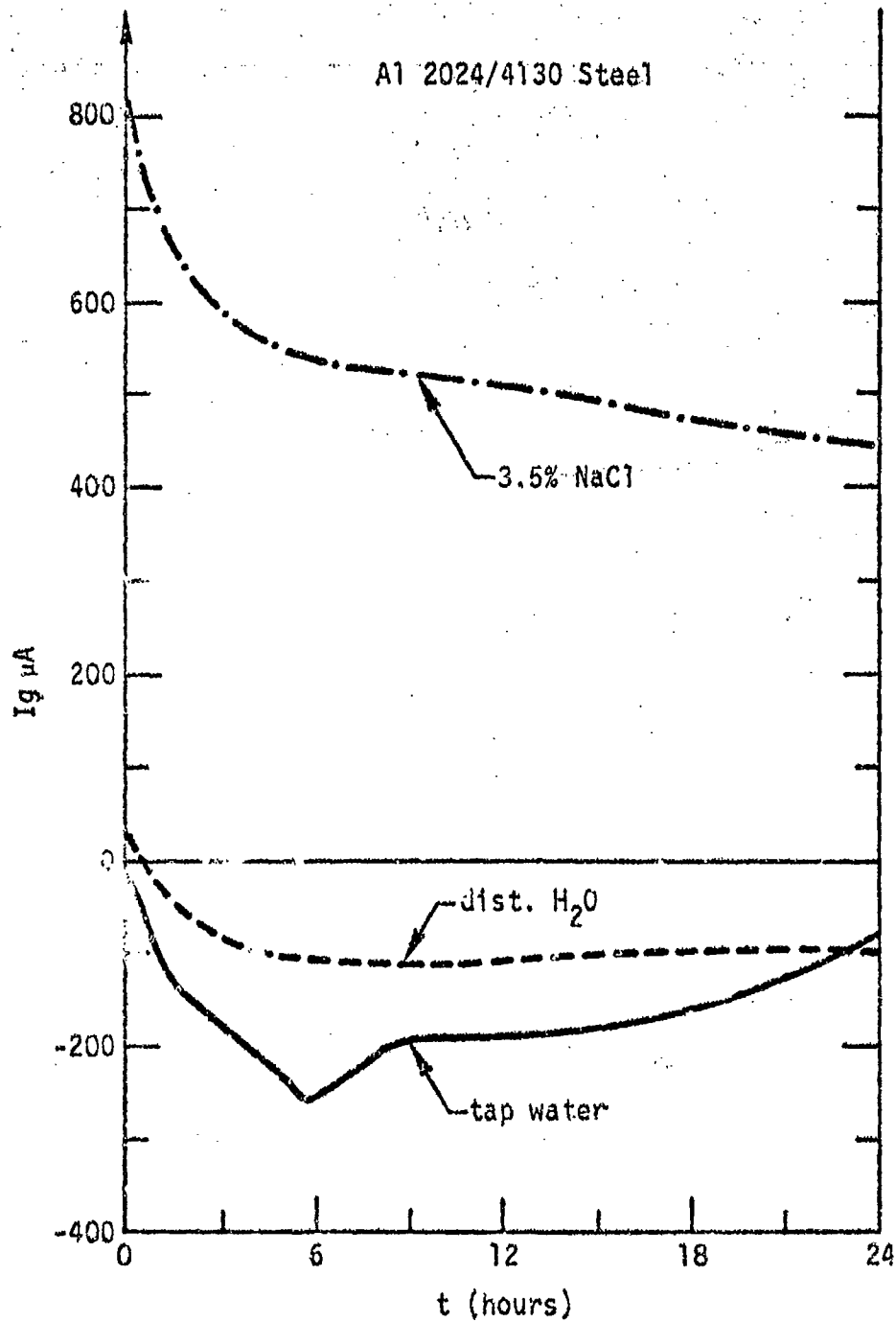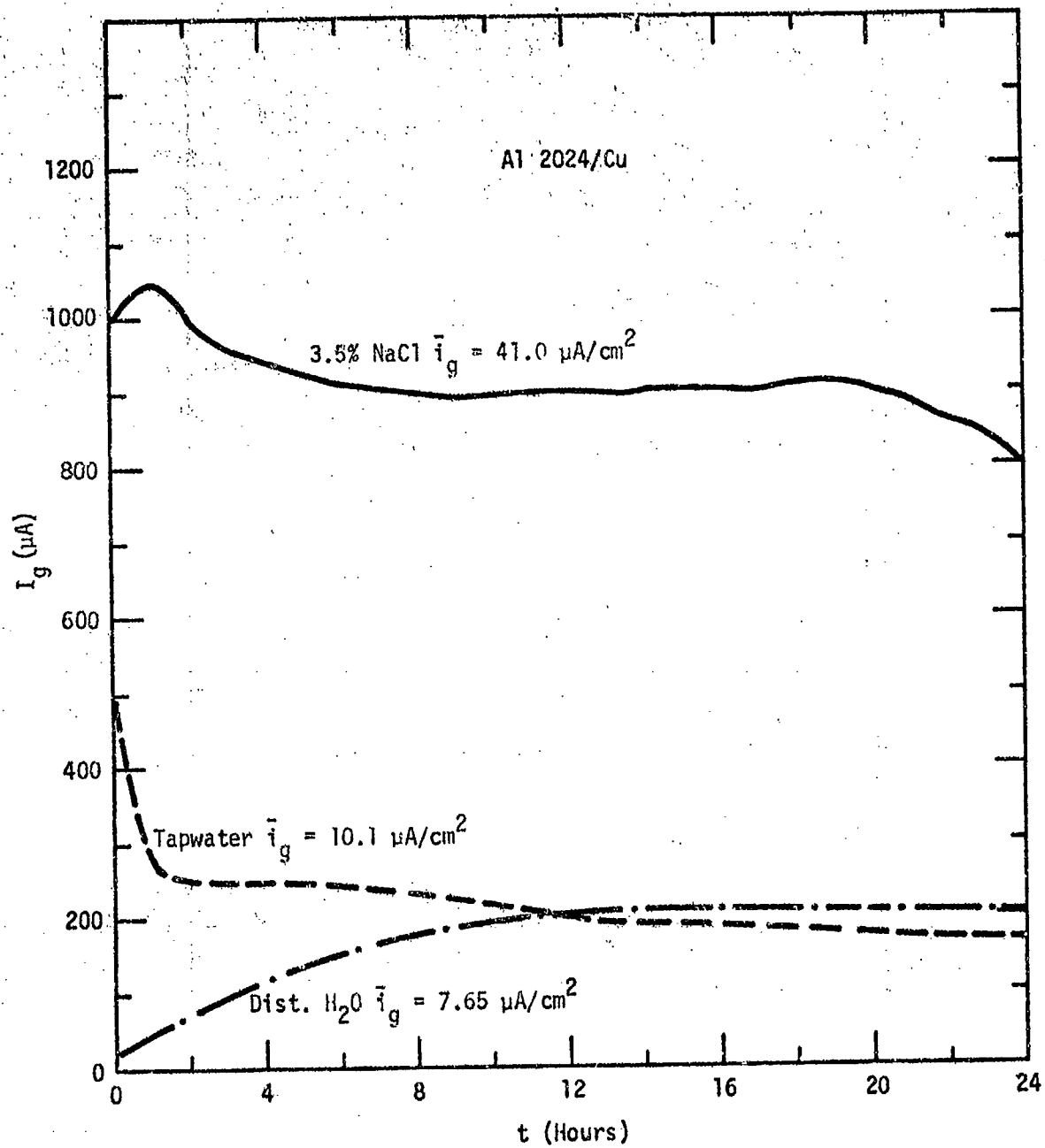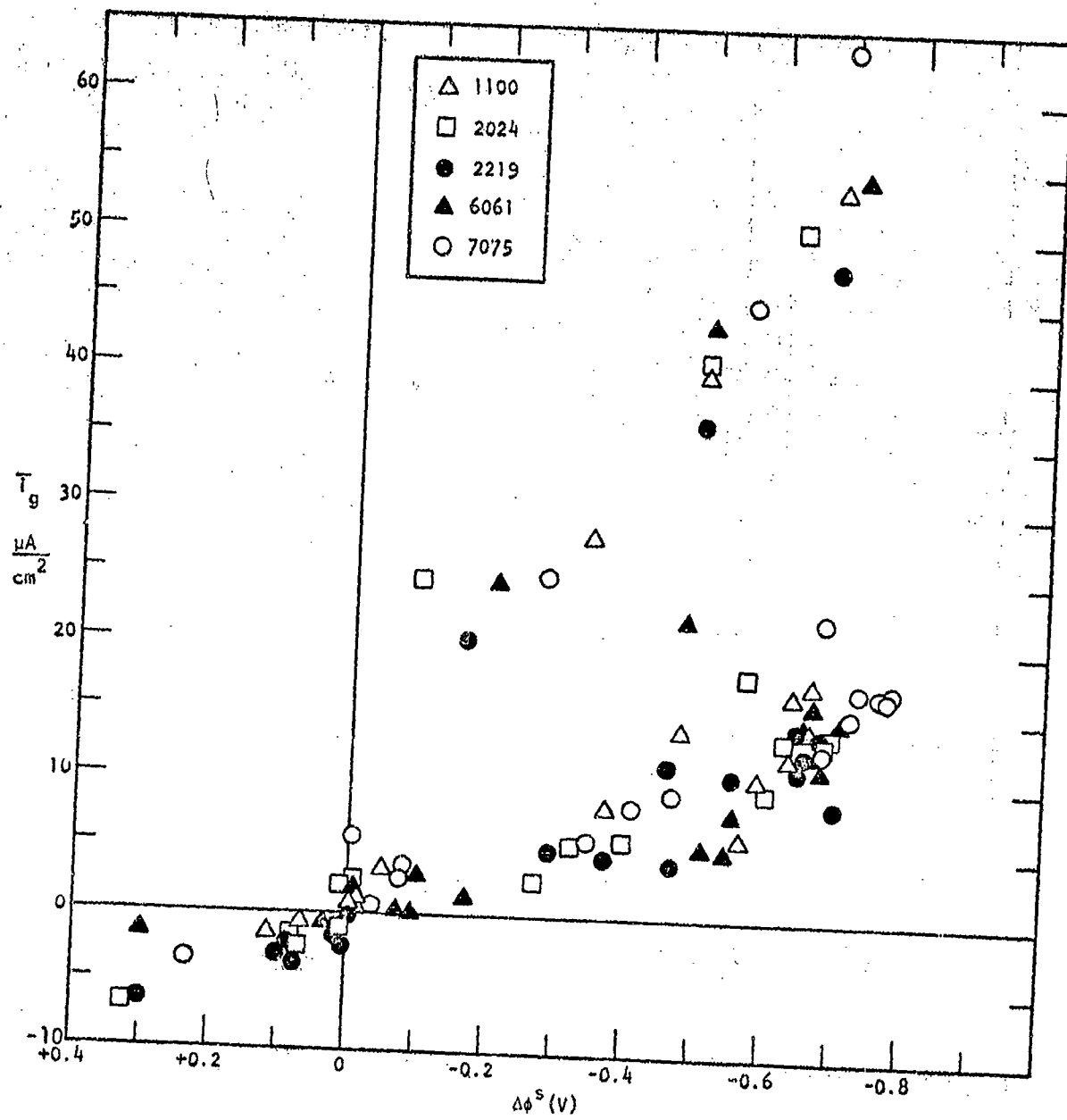
Figure 8a

Figure 8b

Figure 9
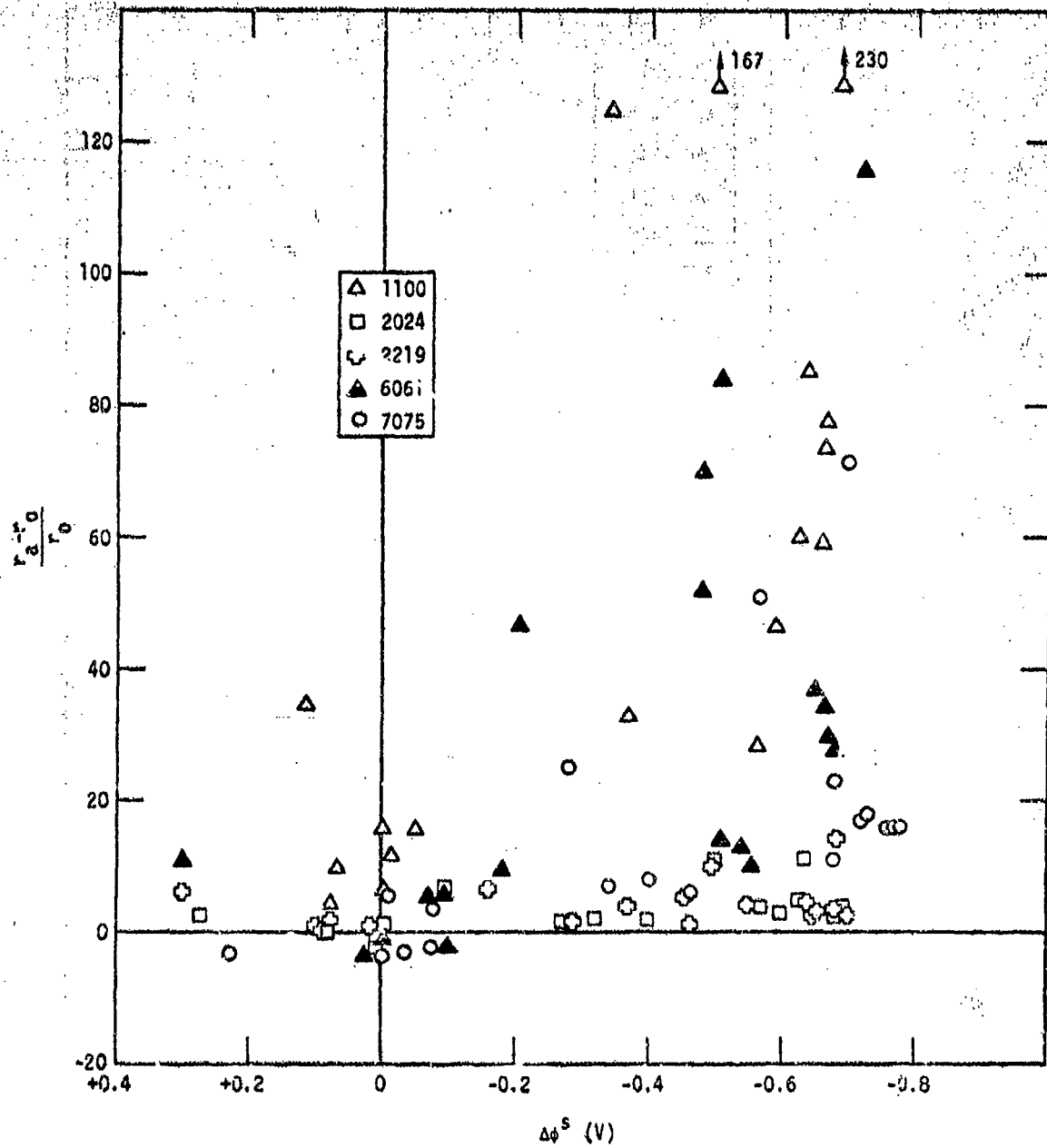
Figure 10

A VERSATILE POLARIZATION CELL SYSTEM

R. E. Geisert
Gould Inc., Cleveland, Ohio
N. D. Greene, V. S. Agarwalla
Institute of Material Science
University of Connecticut
Storrs, Connecticut

INTRODUCTION

A variety of polarization cells for electro-chemical experiments have been reported in the literature with a trend from the earlier complicated designs to simpler designs. Most cells were difficult to make and required custom fitting and careful positioning of their components when assembled. However, even the most recent designs require special glassware and are difficult to modify for special experiments.

With the increasing interest and use of electrochemical techniques for corrosion evaluations, the need for a more improved polarization cell became apparent. A study was made of over thirty polarization cell designs reported in the literature to determine what features should be included in a general use polarization cell. Ideally, a general use polarization cell should: (1) be easily constructed and assembled for use in a variety of experiments, (2) constructed of non-contaminating materials, (3) provide uniform current distribution, (4) have a rugged, readily adjustable Luggin-Haber Probe, and (5) be easily modified for various experiments and electrode configurations.

A new polarization cell system accomplishing the above aims has been designed using commercially available glass pipe and fittings and readily available or easily machined Teflon parts.

BACKGROUND

One of the earliest cell designs was that of Professor R. Piontelli in the early 1950's [1]. His cell consisted of a glass cylinder with a glass stopper holding an externally mounted specimen on one end. The counter electrode was inserted and held in place by a glass stopper in the side of the cylinder. This electrode consisted of a ring positioned parallel to the specimen. The probe assembly was inserted in the cylinder from the side opposite the specimen going through the center of the counter electrode. Piontelli used both a Luggin-Haber probe and his own "side channel probe". With the latter, the sheet specimen had to be ground flat as was the face of the probe so as to prevent any crevice effect. Purified electrolyte was circulated through the cell with an air pump device with inlets and outlets being attached to the body of the cell.

Other early cell designs were equally complicated glass apparatus and were usually designed for one type of experiment. Stern [2] started a trend to a simpler more versatile cell by using a three neck flask with ground glass joints. The two side necks were used for auxiliary electrodes to provide for more uniform current distribution at the working electrode in the center neck. An eccentric joint allowed for some adjustment of the working electrode. Additional openings were added to the flask for a hydrogen electrode, a salt bridge and a gas inlet. This cell design went through several modifications resulting in the now widely used standard polarization cell [3].

The standard polarization cell is a 5 necked distilling flask with the openings for 2 auxiliary electrodes, gas inlet and outlet adaptor, and a thermometer. The working electrode is held in place by an eccentric joint fitting in the center neck allowing for some rotational adjustment of the electrode. The Luggin probe-salt bridge is inserted in the flask through a ball and socket joint which also allows some adjustment. These two adjustments allowed the capilliary tip of the Luggin probe to be located 1 to 3 cm from the working electrode which is necessary to prevent IR drop.

Methods to insure uniform current distribution from the auxiliary electrodes to the working electrode has been approached in several ways. In the Piontelli cell, the auxiliary electrode was the same size as the specimen and placed parallel to it. Another method was to have four tubes from a separate auxiliary electrode compartment encircling the working electrode [4]. In other cells, the auxiliary electrodes were placed in separate compartments and depended on current flow through the electrolyte for uniform current distribution. Another method used an auxiliary electrode ring surrounding the test specimens. With the standard polarization cell, two auxiliary electrodes are used for uniform current distribution.

NEW POLARIZATION CELL DESIGN

The earliest cell designs were complicated glass apparatus that required careful fitting of parts and careful assembly. The present standard polarization cell, while much improved, still has limitations. Fabrication of cell requires the services of a glass blower skilled in scientific glass blowing. Also, modification of the cell for various experimental requirements requires a skilled glass blower. Versatility of the cell is limited since there are no openings available for inserting additional electrodes or other apparatus. Also, specimen size is limited by the diameter of the large neck opening.

From the evaluation of previous polarization cells, it was concluded that a single cell could not be designed with the desired features but without the limitations of these cells. However, following the parameters for a general use polarization cell, a

new cell system was designed based on glass pipe plumbing fittings. These fittings are available in a wide variety of sizes and configurations so that many types of cells can be assembled. For our cell, pipe and fittings with a beaded end configuration were used to facilitate clamping arrangements.

The basic cell (figure 1) consists of a modified end cap fitting with a machined PTFE top, PTFE tube fittings for electrode holders, Luggin Probe, gas diffuser, thermometer, or a condenser. The cell container is made from a 4 inch diameter glass pipe sealed at one end. The depth is 6 3/4 inch to give a volume of slightly more than one liter.

The top is machined from a 5 inch diameter PTFE rod. The circumference is machined with a radius to match the beaded end of the pipe fitting. The top has nine holes that are drilled and tapped for 3/8 inch pipe thread. One hole is in the center, the other are equally spaced on a three inch hole circle (figure 2). With this hole pattern each hole is equidistant from the center hole and the adjacent hole.

The top is held in place with a drain line coupling which consists of a wraparound clamp with a rubber compression liner and a PTFE seal ring. The compression liner and seal ring can also be used with a large worm gear drive hose clamp. This clamping arrangement is easier to use than the more cumbersome clamp for a drain line coupling.

Electrode holders, salt bridge, thermometer and other experimental accessories are held in place by 3/8 x 3/8 PTFE tube fitting screwed into the top. These fittings are designed for 3/8 inch tubing and have a shoulder on the ID to prevent plastic tubing going all the way through. The fittings are drilled and reamed so that 3/8 OD glass tubing can be inserted through the fitting. An aluminum compression nut insures a tight seal on the tubing. Electrode holders and salt bridge are easily made from 3/8 inch heavy wall pyrex tubing for use with these fittings. However, thermometers require a sleeve of teflon tubing to prevent slipping through. Plugs to seal unused holes are machined from 3/4 inch square PTFE rod. These plugs are approximately one inch long and threaded with a 3/8 male pipe thread.

The Luggin probe for this cell is made from 3/8 heavy wall tubing drawn to a capillary tip. The tip extends out from a 1 1/2 inch arm which is bent 90° to the main stem. This design allows the probe to be inserted into any of the holes in the top and brought up to the working electrode in the center.

Two types of salt bridges have been designed for this cell; a thistle tube type (figure 3) and a tube type to an adjacent beaker (figure 1). The thistle tube salt bridge slips into the stem of the Luggin probe. The tip is drawn to a fine point and a means provided for a controlled leak path. One method has been

to embed a quartz fiber. The reference electrode is held in place in the enlarged end with a machined plastic cap. A more conventional salt bridge is a glass tube bent to shape. A filler opening is provided and closed with a small piece of tubing, either rubber or plastic, and a pinch clamp. The thistle tube salt bridge is useful when it is not convenient to have the reference electrode in a separate beaker. Such as, when the polarization cell is placed in constant temperature bath or in a multicompartment cell (figure 4).

Electrode holders are Stern-Makrides mounts using PTFE compression gaskets [3]. These holders are used for cylindrical specimens drilled and tapped for the 5-40 or 6-32 threaded stainless steel rod. A specimen mount for sheet specimens has been modified to be used with the Stern-Makrides mounts.

Versatility of Cell Design

The top for this cell can be used with any 4 inch beaded pipe fitting. Using the tubing adaptors, the specimen mounts, Luggin Probe and other accessories can be made and adjusted in length to any size container. The number of openings in the top allows many experimental variations.

One variation of cell is the three compartment cell shown in figure 4. This is assembled from a 4 x 1 1/2 sanitary tee fitting and two 4 x 1 1/2 quarter bend reducers. The glass fittings are joined by the rubber coupling liners and teflon seal rings using hose clamps for tightness. Each compartment is fitted with a top and the appropriate electrodes and accessories. A two compartment cell can be assembled by using two quarter bend reducers. Any number of cells can be made for various laboratory studies by using different types of fittings. In addition to laboratory studies, corrosion measurements can be made in a process stream of a chemical plant with the use of appropriate glass fittings. Flanged couplings and clamps are available for joining beaded glass pipe to other types of pipe. Using the top for the cells, the electrodes can be placed directly in the process stream for measurements of corrosion rates.

Conclusion

A new polarization cell system has been designed using commercially available glass pipe and fittings and simple Teflon parts. This system can be easily modified, without constructing special components, to perform the following: (1) multi-compartment measurements; (2) multielectrode studies; (3) electrochemical measurements in large electrolyte volumes; (4) flow studies; (5) elevated temperature measurements; (6) optical studies of polarized electrodes; (7) electrochemical measurements in actual process streams; and (8) studies of stressed metal speci-

mens.

These cells can fulfill the exacting requirements of electrochemical experimentation both in university corrosion research laboratories and industrial laboratories.

References

1. R. Piontelli "Electrochemical Behavior of Metals as a Basis for the Study of Corrosion" Corrosion (9) (April 1953)

2. M. Stern "The Electrochemical Behavior, Including Hydrogen Overvoltage of Iron in Acid Environments" Journal of Electrochemical Society 102:11 (1955)

3. N. D. Greene Experimental Electrode Kinetics Rensselaer Polytechnic Institute, Troy, N.Y. 1965

4. A. C. Makrides "Some Electrochemical Methods in Corrosion Research" Corrosion 18:9 (September 1962)
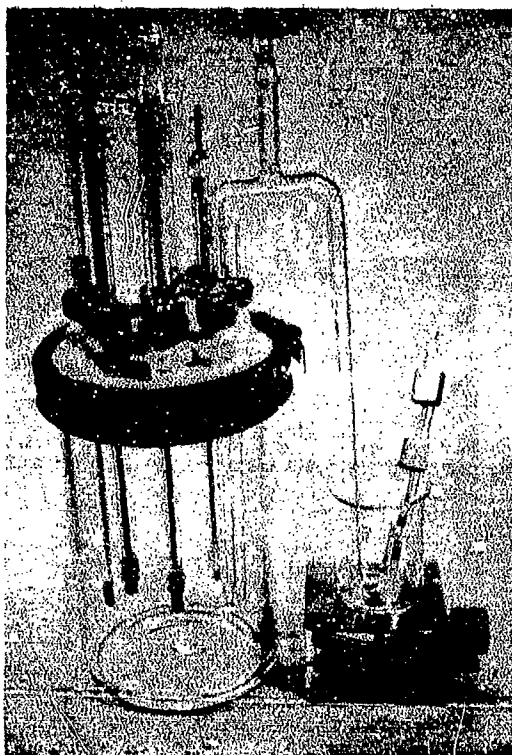
Figure 1   Polarization Cell, Basic Design with Salt Bridge to
separate Beaker
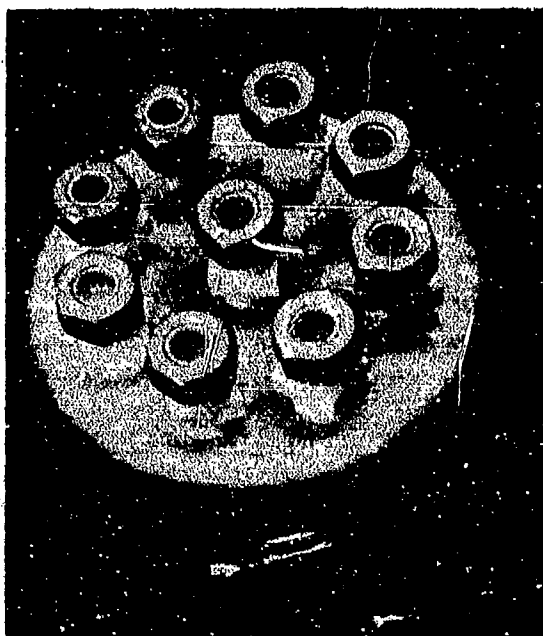
Figure 2   Top, for Polarization Cell snowning arrangement of holes
and Tube Fitting Adaptors
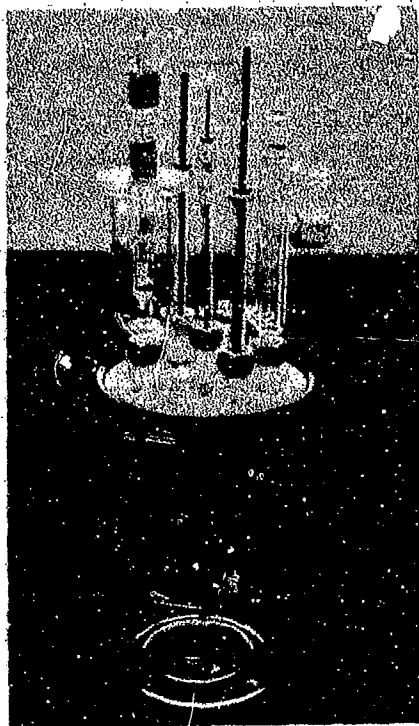
Figure 3   Polarization Cell, Basic Design with thistle tube Salt
Bridge
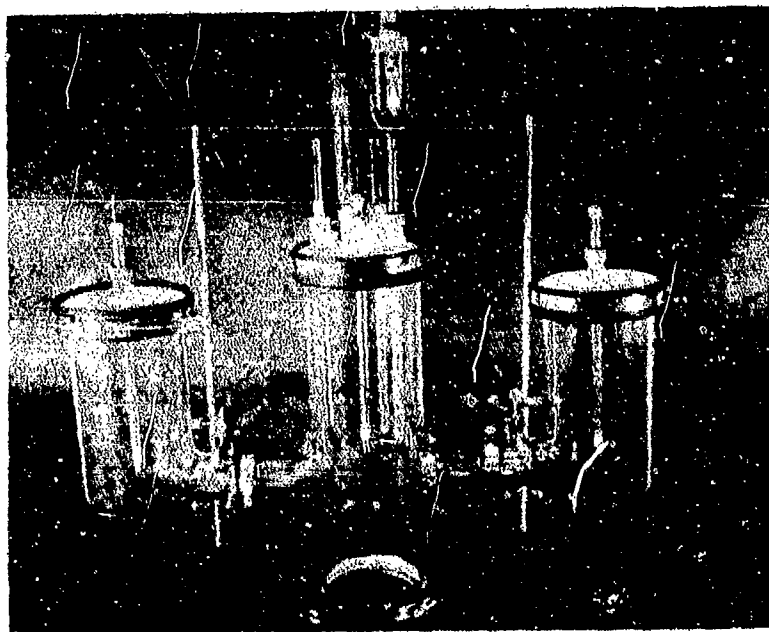
Figure 4   Three compartment cell assembled from a sanitary tee
and two quarter bend reducer

AN ELECTROCHEMICAL TEST TO DETERMINE
CORROSION RATES OF METALS IN
AUTOMOTIVE ENGINE COOLING SYSTEMS

by

Fred F. Lyle, Jr.
Senior Research Engineer
Department of Materials Sciences
Southwest Research Institute
San Antonio, Texas 78284

INTRODUCTION

At the present time, various performance tests are used for evaluating the corrosion behavior of metals in engine coolants which are formulated for corrosion inhibiting and antifreeze properties. These include glassware tests, [1,2,3]* simulated service tests, [2,4] engine dynamometer tests, [5,6] and fleet tests. Depending on the particular method, the test duration ranges from two weeks to a year or more. The tests are either interrupted after specific time intervals or terminated to obtain corrosion rate data by the measurement of coupon weight change or by the examination of actual cooling system components. The engine dynamometer tests are the laboratory methods which most closely reproduce environmental conditions a coolant encounters in service; however, 700[5] to 1200[6] hours are required to perform them. None of the standard tests can be used to monitor instantaneous corrosion rates. Multiple tests are therefore required to evaluate the effects of variations in such environmental parameters as flow rate, pH, temperature, glycol-to-water ratio, inhibitor concentration, impurity concentration, etc. A test which would provide such data in a shorter time without interruption of the test would be a significant improvement over current tests.

Electrochemical linear polarization methods of corrosion rate measurement offer many advantages over weight-change tests of the type used in the standard engine coolant corrosion tests, most important of which is that corrosion rates can be determined instantaneously, _in situ_ without disturbing the corrosion reaction, thereby permitting evaluation of changes in environmental parameters. The technique is based on the fact that the slope of the potential vs applied current density curve at the corrosion potential is related to the corrosion current density (i.e., the corrosion rate) by the following equation:

$$\left(\frac{\Delta i}{\Delta E}\right)_{\Delta E = 0} = \frac{(i_{corr})\,(2.3)\,(\beta_a + \beta_c)}{(\beta_a \beta_c)} \tag{1}$$

where ΔE is the change in electrode potential (mv) with respect to the corrosion potential (i.e., $\Delta E = 0$) produced by Δi, an externally applied current density ($\mu A/cm^2$), i_{corr} is the corrosion current density ($\mu A/cm^2$), and β_a and β_c are the anodic and cathodic Tafel slopes, i.e., the slopes of the curves obtained by plotting the electrode potential as a function of the logarithm of the applied current density in the anodic (+) and cathodic (-) directions, respectively. If the slopes are known, the corrosion rate can be calculated from Eq. (1) by experimentally producing applied current vs potential curves and determining the slope at $\Delta E = 0$. Normally, only a few points within a range of approximately ± 10 mv of the corrosion potential are required.

Linear polarization measurements are normally made using the basic galvanostatic 3-electrode circuit illustrated schematically in Figure 1. The test

---

*Numerals in parentheses refer to List of References.

electrode is made of the metal whose corrosion rate is desired. A current is applied between it and the auxiliary electrode by adjusting the variable resistor. As the current is varied the change in potential of the test electrode with respect to the reference electrode is determined. The high input impedence of the D. C. voltmeter maintains the magnitude of the current flowing between the test and reference electrodes at a very low level, assuring that the potential of the reference electrode remains essentially constant.

This paper describes a test program conducted at Southwest Research Institute to develop a test procedure based on linear polarization techniques to measure corrosion rates of metals exposed in the cooling system of an operating automobile engine.

EXPERIMENTAL PROCEDURES

Use of Linear Polarization to Predict
Long-Term General Corrosion Rates

The objective of this phase of the study was to show that corrosion rates of metals in engine cooling systems determined by the linear polarization method in 100 to 200 hours can be used to predict long-term corrosion rates. This objective was accomplished through a comparative test of linear polarization and weight-change methods. For this purpose the procedures given in a 700-hour test, ASTM Method D2758-68T, "Testing Engine Antifreezes by Engine Dynamometer,"[5] were employed, with the following exceptions: (1) tests to evaluate the antifreeze characteristics other than corrosion were omitted, (2) coupons were removed and weighed only at the end of the test, (3) by-pass and full-flow capsules were replaced by a specially designed full-flow test cell containing coupons and linear polarization electrodes, and (4) the test time for two experiments was reduced from 700 to 200 hours. The coolant used consisted of 40 volume percent technical grade ethylene glycol in corrosive water (prepared by adding 100 ppm each of $NaCl$, Na_2SO_4, and $NaHCO_3$ to deionized water). Throughout the program the engine was operated at a speed of 2500 ± 20 rpm and the coolant temperature was maintained at a temperature of $190 \pm 3 °F$.

A 1967 Oldsmobile engine mounted on a test stand was used. The test cell was fabricated from a steel pipe and was installed in the upper radiator hose, as shown in Figure 2. As constructed, the cell was capable of containing 36 disc-type test electrodes, 6 weight-change coupon test bundles of the type used in ASTM D2758-68T, a disc-type platinum reference electrode, 1 to 4 disc-type stainless steel auxiliary electrodes, and a thermocouple holder.

The electrode assembly used is shown in Figure 3 and is a modification of a design proposed by France.[7] The electrode holder consists of a 3/4-inch pipe plug drilled and tapped to accept a 3/4-inch nylon plug. A flat disc electrode is held in position between the nylon plug and a Teflon gasket. The nylon plug presses against the electrode and compresses the gasket between the front of the electrode

and the steel electrode holder. The Teflon gasket provides a leak-proof seal which minimizes crevice corrosion and controls the exposed surface area. The inside diameter of the gasket is 1.128 cm, which exposes a surface area of 1 cm^2 so that the measured corrosion current is also the corrosion current density to which corrosion rate in standard units such as mils per year (mpy) can be easily equated. Electrical contact between the electrode and the exterior of the test chamber is made with a brass screw through the nylon plug to the back of the electrodes. This electrode assembly is capable of accommodating specimens ranging in thickness from a few mils to approximately 1/4-inch thick.

Electrodes used in this study consisted of the following five metals specified in ASTM Method D2758-68T: (1) SAE 1020 Steel; (2) SAE 71 Copper; (3) SAE CA 268 Brass; (4) SAE 120 Cast Iron; and (5) SAE 329 Cast Aluminum. In the latter stages of the program AISI 6061 aluminum alloy was substituted for SAE 329 aluminum. A platinum reference electrode and two Type 304 stainless steel auxiliary electrodes were used. The basic circuit shown in Figure 1 was used for all polarization measurements.

Linear polarization measurements were made on each test electrode at regular intervals of 24 or 48 hours throughout each test run, and the corrosion rate was calculated from Eq. (1). Potentials were measured after 5 minutes of current application based on results of studies by Greene and Jones[8] which indicated that significant errors can result in $\Delta E/\Delta i$ slopes determined from potential readings taken after shorter times, but that no essential benefit was obtained from taking the potential readings after longer periods. Anodic and cathodic Tafel slopes were calculated from anodic and cathodic logarithmic polarization curves made on each test metal during each test run. The corrosion potential of each metal, relative to the platinum reference electrode, was determined at the time polarization readings were made.

Coupons for weight-change measurements were made from the same metals, cut to the size specified in ASTM D2758-68T. Coupons were mounted on machine screws covered with a sleeve of polyethylene for insulation from the screw. Coupons were insulated from one another by Teflon spacers. Three bundles of coupons were exposed. Both electrodes and coupons were prepared for exposure by grinding to a 600-grit finish with silicon carbide paper, followed by ultrasonic cleaning in detergent solution, rinsing with deionized water, and drying in reagent grade alcohol. Coupons were weighed on a balance which had a sensitivity of ± 0.1 mg. At the end of the exposure period, coupons were cleaned and reweighed, and weight losses were determined. Specimens were cleaned in accordance with specifications given in ASTM G1-67, "Preparing, Cleaning and Evaluating Corrosion Test Specimens."[9] Average corrosion rates were calculated from the weight-loss data using the Faraday equation:

$$i_{corr} = \frac{WnF}{Mt} \qquad (2)$$

where i_{corr} is the corrosion rate ($\mu A/cm^2$), W is the weight loss (g), n is the number of electrons transferred in the corrosion reaction, F is the Faraday constant, M is

286

the atomic weight of the metal or alloy (g), and t is the time of exposure (sec). Average corrosion rates from the polarization data were determined by graphical integration of corrosion-rate-vs-time curves. This procedure allowed comparison of overall corrosion rates measured by the two methods.

Measurement of the Effect of a Corrosion Inhibitor

The objective of this phase of the study was to determine the ability of the linear polarization method to measure the effect of a corrosion inhibitor on the corrosion rates of the test metals. Tests were conducted in the same manner as in the first phase. Prior to the inhibitor evaluation, the engine and test cylinder were carefully cleaned in accordance with specifications given in ASTM D2758-68T. The inhibitor used was a new formulation consisting of 1.0% sodium molybdate and 0.2% benzotriazole adjusted to a pH of 8.3 by addition of sodium hydroxide. This formulation was chosen because 1.0% sodium molybdate is a good inhibitor for all of the metals tested[10] and 0.2% benzotriazole is a particularly good inhibitor for steel and copper alloys.[11]

RESULTS AND DISCUSSION

The first engine test was conducted with uninhibited coolant for the 700-hour period in accordance with specifications given in ASTM D2758-68T. A commercial corrosion rate meter employing the basic circuit shown in Figure 1 was used. Linear polarization readings were made daily during the first 100 hours of the test and at 48- or 72-hour intervals thereafter. Anodic and cathodic Tafel curves were made for each of the test metals after approximately 100 hours and 500 hours of exposure. Engine operation was nominal throughout the test.

Table I compares corrosion rates calculated from weight-change and linear polarization measurements after 700 hours of exposure. Correspondence between average corrosion rates determined from polarization measurements and those calculated from weight-change data was good for cast iron and steel, but was poor for the nonferrous metals. The discrepancy in the result for aluminum was attributed at least in part to severe localized attack of the weight-change coupons at the interface between the coupons and the plastic spacers used to separate them. However, no such rationalization was obvious for the other discrepancies.

After analyzing the results it was concluded that the most probable sources of discrepancy were the specimen design and/or errors in polarization voltage measurements resulting from the resistance of the test fluid and the inherent characteristics of the commercial corrosion rate meter. The specimen design is such that some crevice corrosion of the electrodes is possible at the electrode-Teflon seal interface. A small amount of crevice attack was observed on the copper and brass specimens while no crevice attack was present on the other specimens. Cylindrical electrodes with larger surface areas have been used by other investigators with good results.

Regarding resistance effects, in the standard 3-electrode circuit used in this test, the potential measured consists of two components: (1) activation polarization, i.e., the potential change induced by the flow of current between test and auxiliary electrodes, and (2) an IR drop, i.e., the change in potential resulting from current flow required for voltage measurement between the reference and test electrodes. The IR drop is the product of this current flow and the resistance between the test and reference electrodes; the resistance is the sum of the electrolyte resistance and the resistance of any deposits on electrode surfaces. For polarization measurements to be meaningful, the IR drop must be insignificant compared to the activation polarization component, i.e., the current required for the voltage measurement must be kept very small, the solution resistivity must be low, or the IR drop must be eliminated. In cases where the resistivity of the electrolyte is high, a Wheatstone bridge circuit may be used to balance out the IR drop. The commercial corrosion rate meter used in this test reportedly contained such a circuit.

A 264-hour laboratory experiment was conducted to measure the IR drop. Two cylindrical copper electrodes (18 cm^2 exposed surface area) and one cylindrical steel electrode (9 cm^2 exposed surface area) were tested in a sample of the glycol-water mixture taken from the engine at the end of the 700-hour test. As in the engine test, corrosion rates determined by weight-change measurements were compared to corrosion rates obtained from polarization data. To measure the IR drop a recorder was connected to the corrosion rate meter and current was interrupted at the end of each polarization measurement. Since the IR drop is entirely dependent upon current flow between reference and test electrodes, it disappears instantaneously when the current is interrupted. Measurements on the electrodes showed that an IR drop of approximately 0.13 mv was produced for every microampere of current applied. The most significant result of such an error is the influence it has on the calculation of the Tafel slopes. The corrosion current calculated from the uncorrected Tafel curve for copper (obtained by extrapolating the linear portion of the curve to zero polarization) was found to be 26.5% larger than the rate obtained from IR-corrected polarization data. The IR-drop error is of less significance for rapidly corroding materials; therefore, the error for ferrous metals is expected to be lower. Correlation between corrosion rates calculated from weight-change and linear polarization using slopes from IR-corrected Tafel curves was good for both copper and steel. In the engine test both the distance between electrodes and the corrosion rates were greater than in the laboratory tests and a larger error therefore would be expected. A factor in the engine test not present in the laboratory test was sludge buildup on electrode surfaces, which may have increased the resistance component of the IR drop. It was concluded, therefore, that errors caused by the IR drop in Tafel curve determinations were responsible for the difference between polarization and weight-change corrosion rates in the 700-hour engine test.

Two additional engine tests of 200 hours each, one in uninhibited coolant and the other in inhibited coolant, were conducted. To evaluate the influence of electrode

288

design on corrosion rates, two types of electrodes were used in these tests. Cast iron and brass electrodes were of the same design used in the 700-hour test. Copper, steel, and aluminum electrodes were cylindrical and were mounted on pipe plugs, three per plug, as shown in Figure 4. As installed, they extended into the center of the test chamber where they were exposed to the full coolant flow. Cast aluminum electrodes were not available so aluminum alloy 6061 electrodes were substituted. The exposed surface area of the electrodes was as follows: copper - 18 cm^2; mild steel and aluminum - 9 cm^2; brass and cast iron - 1 cm^2. Weight-change data were obtained directly from the electrodes rather than from separate coupons. As before, a platinum reference electrode and two Type 304 stainless steel auxiliary electrodes were used. A DC electrometer with an input impedance of 10^{14} ohms was used to measure potentials. A Wheatstone bridge circuit, developed by Jones, [12] was used to eliminate the IR drop. To balance the bridge, a procedure employed by Wilde for studies in high-resistivity water was followed. [13] Linear polarization measurements were made daily on each electrode, with the exception of weekends, when 72 hours elapsed between readings.

Resistances required in the bridge circuit to balance the resistance between reference and test electrodes for both tests are given in Table II. The larger resistances required for the smaller recessed brass and iron electrodes are believed to have resulted from surface deposits. Post-test examination of all the electrodes revealed buildup of sludge on the iron and brass electrode surfaces, while the other electrodes, all of which were cylindrical and extended into the coolant, were free of deposits. The significantly higher resistances required for ferrous and cuprous metals in the inhibited coolant suggest that the inhibitor promoted formation of a protective film on these metals. Conversely, the lower resistance required for aluminum in the inhibited coolant indicates that the inhibitor tended to remove any such film on the aluminum electrodes.

Corrosion rates calculated from weight-change and linear polarization data, steady-state corrosion potentials, and linear polarization constants for both tests are given in Tables III and IV. Correlation of average corrosion rates in the uninhibited coolant determined by linear polarization with average corrosion rates determined from weight-change data was very good for the ferrous and cuprous metals, but was poor for aluminum. Comparison of corrosion rates in the two coolants shows that the inhibitor reduced the corrosion rates of ferrous and cuprous metals by two or more orders of magnitude, but increased the corrosion rate of aluminum. A reasonably good correlation between average linear polarization and weight-change corrosion rates was obtained for aluminum in the inhibited coolant, but the large variation in polarization data for the three aluminum samples casts doubt on the validity of the average rate. The very low corrosion rate data obtained from the inhibited coolant show the superior sensitivity of the polarization method.

The instantaneous nature of linear corrosion rate measurement permits an investigator to follow changes in corrosion rate with time as illustrated in Figure 5 for cast iron and brass, or, if desirable, to continuously monitor corrosion rates. For example, the corrosion rate of cast iron in the uninhibited coolant initially increased somewhat in the first 100 hours of exposure to a rate of 40 μA/cm^2 before decreasing to a relatively constant rate of 20 μA/cm^2 after approximately 125 hours of exposure. The curve for brass in the uninhibited coolant is similar. Such behavior is typical of slowly-forming protective oxide films which lead to reduction of the initial corrosion rates.

It is evident from the curves in Figure 5 that the inhibitor produced a hundred-fold reduction in the brass corrosion rate and a thousandfold reduction in the iron rate within the first few hours of exposure and maintained these low rates throughout the 200-hour exposure period. By contrast, the weight-change method yields only one item of data, the average corrosion rate over the test period.

Table V compares the average corrosion rates determined by weight-change for the five metals exposed to uninhibited coolant for 700 hours (from Table I) with the steady-state rates obtained in the 200-hour uninhibited test. If the steady-state rate is used to predict the long-term corrosion rate, the 700-hour weight-change data differ by approximately a factor of 2, with the exception of aluminum. This is an acceptable difference, considering that corrosion rates determined by weight-change tests commonly differ by a factor of four or more.

It is not known with certainty why satisfactory correlation between weight-change and polarization was not achieved for aluminum. However, the results obtained may be explained by the fact that aluminum is an active-passive metal, i.e., it corrodes at a low rate over a given potential range (the "passive" range) because of the formation of a protective oxide film, but at lower potentials (the "active" range) the film is destroyed and the corrosion rate is greatly increased. In general, the corrosion rate of a metal is reduced if its electrode potential is decreased. Note that this is the case for the ferrous and cuprous metals in the 200-hour engine tests (Tables III and IV). However, if the electrode potential of a metal corroding in the passive range is lowered, the metal becomes active, and its corrosion rate increases. This appears to be the case for the aluminum alloy tested. In the inhibited coolant the potential was lowered and the corrosion rate (as measured by polarization) was increased by a factor of about 20, as compared to the uninhibited coolant. A second factor that should be noted is that excessive errors in the determination of the corrosion rate of passive aluminum by the weight-loss method have been reported.[2] This is because the protective films formed are dissolved by normal cleaning procedures and such weight loss cannot be distinguished from corrosion loss. This would explain the order-of-magnitude difference between weight-loss and polarization corrosion-rate data for aluminum in the uninhibited coolant and would indicate that the polarization method is superior for determining corrosion rate of aluminum corroding in the passive state.

CONCLUSIONS

The results of these tests have demonstrated the successful application of linear polarization techniques for measuring corrosion rates of ferrous and cuprous metals in an automotive engine cooling system under operating conditions. Specifically, the data have demonstrated that: (1) in situ linear polarization measurements provide instantaneous corrosion rates of acceptable accuracy in uninhibited and inhibited ethylene glycol solutions at a temperature of 190°F and an engine speed of 2500 rpm; (2) long-term corrosion rates may be predicted from linear polarization data taken after 100 to 200 hours of engine operation; (3) the linear polarization method is well suited for evaluation of inhibitors; a new inhibitor formulation based on sodium molybdate was demonstrated to be very effective; (4) very low corrosion rates are easily measured by the linear polarization method and (5) the linear polarization method is capable of yielding information concerning transient phenomena which cannot be obtained by the weight-change method. Each of these points represents a significant advance over conventional weight-change techniques. Discrepancies between weight-loss and polarization data for aluminum suggest that the linear polarization method may be superior for measuring corrosion rates of aluminum corroding in the passive state. Additional studies are needed to define this point and to verify the suitability of the linear polarization method for measurement of corrosion rates of aluminum.

ACKNOWLEDGEMENTS

REFERENCES

1. ASTM D 1384, "Standard Method for Glassware Corrosion Test for Engine Antifreezes," American Society for Testing and Materials, Philadelphia, Pa.

2. GM 1899-M, "Automotive Engine Coolant, Antifreeze Concentrate-Ethylene Glycol Type," General Motors Engineering Standards, July 1965.

3. BL1-1, "Corrosion Test for Ethylene Glycol Antifreeze, Ford Motor Company Quality Laboratory and Chemical Engineering Physical Test Methods, Jan. 24, 1961.

4. ASTM D 2570, "Tentative Method for Simulated Service Corrosion Testing of Engine Antifreezes," American Society for Testing and Materials, Philadelphia, Pa.

5. ASTM D 2758, "Tentative Method of Testing Engine Antifreezes by Engine Dynamometer," American Society for Testing and Materials, Philadelphia, Pa.

6. BL2-1, "Engine Test for Coolants," Ford Motor Company Quality Laboratory and Chemical Engineering Physical Test Methods, Jan. 16, 1962.

7. France, Jr., W.D., "A Specimen Holder for Precise Electrochemical Polarization Measurements on Metal Sheet and Foil," Journal of the Electrochemical Society, Vol. 114, No. 8, Aug. 1967, pp. 818-819.

8. Greene, N.D., and Jones, D.A., "Electrochemical Measurement of Low Corrosion Rates," Corrosion, Vol. 22, No. 7, July 1966, pp. 198-205.

9. ASTM G1-72, "Recommended Practice for Preparing, Cleaning, and Evaluating Corrosion Test Specimens," American Society for Testing and Materials, Philadelphia, Pa.

10. Brophy, J.E., Fitzsimmons, V.G., O'Rear, J.G., Price, T.R., and Zisman, W.A., "Aqueous Nonflammable Hydraulic Fluids," Industrial and Engineering Chemistry, Vol. 43, No. 4, Apr. 1951, pp. 884-896.

REFERENCES (Cont'd.)

11.   Mansfeld, F., Smith, T., and Parry, E.P., "Benzotriazole as
      Corrosion Inhibitor for Copper," Corrosion, Vol. 27, No. 7,
      July 1971, pp. 289-294.

12.   Jones, D.A., "Polarization in High Resistivity Media," Corrosion
      Science, Vol. 8, 1968, pp. 19-27.

13.   Wilde, B.E., "Adaptation of Linear Polarization Techniques for
      In-Situ Corrosion Measurements in Water Cooled Nuclear Reactor
   Environments," Corrosion, Vol. 23, Dec. 1967, pp. 379-384.
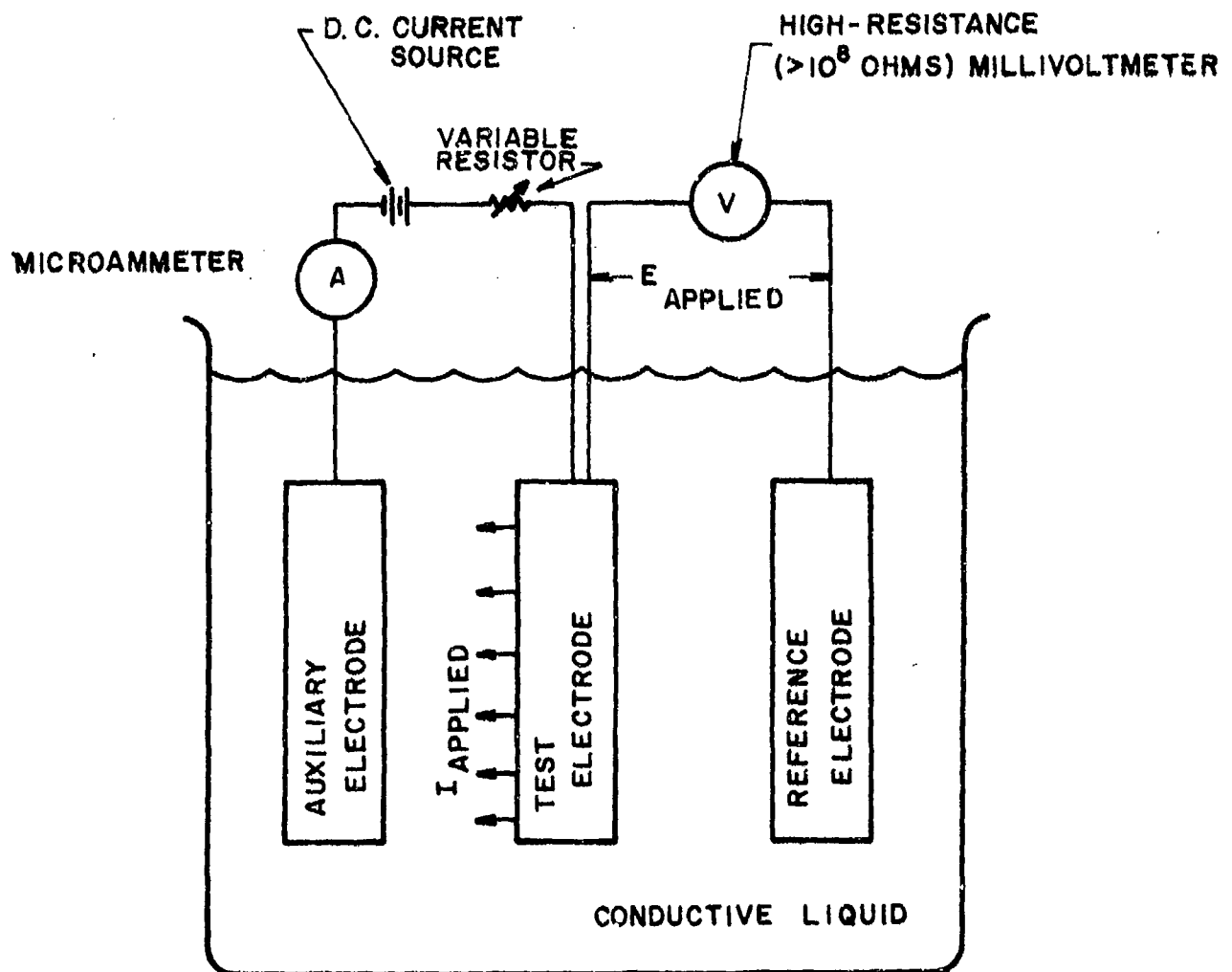
FIGURE 1. BASIC 3-ELECTRODE LINEAR POLARIZATION TEST CIRCUIT.
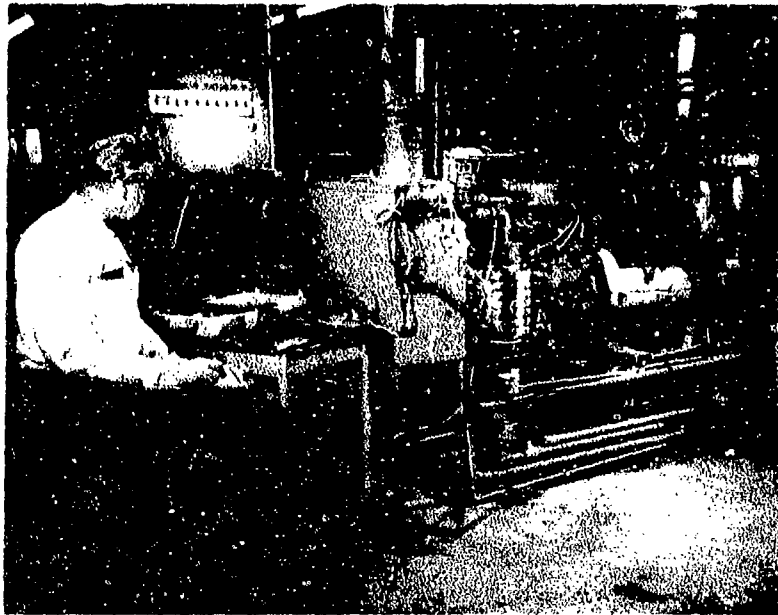
02-18590

(a) Overview of Engine, Test Chamber, and Instrumentation
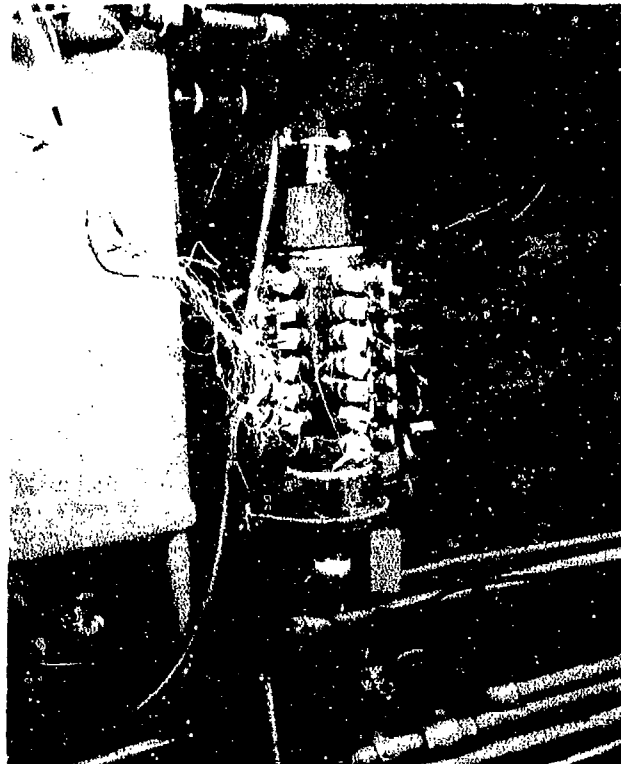
02-18592

(b) Test Chamber Mounted in Upper Radiator Hose

FIGURE 2.   ENGINE TEST FACILITY.
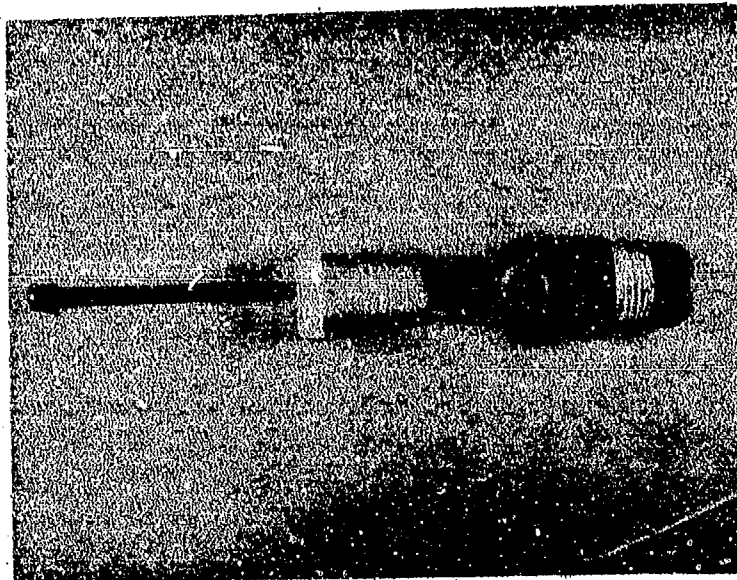
02-18596

(a) Components
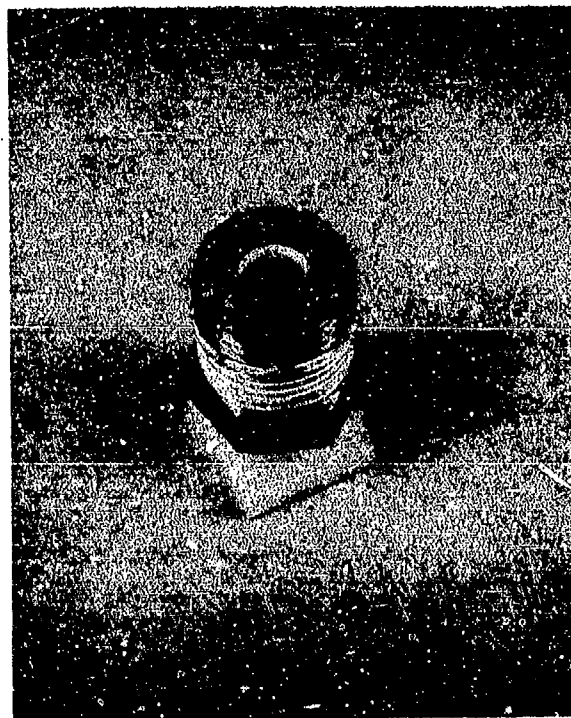
02-18597

(b) Assembled

FIGURE 3. ELECTRODE DESIGN. The threaded nylon plug presses
the specimen against the Teflon gasket and compresses
the gasket against a lip inside the steel plug. The brass
screw through the nylon plug provides external electrical
connection to the specimen.

FIGURE 4. CYLINDRICAL ELECTRODES AND HOLDER.
The holder was mounted through a coupling
welded to the test chamber such that the
electrodes extended into the center of the test
chamber.
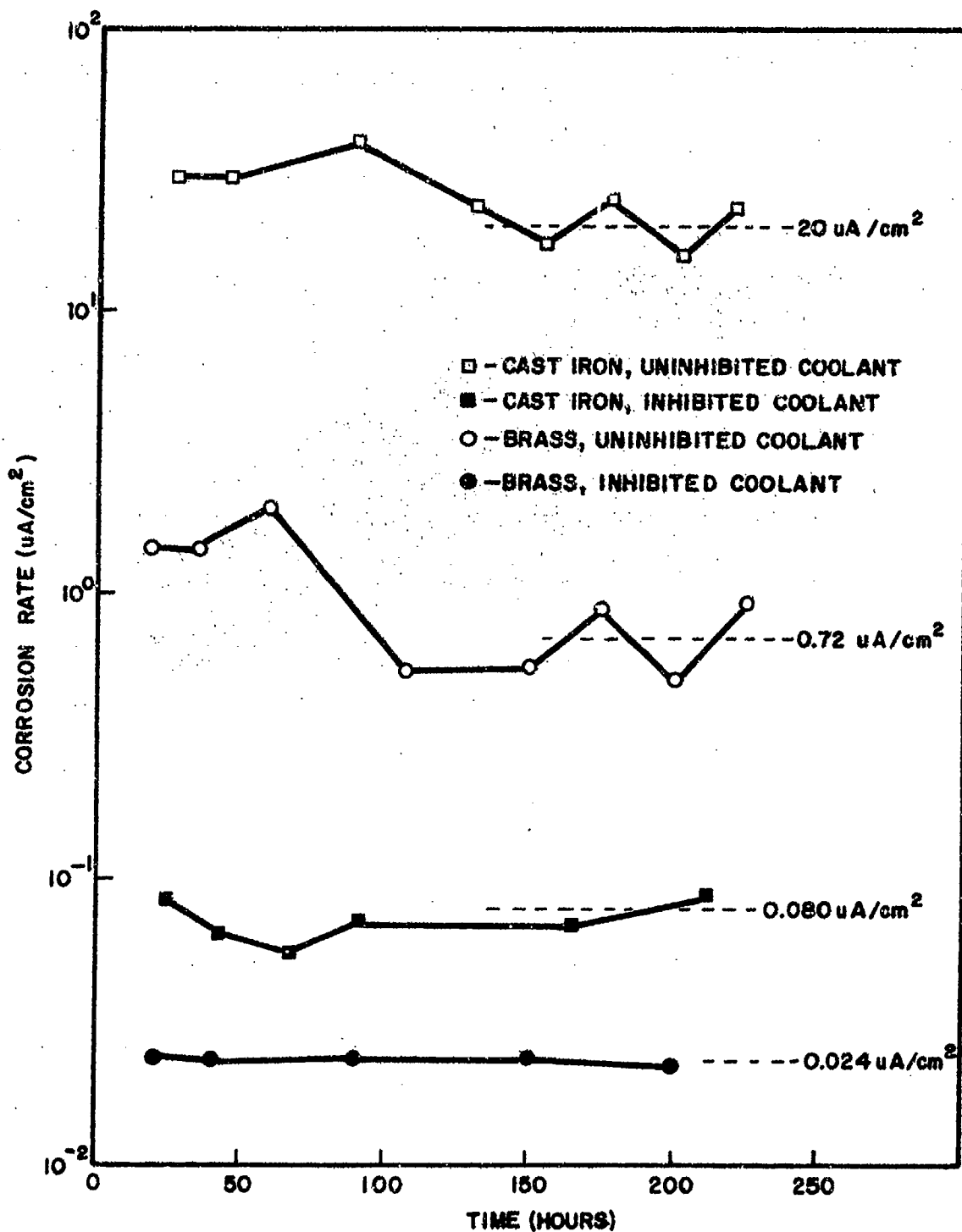
FIGURE 5. CORROSION RATES VS TIME FOR CAST IRON AND
BRASS IN INHIBITED AND UNINHIBITED COOLANT.
Dashed lines indicate steady-state rates.

TABLE I

COMPARISON OF CORROSION RATES IN 700-HOUR
ENGINE TEST - UNINHIBITED COOLANT

Material		Linear Polarization		Weight Change
Copper		3.96		0.527
		6.38		0.389
		5.80		0.381
	Ave.	4.38 uA/cm^2	Ave.	0.436 uA/cm^2
		(2.01 mpy)		(0.200 mpy)
Brass		4.84		0.386
		3.22		0.349
		7.01		0.282
	Ave.	5.02 uA/cm^2	Ave.	0.339 uA/cm^2
		(2.16 mpy)		(0.145 mpy)
Mild Steel		26.5		24.8
		18.8		19.1
		19.1		37.0
	Ave.	21.5 uA/cm^2	Ave.	27.0 uA/cm^2
		(10.3 mpy)		(12.9 mpy)
Aluminum		0.20		2.20
		0.28		4.06
		0.33		2.11
	Ave.	0.27 uA/cm^2	Ave.	2.79 uA/cm^2
		(0.12 mpy)		(1.21 mpy)
Cast Iron		24.0		29.5
		26.9		38.1
		23.0		30.2
	Ave.	24.6 uA/cm^2	Ave.	32.6 uA/cm^2
		(11.8 mpy)		(15.6 mpy)

TABLE II

WHEATSTONE BRIDGE RESISTANCES REQUIRED TO BALANCE IR DROP FOR 200-HOUR ENGINE TESTS

Material	Resistances in Uninhibited Coolant (ohms)	Resistances in Inhibited Coolant (ohms)
Mild Steel	150	500
Cast Iron	1,100	10,000
Copper	100	1,000
Brass	1,100	20,000
Aluminum	180	50

TABLE III

CORROSION DATA FOR 200-HOUR ENGINE TEST

	Uninhibited Coolant		
	Corrosion Rate		Steady State
Material	Wt. Change[1]	Polarization	Corrosion Potential
Mild Steel	10.8	27.7	-120
	40.5	29.2	-150
	33.1	17.8	-120
Ave.	28.1 μA/cm^2	24.9 μA/cm^2	-130 mv
	(13.4 mpy)	(11.9 mpy)	
Cast Iron	43.4	31.6	-180
	30.1	31.4	-180
	27.5	36.1	-180
Ave.	33.7 μA/cm^2	33.1 μA/cm^2	-180 mv
	(16.1 mpy)	(15.9 mpy)	
Copper	0.67	0.81	+ 8
	0.93	0.73	+ 12
	0.65	0.79	+ 8
Ave.	0.76 μA/cm^2	0.78 μA/cm^2	+ 10 mv
	(0.35 mpy)	(0.36 mpy)	
Brass	1.54	1.12	- 6
	1.16	0.99	- 25
	1.16	1.02	- 25
Ave.	1.29 μA/cm^2	1.04 μA/cm^2	- 20 mv
	(0.55 mpy)	(0.45 mpy)	
Aluminum	11.03	0.82	-200
	13.20	0.87	-200
	10.28	1.18	-130
Ave.	11.50 μA/cm^2	0.96 μA/cm^2	-175 mv
	(4.9 mpy)	(0.42 mpy)	

[1] Calculated from the Faraday Equation using the following values for atomic weights: Cast iron and mild steel - 55.85; Copper - 63.54; Brass - 63.54; 6061 Aluminum - 26.98.

TABLE IV

CORROSION DATA FOR 200-HOUR ENGINE TEST

| Material | Inhibited Coolant | | Steady State |
| | Corrosion Rate | | |
	Wt. Change[1]	Polarization	Corrosion Potential
Mild Steel	NM[2]	0.221	-220
	NM	0.197	-200
	NM	0.240	-220
Ave.	NM	0.219 $\mu A/cm^2$ (0.105 mpy)	-215 mv
Cast Iron	NM	0.064	-375
	NM	0.062	-350
	NM	0.095	-350
Ave.	NM	0.074 $\mu A/cm^2$ (0.0035 mpy)	-360 mv
Copper	NM	0.007	-175
	0.13	0.011	-175
	NM	0.005	-175
Ave.	NM	0.008 $\mu A/cm^2$ (0.0036 mpy)	-175 mv
Brass	NM	0.055	-200
	NM	0.011	-160
	NM	0.009	-200
Ave.	NM	0.025 $\mu A/cm^2$ (0.011 mpy)	-180 mv
Aluminum	18.90	7.40	-300
	31.90	9.30	-400
	33.90	37.60	-300
Ave.	27.90 $\mu A/cm$ (11.95 mpy)	18.10 $\mu A/cm^2$ (7.75 mpy)	-330 mv

---

[1] Calculated from the Faraday Equation using the following values for atomic weights: Cast iron and mild steel - 55.85; Copper - 63.54; Brass - 63.54; 6061 Aluminum - 26.98.

[2] NM - None measured.

302

TABLE V

COMPARISON OF CORROSION RATES DETERMINED FROM 700-HOUR WEIGHT-CHANGE DATA AND 200-HOUR STEADY-STATE LINEAR POLARIZATION DATA - UNINHIBITED COOLANT

Material	700-Hour Weight-Change (uA/cm^2)	200-Hour Linear Polarization Steady State (uA/cm^2)
Mild Steel	27.0 (12.9 mpy)	18.8 (9.0 mpy)
Cast Iron	32.6 (15.6 mpy)	20.0 (9.6 mpy)
Copper	0.436 (0.201 mpy)	0.970 (0.447 mpy)
Brass	0.339 (0.144 mpy)	0.720 (0.306 mpy)
Aluminum	2.79 (1.19 mpy)	0.343 (0.146 mpy)

Observations on the Stress Corrosion Cracking of High Strength Aluminum Alloys:
The Effect of Solution pH

by

E. L. MacNamara
Pitman-Dunn Laboratory
U. S. Army Frankford Arsenal
Philadelphia, Pa.   19137

Abstract

The effect of pH on crack initiation in aluminum alloys, 7178-T6 and 2014-T6
has been studied using dynamic as well as static techniques. Under the conditions
for cracking, current increased with time at constant potential. Specimens stressed
below the respective yield strengths cracked when the solution pH was not controlled
but not in alloy 7178-T6 in solutions buffered to a specific pH. Cracking was ef-
fected in alloy 2014-T6 only at pH 8.

Introduction

There presently is no reliable theory of stress corrosion cracking in any alloy
environment system which can be used to predict the performance of material (1).
Researchers have attacked the problem by studying structural defects, mechanical
faults, composition and manufacturing history of the alloy and the influence of var-
ious environments.

One technique for evaluating the mechanism of stress corrosion cracking in mul-
tiphase alloys or polycrystalline material is electrochemical. Anodic dissolution
is accelerated by yielding in pure metals which are normally immune to stress corro-
sion cracking, but in alloys that are non-susceptible such an effect is not seen.
In susceptible alloys plastic deformation, as opposed to elastic strain, produced
large changes in corrosion rates (2). In high strength aluminum alloys it may be
possible for microregions of plastic strain to exist in the elastic range, the size
of which are dependent upon the level of yield stress. The plastic yielding would
generate electrical potential changes (3) which could be measured, thereby allowing
the characterization of crack initiation and propagation. If the changes were large
enough in these preferred sites to enhance the corrosion reaction, cracking might be
initiated.

Experimental Procedure

Extruded wires, 0.20 cm diameter x 7.5 cm, of alloys 7178-T6 and 2014-T6 were
threaded on each end, placed into 0.635 cm aluminum stock fitted through lucite
blocks and fastened in the jaws of an Instrom T.M. Tester. The lower rod was passed
through a rubber stopper in the bottom of a glass tube, 45 mm diameter. With auxil-
iary platinum electrodes, a standard calomel electrode and the electrolyte solution,
this configuration comprised the cell in which the electrochemical measurements were
made. The surfaces to be exposed were prepared immediately before the specimens were

---

Key words: stress corrosion, aluminum alloys, pH polarization

assembled in the holders. The wires, with threads protected, were placed in a Jacobs chuck attached to a constant speed motor. The specimens were abraded with moist 600 carbide paper, 400A and finally 4/6 emery paper, while being rotated, to expose a "fresh" surface. The polarization characteristics of these specimens were obtained in 0.1N KCl using an Anatrol Model 4100 Potentiostat. Scans were made by increasing the potential fifty millivolts every sixty seconds beginning with −1500 mv and the current was recorded immediately before each adjustment. The electrolyte was unstirred and open to the atmosphere. Fresh solution was used for each run. Adjustments in the pH of the 0.1N KCl were made using buffer reagents, which would give round values of pH, prepared in accordance with published procedures (4). There were no effects due to "foreign ions" introduced by the buffer salts.

Results and Discussion

Potential-current profiles were obtained potentiostatically in 0.1N KCl for alloys 7178-T6 and 2014-T6 while stressed at 50% Y.S. and 75% Y.S.[*] respectively and compared to similar data obtained on unstressed specimens of the same material. Chemical analyses of the as-received material revealed the following composition:

	7178-T6	2014-T6
Cu	1.87%	4.62%
Si	0.1-.2%	0.7/1.2%
Fe	0.2-.4%	0.4/0.7%
Mn	less than 0.01%	0.44%
Zn	6.75%	0.1/0.2%
Mg	2.7%	0.39%
Ti	0.06%	None detected
Cr	0.2-.4%	less than 0.05%
Sn-Pb	none detected	none/less than 0.02%
Ni	less than 0.01%	less than 0.01%
Al	remainder	remainder

Cracking occurred in the stressed specimens used to obtain the potential-current profiles. Fissures, rather than complete fractures, were obtained which were parallel to each other and normal to the direction of the applied tension. To corroborate these observations, specimens of alloy 7178 were loaded to 50% Y.S., the previous maximum stress, and subjected to an applied potential just cathodic to the corrosion potential previously observed in the potential current profiles. Within three minutes, the current becoming anodic changed direction. After this experiment, several cracks were observed in the specimen which were identical to those seen in the earlier specimens. The second alloy cracked in the same manner, but only after periods of sustained loading at 75% Y.S. (In this case the load was identical to that used for the other alloy.) Since the materials used in this study were extrusions, specimens were oriented in the longitudinal direction. Tensile stress was applied parallel to the grain orientation. Cracking occurred normal to the direction of stress and prevailing grain orientation. A precipitate formed in the electrolyte, and the pH had increased markedly. A slight change in the pH is expected since the electrode

---

[*] Yield Strength 2014-T6 = 65,000 psi
                    7178-T6 = 83,000 psi

reaction proceeds with the scan, changing the environment. However, this obvious change did necessitate a control on the electrode reaction in order to define the parameter of crack initiation. With this in mind, portions of the electrolyte stock solution (0.1N KCl) were buffered to definite pH levels, and with other conditions unchanged, polarization characteristics were reexamined through the range of buffered pH. Two major trends were noted in the curves generated from this data: curves were displaced toward the anodic direction with increased pH; curves were displaced to higher decades of current density with decreased pH. Within a pH unit, potentials of alloy 2014-T6 under stress were approximately 100 mv more positive than that of unstressed specimens. Specimens of alloy 7178 under stress usually displayed potentials more negative than those of their unstressed counterparts.

The surface of specimens subjected to the buffered electrolyte in the polarization studies was noticeably different when compared to specimens from the various pH levels and to those from solutions in which the pH was not controlled. Specimens from the uncontrolled solution were dark and rough, whereas specimens from the controlled solutions were smooth and somewhat tarnished with a sheen. There were some discrete dark gray areas, apparently the sites of selective reaction but with no evidence of erosion or corrosion products. Specimens treated at the pH 3 and 5 levels were compared under a magnification of 30 x. Stressed specimens at both levels of pH were pitted; those at the lower pH were peppered with minute but distinct pits surrounded by strains. The remainder of the surface was dull and mottled. At the higher pH there were a few, large, isolated pits as well as some darkened areas roughened by erosion. There was no pitting at either level of pH in the unstressed specimens. In the more acid pH, surfaces were silvery although dulled by contact with the solution and were "freckled" with darker gray, non-uniform areas. At the higher pH, the surfaces were very dull gray with well defined black spots. There were no precipitates in these buffered solutions at the end of the polarization experiment, although a white flocculent precipitate was present in the unbuffered solutions in which cracking occurred. When pH was controlled cracking could not be effected in alloy 7178-T6 through the range to pH 9. Cracking occurred at pH 8 but at no other level in alloy 2014-T6. Examination of the micro structures showed a uniform grain size and some undissolved precipitate in alloy 2014-T6 and a slight grain elongation and grain boundary precipitate in alloy 7178-T6.

The electrochemical characteristics of the alloys in the T6 condition were further examined under constant applied potential as a function of pH, using the aforementioned buffered electrolyte. The current was recorded at each applied potential. When the current became constant, tension was applied to the specimen without interrupting the experiment. Recording of the current continued as the load varied at a constant strain rate to the maximum value which represented 50% Y.S. The points at which tension was initially applied and maximum load was attained are noted in Fig. 1. The experiment continued until the current reached zero or was constant. The results for alloy 7178 were compared to data collected in the unbuffered electrolyte. At pH 3 little current flowed initially, but after a short time reached a maximum of 5.9 ma. Over the next ten minutes the current dropped by approximately 1.5 ma and remained at this level through loading. At pH 5 the maximum current recorded at zero time decreased steadily reaching a plateau. There was then another rapid decrease in the current through loading which reached a constant value coincident with attainment of maximum load, with a subsequent slight decrease through the end of the test. In the unbuffered solution the current gradually dropped from the initial maximum of 6 ma to a constant value of approximately 4.2 ma. When tension was applied the current dropped immediately to 3 ma, then increased rapidly until at

maximum load it had returned to the no load plateau of 4.2 ma. At pH 7 there was a
sharp decrease in the current from 6 ma to 3 ma until the initial point of loading.
During the loading, current continued to decrease at a slow rate, reaching 2.6 at
maximum load. The current leveled off at 2.2 ma and after several minutes the ex-
periment was discontinued. Alloy 2014-T6 was much more active at this pH, and the
initial current doubled during the loading period (Fig. 2). It reached a maximum
of 4 ma at maximum load. Very little current flowed at pH 5. In the first eight
minutes, the current decreased from 0.03 to 0.015 ma, then increased to .02 ma at
maximum load. The current stabilized at 0.024 ma after a period of slight fluctua-
tions. At pH 3 this alloy was quite active with the initial current pulsating
rapidly, at times exceeding the recorder limits. However when loading began, the
current stabilized at 3.5 ma through the loading period with no change on reaching
maximum load.

Current versus time curves were also recorded at -750 mv in 0.1N KCl, unbuf-
fered with specimens of the 7178-T6 alloy. Maximum load was attained before apply-
ing the potential. Under these conditions the current passed through a maximum
during the first three minutes and approached zero after thirteen minutes. On the
other hand, if tension was not applied, there was a slight increase in current flow
with a steady maximum being reached in five minutes. The total increase was 50
microamps.

Through the range of pH 7-9, current measurements were made at definite load
levels of two minute duration. The zero time value represents current density after
two minutes, with each successive two minute interval representing 10% Y.S. incre-
mental increased in load up to the final value of 50% Y.S.

Grain morphology, preferred orientation, directional stress have all been con-
sidered in the control of crack propagation in the intergranular stress corrosion
failure of aluminum alloys. While studying these influences in 7075-T6, Ugiansky
et al., (5) reported greater pitting of unstressed than stressed specimens using
chromate containing chloride solutions at a pH less than 1. "Stifling of the pit-
ting" was attributed to "an internal cathodic protection mechanism" of the cracking
grain areas. The pitting potential of pure aluminum in 1M sodium chloride has been
reported at -0.48 (SHE) volts (6). Although it is independent of pH and tempera-
ture, it does become more active (negative) with increased chloride concentration.
Aluminum alloys containing only small amounts of manganese and magnesium showed
greater tendency to pit, while traces of Cu^{++} accelerated pitting action. Evidence
presented purportedly supports the theory of competitive adsorption to explain the
critical (pitting) potential mechanism. Another theory involves the relative ease
of chloride diffusion through the oxide film to explain the presence or lack of
pits (7).

It was noticed that certain of the specimens exposed in this study did appear
to have a non-continuous film having the color and luster of copper. In particular,
slow (oven) quenched alloy 2014-T_{exp}. containing 4% copper presented such a film
after exposure in 0.1N KCl buffered to pH 8 for forty-eight hours. The specimen was
under an applied tensile stress equal to 45% Y.S. and an applied potential of
-600 mv/(SCE). Prior to the interruption of the experiment an anodic current flow
of 0.1 ma was recorded. There were no pits or fractures, but there was slight gen-
eral corrosion with a few dark spots. From comparison of the polarization data for
this experimental heat treatment (both on stressed and unstressed specimens), with
normal T6 specimens, pitting should be expected if the critical potential is in fact

not pH sensitive. The applied potential was fifty millivolts more negative than the published critical (pitting) potential and the current was double that recorded at this potential in the normal T6 potentiodynamic scan. Furthermore under stress, the corrosion potential was 100 mv more anodic than that at zero load. The applied potential was anodic to the corrosion potential. This work will be the subject of another paper.

The apparent dependence of crack initiation upon pH of the electrolyte is significant. When the solution pH was controlled and a potential applied to alloy 7178-T6, the current decreased with time indicating that the electrode reaction rate, i.e. film formation, was under dissolution control. In the unbuffered electrolyte (the condition under which rapid cracking had occurred) the current increased with load (time) indicating that the reaction in this case was controlled by the rate of film growth (covering surface). With alloy 2014-T6 cracking occurred only after sustained loading in the unbuffered electrolyte. It was clearly demonstrated that when the solution pH was controlled, cracking could be induced at high pH levels and deterred at the same level by adroit changes of the potential. A definite increase in current with time and load occurred at pH 7 but not at any pH below this level (Fig. 2). It would seem therefore, that when the electrode reaction was not influenced in any way, i.e. in applying constant potential, and was permitted to proceed naturally cracks would not be initiated until the solution pH reached the higher level. At this point diffusion through the film already formed could occur readily. It has been reported that the corrosion rate is primarily controlled by transfer of ions and electrons through the film (8). These data support this premise. If the mechanism depends upon diffusion through the film the decrease in current at pH 5 (Fig. 1 and Fig. 2), might be explained in several ways. The solubility of several species might decrease causing rapid thickening in the film. The diffusion of the current carrying species is directly related to porosity and is inversely proportional to the thickness. A complexed layer could form on the surface of the film, which would inhibit diffusion by reducing the porosity of the film. If the films were ductile under the influence of tension, and rupture did not occur, there would be no fresh metal surface exposed to the corrodent. Diffusion could continue to be hindered by either complexing or precipitation of current carrying species and the corrosion process stopped.

Conclusions

From data reported here crack initiation in high strength aluminum is pH dependent. This dependence is evidence for the participation of surface films in the cracking mechanism and reinforces information previously reported suggesting the major role of these films.

References

1. R. W. Staehle, Ed. Fundamental Aspects of Stress Corrosion Cracking, Proceedings of the Conference, Sept. 1967, Ohio State University.

2. A. R. Despic, R. G. Raicheff and J. Bockris, J. Chem. Physics, 49, 926 (1968).

3. A. G. Funk, J. C. Giddings, C. J. Christensen and H. Eyring, J. Phys. Chem., 61, 1179 (1957).

4. R. A. Robinson and R. H. Stokes, "Electrolyte Solutions," 2nd ed., Butterworths, London: Academic Press, Inc., N. Y., 1959.

5. G. M. Ugiansky, L. P. Skolnick and S. W. Stiefel, Corrosion, <u>25</u>, 77 (1969).

6. H. Bohni and H. H. Uhlig, J. Electrochem. Soc., <u>116</u>, 906 (1969).

7. M. Streicher, J. Electrochem. Soc., <u>103</u>, 375 (1956).

8. M. C. Pryor, J. Electrochem. Soc., "News Notes," May 1971.
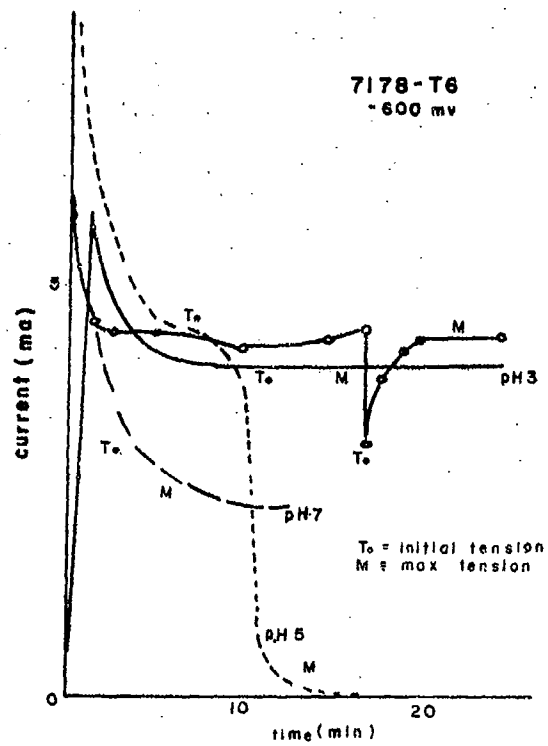
FIGURE 1. The effect of pH and variable load on current flow at fixed applied potential in alloy 7178 T6.
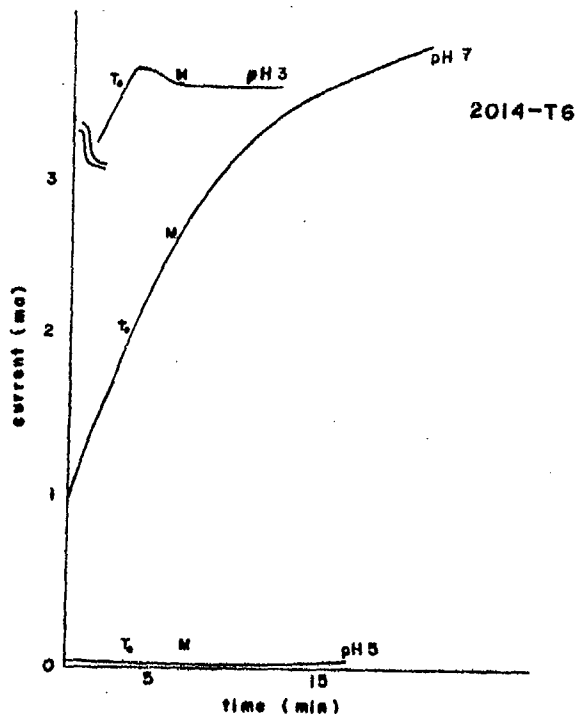
FIGURE 2. The effect of pH and variable load on the current flow at fixed potential in alloy 2014 T6.

311

SESSION VII

PROTECTIVE LONG-TERM STORAGE TECHNIQUES FOR MILITARY EQUIPMENT

DESERT STORAGE TEST PROGRAM

Capt W. C. Connors, 1Lt J. A. Blind and 1Lt L. R. Klein
Military Aircraft Storage and Disposition Center
Davis-Monthan Air Force Base, Arizona 85707

INTRODUCTION

The Desert Storage Test Program was conducted at the Military Aircraft Storage and Disposition Center (MASDC) from January 1972 to February 1974. MASDC is the single DOD operating agency for the storage of non-active inventory military aircraft. It is located on the eastern edge of the Sonoran Desert adjacent to Davis-Monthan AFB in Tucson, Arizona. The desert environment of MASDC makes it an excellent place in which to store aircraft and many of the approximately 6000 aircraft at MASDC are in long-term storage awaiting reactivation, cannibalization, or sale as scrap. The techniques used to preserve aircraft for long-term storage have for years been based upon engineering judgment without any actual technical data on internal aircraft environment and its effect on materials during storage. In recognition of this fact, technical and management personnel from the Army, Navy, and Air Force met at MASDC in January 1972 in order to develop a test program capable of providing the data needed to simplify, standardize, and revalidate MASDC long-term aircraft storage procedures. This Desert Storage Test Program was initiated to provide data on the most effective and least costly methods of aircraft preservation and to revise the <u>Desert Storage Preservation and Process Manual for Aircraft</u> (T.O. 1-1-686/NAVAIR 15-01-4/TM 55-1500-331-34).

EXPERIMENTAL PROCEDURE

The primary goal of the program was to determine the temperature and relative humidity conditions inside stored aircraft and to evaluate the effect of these conditions on aircraft materials. Figure 1 lists the 53 aircraft which were committed for use in the test. These aircraft provided a representative sample of aircraft types in storage at MASDC; i.e., fighter, bomber, cargo, utility, and helicopter. Each of the aircraft were preserved for storage by one of the preservation processes depicted in the figure. The Air Force and Navy Processes involved preservation and sealing in accordance with existing MASDC operating technical directives. The major difference between Air Force and Navy procedures was a requirement for extensive corrosion control for the Navy process. No sealing or preservation was done to Minimum process aircraft except

for the treatment of engines and fuel systems. The aircraft grouped in the State-of-the-Art category were used as test beds for the testing of a number of new preservation materials and techniques such as tapes, coatings, and sealing methods. However, in this paper, we will confine our discussions to the main area of the program which involved only the Air Force, Navy, and Minimum Process aircraft. The material used to seal all aircraft was a water based sprayable, strippable, plastic coating (Mil-C-6799, Type II) called Spraylat.

Environmental

Prior to sealing with Spraylat, each of the test aircraft was instrumented with an Abbeon Type M2A4 Temperature/Relative Humidity instrument in a manner similar to that depicted in Figure 2. A comparison of the ambient condition data generated by these instruments with similar data obtained from official sources indicated that the M2A4 instruments retained good accuracy during the storage period. A total of 134 M2A4 instruments were placed in selected areas of the 53 test aircraft including cockpits, camera bays, fuselage windows, and engine intakes and exhaust locations. Instrument readings were taken manually twice daily, once at the time of projected minimum ambient temperature and once at the time of maximum ambient temperature. The environmental data generated was computer processed to reveal significant trends.

Material

The internal aircraft environment was related to material condition changes during storage using two separate techniques. The first method involved visual observation and photographic documentation of the before and after conditions of selected aircraft areas and components. Material condition changes were also evaluated by placing test plates of representative metallic materials inside aircraft prior to sealing. The extent of corrosion initiation and growth on the test plates was determined at the end of the test. The sizes and types of test plates used in the program are listed in Figure 3.

RESULTS AND DISCUSSION

Several significant trends were found in the environmental and material condition change data.

Temperature

Temperatures inside various aircraft locations followed two general patterns. Air temperatures inside fuselage and engine locations, as shown in Figure 4, tended to follow ambient temperatures closely. Sealing was found to have little effect on temperatures in these areas. However, in areas exposed to direct sunlight such as uncovered cockpits, this was not the case, as shown in Figure 5. While temperatures in Spraylat-covered cockpits stayed within ± 10°F of ambient, the temperatures in uncovered cockpits rose considerably higher. The temperatures inside the uncovered bubble-type canopies exceeded 160°F for over one-third of the test period, mainly during the summer months. Temperatures as high as 190°F were recorded. The absorption of solar energy by seats, panels, and other structures inside uncovered cockpits resulted in the development of these significantly elevated, potentially damaging air temperatures. Extended exposure to elevated temperatures can damage many plastic and elastomeric materials in aircraft cockpits. Figure 6 shows severe delamination of an uncovered EB-66E test aircraft canopy which occurred as a result of the high temperatures and high ultraviolet radiation exposures encountered during storage. O'her more minor effects of heat and ultraviolet radiation were noted.

Relative Humidity

Literature research[1,2,3,4,5,6] has indicated that for ferrous materials little or no corrosion growth occurs below about 40% relative humidity (R/H). Between 40% and 70% mild corrosion growth occurs, and above 70%, corrosion growth is extensive. For non-ferrous materials, these ranges are not as well defined but some relationship of increasing corrosion to increasing relative humidity does exist. The 40% and 70% levels were

used as reference points in evaluating the test program
relative humidity data. As with temperature, the relative
humidity levels were found to vary from one location within
an aircraft to another. On the whole, relative humidity
inside aircraft fuselages tended to follow the pattern shown
in Figure 7. The relative humidity in these locations was
independent of sealing and fell somewhat below ambient. How-
ever, sealing was a factor in engine and cockpit locations.
As shown in Figure 8, the relative humidity inside sealed
engines remained consistently below ambient while the rela-
tive humidity in uncovered engines was on the average above
ambient. The level of relative humidity inside cockpits
and engines is dependent on sealing because the relative iso-
lation of cockpits and engines from adjacent aircraft areas
makes the sealing process more effective. On the otherhand,
the sealing of fuselages is less effective due to the large
number of seams and the need to leave undersides unsealed
to provide drainage.

Test Plates

The relative humidity level correlated closely with corrosion
data obtained from photographs and test plates where ferrous
materials were involved. Overall, test plate corrosion was
not severe. Type 4340 steel and type AZ-31B magnesium alloy
exhibited the most severe corrosion. Test plates in aircraft
in which relative humidity exceeded 40% for the greatest amount
of time tended to exhibit the greatest degree of corrosion.
Lower test plate corrosion levels were noted in sealed cock-
pits. The amount of corrosion on test plates located in fuse-
lage areas appeared to be unrelated to the extent of aircraft
sealing.

Photographic Documentation

The before and after photographs of aircraft components showed
very few cases of significant corrosion growth. The majority
of the corrosion involved rusting of exterior surface steel
components. Corrosion growth on interior or exterior non-
ferrous components was not found to a significant extent.
Corrosion increases were independent of the preservation tech-
nique used.

317

SUMMARY

In summary, the temperature and relative humidity levels, with the resulting effects on aircraft materials, determined the extent of sealing required for various locations. Fuselages, with the exception of water entrapment areas, require a minimum amount of sealing. These and other test program related changes to existing procedures were recommended to and adopted by the Triservice Task Group in May of this year and have since been implemented into the operating technical directives at MASDC.

ACKNOWLEDGMENT

REFERENCES

(1) N. D. Tomaskov, "Development of the Electrochemical Theory of Metallic Corrosion". Corrosion, Vol 20, No. 1, Jan 1969.

(2) Glen Greathouse and Wessel, Deterioration of Materials, Causes and Preventive Techniques, New York: Reinhold Inc., 1954, p. 721.

(3) Preservation, Packaging, and Packing of Military Supplies and Equipment Preservation and Packaging, Vol I, NAVAIR 15-01-1, Jan 1968, p. 48.

(4) Herbert Uhlig, Corrosion and Corrosion Control, New York: John Wiley and Sons, Inc., 1963, pp. 146-147.

(5) Joseph Bosick, Corrosion Prevention for Practicing Engineers, New York: Barnes and Noble, Inc., 1970, pp. 92-93.

(6) Hugh Godard, W. Jepson, M. Bothwell, and Robert Kane, The Corrosion of Light Metals, New York: John Wiley and Sons, Inc., 1967, p. 95.

PROCESSES

	FIGHTERS	BOMBERS	CARGO	UTILITY	HELICOPTER
AIR FORCE	TF9J	KA3B	RC45J	OVI	UH1A
	F4B	EB66E	WC121N	U6A	OH23D
	RF101H		C119J	T33A	CH34C
NAVY	TF9J		RC45J	OVI	UH1A
	F4B	EB66E	WC121N	U6A	OH23G
	RF101H		C119J	T33A	CH34C
MINIMUM	TF9J	KA3B	RC45J	OVI	UH1A
	F4B	EB66E	C121J	U6A	OH23D
	RF101H		C119J	T33A	CH34C
STATE OF THE ART	TF9J		RC45J	OVI	UH1A
		EB66E	NC121K	U6A	OH23D
	RF101H		C119J	T33A	CH34C

FIGURE I. STORAGE TEST AIRCRAFT

FIGURE 2. INSTRUMENTED TEST AIRCRAFT

Small Type Test Plates

Designation	Size (in)	Material
A	1 x 2	4340 Steel
B	1 x 2	1020 H-24 Steel
C	1 x 2	1100 Aluminum
D	1 x 2	7178 T-3 Aluminum
X	1 x 3	7075 T-6 Aluminunm
Y	1 x 2	AZ31B Magnesium

Large (Pacer Lime) Type Test Plates

Designation	Size (in)	Material
A	5 x 6	2014 T-3 Clad in contact with AZ31B Magnesium. Total weight of both panels
B	5 x 6	2024 T-3 - 7075 T-6
C	5 x 6	AZ31B Magnesium
D	5 x 6	7075 T-6 Aluminum
E	5 x 6	7079 T-6 Clad Aluminum
F	5 x 6	4130 Steel

FIGURE 3. COMPOSITION OF TEST PLATES
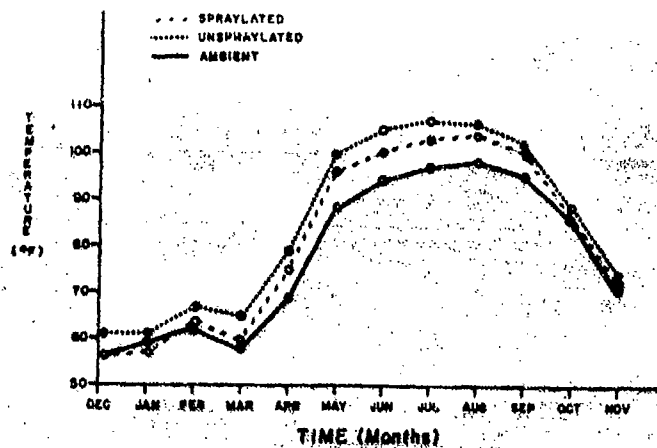
FIGURE 4. C-119J FUSELAGE TEMPERATURE VS. AMBIENT TEMPERATURE

Legend:
- - - SPRAYLATED
.... UNSPRAYLATED
——— AMBIENT
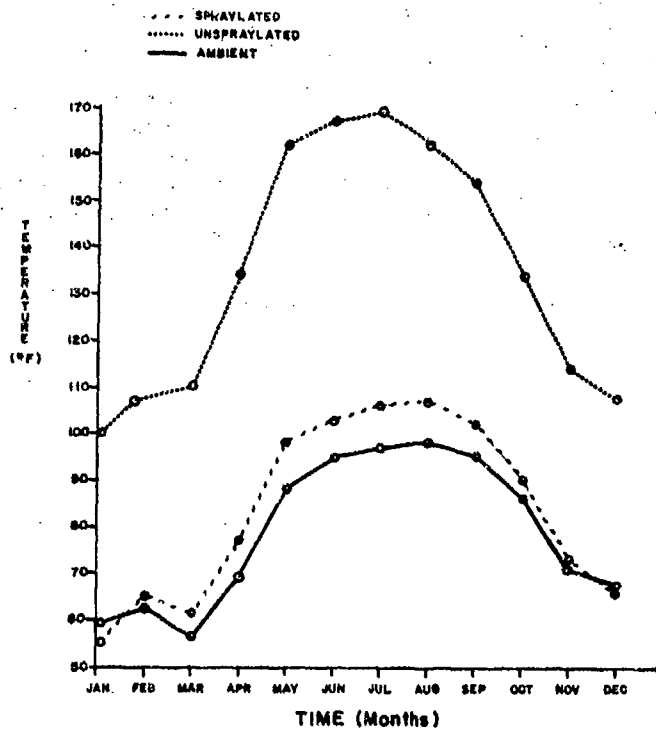
FIGURE 5. TF-9J COCKPIT TEMPERATURE VS. AMBIENT TEMPERATURE
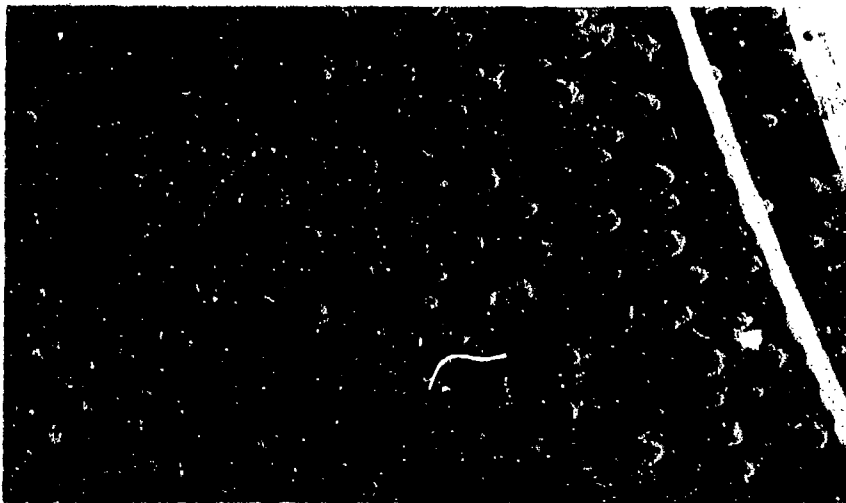
FIGURE 6. EB-66E CANOPY BUBBLES
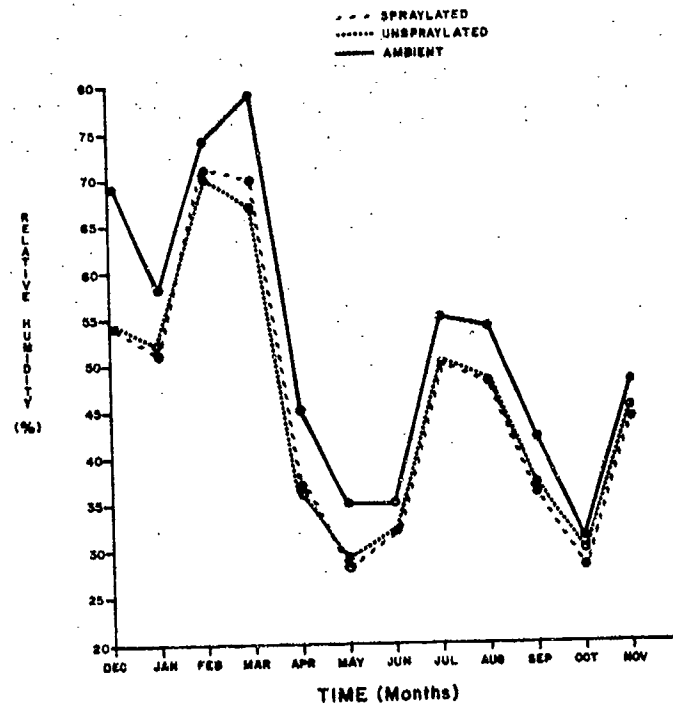
FIGURE 7. C-119J FUSELAGE RELATIVE HUMIDITY VS. AMBIENT
RELATIVE HUMIDITY
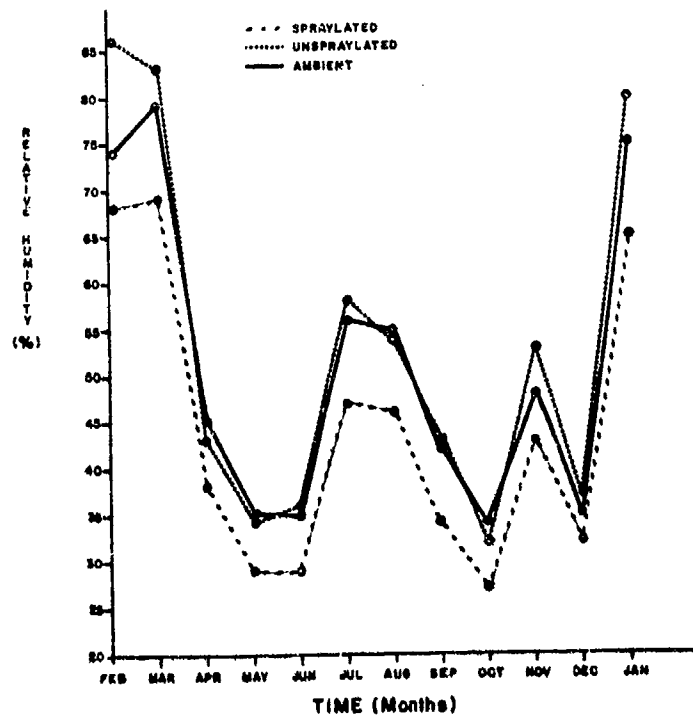
FIGURE 8. F-4B ENGINE RELATIVE HUMIDITY VS. AMBIENT
RELATIVE HUMIDITY

323

WEATHER DATA AND ITS USE IN CORROSION STUDIES

by

Oscar E. Richard
and
Hilda J. Snelling

We represent the USAF Environmental Technical Applications Center (commonly called ETAC), an organization of the Air Weather Service. The mission of ETAC is to provide quantitative advice and studies on the effects of the natural environment across a broad range of DoD activities -- planning, operations, design, development, test, engineering, intelligence. Our products are tailored to the particular problem at hand, in this case corrosion and more specifically corrosion control.

Recently, summaries of hourly weather observations in specified formats were given to the AFLC Corrosion Management Office for Project "RIVET ERIGHT." Efficient use of these and other weather data demands that those needing it know what to ask for, what they are getting, how the elements are observed and summarized, and the realistic limits of the observed values. Our briefing will discuss these items and how the use of weather data must be tailored to the problem addressed.

Let us consider first relative humidity. This parameter is not observed directly at a weather station as it is in many homes with handy wall weather units. It is derived from the coincident observations of the dry bulb temperature and the dewpoint temperature. Relative humidity is just that, a relative evaluation of the humidity. It is not a measurement of the actual water content in a parcel of air. For example, with a dry bulb temperature of 80°F and a dewpoint of 70°F, the relative humidity is approximately 70% and water content is 110 grains of water vapor in one pound of dry air. With a dry bulb temperature of 50°F and a dewpoint temperature of 41°F, the relative humidity is again 70%, but the actual water content decreases to 38 grains of water vapor per pound of dry ice.

The dewpoint temperature is directly related to the amount of moisture in the air. Condensation will occur when an air parcel is cooled to its dewpoint temperature. The amount of moisture in the air will vary with the temperature; the

warmer the air, the greater its capability to hold moisture and vice versa. As an example, air with dry bulb temperature of 80°F and a 4° spread between the dry bulb temperature and the dewpoint temperature can hold 136 grains of water vapor per pound of dry air; whereas, with the same 4° spread at a dry bulb temperature of 50°F, the air can hold only 47 grains of water vapor.

It is a characteristic of the dewpoint temperature that a spread of 4° or less may occur only around sunrise at some stations in a continental climate. In maritime or tropical climates this spread may continue for as long as the entire day. We presented to the Corrosion Office a summary showing days with 3 or more consecutive hours of less than 4°F spread between the dry bulb temperature and its dewpoint temperature. Is this the critical statistic? Or is it water content? If the actual water content is important in the corrosion process, a detailed study of this parameter might be a better way to evaluate corrosion.

Precipitation is another element involved in the corrosion process. It has a dual role or effect. It can both cause corrosion by its presence and also prevent corrosion by washing away corrosive elements. Both the amount and rate of precipitation must be considered. Moderate and heavy precipitation appear to be most effective in the washing process. We define moderate precipitation when 0.11 inches to 0.30 inches of precipitation has fallen in the last hour or 0.01 to 0.03 inches falls in a 6-minute period. Heavy precipitation is recorded when the rainfall rate is in excess of these amounts. Precipitation durations might be a critical factor in studying corrosion. Light rain falling continuously for several hours may result in a greater accumulation of precipitation than moderate or heavy rain over shorter periods of time, thus becoming more effective in the washing process.

The occurrence or nonoccurrence of cloud cover was used in the corrosion study to determine the availability of sunshine for evaporative purposes. Ceilings are defined when more than 5/10 of the sky is covered by opaque clouds. Evaporation occurs when more than half of the sky is covered with clouds as well as when there is "no ceiling." Considerable radiation for drying purposes may occur when ceilings are reported or with an overcast of high, thin (transparent) clouds. A limited number of observing stations have instruments which record both direct and diffused solar radiation, as well as the total solar radiation. Although solar radiation is available at only one or two Air Force Bases, it can

326

be interpolated for others. Direct measurements or estimates of solar radiation may give a better resolution of evaporation than "just sunshine" as defined by "no ceiling" or other cloud statistics.

Wind is used in determining both evaporation rates and the transport of aerosols. Its velocity, until recently, could not definitively be recorded below 3 MPH. Any wind velocities below 3 MPH may be inaccurate and, more often than not, recorded as calm. Any attempt to define wind categories based on winds below 3 MPH is unrealistic. The influence of water and/or salt sources (proximity to the sea) is affected by air-mass flow or, more simply, by the wind direction and speed. If the wind is flowing offshore (from land to sea), little or no salt spray will affect equipment onshore. On the other hand, a strong onshore wind could carry a heavy dosage of salt spray several miles inland. This factor could vary considerably; its overall effect on any corrosion classification system being strongly dependent on wind direction and speed and time of day, as in the case of land-sea breezes. It is possible that the meteorologists should be providing fallout patterns for salt spray based on available wind statistics.

Next, we would like briefly to discuss the availability of weather data for a specific site of interest. If no data exist for the site, and time permits, an observation site should be established. The data taken at this site can then be correlated with the nearest weather reporting station to determine the site's longer weather regime for the correlation statistics. Weather, as you know, is dependent on the local terrain, its roughness, type of vegetation, and exposure. A weather station 10 miles away could give a very good description of the site of interest but, on the other hand, the actual site weather could be vastly different as a result of its locale. The accuracy of the data required will often determine the use of substitute sites directly. The accuracy of other elements of the study used in conjunction with weather statistics will also help determine the accuracy requirements of the weather data.

In summary, our briefing boils down to just one point: better communication between the applied climatologist and the project manager to define the total study requirements. Only then can we tailor our product to provide an optimum weather input, which in turn leads directly to improved models and defense savings.

U.S. ARMY - EXPERIMENTAL LONG-TERM STORAGE PROGRAM COMPREHENSIVE REPORT

A. Gallaccio, W. J. Shields, and W. F. McTeague

Materials Engineering Division
Pitman-Dunn Laboratory
Frankford Arsenal
Philadelphia, Pennsylvania

SUMMARY

A brief history of the Experimental Long-Term Storage Program is presented. Based on observations over an eight-year period, several methods for long-term preservation of Ordnance materiel are evaluated. Successful methods include storage of materiel in unit or multi-unit containers of metal or plastic in which an atmosphere with an average relative humidity of less than 40 percent is maintained.

During the eight years of this program 713 of the original 1028 containers have been opened and the inspected.

The applications of the various methods of preservation utilizing low humidity atmospheres without other preservatives have been found adequate for small arms, field or antiaircraft artillery, automotive materiel, and fire control equipment.

Low humidity air has been found to provide preservation equal to low humidity nitrogen, and to be more practical from the economic and versatility standpoints.

The solar radiation breather has been found highly effective in maintaining a low humidity atmosphere within a balanced pressure container.

Unexercised assembled recoil systems and motor driven generators in de-humidified storage have been found serviceable after eight years.

Immersion in oil has provided adequate preservation of metal but, as expected, has been detrimental to rubber. This method of preservation is not recommended because of its high cost and weight.

The use of volatile corrosion inhibitors is not feasible for the mass preservation of complex ordnance items.

INTRODUCTION

Principally, the results are concerned with the seven years of the program under Frankford Arsenal supervision, but earlier information, accumulated prior to 1948 under contract, is included since this report is intended to be comprehensive.

Much of the data on which evaluations of storage methods are based herein are given in greater detail in Frankford Arsenal Memorandum reports of teardown inspections which have been issued on inspections made since January 1948. Numerous references to the Memorandum Reports have been included in order to assist the reader in gaining access to the specific data which he might require or for which he has special interest.

HISTORICAL BACKGROUND

During the latter part of 1944, the Office, Chief of Ordnance, Artillery Division, Industrial Services (OCO-ORDIR), became acutely concerned with the problem of storage of Ordnance materiel and was instrumental in starting an investigation of long term storage methods. This concern was fostered by the anticipated return to this country of large quantities of materiel from the theaters of war, and the preservation of newly manufactured materiel. In pursuance of this, Office, Chief of Ordnance, ORDIR, in September 1944, assigned to Engineering and Inspection Control Branch (SPOIR) the responsibility of accomplishing a literature survey and of making inquires of the various agencies believed to have knowledge or technical experience in longterm preservation methods for ordnance materiel.

Originally, Army Ordnance planned to store materiel in disassembled condition, but by early 1945 decided to inaugurate the experimental program of storing semi-assembled materiel in metal containers. A proposal of an experimental method of long-term protection of materiel in individual metal containers was outlined in a memorandum[10] issued by the Office, Chief of Ordnance.

The memorandum[10] from the Chief of Ordnance also stated that "contact will be maintained with the Navy, Air Force, and any other Government agency for exchange of information on this program."

A comprehensive literature survey relative to storage and preservation was provided in several reports[72] issued in late 1945 and early 1946 by Battelle Memorial Institute.

The first general meeting on the use of steel containers for long-term storage was held and recorded[14] at Frankford Arsenal on 26 April 1945.

Representatives of each service, technical agency, and the prime industrial contractor concerned with this program at the time were present. The division of assignments between Frankford Arsenal (FSCO), American Bridge Company, and International Harvester Company, was given as follows:

Frankford Arsenal - Design of metal containers for all types of fire control equipment;

American Bridge Company - Design of metal containers for all types of large weapons;

International Harvester Company - Design of metal containers for all types of small arms.

A request[15] was made by ORDIR to investigate thin wall metallic barriers with special breathers for equalizing container pressures with the outside atmosphere. The special breathers (solar radiation type) and containers (sheet aluminum) were suggested by the Davison Chemical Corporation. This phase on the thin wall, balanced pressure containers was placed under the direction of the Fire Control Sub-Office, Frankford Arsenal, who assigned it, under contract, to the Davison Chemical Corporation.

The completion date for placing various items in individual steel and aluminum containers was originally given as 1 September 1945 (later changed to 15 October 1945 by ORDIR) in a memorandum[15] from the Chief of Ordnance to his special representative. A memorandum[16] issued by Office, Chief of Ordnance, 20 July 1945, presented a listing of the various containers, the materiel to be placed in them, and the quantity of each item.

A total of 1992 containers were required to store the items referred to in the Office, Chief of Ordnance memorandum.[17] The construction of containers, however, was curtailed in June 1946, at which time 1041 containers had been completed.

In the preliminary stages of the Long-Term Storage Program, several types of experimental containers, filled with materiel, were placed on outdoor exposure and observed as an aid in the selection of containers which would be serviceable in the extended program. These were: strippable vinyl film, steel, and aluminum unit containers with combat tanks, weasels, command cars, and high-speed tractors, 14 total; steel, multi-unit containers with assorted materiel, 10 total.

Approval of a selection of outdoor storage sites, referred to as exposure sites, was requested in a memorandum[18] from ORDIR to ORDFM. Approval of the selection, slightly revised, was granted. Consequently, by January 1946, distribution of items in the experimental containers was made to five sites located within continental USA and two sites located outside the continental limits. These sites were:

Aberdeen Proving Ground   Tooele Ordnance Depot
Erie Ordnance Depot   Watertown Arsenal
Pueblo Ordnance Depot   Panama Canal Zone

A typical exposure site is shown in Figure 1.

In June 1948, by authority[19] of the Office, Chief of Ordnance, an arctic storage site, Fort Churchill, Canada, was added. Four Ambridge steel containers, two hermetically-sealed and two balanced pressure, were to undergo outdoor exposure and periodic inspection over a period of two years. Inspection procedures were to be established by the assigned technical coordinating unit at Frankford Arsenal.

Frankford Arsenal assumed technical supervision of the Experimental Long Term Storage Program on 31 December 1947.

The laboratory division (Pitman-Dunn Laboratories) at Frankford Arsenal was assigned the responsibility of technical supervision and surveillance of the Experimental Long-Term Storage Program.

MATERIALS, CONDITIONS, INSTRUMENTS, AND EQUIPMENT

Containers and Materiel

The Ordnance Corps and the various contractors agreed on the designs of metal containers for use in the Experimental Long-Term Storage Program.[14] Certain practical and economic factors were considered:

(1) Containers should be easily produced in quantity and constructed to properly confine the storage medium (e.g., to withstand pressures greater than ambient in the case of sealed containers), and should require very little maintenance.

(2) The equipment should be transportable in the container for relocation to strategic or combat areas.

(3) All items should be stored in completely assembled conditions and if this is not feasible, disassembly should be held at a minimum so that the materiel could be put to use in a short time on removal from the container.

(4) First echelon components, tools, and accessories, where feasible, should be stored with the item, to provide a complete combination.

A complete tabulation of all materiel in the Experimental Long-Term Storage Program, under the Industrial Account, is given in Table I; items removed from containers for purposes of inspection are shown. Tables II, III, IV and V list materiel not included under the Industrial Account.

Measurement of all containers, weights of containers, and stored items can be obtained from Pitman-Dunn Laboratories Group, Frankford Arsenal.

AMBRIDGE PRESSURIZED CYLINDRICAL CONTAINERS FOR ARTILLERY WEAPONS AND HOWITZERS

Two hundred fifty Ambridge pressurized cylindrical containers (Figure 2) for artillery weapons and howitzers, were fabricated by the American Bridge Company, Pittsburgh, PA. These are modified cylindrical containers with convex ends and are of 1/4 inch steel plate, of welded construction. They were designed so that a positive internal pressure could be maintained over a temperature range of -60° to $+150^{\circ}$F when initially charged to 6 psi at 70°F. The container base serves as the pallet on which the item is secured. A valve, through which pressure determinations and nitrogen repressurizations could be made, was provided on each container.

One weapon only of the following types was stored in each: 40 mm and 90 mm AA weapons, 105 mm and 155 mm Howitzers.

AMBRIDGE PRESSURIZED RECTANGULAR CONTAINERS FOR 75 mm PACK HOWITZER

One hundred Ambridge pressurized rectangular containers (Figure 3) for 75 mm pack Howitzers, were fabricated by the American Bridge Company, Pittsburgh, PA. These are rectangular, stackable containers, and are of welded 1/4 inch steel plate construction. They were designed so that a positive internal pressure could be maintained over a temperature range of -60° to $+150^{\circ}$F when charged initially to 6 psi at 70°F. The container base serves as the pallet on which the item is secured. Each container is provided with a valve through which nitrogen repressurizations are made. Fifty containers were equipped with an adaptor for exercising the recoil mechanism.

One item (75 mm pack Howitzer) was stored in each container.

AMBRIDGE BALANCED PRESSURE CONTAINER FOR 90 mm AA WEAPONS

Sixteen of the 250 Ambridge pressurized (hermetically sealed) cylindrical containers were modified to balanced pressure containers during field tests in 1947 and 1948, by adapting solar radiation breathers (Figure 4). The modified containers were prepared for a controlled field study of solar radiation breathers. Only containers of 90 mm weapons were selected.

DRAVO PRESSURIZED CYLINDRICAL AND RECTANGULAR CONTAINERS FOR FIRE CONTROL ITEMS

Seventy pressurized cylindrical and rectangular containers, three sizes, for five control items, were fabricated by the Dravo Corporation, Pittsburgh, PA. These containers were of 1/8 inch steel sheet, welded construction. The smallest and largest containers were cylindrical, the smallest for the storage of height finders, the largest for M9 and M10 directors (Figure 5). The rectangular container was for the storage of the M7A1 generator (Figure 6). Each container housed only one item. The containers were designed so that a positive internal pressure could be maintained over a temperature range of -60° to $+150^{\circ}$F when charged initially to 6 psi at 70°F.

H and H PRESSURIZED CYLINDRICAL CONTAINERS
FOR DIRECTORS AND CABLE SYSTEMS

Sixty pressurized cylindrical containers, two sizes, for directors and cable systems, were fabricated by the Harlan and Hollingsworth Company, Wilmington, DE. These containers have a convex top and are of 1/8 inch steel sheet, welded construction (Figure 7). They were designed so that a positive internal pressure could be maintained over a temperature range of $-60°$ to $+150°F$ when charged initially to 6 psi at $70°F$. Each container was provided with a ball check valve for pressure determinations and nitrogen repressurizations.

Directors and cable systems were stored in these containers, one in each.

STEIKER PRESSURIZED CYLINDRICAL CONTAINERS
FOR MORTARS

Eighty-eight pressurized cylindrical containers, four sizes, for various items, were fabricated by the Steiker Division of Federal Auto-Body Corporation, Patterson, NJ. The containers are drums of 20 gage steel sheet, welded construction (Figure 8). They were designed so that a positive internal pressure could be maintained over a temperature range of $-20°$ to $+150°F$ when charged initially to 3 psi at $70°F$. Each container is provided with a ball check valve for pressure determinations and nitrogen repressurizations. (In one container, oil was used as the preservative.)

Materiel stored in these containers consisted of 81 mm mortars, two to a container; 60 mm mortars, four to a container; 20 mm guns, 12 to a container; 37 mm guns, two to a container; and height finders, one to a container.

FRANKFORD ARSENAL DRUMS, PRESSURIZED
FOR OPTICAL FIRE CONTROL INSTRUMENTS

Two hundred five commercial steel drums, 55-gal size, were modified at Frankford Arsenal for the storage of optical fire control instruments (Figure 9). These drums were provided with a ball check valve through which pressure determinations and repressurizations with nitrogen were made.

The drums were designed so that a positive internal pressure could be maintained over a temperature range of $-20°$ to $+150°F$ when charged initially to 3 psi at $70°F$.

ROCK ISLAND ARSENAL RECTANGULAR CONTAINERS
FOR RECOIL MECHANISMS

Fifty rectangular containers were fabricated at Rock Island Arsenal. These were fabricated of 3/16 inch steel sheet, welded construction (Figure 10). They were designed so that a positive internal pressure could be maintained over a temperature range of $-20°$ to $+150°F$ when charged initially to 3 psi at $70°F$. The containers were not provided with valves. In twelve of these containers, oil was used as the preservative.

Materiel stored in these containers consisted of completely disassembled recoil mechanisms for 105 mm Howitzers, two to a container.

IGLOOS, BALANCED PRESSURE RECTANGULAR CONTAINERS

Six igloos, balanced pressure rectangular containers (Figure 11), were erected at Aberdeen Proving Ground by A.O. Smith Corporation. These were fabricated of 7/16 inch steel plate, welded. The base of the container was provided with a removable port, approximately 2½ ft. in diameter. Equilization of pressure in the containers with ambient conditions was provided by various vents, such as solar radiation breathers, open tubes, and tubes connected to the dynamic dehumidification machine.

Various items of ordnance were stored in each of the containers.

SURPLUS GASOLINE STORAGE TANKS

Ten surplus gasoline storage tanks (Figure 12) were erected at the Aberdeen Proving Ground Storage Site by the Columbia Company. These were of four sizes. Eight were dynamically dehumidified, one statically dehumidified and vented, and another, used to evaluate a volatile rust inhibitor in a mass storage test, was not dehumidified. Five tanks, each 55 ft. in diameter, were erected at Red River Arsenal and Lima Ordnance Depot. One of the tanks at Red River Arsenal was used in the volatile corrosion inhibitor evaluation.

Various types of artillery and automotive materiel were stored in the containers at Aberdeen Proving Ground.

MARTIN BALANCED PRESSURE RECTANGULAR CONTAINERS
FOR ANTI-AIRCRAFT WEAPONS

Two hundred five balanced pressure containers (Figure 13) were fabricated by the Glenn L. Martin Company, Baltimore, MD, under a sub-contract to the Davison Chemical Company. These were rectangular, with an asymmetric gabled roof, constructed of welded light gage sheet aluminum alloy. Equalization of pressure in the container with ambient conditions, and maintenance of established low humidity levels inside the container were accomplished by means of a solar radiation breather.

Materiel stored in these containers, one item in each, were one hundred fifty-two 40 mm, fifty-two 90 mm, and one 120 mm anti-aircraft weapons.

SPECIAL STEEL CONTAINERS FOR COMBAT VEHICLES

Eleven special steel containers (Figure 14) were fabricated by several manufacturers under the direction of Detroit Ordnance District. These were of various shapes and sizes, and of welded construction. Not more than one of the following units was stored in each container: combat tank, cargo carrier, command car and high speed tractor.

SPECIAL ALUMINUM CONTAINERS FOR 76 mm MOTOR GUN CARRIAGE

Two special containers (Figure 15), different sizes, of welded aluminum sheet, were fabricated by the Goodyear Aircraft Corporation, Akron, OH, at the direction of the Detroit Ordnance District. These were used to house a single 76 mm M18 motor gun carriage.

SPECIAL BALANCED PRESSURE VINYL CONTAINERS

Fourteen 90 mm AA M1A1 weapons were individually envelop in a 0.040 inch thick vinyl film, spray-applied, at Erie Ordnance Depot, early in 1945. Approximately 90 pounds of silica gel, in bags, was placed inside each vinyl container which was immediately sealed and equipped with a breather vent. The vent consisted of an iron pipe containing a bed of silica gel. Seven of these containers were given a topcoating of sprayable mastic compound, approximately 1/8 inch thick. On a production scale, vents were not installed on vinyl containers (Figure 16).

SPECIAL VINYL CONTAINER

One completely assembled 76 mm Mortar Gun Carriage, M18, was inclosed in a special vinyl container (Figure 17). It was prepared by the Goodyear Aircraft Corporation, Akron, OH, under the direction of Detroit Ordnance District.

Storage Media

Four media of storage are employed in this program. These are: (1) low humidity air, (2) low humidity nitrogen, (3) oil, and (4) volatile corrosion inhibitor (without regard to humidity).

Low humidity air is attained by static or dynamic methods. Silica gel is used for static dehumidification. Similar material, in bulk, is used for dynamic dehumidification.

Low humidity nitrogen is attained by static dehumidification in hermetically sealed containers. Commercial grade oil-pumped nitrogen is used because of its availability at ordnance depots and its low oxygen and water content.

Items stored in oil medium are completely submerged in light machine gun oil prior to sealing the container. The oil complied with Specification 2-27E.

Experimental use of volatile corrosion inhibitor was first tried in this program for bulk storage of Ordnance materiel in two surplus gasoline storage tanks. A selection of artillery field pieces, various small arms, and a variety of prepared metal specimens were stored in each tank.[24] The corrosion inhibitive medium was attained by covering items with kraft paper impregnated with inhibitor and dispersing inhibitor crystals on the container floor. The volatile corrosion inhibitor was dicyclohexylammonium nitrite, VPI-260, product of Shell Development Company.

Storage Sites

LOCATIONS

Representative groups of the filled containers were located at various widely separated locations where different climatic conditions prevailed. Five of the sites were located in the United States; one in the Panama Canal Zone; one in the Territory of Hawaii; and one in Canada.

The domestic sites were at Aberdeen Proving Ground, Aberdeen, MD; Watertown Arsenal, Watertown, MA; Erie Ordnance Depot, LaCarne, OH; Tooele Ordnance Depot, Tooele, UT; and Pueblo Ordnance Depot, Pueblo, CO.

The overseas site in the Territory of Hawaii was located for a time at Kipapa Air Field, but later the containers were moved to an area in Schofield Barracks. In the Panama Canal Zone, one group of containers was located at Corozal, on the Pacific side of the isthmus, and a second group was located at Fort Davis, on the Atlantic side. These sites were selected because of differences in rainfall at the two locations.

The Canadian site, at Fort Churchill, Manitoba, on the shore of the Hudson Bay, was installed following a suggestion made to Office, Chief of Ordnance, in 1948, for the establishment of a subarctic site.

CLIMATIC CONDITIONS

The following descriptions of weather conditions prevailing at the sites are based on U.S. Department of Commerce[26] and Panama Canal Company meteorological reports, information presented in Frankford Arsenal reports pertaining to Fort Churchill[86] and Panama Canal Zone,[87] and "Summer Weather Data."[25]

Aberdeen Proving Ground. Weather changeable; temperature fluctuations not too abrupt; annual mean temperature, 56°F; annual mean relative humidity, 67 percent; annual mean hours possible sunshine, about 60 percent.

Watertown Arsenal. Weather changeable; temperature fluctuations not too abrupt; annual mean temperature, 50°F; annual mean relative humidity, about 66 percent; annual mean hours possible sunshine, approximately 57 percent.

Erie Ordnance Depot. Excessive cloudiness and high relative humidity characterize the climatological conditions at this site; annual mean temperature, about 50°F; annual mean relative humidity, about 72 percent; annual mean hours possible sunshine, about 50 percent.

Tooele Ordnance Depot. The storage site at Tooele is situated about 4500 feet above sea level; wide daily ranges of ambient temperature (90° to 60°F) occur in summer. The annual mean temperature is about 53°F; relative humidity, about 56.5 percent; and possible hours sunshine, about 65 percent.

Pueblo Ordnance Depot. The elevation of the Pueblo site is about 4600 feet. The climate is semi-arid; wide temperature variations occur daily;

plentiful sunshine moderates winter temperatures, but readings of $0^\circ F$, or lower, are registered about eight times each winter. The annual mean temperature is about $51.5^\circ F$; relative humidity, about 51 percent; and possible hours sunshine, about 74 percent.

Hawaii Ordnance Depot. The Hawaiian site is situated on the Island of Oahu, which is near the northern limit of the tropics. The annual mean temperature is about $72^\circ F$; relative humidity, about 70 percent; and possible hours sunshine, 62 percent.

Panama Canal Zone. Wet tropical conditions are characteristic at the Canal Zone Sites on the Atlantic and Pacific sides. Rainfall is greater on the Atlantic than on Pacific side. The annual mean temperature is about $86^\circ F$; relative humidity, about 83 percent; and possible hours sunshine, about 51 percent.

Fort Churchill. Temperatures in winter and early spring usually are below $0^\circ F$; a low of $-50^\circ F$ is sometimes registered in winter. Constant northerly winds from five miles per.hour to gale velocities carry dry snow and frequently cause low visibility. In summer, daily temperatures range between 55° and $90^\circ F$ and the relative humidity is high; southerly winds predominate. In winter the daylight hours are few; in midsummer sunlight and twilight prevail throughout the 24 hours.

Instruments and Equipment

PRESSURE GAGES

Each Ambridge container was equipped with a Fulton-Sylphon pressure gage.

RELATIVE HUMIDITY AND TEMPERATURE INDICATORS

Friez Indicator. Each aluminum container was equipped with a Friez hair element hygrometer.

Silica Gel Indicator. Each aluminum container was equipped with an indicator consisting of silica gel impregnated with cobalt salts which indicated humidity conditions by color change.

Temperature and Humidity Sensing Element. A Dunmore cell-type hygrometer and temperature sensing instrument was installed in approximately 50 percent of the Martin and Ambridge containers.

Dew Point and Dry Bulb Sensing and Recording Instrument. The Foxboro Dewcel with recorder, was installed on containers undergoing special tests.

Multiple Point Temperature Sensing and Recording Instrument. In special tests, temperatures at various locations in the storage tanks and igloos were recorded intermittently on a time chart by means of a multiple point temperature sensing and recording instrument.

338

SOLAR RADIATION BREATHER

This breather was developed by the Division Chemical Corporation, Baltimore, MD, for the balanced pressure containers (Figure 18).

DYNAMIC DEHUMIDIFICATION MACHINES

Kemp (20 cfm) and the Cargocaire (500 cfm) dynamic dehumidification machines, were used experimentally at the Aberdeen Proving Ground Site.

METHODS

Preparation and Storage of Materiel

The Office, Chief of Ordnance, selected the materiel and determined the quantity of each item to be stored in containers. It was required that each item be completely overhauled and modified prior to packing in the container.[17]

A brief description of procedures followed in preparing items for storage in containers follows. Full details in some instances, have been given in previous publications.

90 mm AA M1A1 WEAPONS

One hundred fifty 90 mm M1A1 weapons were overhauled and modified at Erie Proving Ground and Cresona Ordnance Depot for this program. They were inclosed in strippable vinyl film barriers and statically dehumidified.

One hundred of the weapons were put into Ambridge containers. The container for this weapon was not designed to permit periodic exercising of the recoil system while in storage.[28]

Fifty 90 mm weapons were sent to the Glenn L. Martin Company to be placed in mobile balanced pressure aluminum containers, statically dehumidified and equipped with solar radiation breathers.

40 mm AA M2A1 WEAPONS

Two hundred two 40 mm AA M2A1 weapons were overhauled and modified at the Erie Ordnance Depot. They were inclosed in statically dehumidified strippable vinyl film barrier.

Fifty were sent to the American Bridge Company and placed in steel containers.[31]

75 mm HOWITZER

One hundred Pack Howitzers, 75 mm, M1A1, with Carriage, M8, were overhauled at Aberdeen Proving Ground and shipped by covered truck to the Ambridge plant for packing in hermetically sealed, nitrogen pressurized,

dehumidified steel containers.

105 mm M2A2 HOWITZER AND MOUNT

Fifty of these howitzers were overhauled at Erie Ordnance Depot. They were then shipped to the American Bridge Company plant to be stored in steel containers.

155 mm M1A1 HOWITZER AND MOUNT

Fifty of these howitzers were overhauled and modified at Erie Ordnance Depot. These weapons were shipped to the American Bridge Company plant for packing in steel containers.

M7A1 and M15A1 UNIT GENERATORS

Forty unit generators M7A1 and ten unit generators M15A1 were inspected and modified at Frankford Arsenal. They were stored in Dravo hermetically sealed containers.

M9A1 and M10 AA DIRECTORS

Ten, each, M9A1 and M10 AA directors were overhauled at Frankford Arsenal and shipped as units to the Dravo Corporation.

M5A2 and M7A1B1 AA DIRECTORS

Twenty-five, each M5A2 and M7A1B1 AA directors were overhauled and modified at Frankford Arsenal. They were then shipped to the Harlan and Hollingsworth Company plant for packing in individual containers.

M1 CABLE SYSTEM

Ten M1 cable systems were inspected and prepared at Frankford Arsenal for storage. Each system was packed in a separate nitrogen pressurized container.

PERISCOPES AND TELESCOPES

The periscope and elbow telescopes were inspected, overhauled, modified, and packed at Frankford Arsenal. All were packed on removable metal racks in standard 55-gallon steel drums.

M7A1 COMPUTING SIGHTS

Fifty M7A1 computing sights were overhauled and inspected at Frankford Arsenal. Two of these sights were packed on removable metal racks in each of 25 double length steel drums.

60 mm M2 MORTARS AND 81 mm M1 MORTARS

One hundred each of 60 mm M2 and 81 mm M1 mortars were obtained new. All were packed in modified 55-gallon steel drums on removable steel racks.

20 mm AA M3 GUN AND 37 mm M10 AUTOMATIC GUN

These weapons were stored in twelve steel drum containers.

105 mm HOWITZER RECOIL MECHANISM

One hundred completely disassembled recoil mechanisms for 105 mm howitzers were overhauled, modified, and packed at Rock Island Arsenal[35] in dehumidified steel containers.

SPECIAL ITEMS

The following items were placed in experimental containers which were later assigned to the responsibility of this program:

(1) Artillery Materiel - in storage tanks and igloos at Aberdeen Proving Ground;

(2) Combat Automotive Materiel - in special containers at Lima Ordnance Depot;

(3) Artillery Materiel - in strippable vinyl barriers.

DISTRIBUTION TO STORAGE SITES

All of the loaded containers were separated in groups and shipped to the seven original exposure sites. These sites are discussed under the section Exposure Sites of this report.

Observations

TEMPERATURE

Temperature in the aluminum container is read on the thermometer of the Friez hygrometer, which is mounted behind a glass port in the access door.

Temperatures in various locations in the steel igloos and surplus gasoline storage tanks at the Aberdeen site are recorded by means of multipoint recording instruments.

Ordinary glass thermometers are used for occasional temperature checks on, and in adjustments of, the mechanical temperature indicating equipment.

Electric hygrometers (Dunmore cell type) was installed in about 50 percent of all Martin (aluminum) and Ambridge (steel) containers.

RELATIVE HUMIDITY

Direct readings of relative humidity conditions inside aluminum containers were taken from the indicating scale of the Friez hygrometer. Determinations at the Aberdeen Proving Ground site and 14 Ambridge balanced pressure containers at various sites, were made from the Foxboro instrument installed in each container. Relative humidities inside the steel igloos at Aberdeen Proving Ground also are determined from dew point records of Foxboro instruments.

In case of the nitrogen pressurized containers, the dew point cup method was used for obtaining relative humidity measurements of the container atmosphere.

PRESSURE

Pressures inside the hermetically sealed containers are measured by means of a mercury manometer.

Opening Containers for Teardown Inspections

PRESSURIZED CONTAINERS

The first requirement in opening any pressurized container is to release the pressure. This is accomplished by opening the charging valve to alloy escape of nitrogen. The containers are then opened as follows.

The Ambridge cylindrical container is cut along the base with an acetylene torch to permit removal of the upper shell. The flame is directed as closely as possible along the original weld line at the base. When the cutting is completed, the shell is lifted vertically by means of a crane. This operation requires caution since the shell will tilt somewhat, and, since clearance between the shell and materiel is close, damage to the materiel might occur.

The Ambridge rectangular container for 75 mm Howitzers is flame-cut at the edges of the top plate, at an angle, so that the top and side juncture is cut away. After the top plate is removed, the two wheels are unfastened from its underside. The hose connection between the assembled recoil mechanism and the container wall is uncoupled and the howitzer and trail assembly are hoisted from the container. The tools and canvas covers are removed from side compartments on the inner container wall.

The Dravo rectangular container is opened by flame-cutting the front end at the edges. The end is then pulled off by means of a shop tractor. The generator is best removed by blocking up the front of the generator to clear the skid rail of the container; cables are attached to the generator to slide it out. A necessary precaution is to place wooden blocks outside the container almost flush to the skid rail so as to prevent damage to the rear apron as the generator clears the container.

The Frankford Arsenal and Steiker cylindrical containers of optical equipment and 20 mm, 60 mm, and 81 mm mortars, are opened by flame-cutting around the top chime. These containers may also be opened by cutting around the top stiffening rib, using an air-operated chisel. The materiel, attached to prefabricated frame supports, are lifted by crane or tackle.

The Dravo and Harlan and Hollingsworth cylindrical containers, in which directors and cable systems are stored, are opened by directing the flame of the torch on a line just above the original weld around the base. An alternate method is to make a circumferential cut with an air operated chisel around the lowest stiffening rib. A cable hook is placed in the lifting eye at the top of the container so that the shell can be raised clear of the materiel.

The Rock Island Arsenal containers in which disassembled recoil mechanisms are stored, are either nitrogen pressurized or oil filled. Those containing oil must be drained before any attempt is made to remove the top plate by flame-cutting. When the top plate has been removed, the mechanism may then be lifted out by means of a sling and a hoisting device. Some recoil mechanism parts must be detached from each of the end plates. Nitrogen-filled containers are opened in the same matter after reducing the nitrogen pressure by removing the drain plug.

BALANCED PRESSURE CONTAINERS

The Ambridge cylindrical container requires removal of the solar radiation breather and the temperature and dew point elements and recorders before opening. Opening is performed using a cutting-torch following the procedure described for the pressurized Ambridge container.

The Martin aluminum container for the 40 mm and 90 mm AA weapons is opened by means of an air-operated chisel or by an electric-arc cutter. The cap around the lifting eye on the 40 mm and 90 mm container is cut with an air chisel; in the case of the 90 mm container, the cap around the pintle is also cut. The canopy is separated from the base by directing the chisel along the cutting line marked near the bottom of the barrier. A hole is punched in the side opposite the access door so that the rigging lines can be attached to the shell, which is then lifted from the base with a crane. On 90 mm barriers, the wheel well fenders (which are part of the base) are removed so that the weapon can be lifted off the aluminum base. This is a difficult operation since the brake and wheel assembly and a series of bolts must be removed. The air chisel can then be used to cut through to the axle.

The use of electric-arc cutting for the removal of the aluminum barrier is considerably faster, but must be performed outdoors because of fumes evolved. The canvas covers must be removed from the container prior to the cutting operation to protect them from damage by fire.

A variation is to be noted on the 40 mm AA M2A1 weapon, since the weapon is not mobile and is fastened to the beams of the floor of the container, in firing position, by special fasteners. After the shell and fasteners are removed, the weapon is raised from the floor by a crane. The wheels are replaced and the weapon lowered to the ground. The retracted running gear is then returned to the traveling position using proper safety precautions since the safety lock modification is not present on these weapons.

Inspection of Materiel

Teardown inspections are performed by depot inspectors and mechanics. A representative of the Long-term Storage Section of Frankford Arsenal is in attendance to direct teardown inspections in order to derive first-hand information regarding the extent of preservation afforded by the experimental container methods of storage.

When a container is opened, a visual inspection is made to determine the general condition of the materiel. Notes are taken regarding rust, corrosion, mildew, mechanical damage, or any condition which could be considered as evidence of failure of the method of preservation. The materiel is then dismantled to the extent required for existing overhaul and modification to render the materiel ready-for-issue. Conditions uncovered in the dismatling, which were not detectable in the preliminary visual inspection, are noted and, if considered unusual, are photographed. A comparison is made of the conditions found and those recorded in the original packaging inspection report which usually, but not always, is found with the materiel in the container. A report is then issued summarizing the teardown inspection results; opinions, considerations, and conclusions of the inspectors are considered.

Breather Tests

A study and evaluation of the solar radiation breather was made at Pennsylvania State College Engineering Experimental Station under Contract DA-19-020-ORD-5915.[39]

Concurrently, at Aberdeen Proving Ground, several Martin balanced pressure aluminum containers equipped with solar radiation breathers were selected for field evaluation of the breather to maintain a constant low relative humidity.[40]

The breathers at Aberdeen Proving Ground had been filled with known quantities of silica gel preloaded with water to present a series from approximately 2 percent (control) to 35 percent saturation. The container humidities were approximately 30 percent. The container humidities and breather weights were checked monthly.

RESULTS AND DISCUSSIONS

Teardown Inspections

Low humidity nitrogen and air atmospheres in hermetically sealed and balanced pressure containers, respectively, are the two principal storage

media with which this Experimental Long-Term Storage Program is concerned. Vapor phase corrosion inhibitor and oil media are involved to a lesser degree. Results of teardown inspections or periodic evaluations of stored materiel for the eight-year duration are discussed in this section for each medium separately.

Low Humidity Nitrogen Atmosphere

GENERAL

Items stored in the various hermetic containers, pressurized with nitrogen and maintained at low humidity, were found, on inspection, to be in an excellent state of preservation.

RECOIL MECHANISMS

In addition to the general inspection of the items stored, particular attention was directed to the operation of weapons. Whenever possible, proof-firing tests were performed. Mechanical exercising and visual examination of internal surfaces of recoil mechanisms were accomplished in order to ascertain the efficiency of the storage method for preserving the recoil mechanism.

Real disagreement and lively differences of opinion exist concerning the need of exercising recoil mechanisms while in storage. It seems apparent from the information acquired since the initiation of this program that assembled and unexercised recoil mechanisms stored in low humidity nitrogen or air atmospheres below 40 percent relative humidity can be expected to remain unaffected and serviceable. This is an accepted fact for the Monel recoil mechanisms of the 90 mm AA weapons.[28]

Evidences have been and are being collected [84,85] for the steel mechanisms from some of the 75 mm howitzers which have been in storage beyond eight years and on which exercisings have not been conducted for over four years because of low nitrogen pressures in the recoil cylinders. In the 155 mm howitzers, leakage of oil around the purge packings has been observed. Disassembled recoil mechanisms have remained intact; i.e., highly polished surfaces have remained untarnished. Additional information follows for recoil mechanisms of the various weapons stored.

FIRE CONTROL EQUIPMENT

The fire control electrical systems of 90 mm and 40 mm weapons consistently have been found in remarkably good condition. Immediately on removal from consulation of the circuits have been found to be higher, generally, than resistances which had been measured prior to storage, as ascertained from records with the stored item. This should be expected in view of the desorption of moisture by the insulation in the low humidity atmosphere of the storage container. After 24 to 48 hours exposure to ambient conditions, the resistance measurements were found to approach the values indicated in the pre-storage records.

OPTICAL INSTRUMENTS

About one-third of the containers of M6 periscopes have been opened after four to six years of storage. None of the periscopes showed condensate on the prisms; their condition was excellent throughout.[37,41]

None of the 672 M17 Az or El telescopes removed from 28 Frankford Arsenal containers over various periods of storage (up to seven years) showed any changes over the original conditions as noted on the inspection sheets inclosed with them.[37,41,49]

Twelve-hundred M1 panoramic telescopes were removed from 25 containers after six years' storage. According to original inspection records in the containers, no overhaul of the telescopes was made prior to storage because of the need of meeting the storage "deadline." Telescopes (432) in nine containers had undergone no change in storage; 768 in 16 containers apparently showed a 25 percent increase in condensate on lenses and prisms.[50]

None of the 24 computing sights which have been removed from 12 Frankford Arsenal containers showed deterioration or change after storage for seven years. The items were in serviceable condition.[45]

MORTARS

The 60 mm and 81 mm mortars examined after six years' storage were very well preserved.[52]

GUNS

Nine containers, each with twelve 20 mm M3 guns, and one container of two 37 mm automatic guns, were opened in 1950. All of the guns were found in excellently preserved condition, free of corrosion, and entirely serviceable.

BALANCED PRESSURE CONTAINERS

Martin aluminum and Ambridge steel containers, equipped with solar radiation breathers, have been evaluated as balanced pressure containers.

It should be recognized that certain construction faults with which the aluminum container was fraught had not been foreseen in 1945. For example, the edge welded seam, the spot welded stiffener rods, and the thin gage sheet utilized, each contributed to the inherent leaky characteristic of the container. At this point it is desires to emphasize that the aluminum containers were not able to withstand the strain and stress of normal expansion and contraction under ambient temperature extremes.

Because of leakages in the containers, and not because of inefficiency of the solar radiation breather, a large percentage of balanced pressure aluminum containers could not maintain a low humidity atmosphere; hence these containers required maintenance to provide adequate preservation for more than two years.

Aluminum containers which were regularly checked for leaks and in which leaks had been found and repaired without delay, have given excellent pro-

tection for eight years. These and leak-free Ambridge balanced pressure containers in which low humidity air atmosphere could be maintained by means of solar reactivation of the breather desiccant, attest to the value and importance of low humidity balanced pressure air atmosphere as an excellent preservative medium for ordnance materiel.

Special Storage Tests

COMBAT VEHICLES IN LOW HUMIDITY NITROGEN MEDIUM

Thirteen metal containers (eleven steel and two aluminum) and one strippable vinyl film barrier had been fabricated during 1946 by several contractors, under the supervision of the Office, Chief of Ordnance (Detroit), for the storage of automotive materiel at the Lima Ordnance Depot.

The material in all but two of the steel containers was well preserved.

ARTILLERY IN LOW HUMIDITY AIR MEDIUM

The artillery weapons removed from the statically dehumidified strippable film barriers have been found to be well preserved from rust and corrosion. Electrical resistance of the insulation of the fire control wiring has been reported as above that observed at the time of placing the weapons in the barriers.

MISCELLANEOUS MATERIEL IN VOLATILE CORROSION INHIBITING MEDIUM

The test to determine the feasibility of mass storage of materiel in large containers, using a volatile corrosion inhibiting agent as the means of preservation, was unsuccessful and was terminated after little more than one year.[56] It should not be inferred from this that the failure is attributable to the ineffectiveness of the inhibiting agent. Several factors contributing to the adverse results have been discussed in an earlier report.[24]

Vapor phase corrosion inhibitors in non-hermetic or gas permeable containers cannot be relied upon for protection of stored items over long periods of time. Containers which permit an exchange of atmosphere with the outside will allow dilution of the protective vapor below effective concentration if the exchange is rapid or if the time is long enough, and will eventually allow complete dissipation of the inhibitor. The successful application of volatile corrosion inhibitors depends on maintaining the recommended concentrations of the inhibitor vapors; the more hermetic the storage container, the longer will be the time of protection afforded. Generally, large containers are difficult to make hermetic or nearly so. An alternate method of atmosphere control, such as dehumidification, has been demonstrated in this program to be completely successful for long-term storage.

Vapor phase corrosion inhibitors are suitable for use in small packages because of the simpler methods of sealing. The length of time of effective preservation can be predicted, depending on the construction of the

package and conditions under which it is to be stored.

Production Storage

DEHUMIDIFIED STORAGE TANKS

The progress report[59] on the condition of the materiel removed from these tanks indicated that the materiel was well preserved after eight years of storage.

STRIPPABLE VINYL FILM CONTAINERS

Vinyl strippable film as a barrier materiel for the storage of assembled equipment was developed by the Naval Ordnance Laboratory in 1944. The Ordnance Corps adopted this barrier in 1945 for field storage of assembled equipment. Ordnance has modified and improved the strippable film system for its specific applications. Several experimental statically dehumidified plastic containers, consisting of vinyl film and mastic topcoating, have preserved AA weapons in outdoor storage for eight years.

The ease and low-cost of preparation of the spray-applied container or barrier, and the readiness and mobility of the completed units which have been stored therein are the outstanding merits of the strippable container. To envelope a 90 mm AA M1A1 weapon requires about 35 man-hours.

The strippable vinyl film container has given outstanding service for short-term and interim storage, and has been demonstrated to be notably valuable for shipping purposes. Considerably more attention and wider use should be given it.

Aberdeen Proving Ground Tests

The experimental storage tests with igloos and surplus tanks at the Aberdeen Proving Ground site over an eight year period have demonstrated that dynamic dehumidification is more practical than the static method for acquiring low humidity atmospheres for long-term preservation of materiel in mass. Over-all costs for the eight year period are only very slightly higher for the dynamic method, because of higher initial expenditures for equipment and equipment installation.

Recoil Mechanisms

In the early planning of the Experimental Long-Term Storage Program, consideration was given to periodic exercising of recoil mechanisms in storage. It was decided, on the basis of established M1S procedures, that all steel mechanisms on 75 mm and 155 mm howitzers stored in low humidity nitrogen should undergo periodic exercising inside containers which would be constructed to permit this.

All of the exercised steel mechanisms gave very satisfactory performances in all tests to which subjected, and examinations of internal sur-

faces of some of these mechanisms have shown complete absence of corrosion.
At Erie Ordnance Depot, teardown inspections have been accomplished on
four assembled recoil mechanisms in dehumidified storage which had failed
to return to battery position because of low nitrogen pressures or oil
leakages and which, consequently, had not been exercised for approxi-
mately four years. These mechanisms were found to be completely free
from corrosion.[84]

Generator Units

On removal from the container and servicing with motor oil, coolant,
spark plugs, gasoline, and a new battery, each of 88 generator units was
completely operable in conformance with inspection standards. Five were
found inoperable because of low compression. Inspection reports inclosed
with these items revealed that the engines had not been overhauled prior
to storage.

Preservative Compounds

It was observed that in containers where relative humidities were below
40 percent during the storage period, weapons stored without a preservative
coating were in as good condition as those stored with preservative coating.
For this reason it is considered that the use of thick or thin film pre-
servative compounds on material stored in air or nitrogen atmospheres held
below 40 percent relative humidity is unnecessary.

It is of interest to note that in the defective aluminum containers,
where high relative humidities prevailed during the storage period, items
were found to be heavily corroded despite the fact that they were liberally
coated with rust preventive preservative compounds.[64]

Breathers

In the balanced pressure containers, it is endeavored to maintain a rela-
tive humidity of approximately 30 percent by static dehumidification, for
proper preservation of materiel. Although this 30 percent level is lower
than may be tolerated, since preservation over prolonged periods has been
accomplished with humidity levels as high as 40 percent, it is easily at-
tainable by static dehumidification with suitable desiccant.

The "breathing" of a container through a simple orifice or a long tube
will, in a relatively short time, result in an increase of relative humid-
ity of the container atmosphere. An ordinary desiccant type water-vapor
trap only serves to delay container atmosphere humidification; it becomes
progressively more ineffectual as the breather desiccant approaches satur-
ation. But, very effective and complete humidity control of balanced pres-
sure containers is attainable with solar radiation breathers.

SOLAR RADIATION BREATHER

The solar radiation breather could be referred to more descriptively as
a solar reactivated breather. It is assigned to utilize solar radiation
to reactivate silica gel desiccant, which it contains (Figure 23).

The breather is always located on the top of the container and is black to increase efficiency of solar heating. The breather desiccant is reactivated under solar heating. Under the same influence, container gases expand and escape through the breather, sweeping water-vapor from the breather desiccant into the ambient atmosphere. As the container atmosphere contracts with the waning of solar heat and resultant drop in container temperature, water-vapor in the ambient atmosphere which would enter the container via the solar radiation breather, is absorbed by the reactivated breather desiccant. Each cycle of this process is dynamic. Under all climatic conditions from subarctic to tropical zones, when exposed to solar radiation, the breather is completely effective in maintaining near-constant humidity control inside balanced pressure storage containers for at least 7 years, as ascertained in this program (Figure 24).

TUBULAR BREATHER

Tubular vents having a length-diameter ratio of 10:1 up to a diameter of one inch are claimed to permit breathing of containers, yet to prevent entrance of water vapor on in-breathing.[66] This has not been borne out in experiments conducted in this program.

Dynamic Dehumidification

The 20 cfm Kemp machine at Aberdeen Proving Ground has operated for about nine years and has been inactivated once for a period of two weeks to permit repairs. During this period of inactivation, the humidity of the container atmosphere did not exceed 35 percent.

Cargocaire machines at Aberdeen Proving Ground were in operation on two series systems of about 90,000 cubic feet each, for seven years, without any prolonged period of inactivity. The operating time on these machines has also been about 10 percent of the time, with the removal of slightly over 18 pounds of water per day from each of the two systems. Unofficial information has been received to the effect that operation of Cargocaire machines in similar dynamic systems of the Production Storage Tank Farms has provided almost identical data. The systems were series connected tanks having a total volume of about 280,000 cubic feet.

Evaluation of Storage Methods

Consistently good results have been obtained with low humidity air or nitrogen atmospheres in all types of containers throughout this program. Total immersion in oil in a hermetic container has been found effective for long term preservation of metallic components and assemblied, but detrimental to rubber and leather components. The volatile corrosion inhibitive agent for mass preservation of materiel as evaluated in the non-hermetic surplus tank was ineffectual.

CONCLUSIONS

1. Materiel in low humidity nitrogen or air atmospheres has been preserved satisfactorily over nine years.

2. Low humidity air is equal to low humidity nitrogen in preservative effectiveness, but low humidity air is more easily obtained either statically with desiccants or dynamically with dehumidification machines.

3. For very large containers or buildings (storage tanks or warehouses), dynamic dehumidification is practical. For transportable containers of single, complete units, in outdoor storage (e.g., 90 mm weapons in aluminum containers), the static method of dehumidification using the solar radiation breather is practical. For small hermetic containers, static dehumidification is most practical.

4. It is unnecessary to apply thin or thick coat preservatives on bare metal surfaces which are stored in low humidity atmospheres.

5. The use of vapor phase corrosion inhibitors for the mass preservation of materiel in large, nonhermetic containers was found to be ineffective. However, such inhibitors are suitable for extended storage of steel in small containers.

6. Total immersion of metallic items in specified oils or greases is effective for long-term preservation (for more than nine years). These media, however, are deleterious to rubber and leather components.

7. Highly effective, low cost, mobile, interim or long-term storage or shipping containers may be fabricated by application of strippable vinyl film which conforms closely to the contour of the item.

8. Exercising of assembled recoil mechanisms during long-term storage in low humidity air or nitrogen atmospheres is not necessary.

9. Exercising of generators and engines during long-term storage in low humidity air or nitrogen atmosphere is not necessary.

10. Rubber items removed from prolonged storage in low humidity air or nitrogen atmospheres apparently have not deteriorated.

RECOMMENDATIONS

1. It is recommended that the methods of long-term preservation of materiel which have been successfully utilized in this program be considered for applicability by all Corps of the Army.

2. Specific recommendations for immediate consideration are:

a. Lightweight, balanced pressure containers made of metal or plastic and equipped with solar radiation breathers should be adopted for the extended storage of individual field and anti-aircraft artillery and mobile vehicles; hermetically sealed cylindrical containers made of metal should be adopted for extended storage of small arms, optical, and fire control equipment.

b. Wherever possible, rubber tires should be stored in the container with the item.

c. Mechanically dehumidified gasoline storage type tanks or warehouses should be used for bulk storage of artillery, vehicles, and similar materiel.

d. Low humidity air should be employed as a preservative medium.

e. Supplementary preservative films, other than a light oil, should not be applied on items placed in low humidity, long-term storage.

f. More extensive tests should be carried out on serviceable recoil mechanisms to provide additional information as to the possibility of discontinuing of the requirement for periodic exercising while in dehumidified storage.

g. Consideration should be given to the long-term storage in low humidity atmospheres, of internal combustion engines, without exercising.

REFERENCES

1. Major Max F. Mueller, "Long-Term Storage of Ordnance Materiel - Progress Report," Frankford Arsenal, 15 Aug 1945.

2. "Long-Term Storage of Ordnance Materiel - Comprehensive Report," Engineering Division of the Davison Chemical Corporation, 1948.

3. Office Memorandum, "Long-Term Storage of Artillery Materiel," Col V. T. Fahringer, Engineering and Inspection Control Branch (SPOIR), to Col G. B. Welch, Chief, Fire Control Sub-office (FCSO), Frankford Arsenal, 8 Sep 1944.

4. 1st Ind to Reference 3, Col G. B. Welch to Col V. T. Fahringer, 23 Sep 1944.

5. Fire Control Sub-office Memorandum No. 132, Maj. B. P. Shirey, 6 Nov 1944.

6. Fire Control Sub-office Memorandum No. 132, Addendum 1, Maj B. P. Shirey, 7 Dec 1944.

7. Memorandum, "Establishment of Long-Term Storage Unit in Fire Control Sub-office" (at Frankford Arsenal), Col F. Mitchell, Fire Control Sub-office, Frankford Arsenal, 23 Nov 1944.

8. Teletype, 232037Z, Engineering and Inspection Control Branch, Jackson, 23 Nov 1944.

9. Minutes, "Conference Between Army and Navy Representatives of Pre-

servation of Ordnance Equipment," held in Room 0144, Navy Department, Bureau of Ordnance, Washington 25, D. C., 10 Oct 1944.

10. Memorandum, "Proposed Method of Long Range Preservation of Certain Types of Ordnance Equipment by Use of Sealed Containers," Maj Gen L. H. Campbell, Jr., Chief of Ordnance, Department Army, Washington, D. C. 12 Apr 1945.

11. Memorandum For Record, "Proposed Method of Long Range Preservation of Artillery Materiel by Use of Sealed Containers," Gen F. M. Wells, Chief, Artillery Division, Industrial Service, Office, Chief of Ordnance (ORDIR), Washington, D. C., 13 Apr 1945.

12. Memorandum, "Outline of Intent, Purpose, and General Basis of Storage Development Program Proposed to be Undertaken by Davison Chemical Corporation," Maj A. H. Sundfor, Fire Control Engineering Office, Frankford Arsenal, 10 May 1945.

13. Memorandum, "Experimental Packaging," Col F. I. Gilbert, Special Representative of Chief of Ordnance, for Chief, Experimental Packaging, Industrial Service, 24 Apr 1945.

14. Record of First General Meeting, "Steel 'Canning' as Applied to Long Term Storage," held at Frankford Arsenal, 30 Apr 1945.

15. Memorandum, "Long-Term Storage," Maj F. A. Doeppers, Acting Chief, Engineering and Inspection Control Branch, Artillery Division, Industrial Service, Office, Chief of Ordnance, 1 May 1945.

16. Office Memorandum, "Canning Operation Equipment," Lt Gen L. H. Campbell, Jr., Chief or Ordnance, to Col F. I. Gilbert, Special Representative of the Chief of Ordnance, 19 Jul 1945.

17. Office Memorandum, "Canning Operation Experiments," Brig Gen G. M. Wells, Chief, Artillery Division, Industrial Service, Office, Chief of Ordnance, 20 Jul 1945.

18. Memorandum, "Exposure Sites for Long-Term Storage Experiments," Chief, Artillery Division, Industrial Service, to Chief, Returned Material Branch, Maintenance Division, Field Service, 16 Oct 1945.

19. Letter of Authorization, "Arctic Tests of Long-Term Storage Packs," (OO 400.112/1358, FA 400.112/14157) 11 Mar 1948, and 1st Ind, 21 Apr 1948.

20. Artillery Division Memorandum 1-46, "Long-Term Storage Program," Col T. A. Wehyer, Chief, Artillery Division, Industrial Service, Office, Chief of Ordnance, 10 Jan 1946.

21. Artillery Division Memorandum 1-47, "Long-Term Storage Program, Col J. F. Gamber, Chief, Artillery Division, Industrial Service, Office, Chief of Ordnance, 14 Jan 1947.

22. Minutes of Meeting, "Continuance of Contracts 3619 and 3771 with Davison Chemical Corporation and Establishment of Surveillance Unit for Long-Term Storage Activities," J. O. Bluhm, Chief, Instrument Division, Frankford Arsenal; meeting held at Frankford Arsenal 9 Jan 1947.

23. Office Memorandum, "Responsibility for Long-Term Storage Surveillance," Brig Gen E. E. MacMoreland, Commanding Officer, Frankford Arsenal, to Director, Laboratory Division; Division Officer, Fire Control Development Division; Chief, Instrument Division; 15 Jan 1947.

24. W. J. Shields and A. Gallaccio, "Gasoline Storage Tank - Vapor Phase Corrosion Inhibitor Test," Frankford Arsenal Memorandum Report No. MR-508, Aug 1952.

25. Summer Weather Data, Kansas, The Marley Company, 1944.

26. "Local Yearly Climatological Summaries," U.S. Dept of Commerce, Weather Bureau.

27. "Instructions for Overhaul, Preparation, Disassembly, and Hermetically Sealed Canning Gun, 90 mm, M1," Tentative AB-6, Erie Proving Ground, Sep 1945.

28. "Long-Term Storage of Artillery Materiel," American Bridge Company Technical Report, 1946.

29. "Instructions for Overhaul, Preparation, Disassembly, and Canning, Gun, 90 mm, M1, in Balanced Pressure Barrier," Tentative AB-5, Erie Proving Ground, Oct 1945.

30. "Instructions for Overhaul, Preparation and Hermetically Sealed Canning Automatic Gun, 40 mm, M1," Tentative AB-2, Erie Proving Ground Oct 1945.

31. "Instructions for Overhaul, Preparation, and Canning Gun, Automatic, 40 mm, M1, in Balanced Pressure Barrier," Tentative AB-3, Erie Proving Ground, Oct 1945.

32. "Instructions for Overhaul, Preparation, and Hermetically Sealed Canning Howitzer, 75 mm, M1A1," Tentative AB-4, Erie Proving Ground, Dec 1945.

33. "Instructions for Overhaul, Preparation, and Hermetically Sealed Canning Howitzer, 105 mm, M2A1," Tentative AB-8, Erie Proving Ground, Dec 1945.

34. "Instructions for Overhaul, Preparation, and Hermetically Sealed Canning Howitzer, 155 mm, M1," Tentative AB-9, Erie Proving Ground, Dec 1945.

35. Notes on the Metal Packing Containers for Extended Storage of Two 105 mm Howitzer Recoil Mechanism, M2A1, Rock Island Ordnance Center, Oct 1945.

36. Long-Term Storage Exposure Site Bulletin No. 15, Davison Chemical Corp., 15 Dec 1947.

37. "Long-Term Storage of Ordnance Material," Davison Chemical Corporation Quarterly Report, Oct 1947.

38. Memorandum, Executive to Chief, Operations Branch, Field Service Division, to Chief, Weapons Section, Maintenance Branch, Field Service Division, 19 Mar 1948.

39. "Test of Solar Radiation Breather on Aluminum Balanced Pressure Barrier Containing 40 mm Gun and Carriage," Engineering Experiment Station, Pennsylvania State College, 31 Dec 1946.

40. Monthly Progress Reports, Davison Chemical Corporation, prior to 1947.

41. W. J. Shields, "Experimental Long-Term Storage Program - Complete Teardown Inspection and Deactivation of Exposure Site at Oahu, Territory of Hawaii," Frankford Arsenal Memorandum Report MR-535, Feb 1953.

42. W. J. Shields, "Experimental Long-Term Storage Program - Complete Teardown Inspection, Erie Ord Depot, 20 Jun to 1 July 49," Frankford Arsenal Memorandum Report MR-428, Jan 1950.

43. W. J. Shields, "Experimental Long-Term Storage Program - Teardown Inspection of Twenty-one Howitzer, 105 mm, M2A1, Aberdeen Proving Ground, January and February 1951," Frankford Arsenal Memorandum Report MR-563, July 1953.

44. M. A. Pelensky, "Long-Term Storage Experimental Program - Teardown Inspection, Aberdeen Proving Cround, 13 June to 24 June 49," Frankford Arsenal Memorandum Report MR-424, Jan 1950.

45. M. A. Pelensky, "Long-Term Storage Experimental Program - Teardown Inspection, Panama Canal Zone, 1 to 23 Feb 50," Frankford Arsenal Memorandum Report MR-448, Nov 1950.

46. W. F. McTeague, "Experimental Long-Term Storage Program - Teardown Inspection, Panama Canal Zone, 25 February to 24 March 1952," Frankford Arsenal Memorandum Report MR-548, Apr 1953.

47. W. J. Shields, "Experimental Long-Term Storage Program - Teardown Inspection at Raritan Arsenal, 9 to 22 December 1950," Frankford Arsenal Memorandum Report MR-507, July 1952.

48. W. J. Shields, "Experimental Long-Term Storage Program - Teardown Inspection of Unit Generators, M7A1, at Tooele Ordnance Depot, May 1951," Frankford Arsenal Memorandum Report MR-561, July 1953.

49. W. J. Shields, "Experimental Long-Term Storage Program - Teardown Inspection of Telescopes, Elbow, M17, in Two Defective Containers

at Panama Canal Zone, May 1950," Frankford Arsenal Memorandum Report MR-544, Feb 1953.

50. W. J. Shields, "Experimental Long-Term Storage Program, Teardown Inspection at Frankford Arsenal of Telescopes, Panoramic, M1, in Sixteen Containers Received from Watertown Arsenal January 1951," Frankford Arsenal Memorandum Report MR-560, July 1953.

51. G. F. Nordblom, "Condensate Formation on the Interior Optical Surfaces of 6x30 Binoculars," Frankford Arsenal Memorandum Report MR-379, Nov 1947.

52. W. J. Shields, "Experimental Long-Term Storage Program - Teardown Inspection of 60 mm and 81 mm Mortars with Mounts at Aberdeen Proving Ground and Erie Ordnance Depot, 25 April to 1 May 1951," Frankford Arsenal Memorandum Report MR-566, Aug 1953.

53. Memorandum for Record, "Long-Term Storage Experimental Program Conference, Aberdeen Proving Ground, 13 and 14 Dec 1948, Frankford Arsenal Jan 1949.

54. W. J. Shields, "Long-Term Storage Experimental Program - Teardown Inspection of Defective Aluminum Containers, Aberdeen Proving Ground, June to August 1948," Frankford Arsenal Memorandum Report MR-450, Dec 1950.

55. W. J. Shields and A. Gallaccio, "Teardown Inspection of Ordnance Automotive Materiel in 14 Containers Exposed Two Years at Lima Ordnance Depot," Frankford Arsenal Memorandum Report MR-425, Jan 1950.

56. Quarterly Report, "Long-Term Storage of Ordnance Materiel, Exposure Site Analysis," The Davison Chemical Corporation, p 33, 34 July 1947.

57. "Volatile Corrosion Inhibitors," Ordnance, Sep-Oct 1950 and Iron Age, 7 Jun 1951.

58. 1st Ind., Letterkenny Ordnance Depot (ORDKE 400.112/114), "Vapor Phase Inhibitor Report," 8 Nov 1951.

59. Communications from Aberdeen Proving Ground on Tank Farm Operation, FA 400.23/315-1, 30 Sep 1948.

60. Correspondence reporting hail damage Pueblo Ordnance Depot, Tooele Ordnance Depot, and San Antonio, 29 Dec 1947.

61. Communication from Erie Ordnance Depot, 15 Apr 1945.

62. Long-Term Storage Exposure Site Bulletin No. 14, Davison Chemical Corporation, 15 Oct 1947.

63. Quarterly Report, "Long-Term Storage of Ordnance Materiel, Exposure

Site Analysis," The Davison Chemical Corporation, Apr 1947.

64. Quarterly Report, "Long-Term Storage of Ordnance Materiel, Exposure Site Analysis," The Davison Chemical Corporation, 1 Jan 1948.

65. "The Balanced Pressure Barrier of Aluminum Construction," Davison Chemical Corporation and Glenn L. Martin Company, 3 Jul 1944.

66. M. H. Bradford, "Protection of Ordnance Instruments by Silica-Gel Vapor Phase Inhibitor and Breather Tubes," U. S. Naval Gun Factory Technical Report No. NGF 95-47, 3 Nov 1947; and H. W. Ritter and M. H. Bradford, "Effect of Breather Tubes on the Amount of Moisture-Vapor Entering Sealed Containers when these Containers are Subjected to a Severe Temperature and Humidity Cycle," U. S. Naval Gun Factory Technical Report No. NGF 95-47, Second Test, 3 Aug 1948.

67. W. F. Hicks, "Humidity Measurement by a New System," Foxboro Company, Reprint, Refrigerator Engineering, Oct 1947.

68. "Aging of Natural and Synthetic Rubbers," Firestone Tire & Rubber Co., Final Report, Contract DA-33-019-ORD-723, 10 Feb 1953.

69. Memorandum, "Storage," Maj F. A. Doeppers, Acting Chief, Engineering and Inspection Control Branch, Artillery Division, Industrial Service, Office, Chief of Ordnance to Fire Conrrol Sub-Office, Frankford Arsenal, 9 Jul 1945.

70. Letter of Instructions, Office, Chief of Ordnance, ORDIR (FA 400.23/312) 22 Jan 1948.

71. Training Film, "Strippable Film Application," U. S. Army Signal Corps Technical Film Bulletin No. 179 9-34.

72. Literature Surveys Relative to the Storage and Preservation of Materials - Battelle Memorial Institute Reports issued during 1945-1946.

73. A. Wachter, T. Skei, and N. Stillman, "Dicyclohexylammonium Nitrite, a Volatile Corrosion Inhibitor for Corrosion Prevention," Shell Development Company, 1951.

74. "Aging of Natural and Synthetic Rubbers," Firestone Tire & Rubber Co., Final Report, Contract DA-33-019-ORD-723, 10 Feb 1953.

75. Hayward R. Baker, "Volatile Rust Inhibitors," Naval Research Laboratories Report 4319, 10 May 1954.

76. W. J. Shields, "Long-Term Storage Experimental Program, Annual Teardown Inspection, Erie Ordnance Depot, 20 Jun to 1 Jul 1949," Frankford Arsenal Memorandum Report MR-428, Jan 1950.

77. W. J. Shields, "Long-Term Storage Experimental Program, Annual

Teardown Inspection, Pueblo Ordnance Depot, 24 Oct to 4 Nov 1949," Frankford Arsenal Memorandum Report MR-430, Feb 1950.

78. M. A. Pelensky, "Long-Term Storage Experimental Program - Annual Teardown Inspection, Watertown Arsenal, 14 Nov to 7 Dec 1949," Frankford Arsenal Memorandum Report MR-432, Jun 1950.

79. W. J. Shields, "Experimental Long-Term Storage Program - Teardown Inspection at Augusta Arsenal, 30 Oct to 10 Nov 1950," Frankford Arsenal Memorandum Report No. MR-510, Jun 1952.

80. W. J. Shields, "Experimental Long-Term Storage Program, Annual Teardown Inspection - Teardown Inspection Pueblo Ordnance Depot, Nov-Dec 1951," Frankford Arsenal Memorandum Report MR-559, Jul 1953.

81. W. J. Shields, "Experimental Long-Term Storage Program - Teardown Inspection of Three 90 mm M1A1 AA Weapons at Tooele Ordnance Depot, 8 to 25 Nov 1951," Frankford Arsenal Memorandum Report MR-579, Feb 1954.

82. W. J. Shields, "Experimental Long-Term Storage Program - Teardown of Two 40 mm AA Weapons in Damaged Aluminum Containers at Erie Ordnance Depot, 27 Aug 51," Frankford Arsenal Memorandum Report MR-583, Mar 1954.

83. W. F. McTeague, "Experimental Long-Term Storage Program - Teardown Inspection of 40 mm Antiaircraft Guns at Anniston Ordnance Depot: February to June 1953," Frankford Arsenal Memorandum Report MR-588, Aug 1954.

84. Ltr, Erie Ordnance Depot to Frankford Arsenal, Subject: "Removal of Ordnance Weapons from Long-Term Storage Containers," FA 400.23/15, Incl 10 and 11, 15 Apr 1955.

85. Ltr, Frankford Arsenal to Erie Ordnance Depot, Subject: "Experimental Long-Term Storage - Exercising of Assembled Hydropneumatic Recoils," 25 May 1955.

86. A. Gallaccio and W. J. Shields, "Initiation of Long-Term Storage Experimental Site at Fort Churchill, Manitoba, Canada," Frankford Arsenal Memorandum Report MR-419, Sep 1949.

87. L. Teitell, "Weather at the Panama Canal Zone Tropical Testing Station," Frankford Arsenal Report R-742, Oct 1946.

88. Recent data, unpublished.

NOTE: This paper is a shortened version of Frankford Arsenal Report R-1269. As a consequence, certain references and figures contained in the original report have been omitted from the body of this paper. The original number of the reference or figure shown has been retained.

Table I. Inventory of Material and Containers in Industrial Account

Storage Unit	Item	Medium	No. of Item	Aberdeen Proving Ground			Erie Ordnance Depot			Hawaii Ordnance Depot			Panama Canal Zone			Pueblo Ordnance Depot			Toele Ordnance Depot			Watertown Arsenal			Frankford Arsenal			Raritan Arsenal			Augusta Arsenal			Anniston Ordnance Depot			Red River Arsenal			Totals		
				A	B	C	A	B	C	A	B	C	A	B	C	A	B	C	A	B	C	A	B	C	A	B	C	A	B	C	A	B	C	A	B	C	A	B	C

*A - Original inventory
B - Reserved for inspection
C - Remainder
** disassembled

Table IV. Materiel Stored at Lima Ordnance Depot
Not under Industrial Account

Storage Unit	Item	Medium	Items per Container	Total[*]		
				A	B	C
Steel						
	Tank, M24	N_2	1	2	2	0
	Tank, M4A3	N_2	1	1	1	0
	Tank, M36B2	N_2	1	1	1	0
	Car, Armored, M8	N_2	1	1	1	0
	Car, Armored, M20	N_2	1	2	2	0
	Carrier, Cargo, M29C	N_2	1	2	2	0
	Tractor, HS, M6	N_2	1/2	2	2	0
Aluminum						
	Carriage, Motor, Gun, M18	N	1/2	2	2	0
Strippable film						
	Carriage, Motor, Gun, M18	Air	1	1	1	0
	Total			14	14	0

[*]Ibid

Table V. 90 mm AA M1A1 Weapons in Strippable Vinyl Film Containers
Not under Industrial Account

Location	Medium	Items per Container	Total[*]		
			A	B	C
Black Hills Ordnance Depot	Air	1	2	2	0
Pueblo Ordnance Depot	"	1	2	2	0
Tooele Ordnance Depot	"	1	2	2	0
Mt Rainier Ordnance Depot	"	1	2	2	0
San Antonio Ordnance Depot	"	1	2	2	0
Erie Ordnance Depot	"	1	2	2	0
Frankford Arsenal	"	1	2	1	1
	Total		14	13	1

*Ibid

Table II. Material Stored at Aberdeen Proving Ground
Not under Industrial Account

Storage Unit	Item	Totals*		
		A	B	C
10 Gasoline Storage Tanks**				
	Carriage, 240 mm, M1, w/Wagon, M3A1	3	3	0
	Gun, 90 mm, M2, w/Mount, M3	6	6	0
	Howitzer, 155 mm, M1, w/Carriage, M1A1 or M1A2	20	20	0
	Gun, 40 mm, M1, w/Carriage, M2A1	64	64	0
	Gun, 57 mm, M1, w/Carriage, M2	20	20	0
	Howitzer, 75 mm, Pack, M1A1, w/Carriage, M1 or M8	128	128	0
	Total	241	241	0
6 Igloo, 40 ft x 10 ft x 8 ft				
	Howitzer, 240 mm, M1, w/Wagon, M2A1	6	0	6
	Gun, 40 mm, M1, w/Carriage, M2A1, removed	2	2	0
	Howitzer, 75 mm, M1A1, w/Carriage, M1	70	0	70
	Total	78	2	76

*A - Original inventory
B - Removed for inspection
C - Remainder

**3 - 55 ft x 16 ft
3 - 38 ft x 8 ft
2 - 29 ft x 8 ft
2 - 21 ft x 8 ft

Table III. Material Stored at Frankford Arsenal
Not under Industrial Account

Storage Unit	Item	Total*		
		A	B	C
13 containers	Periscope, M6 (36 per container, 468 total	13	0	13

*Ibid
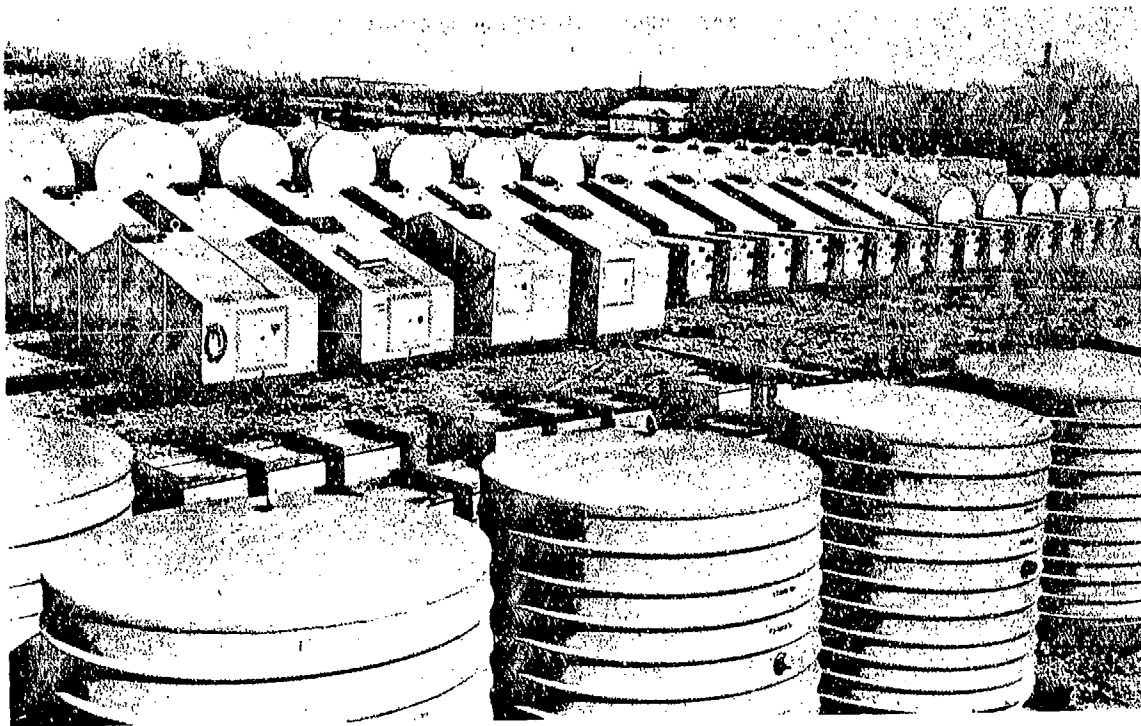
Figure 1. Typical exposure site
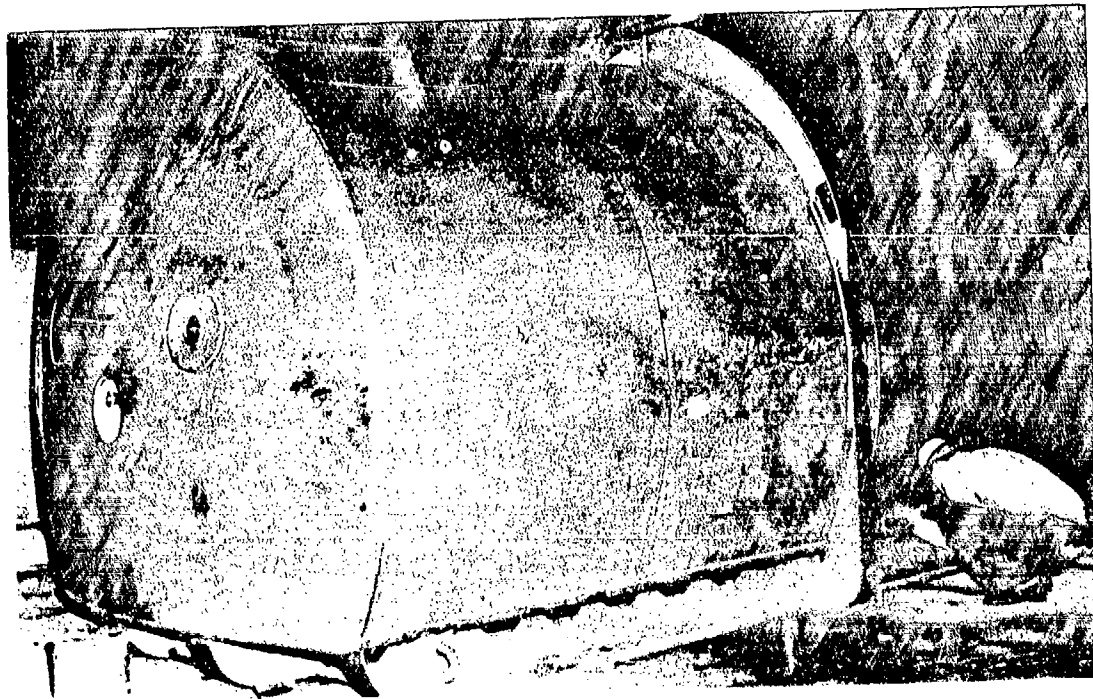
Figure 2. Ambridge cylindrical container

362
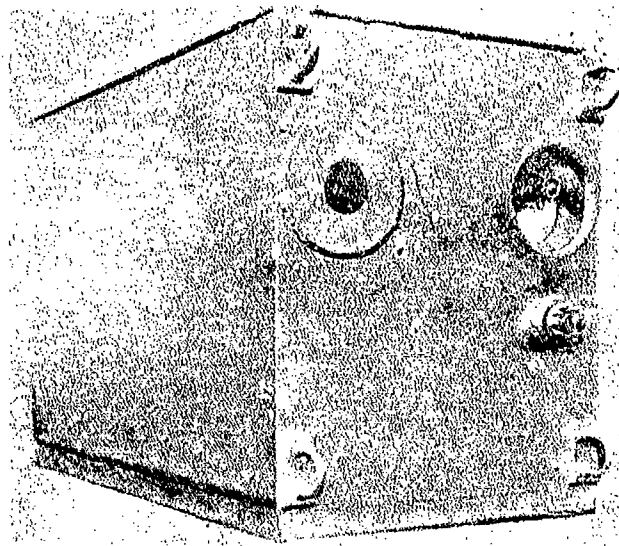
Figure 3. Ambridge rectangular container
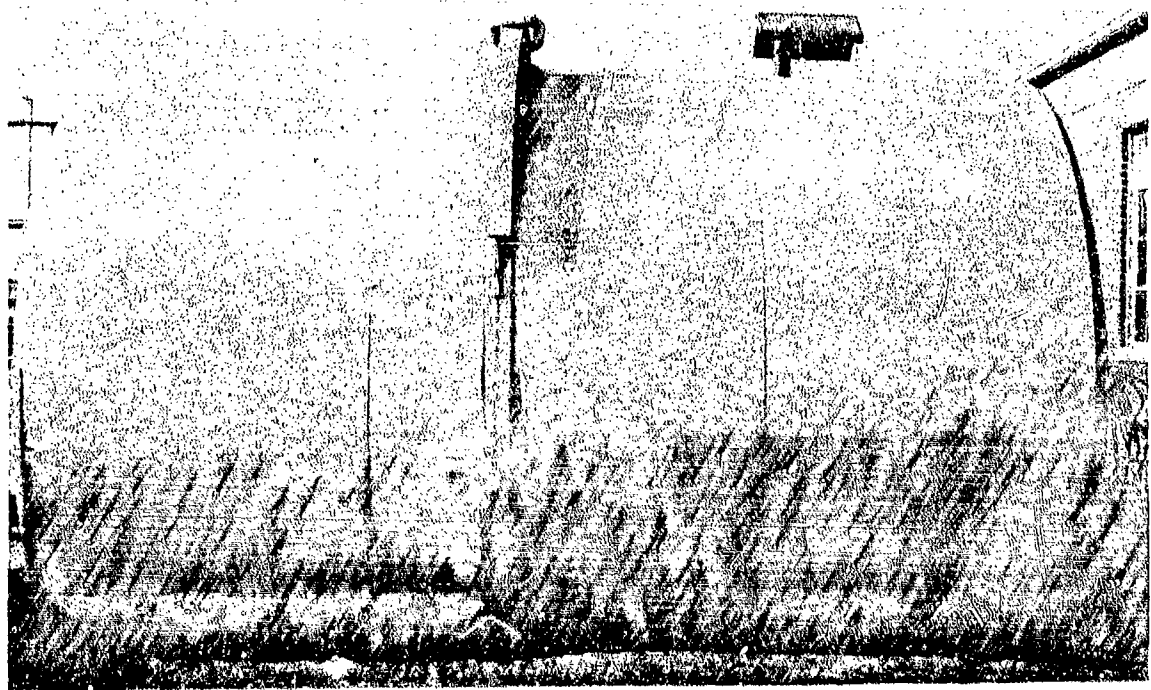
Figure 4. Ambridge container modified with solar radiation breather
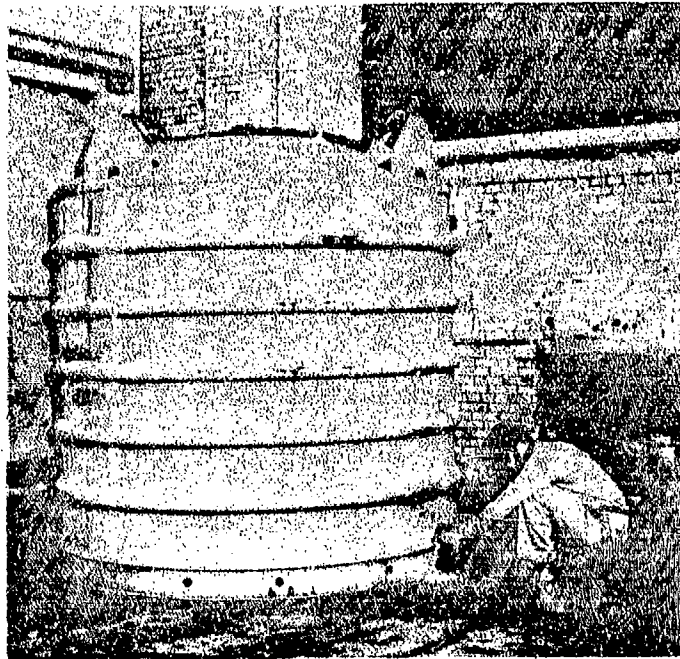
Figure 5. Dravo cylindrical container
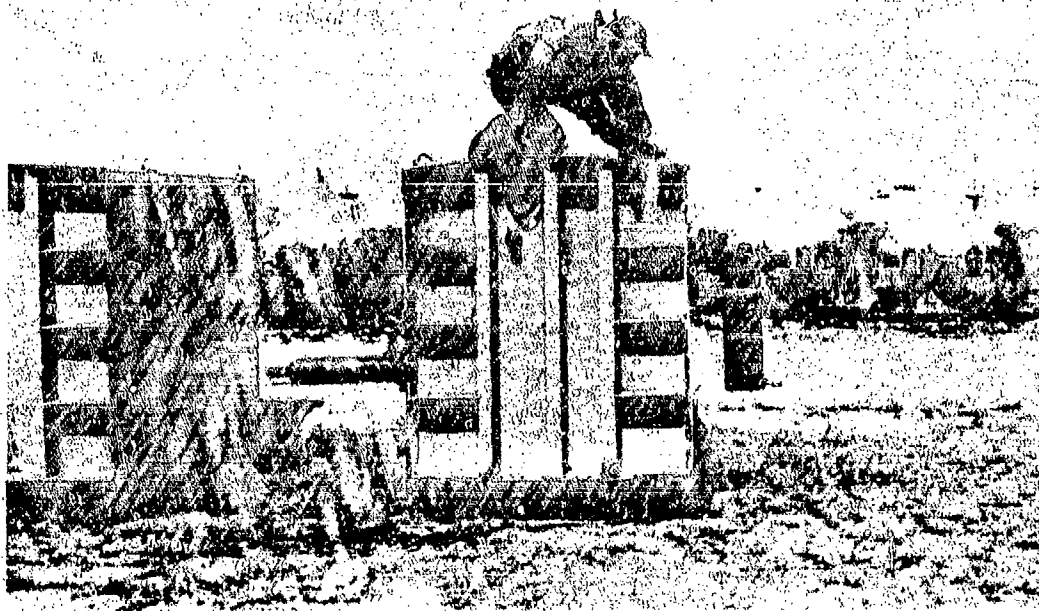

Figure 6. Dravo rectangular container
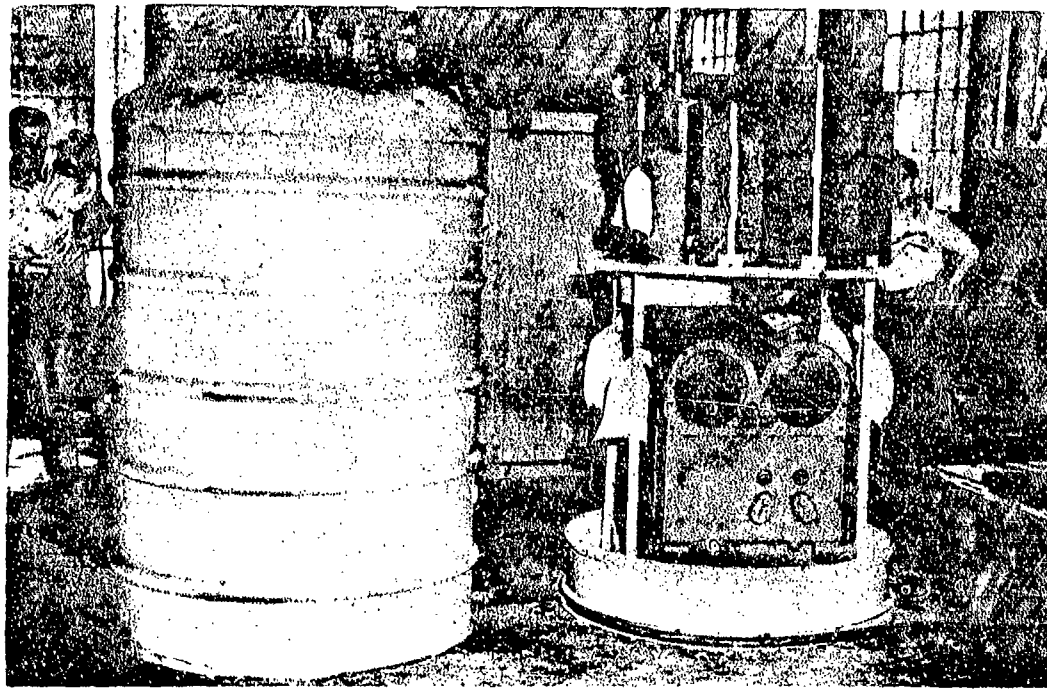
Figure 7. Harlan and Hollingsworth container


Figure 8. Steiker containers
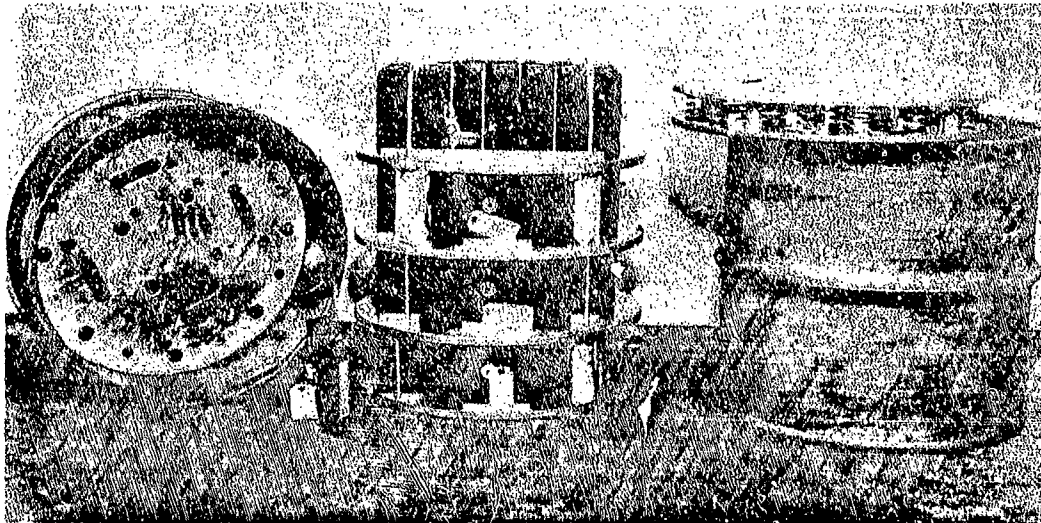
Figure 9. Frankford Arsenal container


Figure 10. Rock Island Arsenal containers
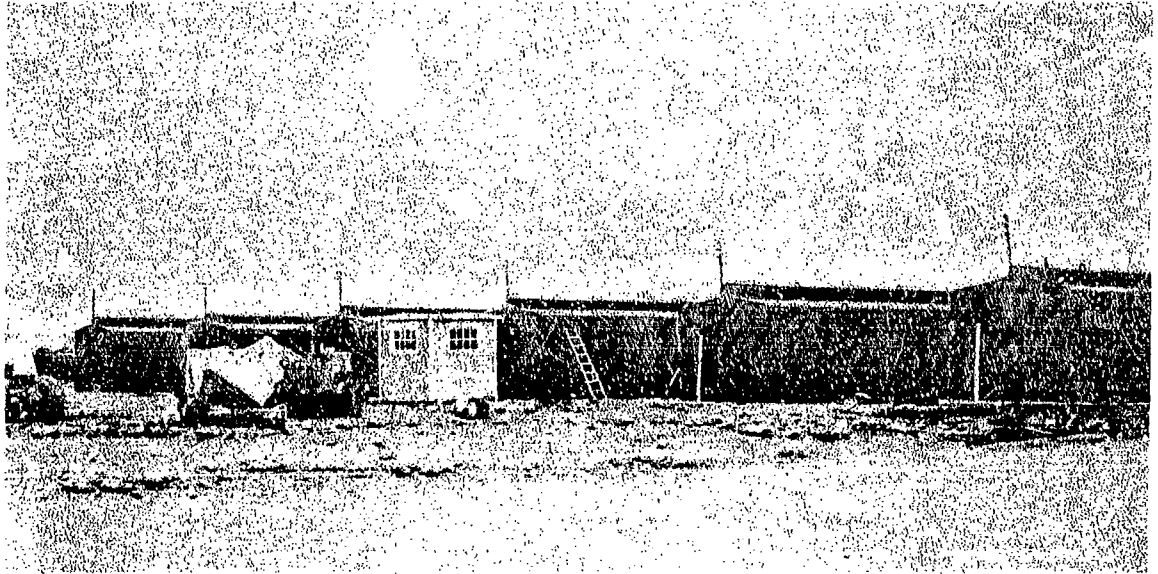
Figure 11. Igloos
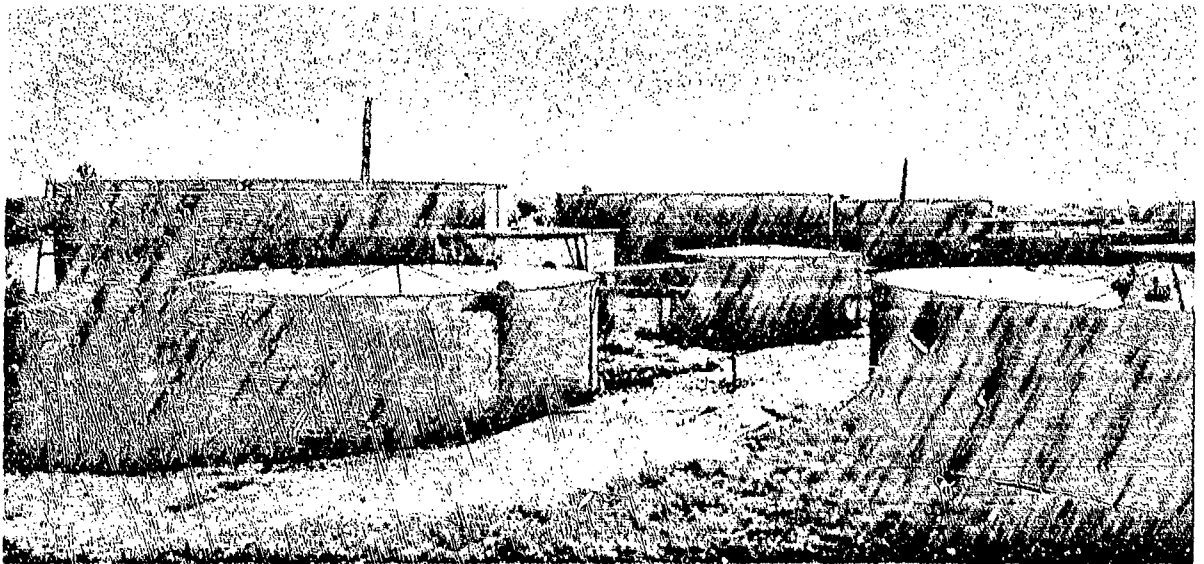
Figure 12. Storage tanks
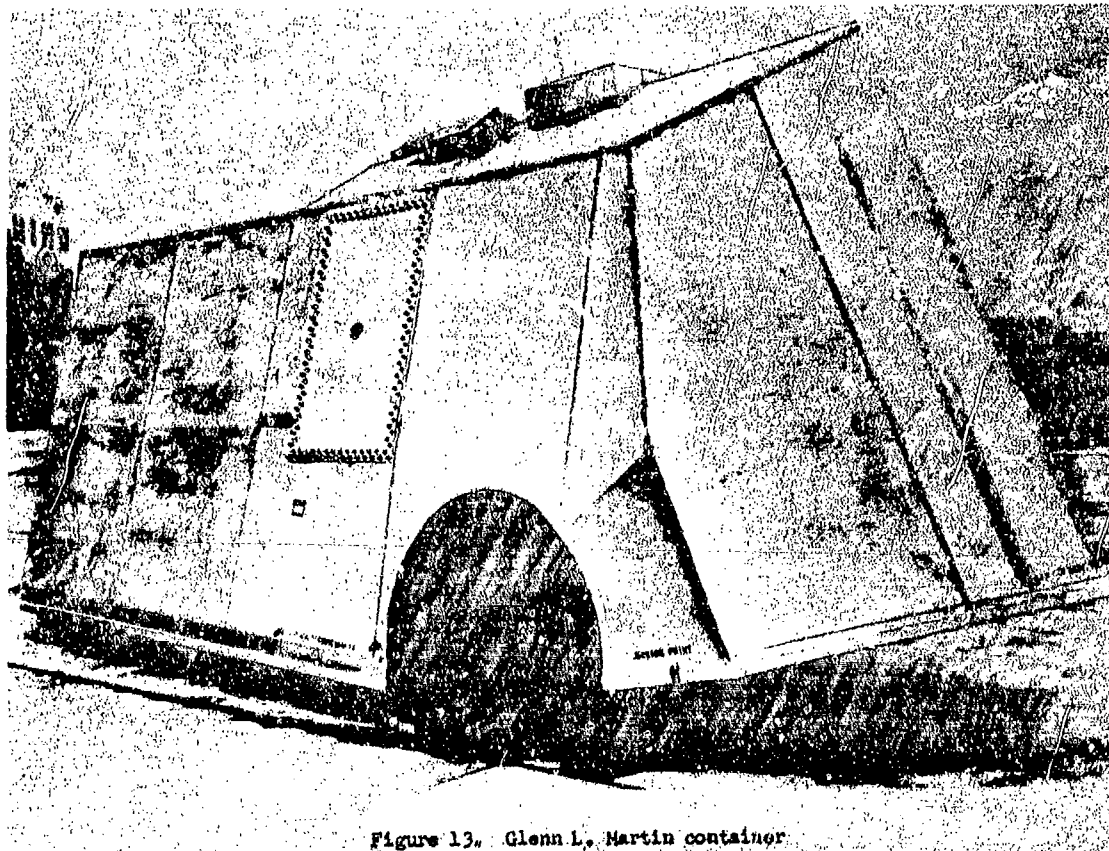
Figure 13. Glenn L. Martin container
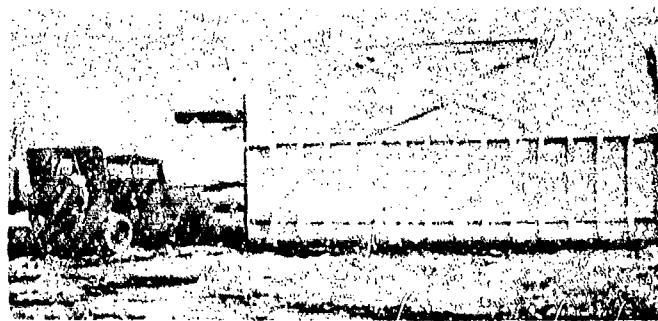
Figure 14. Special container

368
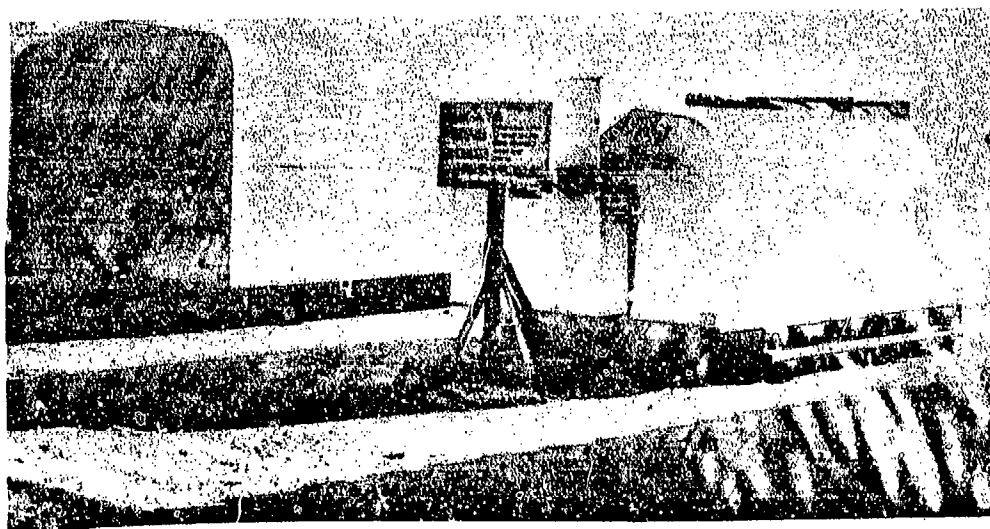
Figure 15. Special container
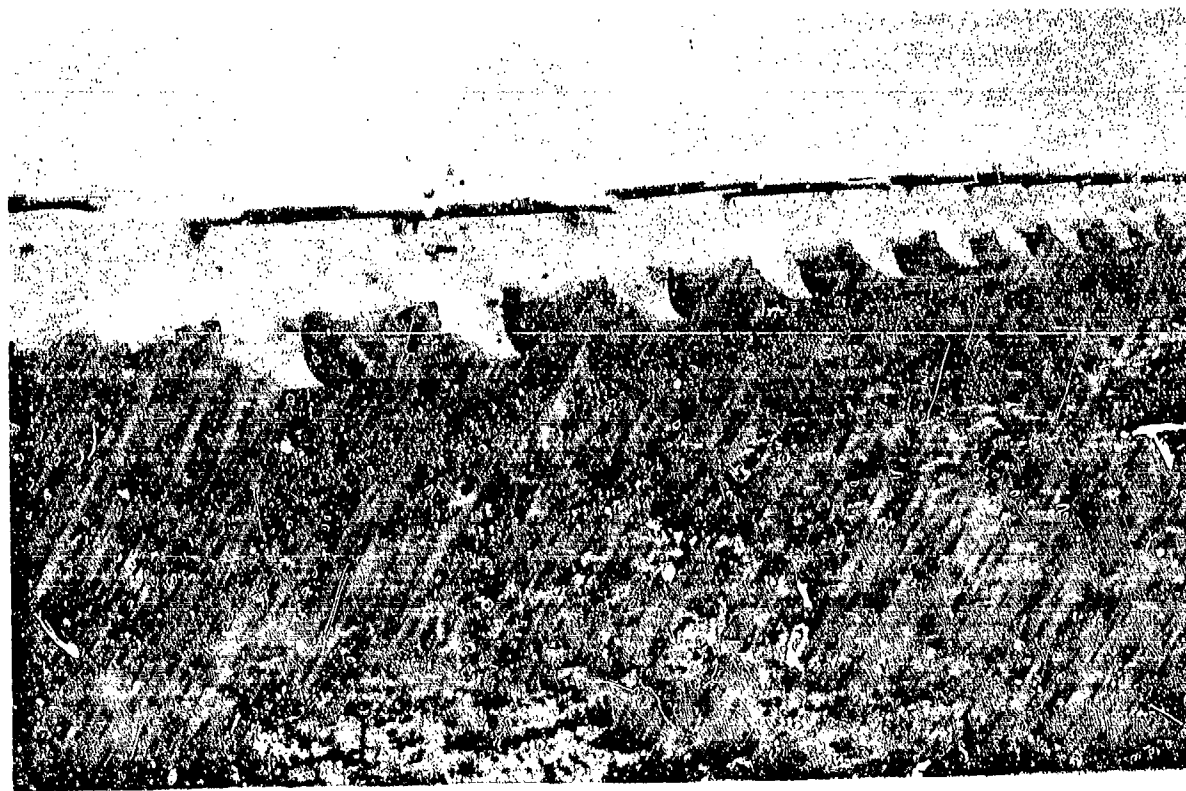

Figure 16. Vinyl containers
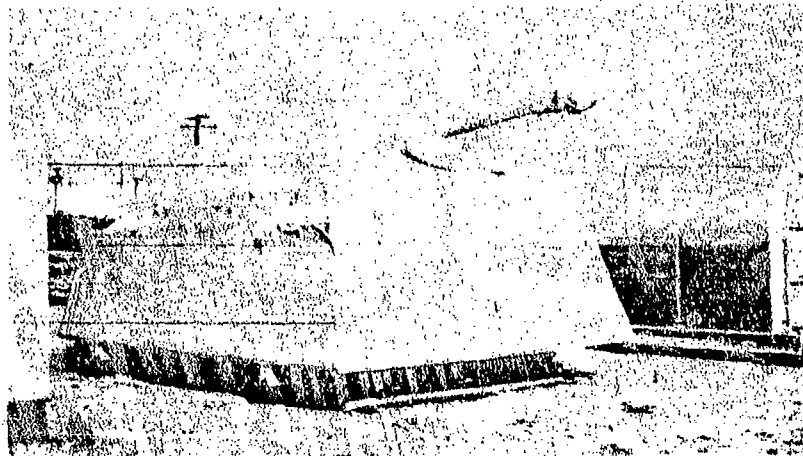
Figure 17. Special vinyl container
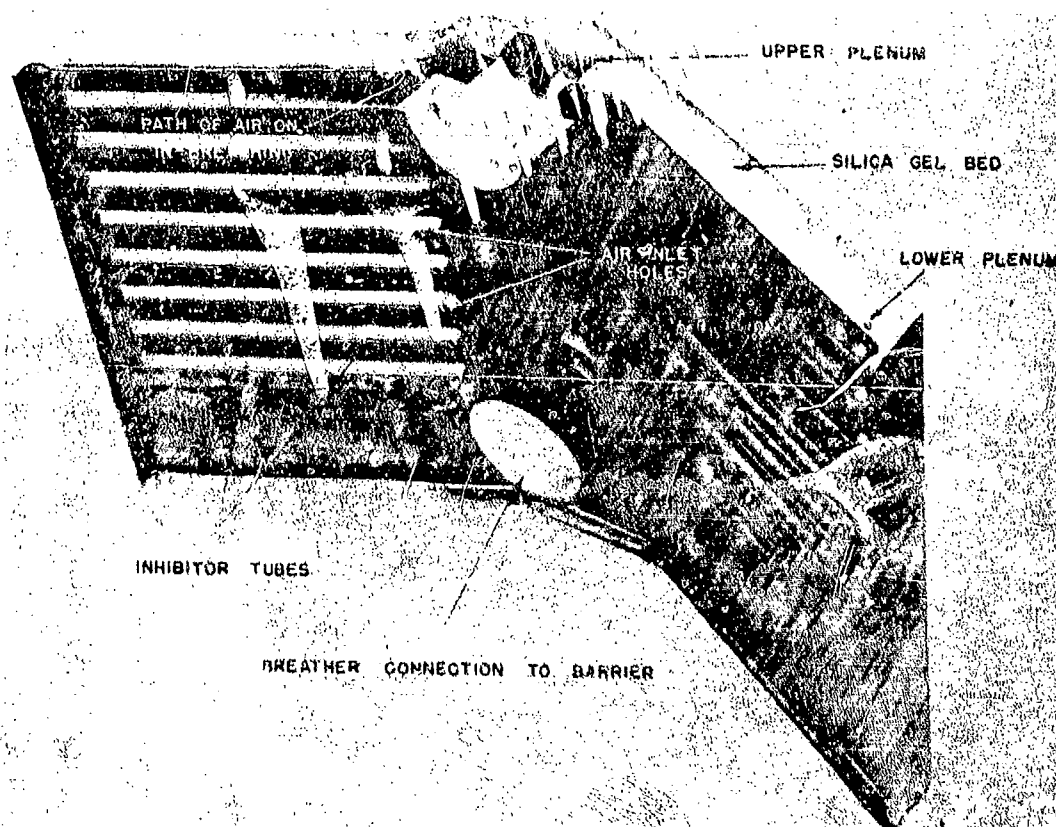
Figure 18. Solar radiation breather
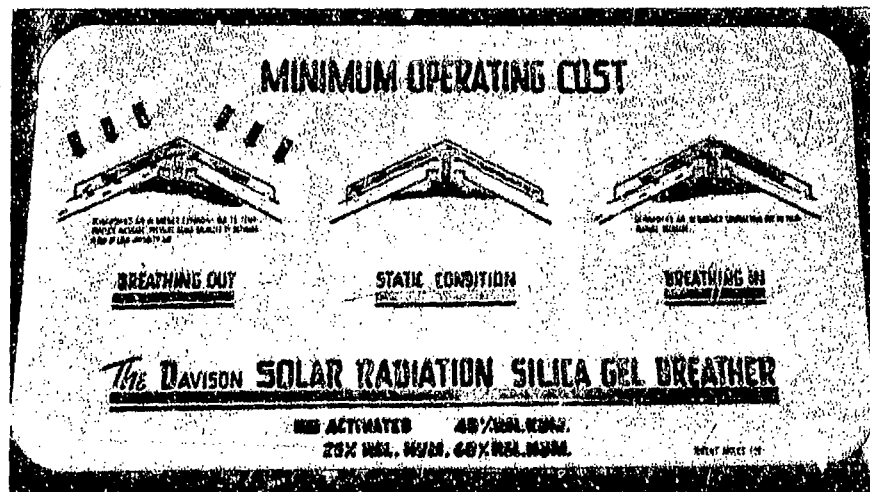
Figure 23. Cross-section of solar radiation breather
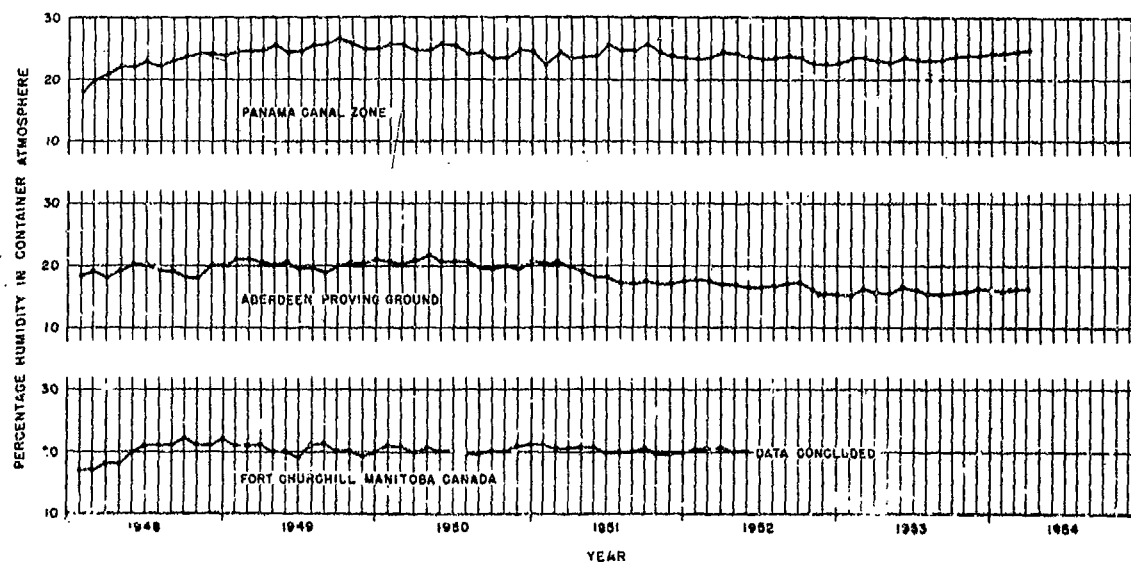
Figure 24. Relative humidity in container with solar radiation breather